MONTHLY NOTICES

OF THE

ROYAL ASTRONOMICAL SOCIETY

Vol. 114 No. 1 1954

Published and Sold by the
ROYAL ASTRONOMICAL SOCIETY
BURLINGTON HOUSE
LONDON, W. 1

Price Thirteen Shillings and Sixpence

NOTICE TO AUTHORS

1. *Communications.*—Papers must be communicated to the Society by a Fellow. They should be accompanied by a summary at the *beginning* of the paper conveying briefly the content of the paper, and drawing attention to important new information and to the main conclusions. The summary should be intelligible in itself, without reference to the paper, to a reader with some knowledge of the subject; it should not normally exceed 200 words in length. **Authors are requested to submit MSS. in duplicate. These should be typed using double spacing and leaving a margin of not less than one inch on the left-hand side. Corrections to the MSS. should be made in the text and not in the margin.** Unless a paper reaches the Secretaries more than seven days before a Council meeting it will not normally be considered at that meeting. By Council decision, MSS. of accepted papers are retained by the Society for one year after publication; unless their return is then requested by the author, they are destroyed.

2. *Presentation.*—Authors are allowed considerable latitude, but they are requested to follow the general style and arrangement of *Monthly Notices*. References to literature should be given in the standard form, including a date, for printing either as footnotes or in a numbered list at the end of the paper. Each reference should give the **name and initials** of the author cited, irrespective of the occurrence of the name in the text (some latitude being permissible, however, in the case of an author referring to his own work). The following examples indicate the style of reference appropriate for a paper and a book, respectively :—

A. Corlin, *Zs. f. Astrophys.*, **15**, 239, 1938.
H. Jeffreys, *Theory of Probability*, 2nd edn., section 5.45, p. 258, Oxford, 1948.

3. *Notation.*—For technical astronomical terms, authors should conform closely to the recommendations of Commission 3 of the International Astronomical Union (*Trans. I.A.U.*, Vol. VI, p. 345, 1938). Council has decided to adopt the I.A.U. 3-letter abbreviations for constellations where contraction is desirable (Vol. IV, p. 221, 1932). In general matters, authors should follow the recommendations in *Symbols, Signs and Abbreviations* (London : Royal Society, 1951) except where these conflict with I.A.U. practice.

4. *Diagrams.*—**These should be designed to appear upright on the page, drawn about twice the size required in print and prepared for direct photographic reproduction except for the lettering, which should be inserted in pencil. Legends should be given in the manuscript indicating where in the text the figure should appear.** Blocks are retained by the Society for 10 years; unless the author requires them before the end of this period they are then destroyed.

5. *Tables.*—**These should be arranged so that they can be printed upright on the page.**

6. *Proofs.*—Costs of alterations exceeding 5 per cent of composition must be borne by the author. Fellows are warned that such costs have risen sharply in recent years, and it is in their own and the Society's interests to seek the maximum conciseness and simplification of symbols and equations consistent with clarity.

7. *Revised Manuscripts.*—When papers are submitted in revised form it is especially requested that they be accompanied by the original MSS.

Reading of Papers at Meetings

8. When submitting papers authors are requested to indicate whether they will be willing and able to read the paper at the next or some subsequent meeting, and approximately how long they would like to be allotted for speaking.

9. Postcards giving the programme of each meeting are issued some days before the meeting concerned. Fellows wishing to receive such cards whether for Ordinary Meetings or for the Geophysical Discussions or both should notify the Assistant Secretary.

MONTHLY NOTICES

OF THE

ROYAL ASTRONOMICAL SOCIETY

Vol. 114 No. 1

MEETING OF 1954 JANUARY 8

Dr J. Jackson, President, in the Chair

The election by the Council of the following Fellows was duly confirmed :—

*Lewis Grenville Bentley, 27 Gracefield Gardens, Streatham, London, S.W.16 (proposed by F. M. Holborn);

Robert John Bray, University Observatory, Oxford (proposed by H. H. Plaskett);

Ronald Edgar Edwards, 14 Leaside Way, Southampton (proposed by E. W. Mason);

*Mavis McIntyre Smith Gibson, H.M. Nautical Almanac Office, Royal Greenwich Observatory, Herstmonceux Castle, Hailsham, Sussex (proposed by D. H. Sadler);

*Raymond Hide, 22 Castle Hills Road, Scawthorpe, near Doncaster, Yorkshire (proposed by S. Chandrasekhar);

*John Noel Hodgson, 123 Cherrydown Avenue, Chingford, London, E.4 (proposed by R. O. Redman);

*Francis John Lowes, Department of Geodesy and Geophysics, Downing Place, Cambridge (proposed by M. N. Hill);

William Scott Matthews, 81 Albert Road, Colne, Lancashire (proposed by W. M. Mason);

*Gilbert Elliott Satterthwaite, 48 Upper Abbey Road, Belvedere, Kent (proposed by A. F. Alexander);

*Gordon Ingram Thompson, Dunsink Observatory, Co. Dublin, Eire (proposed by H. A. Brück); and

William Henry Vale, 11 Edgar Street, Brighton, Victoria, Australia (proposed by J. Boyle).

The election by the Council of the following Junior Member was duly confirmed :—

Philip Henry Vince, Wyeross, 17 Stanley Hill Avenue, Amersham, Buckinghamshire (proposed by A. W. Vince).

Ninety-seven presents were announced as having been received since the last meeting.

The President announced that the Council had awarded the Gold Medal of the Society to Dr Walter Baade, of Mount Wilson Observatory, for his observational work on galactic and extra-galactic objects.

*Transferred from Junior Membership.

ON THE INTENSITIES OF INTERLOCKED MULTIPLET LINES IN THE MILNE–EDDINGTON MODEL

I. W. Busbridge and D. W. N. Stibbs

(Communicated by the Director, University Observatory, Oxford)

(Received 1953 July 11)

Summary

The equations of transfer in the Milne–Eddington model for multiplet lines with a common upper state are solved exactly. It is assumed that no redistribution in frequency takes place other than that due to interlocking, that the ratios of the line absorption coefficients to the continuous absorption coefficient are independent of depth, and that the lower states of the lines are sharp. A linear approximation for the Planck function is used. The solution is found to depend on H-functions of a fairly simple type. The case of a doublet is considered in detail. Values for the H-functions are computed and the residual intensities of the two components are evaluated as functions of $\mu(=\cos\theta)$ for three distances from the centres of the lines. These are compared with the residual intensities for doublet lines when there is no interlocking. It is shown that interlocking causes a small reduction in the difference between the residual intensities of the two lines, the reduction being greater towards the limb. A solution for the doublet intensities based on Eddington's approximation is also considered and it is shown that the errors in the approximate solution are satisfactorily small for $\mu > 0{\cdot}2$.

---

1. *Introduction.*—The theory of the formation of absorption lines by coherent scattering may be applied to multiplets with a common lower state if the lower state itself is sharp and if there is no redistribution in frequency due to collision broadening of the upper states. Under these conditions an atom, once excited to any one of the upper states, can only return to the common lower state. When, however, there is a common upper state, the re-emission will be governed by the transition probabilities corresponding to the various lines and the atom may return to a different state from the one in which it started. Examples of such interlocked lines are

Al I	λ3961 A	and	Ga I	λ4172 A	$^2P_{3/2}-{}^2S_{1/2}$
	3944 A			4032 A	$^2P_{1/2}-{}^2S_{1/2}$
Mg I	λ5184 A		Ca I	λ6162 A	$^3P_2-{}^3S_1$
	5173 A	and		6122 A	$^3P_1-{}^3S_1$
	5167 A			6102 A	$^3P_0-{}^3S_1$

The equations of transfer in the Milne–Eddington model for interlocking without redistribution have been discussed by Woolley and Stibbs in (**5**), where a clear statement of the problem will be found. Taking the Planck function to be linear, they have obtained a solution by means of Eddington's approximation and calculated the residual intensities and the total absorption in the emergent flux for doublet and triplet lines. Although their equations are set out for triplets, they clearly extend to multiplets containing any number of lines with a

common upper state and these equations, suitably generalized, are reproduced in Section 2.

The method of solution (Sections 3–5) is a slight modification of one which has already been applied successfully in (**1**) and (**4**) to problems of non-coherent scattering. It easily gives the exact solution for k interlocked lines in terms of H-functions of a fairly simple type.

When $k=1$, these functions are those already tabulated by Chandrasekhar and Breen (see (**2**) Table XI). In Section 6.1 we describe the method which has been used to compute them when $k=2$ and we give a table of values (Table I). These values are used in Section 6.2 to evaluate the residual intensities for doublet lines at three distances from their centres. The residual intensities are calculated as functions of μ, where $\cos^{-1}\mu$ is the angle which the direction of emergence makes with the outward normal to the surface of the atmosphere. The results are shown in Table II and Fig. 1.

In order to show the effect of interlocking on the centre-to-limb variation of the residual intensity, the corresponding residual intensities are evaluated for a doublet without interlocking (Table III and Fig. 2). It is shown that interlocking reduces the differences between the residual intensities of the two lines for all values of μ. The reduction near the centre of the disk ($\mu=1$) is very small, but it increases towards the limb. The effect is shown clearly in Fig. 3.

The labour involved in computing the H-functions is considerable and it would be even greater for a triplet ($k=3$). For this reason we consider, in Section 6.3, the accuracy of an approximate solution of the equations of transfer for a doublet based on Eddington's approximation, and we show that, in the cases examined, the proportional errors in the residual intensities lie within ± 1 per cent for values of $\mu>0{\cdot}2$.

2. *The equations of transfer.*—Woolley and Stibbs have made certain assumptions in (**5**) which we shall also make here. These are

(i) that the lines are so close together that variations of the continuous absorption coefficient κ and of the Planck function $B(\nu, T)$ with wave-length may be neglected. This also means that the lower states are nearly equal in excitation potential and that they have the same classical damping constant. Then the values of $\eta_1, \ldots, \eta_k$ (the ratios of the line absorption coefficients to κ) are proportional to the transition probabilities for spontaneous emission from the upper state to the respective lower states;

(ii) that $\eta_1, \ldots, \eta_k$ are independent of depth;

(iii) that
$$B(\nu, T)=a+b\tau, \tag{2.1}$$
where $\tau=\int_0^x \kappa\rho\, dx$, x being the depth below the surface of the atmosphere. By (i) a, b and τ are independent of ν;

(iv) that the coefficient ϵ, which is introduced to allow for thermal emission associated with the line absorption, is independent of both frequency and depth.

With these assumptions, the equations of transfer are
$$\mu\frac{dI_r(\tau,\mu)}{d\tau}=(1+\eta_r)I_r(\tau,\mu)-(1+\epsilon\eta_r)(a+b\tau)$$
$$-(1-\epsilon)\alpha_r\sum_{p=1}^{k}\tfrac{1}{2}\eta_p\int_{-1}^{1}I_p(\tau,\mu')\,d\mu' \quad (r=1,\ldots,k), \tag{2.2}$$
where
$$\alpha_r=\eta_r/(\eta_1+\ldots+\eta_k), \tag{2.3}$$
so that
$$\alpha_1+\alpha_2+\ldots+\alpha_k=1. \tag{2.4}$$

In the equations (2.2) the subscript r denotes the quantity corresponding to the line of frequency ν_r. Later it will be convenient to use $I_r(\tau,\mu)$ and η_r when we are considering any frequency ν, but on putting $\nu=\nu_r$, we shall replace them by $I_r(\tau,\mu)$ and η_r.

The equations (2.2) have to be solved subject to the boundary conditions

$$I_r(0,-\mu')\equiv 0 \qquad (0<\mu'\leqslant 1,\ r=1,\ldots,k), \tag{2.5}$$

together with a condition limiting $I_r(\tau,\mu)$ for large τ. We shall assume that $I_r(\tau,\mu)$ is at most linear in τ for large τ.

Exact solutions of (2.2) are easily found, but they do not satisfy (2.5). These are

$$I_r(\tau,\mu)=a+b\left(\tau+\frac{\mu}{1+\eta_r}\right) \qquad (r=1,\ldots,k),$$

as is easily verified with the help of (2.3).

Write

$$I_r(\tau,\mu)=a+b\left(\tau+\frac{\mu}{1+\eta_r}\right)+I_r^*(\tau,\mu) \qquad (r=1,\ldots,k). \tag{2.6}$$

Then $I_r^*(\tau,\mu)$ satisfies the equations of transfer

$$\mu\frac{dI_r^*(\tau,\mu)}{d\tau}=(1+\eta_r)I_r^*(\tau,\mu)-(1-\epsilon)\alpha_r\sum_{p=1}^{k}\tfrac{1}{2}\eta_p\int_{-1}^{1}I_p^*(\tau,\mu')d\mu' \qquad (r=1,\ldots,k), \tag{2.7}$$

together with the boundary conditions

$$I_r^*(0,-\mu')\equiv\frac{b\mu'}{1+\eta_r}-a \qquad (0<\mu'\leqslant 1,\ r=1,\ldots,k). \tag{2.8}$$

Moreover $I_r^*(\tau,\mu)$ must be at most linear in τ as $\tau\to\infty$.

We have here the problem of a scattering atmosphere subject to external radiation, whose intensity is given by (2.8). We want to find the emergent intensity $I_r^*(0,\mu)$ of frequency ν_r. This will be the intensity of the diffusely reflected radiation; it can be calculated when the appropriate scattering function is known.

In the present problem the scattering function splits up into k^2 functions

$$S_{rs}(\mu,\mu') \qquad (r=1,\ldots,k;\ s=1,\ldots,k),$$

but it is convenient to reunite them temporarily in the function

$$p(\nu,\nu')S(\nu,\nu';\ \mu,\mu'),$$

where ν is any one of $\nu_1,\nu_2,\ldots,\nu_k$,

$$p(\nu,\nu')=\alpha_r\sum_{p=1}^{k}\delta(\nu_p-\nu'), \tag{2.9}$$

δ denoting Dirac's δ-function, and

$$S(\nu_r,\nu_s;\ \mu,\mu')=S_{rs}(\mu,\mu'). \tag{2.10}$$

Then the law of diffuse reflection for the atmosphere can be written (*cf.* (4), equation (15))

$$I_\nu^{\mathrm{ref}}(0,\mu)=\frac{1}{2\mu}\int_0^\infty p(\nu,\nu')\,d\nu'\int_0^1 S(\nu,\nu';\ \mu,\mu')I_{\nu'}^{\mathrm{inc}}(0,-\mu')\,d\mu'. \tag{2.11}$$

The equivalent form in terms of the functions $S_{rs}(\mu,\mu')$ is

$$I_r^{\mathrm{ref}}(0,\mu)=\alpha_r\sum_{p=1}^{k}\frac{1}{2\mu}\int_0^1 S_{rp}(\mu,\mu')I_p^{\mathrm{inc}}(0,-\mu')\,d\mu', \tag{2.12}$$

a form to which we shall return in Section 5.

With the aid of (2.9), (2.7) can be written in the form

$$\mu\frac{dI_\nu^*(\tau,\mu)}{d\tau}=(1+\eta_\nu)I_\nu^*(\tau,\mu)-\tfrac{1}{2}(1-\epsilon)\int_0^\infty \eta_{\nu'}p(\nu,\nu')\,d\nu'\int_{-1}^{1} I_{\nu'}^*(\tau,\mu')\,d\mu'. \quad (2.13)$$

This is equation (12) of (**4**), to which we now refer for the general equation for the scattering function.

3. *The scattering functions.*—In (**4**), Stibbs has found the following general equation for the scattering function $S(\nu,\nu';\ \mu,\mu')$:

$$\begin{aligned}\left[\frac{1+\eta_\nu}{\mu}+\frac{1+\eta_{\nu_i}}{\mu_i}\right]p(\nu,\nu_i)\frac{S(\nu,\nu_i;\ \mu,\mu_i)}{1-\epsilon}&=p(\nu,\nu_i)\eta_{\nu_i}\\&+\eta_{\nu_i}\int_0^\infty p(\nu,\nu')p(\nu',\nu_i)\,d\nu'\int_0^1 S(\nu,\nu';\ \mu,\mu')\frac{d\mu'}{2\mu'}\\&+\int_0^\infty \eta_{\nu'}p(\nu,\nu')p(\nu',\nu_i)\,d\nu'\int_0^1 S(\nu',\nu_i;\ \mu',\mu_i)\frac{d\mu'}{2\mu'}\\&+\int_0^\infty p(\nu,\nu'')\,d\nu''\int_0^1 S(\nu,\nu'';\ \mu,\mu'')\frac{d\mu''}{2\mu''}\int_0^\infty \eta_{\nu'}p(\nu'',\nu')p(\nu',\nu_i)\,d\nu'\\&\times\int_0^1 S(\nu',\nu_i;\ \mu',\mu_i)\frac{d\mu'}{2\mu'}. \qquad (3.1)\end{aligned}$$

In this ν_i and μ_i refer to the incident radiation and ν,μ to the emergent radiation.

On substituting the value (2.9) for $p(\nu,\nu')$ and dividing by α_ν, this equation becomes

$$\begin{aligned}\left[\frac{1+\eta_\nu}{\mu}+\frac{1+\eta_{\nu_i}}{\mu_i}\right]\Sigma_s\delta(\nu_s-\nu_i)\frac{S(\nu,\nu_i;\ \mu,\mu_i)}{1-\epsilon}&=\eta_{\nu_i}\Sigma_s\delta(\nu_s-\nu_i)\\&+\eta_{\nu_i}\Sigma_s\delta(\nu_s-\nu_i)\int_0^\infty \alpha_{\nu'}\Sigma_p\delta(\nu_p-\nu')\,d\nu'\int_0^1 S(\nu,\nu';\ \mu,\mu')\frac{d\mu'}{2\mu'}\\&+\Sigma_s\delta(\nu_s-\nu_i)\int_0^\infty \alpha_{\nu'}\eta_{\nu'}\Sigma_q\delta(\nu_q-\nu')\,d\nu'\int_0^1 S(\nu',\nu_i;\ \mu',\mu_i)\frac{d\mu'}{2\mu'}\\&+\Sigma_s\delta(\nu_s-\nu_i)\int_0^\infty \alpha_{\nu'}\Sigma_p\delta(\nu_p-\nu'')\,d\nu''\int_0^1 S(\nu,\nu'';\ \mu,\mu'')\frac{d\mu''}{2\mu''}\\&\times\int_0^\infty \alpha_{\nu'}\eta_{\nu'}\Sigma_q\delta(\nu_q-\nu')\,d\nu'\int_0^1 S(\nu',\nu_i;\ \mu',\mu_i)\frac{d\mu'}{2\mu'}.\end{aligned}$$

On using the properties of the δ-function we get

$$\begin{aligned}\left[\frac{1+\eta_\nu}{\mu}+\frac{1+\eta_{\nu_i}}{\mu_i}\right]\Sigma_s\delta(\nu_s-\nu_i)\frac{S(\nu,\nu_i;\ \mu,\mu_i)}{1-\epsilon}&=\eta_{\nu_i}\Sigma_s\delta(\nu_s-\nu_i)\\&+\eta_{\nu_i}\Sigma_s\delta(\nu_s-\nu_i)\Sigma_p\alpha_p\int_0^1 S(\nu,\nu_p;\ \mu,\mu')\frac{d\mu'}{2\mu'}\\&+\Sigma_s\delta(\nu_s-\nu_i)\Sigma_q\alpha_q\eta_q\int_0^1 S(\nu_q,\nu_i;\ \mu',\mu_i)\frac{d\mu'}{2\mu'}\\&+\Sigma_s\delta(\nu_s-\nu_i)\Sigma_p\alpha_p\int_0^1 S(\nu,\nu_p;\ \mu,\mu')\frac{d\mu'}{2\mu'}\\&\times\Sigma_q\alpha_q\eta_q\int_0^1 S(\nu_q,\nu_i;\ \mu',\mu_i)\frac{d\mu'}{2\mu'}.\end{aligned}$$

When $\nu_i=\nu_s$ the δ-function becomes indefinitely large; hence this equation will be satisfied only if the coefficient of $\delta(\nu_s-\nu_i)$ is zero for $\nu_i=\nu_s$. Hence

$$\left[\frac{1+\eta_r}{\mu}+\frac{1+\eta_s}{\mu_i}\right]\frac{S(\nu,\nu_s;\ \mu,\mu_i)}{1-\epsilon}=\eta_s+\eta_s\sum_p\alpha_p\int_0^1 S(\nu,\nu_p;\ \mu,\mu')\frac{d\mu'}{2\mu'}$$
$$+\sum_q\alpha_q\eta_q\int_0^1 S(\nu_q,\nu_s;\ \mu',\mu_i)\frac{d\mu'}{2\mu'}+\sum_p\alpha_p\int_0^1 S(\nu,\nu_p;\ \mu,\mu')\frac{d\mu'}{2\mu'}$$
$$\times\sum_q\alpha_q\eta_q\int_0^1 S(\nu_q,\nu_s;\ \mu',\mu_i)\frac{d\mu'}{2\mu'}\qquad(s=1,\ldots,k).$$

Finally replacing ν by ν_r, using (2.10), and factorizing, we have

$$\left[\frac{1+\eta_r}{\mu}+\frac{1+\eta_s}{\mu_i}\right]\frac{S_{rs}(\mu,\mu_i)}{1-\epsilon}=\left\{1+\sum_{p=1}^{k}\alpha_p\int_0^1 S_{rp}(\mu,\mu')\frac{d\mu'}{2\mu'}\right\}$$
$$\times\left\{\eta_s+\sum_{q=1}^{k}\alpha_q\eta_q\int_0^1 S_{qs}(\mu',\mu_i)\frac{d\mu'}{2\mu'}\right\},\qquad(3.2)$$

and this holds for $r=1,\ldots,k$, $s=1,\ldots,k$.

From the theory of coherent scattering we know that

$$S_{rr}(\mu,\mu_i)=S_{rr}(\mu_i,\mu).\qquad(3.3)$$

On putting $s=r$ in (3.2), we see that this will be so if

$$\eta_p S_{pr}(\mu',\mu)=\eta_r S_{rp}(\mu,\mu'),\qquad(3.4)$$

a relation which includes (3.3). In the Appendix we prove conversely that (3.2) and (3.3) together imply (3.4). From (3.2) and (3.4) we have

$$\left[\frac{1+\eta_r}{\mu}+\frac{1+\eta_s}{\mu_i}\right]\frac{S_{rs}(\mu,\mu_i)}{\eta_s(1-\epsilon)}=\left\{1+\sum_{p=1}^{k}\alpha_p\int_0^1 S_{rp}(\mu,\mu')\frac{d\mu'}{2\mu'}\right\}$$
$$\times\left\{1+\sum_{p=1}^{k}\alpha_p\int_0^1 S_{sp}(\mu_i,\mu')\frac{d\mu'}{2\mu'}\right\}.\qquad(3.5)$$

Write

$$H_r(\mu)=1+\sum_{p=1}^{k}\alpha_p\int_0^1 S_{rp}(\mu,\mu')\frac{d\mu'}{2\mu},\qquad(3.6)$$

so that

$$\left[\frac{1+\eta_r}{\mu}+\frac{1+\eta_s}{\mu_i}\right]\frac{S_{rs}(\mu,\mu_i)}{\eta_s(1-\epsilon)}=H_r(\mu)H_s(\mu_i),\qquad(3.7)$$

and let*

$$\lambda_r=\frac{1+\epsilon\eta_r}{1+\eta_r},\qquad n_r=\frac{1}{1+\eta_r}=\frac{\lambda_r}{1+\epsilon\eta_r}.\qquad(3.8)$$

Then

$$1-\lambda_r=\frac{\eta_r(1-\epsilon)}{1+\eta_r},\qquad\frac{n_r}{n_s}=\frac{1+\eta_s}{1+\eta_r},\qquad(3.9)$$

and (3.7) can be written

$$S_{rs}(\mu,\mu')=n_r(1-\lambda_s)\frac{\mu\mu'}{n_r\mu+n_s\mu'}H_r(\mu)H_s(\mu').\qquad(3.10)$$

---

* This definition of λ_r agrees with that adopted in (2), Section 84. If $\epsilon=0$, then $n_r=\lambda_r$.

On substituting from (3.10) into (3.6), we have

$$H_r(\mu)=1+\tfrac{1}{2}\sum_{p=1}^{k}\alpha_p(1-\lambda_p)n_r\mu H_r(\mu)\int_0^1\frac{H_p(\mu')}{n_r\mu+n_p\mu'}\,d\mu', \tag{3.11}$$

or

$$\frac{1}{H_r(\mu)}=1-\tfrac{1}{2}\sum_{p=1}^{k}\alpha_p(1-\lambda_p)n_r\mu\int_0^1\frac{H_p(\mu')}{n_r\mu+n_p\mu'}\,d\mu'. \tag{3.12}$$

Consider also

$$\frac{1}{H_s(\mu)}=1-\tfrac{1}{2}\sum_{p=1}^{k}\alpha_p(1-\lambda_p)n_s\mu\int_0^1\frac{H_p(\mu')}{n_s\mu+n_p\mu'}\,d\mu'.$$

From these it at once follows that

$$H_r(x/n_r)=H_s(x/n_s)=H(x)\quad\text{(say)}.$$

Hence

$$H_r(\mu)=H(n_r\mu), \tag{3.13}$$

where, from (3.11),

$$H(n_r\mu)=1+\tfrac{1}{2}n_r\mu H(n_r\mu)\sum_{p=1}^{k}\alpha_p(1-\lambda_p)\int_0^1\frac{H(n_p\mu')}{n_r\mu+n_p\mu'}\,d\mu'. \tag{3.14}$$

Change the variables in this from μ and μ' to x and x' by writing $n_r\mu=x$, $n_p\mu'=x'$. Then

$$H(x)=1+\tfrac{1}{2}xH(x)\sum_{p=1}^{k}\alpha_p(1-\lambda_p)n_p^{-1}\int_0^{n_p}\frac{H(x')}{x+x'}\,dx',$$

or

$$H(x)=1+xH(x)\int_0^1\frac{\Psi(x')H(x')}{x+x'}\,dx', \tag{3.15}$$

where, assuming that

$$\eta_1>\eta_2>\ldots>\eta_k, \tag{3.16}$$

so that

$$0\leqslant n_1<n_2<\ldots<n_k\leqslant 1, \tag{3.17}$$

$$\Psi(x')=\begin{cases}\tfrac{1}{2}\sum_{p=1}^{k}\alpha_p(1-\lambda_p)/n_p & (0\leqslant x'\leqslant n_1),\\ \tfrac{1}{2}\sum_{p=r+1}^{k}\alpha_p(1-\lambda_p)/n_p & (n_r<x'\leqslant n_{r+1}),\\ 0 & (n_k\leqslant x'\leqslant 1).\end{cases} \tag{3.18}$$

Since

$$\int_0^1\Psi(x')\,dx'=\sum_{p=1}^{k}\tfrac{1}{2}\alpha_p(1-\lambda_p)=\tfrac{1}{2}\left(1-\sum_{p=1}^{k}\alpha_p\lambda_p\right)\leqslant\tfrac{1}{2}, \tag{3.19}$$

$\Psi(x')$ satisfies the conditions of (**2**), Chap. V, and the solution of (3.15) can at once be found.

From (3.10) and (3.13) we have

$$S_{rs}(\mu,\mu')=\eta_r(1-\lambda_s)\frac{\mu\mu'}{n_r\mu+n_s\mu'}H(n_r\mu)H(n_s\mu'). \tag{3.20}$$

This is the final form for the scattering function from frequency ν_s and direction $-\mu'$ into frequency ν_r and direction μ.

4. *The H-function.*—Before completing the solution of the problem in question, it is convenient to obtain some properties of the H-function which is the solution of (3.15). In this section all references are to Chap. V of (**2**) and we shall therefore quote (**2**) followed by the number of the relevant formula or by the theorem required.

By (**2**), Theorem 1, and by (3.19),

$$\sum_{p=1}^{k} \tfrac{1}{2}\alpha_p(1-\lambda_p)n_p^{-1}\int_0^{n_p} H(x')\,dx' = 1-\left(\sum_{p=1}^{k}\alpha_p\lambda_p\right)^{1/2},$$

and so

$$\sum_{p=1}^{k} \tfrac{1}{2}\alpha_p(1-\lambda_p)\int_0^{1} H(n_p\mu')\,d\mu' = 1-\left(\sum_{p=1}^{k}\alpha_p\lambda_p\right)^{1/2}. \tag{4.1}$$

By means of (4.1), (3.14) can be re-written in the form (*cf.* (**2**), Theorem 1, Corollary 2)

$$\frac{1}{H(n_r\mu)} = \left(\sum_{p=1}^{k}\alpha_p\lambda_p\right)^{1/2} + \tfrac{1}{2}\sum_{p=1}^{k}\alpha_p(1-\lambda_p)\int_0^1 \frac{n_p\mu' H(n_p\mu')}{n_r\mu+n_p\mu'}\,d\mu'. \tag{4.2}$$

By (**2**), (66) and (67),

$$\ln H(x) = \frac{x}{\pi i}\int_0^{i\infty} \ln T(w)\,\frac{dw}{w^2-x^2}, \tag{4.3}$$

where

$$T(w) = 1-2w^2\int_0^1 \frac{\Psi(\mu)\,d\mu}{w^2-\mu^2} = 1-w^2\sum_{p=1}^{k}\frac{\alpha_p(1-\lambda_p)}{n_p}\int_0^{n_p}\frac{d\mu}{w^2-\mu^2}.$$

This gives

$$T(w) = 1-\tfrac{1}{2}w\sum_{p=1}^{k}\frac{\alpha_p(1-\lambda_p)}{n_p}\ln\frac{w+n_p}{w-n_p}, \tag{4.4}$$

where the principal values of the logarithms have to be taken.

It is simplest now to concentrate on the strongest line of the multiplet and to calculate $H(n_1\mu)$. The changes required for any other line are obvious. In (4.3) and (4.4) put $x=n_1\mu$, $w=in_1\cot\theta$ $(0\leqslant\theta\leqslant\tfrac{1}{2}\pi)$. Then (4.4) simplifies to

$$T(in_1\cot\theta) = 1-\cot\theta\left\{\alpha_1(1-\lambda_1)\theta+\sum_{p=2}^{k}\alpha_p(1-\lambda_p)\frac{n_1}{n_p}\cot^{-1}\left(\frac{n_1}{n_p}\cot\theta\right)\right\}, \tag{4.5}$$

and (4.3) becomes

$$H(n_1\mu) = \exp\left\{-\frac{\mu}{\pi}\int_0^{\pi/2}\frac{\ln T(in_1\cot\theta)}{\cos^2\theta+\mu^2\sin^2\theta}\,d\theta\right\}. \tag{4.6}$$

When $\eta_1,\ldots,\eta_k$ and ϵ are known, α_r, λ_r and n_r $(r=1,\ldots,k)$ can be calculated by means of (2.3) and (3.8) and then $H(n_1\mu)$ can be evaluated from (4.5) and (4.6) by numerical integration. Had the strongest line of the multiplet been formed by coherent scattering (without interlocking) the H-function involved would have been given by (4.6) with

$$T(in_1\cot\theta) = 1-(1-\lambda_1)\theta\cot\theta. \tag{4.7}$$

By comparing this with (4.5) we see the changes introduced by interlocking.

5. *The emergent intensity.*—From (2.8), (2.12) and (3.8), we have

$$I_r^*(0,\mu) = \frac{\alpha_r}{2\mu}\sum_{p=1}^{k}\int_0^1 S_{rp}(\mu,\mu')(bn_p\mu'-a)\,d\mu'.$$

Substituting from (3.20) we get

$$I_r^*(0,\mu)=\tfrac{1}{2}\alpha_r H(n_r\mu)\sum_{p=1}^{k} n_r(1-\lambda_p)\int_0^1 \frac{\mu'(bn_p\mu'-a)}{n_r\mu+n_p\mu'}H(n_p\mu')\,d\mu'$$

$$=\tfrac{1}{2}\alpha_r H(n_r\mu)\sum_{p=1}^{k} n_r(1-\lambda_p)\int_0^1\left\{b\mu'-\frac{(bn_r\mu+a)\mu'}{n_r\mu+n_p\mu'}\right\}H(n_p\mu')\,d\mu'$$

$$=\tfrac{1}{2}\alpha_r H(n_r\mu)\left\{bn_r\sum_{p=1}^{k}(1-\lambda_p)\int_0^1\mu' H(n_p\mu')\,d\mu'\right.$$

$$\left.-n_r(a+bn_r\mu)\sum_{p=1}^{k}(1-\lambda_p)\int_0^1\frac{\mu' H(n_p\mu')}{n_r\mu+n_p\mu'}\,d\mu'\right\}. \tag{5.1}$$

From (2.6),

$$I_r(0,\mu)=a+bn_r\mu+I_r^*(0,\mu). \tag{5.2}$$

By making use of (4.2) multiplied by $H(n_r\mu)$, this can be written in the form

$$I_r(0,\mu)=(a+bn_r\mu)H(n_r\mu)\left\{\left(\sum_{p=1}^{k}\alpha_p\lambda_p\right)^{1/2}+\tfrac{1}{2}\sum_{p=1}^{k}\alpha_p(1-\lambda_p)\int_0^1\frac{n_p\mu' H(n_p\mu')}{n_r\mu+n_p\mu'}\,d\mu'\right\}$$

$$-(a+bn_r\mu)H(n_r\mu)\tfrac{1}{2}\alpha_r n_r\sum_{p=1}^{k}(1-\lambda_p)\int_0^1\frac{\mu' H(n_p\mu')}{n_r\mu+n_p\mu'}\,d\mu'$$

$$+\tfrac{1}{2}b\alpha_r n_r H(n_r\mu)\sum_{p=1}^{k}(1-\lambda_p)\int_0^1\mu' H(n_p\mu')\,d\mu',$$

and thus

$$I_r(0,\mu)=(a+bn_r\mu)H(n_r\mu)\left\{\left(\sum_{p=1}^{k}\alpha_p\lambda_p\right)^{1/2}\right.$$

$$\left.+\tfrac{1}{2}\sum_{p=1}^{k}(\alpha_p n_p-\alpha_r n_r)(1-\lambda_p)\int_0^1\frac{\mu' H(n_p\mu')}{n_r\mu+n_p\mu'}\,d\mu'\right\}$$

$$+\tfrac{1}{2}b\alpha_r n_r H(n_r\mu)\sum_{p=1}^{k}(1-\lambda_p)\int_0^1\mu' H(n_p\mu')\,d\mu'. \tag{5.3}$$

This is the final form for the emergent intensity in the rth line.

We shall use the notation $H(\varpi;\ \mu)$ for the H-function tabulated by Chandrasekhar and Breen (see (**2**), Table XI). Then $H(1-\lambda;\ \mu)$ is the H-function for coherent scattering. When $k=1$, (4.5) reduces to (4.7), $H(n_1\mu)=H(1-\lambda_1;\ \mu)$ and (5.3) becomes Chandrasekhar's solution for coherent scattering ((**2**), Section 84). This solution is also obtained when $\eta_1=\eta_2=\ldots=\eta_k$.

6. *The calculations for a doublet*

6.1. *The H-functions.*—For a doublet,

$$\eta_1:\eta_2=2:1 \quad \text{and} \quad \alpha_1=\tfrac{8}{3},\ \alpha_2=\tfrac{1}{3}. \tag{6.1}$$

Let $\phi(0\leqslant\phi\leqslant\tfrac{1}{2}\pi)$ be defined in terms of $\theta(0\leqslant\theta\leqslant\tfrac{1}{2}\pi)$ by the equation

$$n_1\cot\theta=n_2\cot\phi. \tag{6.2}$$

Then, when $k=2$, (4.5) and (4.6) give

$$H(n_1\mu)=\exp\left\{-\frac{\mu}{\pi}\int_0^{\pi/2}\frac{\ln[1-\alpha_1(1-\lambda_1)\theta\cot\theta-\alpha_2(1-\lambda_2)\,\phi\,\cot\phi]}{\cos^2\theta+\mu^2\sin^2\theta}\,d\theta\right\}, \tag{6.3}$$

and we have the relation

$$H(n_2\mu)=H\left(n_1.\frac{n_2}{n_1}\mu\right). \tag{6.4}$$

The integral (6.3) could be evaluated by numerical integration, but it was decided to calculate the values of the H-functions by means of sequence iterations based on (4.2). For this, good initial approximations for $H(n_1\mu)$ and $H(n_2\mu)$ were needed and these were obtained from (6.2)–(6.4) as follows:

Since $\alpha_1+\alpha_2=1$, (6.3) can be written

$$H(n_1\mu)=\exp\left\{-\frac{\mu}{\pi}\int_0^{\pi/2}\frac{\ln\left(1-[1-\alpha_1\lambda_1-\alpha_2\lambda_2-k(\theta)]\,\theta\cot\theta\right)}{\cos^2\theta+\mu^2\sin^2\theta}\,d\theta\right\}, \tag{6.5}$$

where

$$k(\theta)=\alpha_2(1-\lambda_2)\{1-(\phi\cot\phi)/(\theta\cot\theta)\}. \tag{6.6}$$

As θ increases from 0 to $\frac{1}{2}\pi$, $k(\theta)$ increases from 0 to $\alpha_2(1-\lambda_2)(1-n_1/n_2)$, which is less than $\frac{1}{3}$ in all cases. As a first approximation $k(\theta)$ can be replaced by

$$k_1=\tfrac{1}{2}\alpha_2(1-\lambda_2)(1-n_1/n_2), \tag{6.7}$$

and then (6.5) gives

$$H(n_1\mu)\simeq H(1-\alpha_1\lambda_1-\alpha_2\lambda_2-k_1;\ \mu). \tag{6.8}$$

Thus approximate values for $H(n_1\mu)$, when $0\leqslant\mu\leqslant 1$, can be found from the tables for $H(\varpi;\ \mu)$ in (**2**), interpolating linearly between the values for successive ϖ when necessary.

In order to evaluate $H(n_2\mu)$ from (6.4), it is necessary to know values for $H(n_1\mu)$ not only in the interval (0, 1) but also for $1<\mu\leqslant n_2/n_1$. Since, by (4.2),

$$H(n_1\mu)\to(\alpha_1\lambda_1+\alpha_2\lambda_2)^{-1/2}\quad\text{as}\quad\mu\to\infty, \tag{6.9}$$

fairly reliable values can be obtained by an extrapolation formula of the form

$$H(n_1\mu)=(\alpha_1\lambda_1+\alpha_2\lambda_2)^{-1/2}-(c_1\mu+c_2)^{-1}, \tag{6.10}$$

c_1 and c_2 being determined from the approximate values of $H(n_1\mu)$ for $\mu=0{\cdot}95$ and $1{\cdot}00$. In this way approximate values were also found for $H(n_2\mu)$ $(0\leqslant\mu\leqslant 1)$.

Three cases were considered:

$$\left.\begin{array}{llllll}
\text{I.} & \eta_1=10, & \eta_2=5, & \epsilon=0, & \lambda_1=n_1=\frac{1}{11}, & \lambda_2=n_2=\frac{1}{6};\\
\text{II.} & \eta_1=4, & \eta_2=2, & \epsilon=0, & \lambda_1=n_1=\frac{1}{5}, & \lambda_2=n_2=\frac{1}{3};\\
\text{III.} & \eta_1=1, & \eta_2=\frac{1}{2}, & \epsilon=0, & \lambda_1=n_1=\frac{1}{2}, & \lambda_2=n_2=\frac{2}{3}.
\end{array}\right\} \tag{6.11}$$

In Cases I and II the initial values found by the method described above differed from the final values in the second decimal place; in Case III the difference only occurred in the third decimal place.

The equations (4.2), on which the iterations were based, can be written

$$\left.\begin{aligned}
\frac{1}{H_1(\mu)}&=(\alpha_1\lambda_1+\alpha_2\lambda_2)^{1/2}+\tfrac{1}{2}\alpha_1(1-\lambda_1)\int_0^1\frac{\mu' H_1(\mu')\,d\mu'}{\mu+\mu'}+\tfrac{1}{2}\alpha_2(1-\lambda_2)\int_0^1\frac{\mu' H_2(\mu')\,d\mu'}{\mu n_1/n_2+\mu'},\\
\frac{1}{H_2(\mu)}&=(\alpha_1\lambda_1+\alpha_2\lambda_2)^{1/2}+\tfrac{1}{2}\alpha_1(1-\lambda_1)\int_0^1\frac{\mu' H_1(\mu')\,d\mu'}{\mu n_2/n_1+\mu'}+\tfrac{1}{2}\alpha_2(1-\lambda_2)\int_0^1\frac{\mu' H_2(\mu')\,d\mu'}{\mu+\mu'},
\end{aligned}\right\} \tag{6.12}$$

where $H_1(\mu)=H(n_1\mu)$ and $H_2(\mu)=H(n_2\mu)$. At each stage of the iterations the approximate values of the H-functions at $\mu=0$, 0·1, 0·2, 0·4, 0·6, 0·8 and 1·0

were represented by polynomials of degree six in μ. This enabled the iterations to be carried out with the help of tables of the integral

$$I_m = \int_0^1 \frac{(\mu')^m \, d\mu'}{\mu x + \mu'} \quad (m = 1, 2, \ldots, 7)$$

for $x = 1, n_1/n_2$ and n_2/n_1. These were constructed from the recurrence relation

$$I_m = \frac{1}{m} - \mu x I_{m-1}, \quad I_0 = \ln \frac{1+\mu x}{\mu x}.$$

Let $H_1^{(n)}$ and $H_2^{(n)}$ be the nth iterates of the functions $H_1(\mu)$ and $H_2(\mu)$ and let

$$\Delta_1^{(n-1)} = H_1^{(n)} - H_1^{(n-1)}, \quad \Delta_2^{(n-1)} = H_2^{(n)} - H_2^{(n-1)},$$

so that these are the corrections to the $(n-1)$th iterates. After several iterations it was found that $\Delta_1^{(n)}/\Delta_1^{(n-1)}$ and $\Delta_2^{(n)}/\Delta_2^{(n-1)}$, though alternating in sign, were practically independent of both n and μ. When this state of affairs was reached, the remaining errors in the H-functions were almost completely removed by summing a series of extrapolated corrections as follows:

Let $\beta_1 = |\Delta_1^{(n)}/\Delta_1^{(n-1)}|$, $\beta_2 = |\Delta_2^{(n)}/\Delta_2^{(n-1)}|$, and assume that β_1 and β_2 are independent of n. Then the equations

$$\left.\begin{aligned} H_1(\mu) &= H_1^{(n)} + \Delta_1^{(n)}(1 - \beta_1 + \beta_1^2 - \ldots) = H_1^{(n)} + \Delta_1^{(n)}/(1+\beta_1), \\ H_2(\mu) &= H_2^{(n)} + \Delta_2^{(n)}(1 - \beta_2 + \beta_2^2 - \ldots) = H_2^{(n)} + \Delta_2^{(n)}/(1+\beta_2), \end{aligned}\right\} \quad (6.13)$$

will give the H-functions exactly. Since, however, β_1 and β_2 were not entirely independent of n, the equations (6.13) only gave much improved values for the H-functions. These values were re-iterated until further iteration made no alteration in the fifth decimal place. The extrapolated corrections were so effective that only one or two such iterations proved to be necessary. The final values of the H-functions are given in Table I.

TABLE I

Values of the H-functions for a doublet

μ	I: $\eta_1=10$, $\eta_2=5$		II: $\eta_1=4$, $\eta_2=2$		III: $\eta_1=1$, $\eta_2=\frac{1}{2}$	
	$H_1(\mu)$	$H_2(\mu)$	$H_1(\mu)$	$H_2(\mu)$	$H_1(\mu)$	$H_2(\mu)$
0·0	1·0000	1·0000	1·0000	1·0000	1·0000	1·0000
0·1	1·1440	1·2278	1·1140	1·1647	1·0598	1·0724
0·2	1·2429	1·3745	1·1869	1·2620	1·0935	1·1108
0·4	1·3975	1·5893	1·2936	1·3944	1·1382	1·1591
0·6	1·5197	1·7462	1·3722	1·4844	1·1679	1·1896
0·8	1·6211	1·8684	1·4341	1·5509	1·1896	1·2111
1·0	1·7075	1·9670	1·4844	1·6020	1·2064	1·2271

6.2. *The residual intensities.*—The emergent intensities for the lines of the doublet are given by equation (5.3), and in the continuous spectrum outside the lines we have $I^{(\text{cont})}(0, \mu) = a + b\mu$. The residual intensities, expressed as percentages of the intensity in the continuous spectrum, are

$$r_i(\mu) = 100 I_i(0, \mu)/I^{(\text{cont})}(0, \mu) \quad (i = 1, 2). \qquad (6.14)$$

Values of $r_1(\mu)$ and $r_2(\mu)$ were calculated for Cases I, II and III for a region of the spectrum where $b=\frac{3}{2}a$. The first moments of the H-functions and certain integrals required in the calculations had already been evaluated as part of the iteration process described above. The results are given in Table II and are shown by the curves of Fig. 1, in which the residual intensities are plotted as functions of μ. Since, in the wings of the lines, η is proportional to $(\Delta\lambda)^{-2}$, where $\Delta\lambda$ is the distance from the line centre, the cases I–III of (6.11) lead, respectively, to cross-sections of the line profiles at increasing distances from the centres of the lines. This representation of the results is similar to that adopted by Houtgast in (**3**), where cross-section curves for multiplets in the solar spectrum are given.

In Table III we give the corresponding exact values for a doublet without interlocking. These values are shown by the curves in Fig. 2. They have been calculated from the exact solution in (**2**), Section 84.5, equation (69) and from Tables XI and XXXIII of (**2**). Appropriate interpolations were used when necessary.

TABLE II

Residual intensities for a doublet with interlocking

μ	I: $\eta_1=10$, $\eta_2=5$		II: $\eta_1=4$, $\eta_2=2$		III: $\eta_1=1$, $\eta_2=\frac{1}{2}$	
	$r_1(\mu)$	$r_2(\mu)$	$r_1(\mu)$	$r_2(\mu)$	$r_1(\mu)$	$r_2(\mu)$
0·0	38·57	43·69	56·83	64·02	83·60	89·06
0·1	39·09	46·39	56·88	65·74	82·58	88·80
0·2	38·16	46·35	55·17	64·76	80·24	87·28
0·4	35·86	44·73	51·49	61·81	75·97	84·39
0·6	33·70	42·70	48·28	58·95	72·60	82·07
0·8	31·82	40·75	45·60	56·50	69·96	80·26
1·0	30·18	39·00	43·37	54·41	67·86	78·80

TABLE III

Residual intensities for a doublet without interlocking

μ	I: $\eta_1=10$, $\eta_2=5$		II: $\eta_1=4$, $\eta_2=2$		III: $\eta_1=1$, $\eta_2=\frac{1}{2}$	
	$r_1(\mu)$	$r_2(\mu)$	$r_1(\mu)$	$r_2(\mu)$	$r_1(\mu)$	$r_2(\mu)$
0·0	35·34	48·74	53·55	68·79	82·03	90·97
0·1	36·58	49·71	54·36	68·90	81·44	90·08
0·2	36·12	48·71	53·15	67·07	79·34	88·24
0·4	34·51	46·03	50·12	63·18	75·36	85·00
0·6	32·77	43·45	47·30	59·85	72·16	82·49
0·8	31·17	41·21	44·88	57·12	69·63	80·56
1·0	29·72	39·26	42·81	54·86	67·56	79·03

From Tables II and III and from Figs. 1 and 2 it will be seen that the effect of interlocking is to increase $r_1(\mu)$ and to decrease $r_2(\mu)$ for all μ. Let $d(\mu)$ denote the difference $r_2(\mu)-r_1(\mu)$ in the interlocked case, and let $d_0(\mu)$ denote this difference when there is no interlocking. Then $d(\mu)<d_0(\mu)$ for all μ. The values of $d(\mu)$ and $d_0(\mu)$ in Cases I–III are shown by the full and broken curves respectively in Fig. 3. Near the centre of the disk $d_0(\mu)-d(\mu)$ is very small, but it increases towards the limb in every case and for the sections nearest to the centres of the

lines (Cases I and II) it rises to more than 4 per cent of the continuous spectrum at $\mu = 0{\cdot}2$.

An interesting feature of the curves in Figs. 1 and 2 is the drop in $r_1(\mu)$ and $r_2(\mu)$ near to $\mu = 0$ in Cases I and II. This occurs both when there is interlocking and when there is no interlocking. This result is, however, only of limited interest, since the plane-parallel representation of a stellar atmosphere only applies for values of $\mu > 0{\cdot}2$.

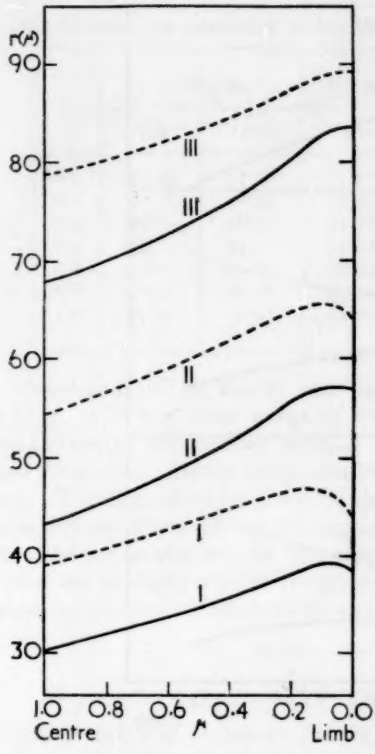

FIG. 1.—*The residual intensities for a doublet with interlocking.*

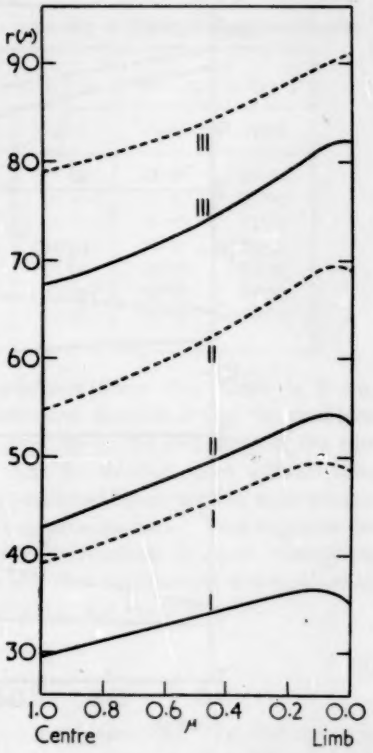

FIG. 2.—*The residual intensities for a doublet without interlocking.*

Both figures show cross-sections of the line profiles at three distances from their centres, the full curves representing the stronger component and the broken curves the weaker component.

6.3. *Eddington's approximation.*—In this section we consider the accuracy of an approximate solution for the residual intensities for interlocked doublet lines based on Eddington's approximation. The details of the solution for the residual intensities in the emergent flux are given in (5). The residual intensities in any direction μ and in a region of the spectrum where $b = \frac{3}{2}a$ are given by

$$\left.\begin{aligned} r_1(\mu) &= 100(1+\tfrac{3}{2}\mu)^{-1}\left\{1+\frac{3}{2}\frac{\mu}{1+\eta_1}+\eta_1\left(\frac{\alpha_1 A_{11}+\alpha_2 A_{21}}{1+\eta_1+\mu p_1}+\frac{\alpha_1 A_{12}+\alpha_2 A_{22}}{1+\eta_1+\mu p_2}\right)\right\}, \\ r_2(\mu) &= 100(1+\tfrac{3}{2}\mu)^{-1}\left\{1+\frac{3}{2}\frac{\mu}{1+\eta_2}+\eta_2\left(\frac{\alpha_1 A_{11}+\alpha_2 A_{21}}{1+\eta_2+\mu p_1}+\frac{\alpha_1 A_{12}+\alpha_2 A_{22}}{1+\eta_2+\mu p_2}\right)\right\}. \end{aligned}\right\} \quad (6.15)$$

In these expressions p_1 and p_2 are, respectively, the larger and smaller positive roots of the equation

$$p^4-(q_{11}^2+q_{22}^2)p^2+q_{11}^2q_{22}^2-q_{12}^2q_{21}^2=0, \tag{6.16}$$

where

$$\left.\begin{aligned} q_{12}^2&=3\eta_1(1+\eta_1)\alpha_2, & q_{21}^2&=3\eta_2(1+\eta_2)\alpha_1,\\ q_{11}^2&=3(1+\eta_1)\{1+\eta_1(1-\alpha_1)\}, & q_{22}^2&=3(1+\eta_2)\{1+\eta_2(1-\alpha_2)\}. \end{aligned}\right\} \tag{6.17}$$

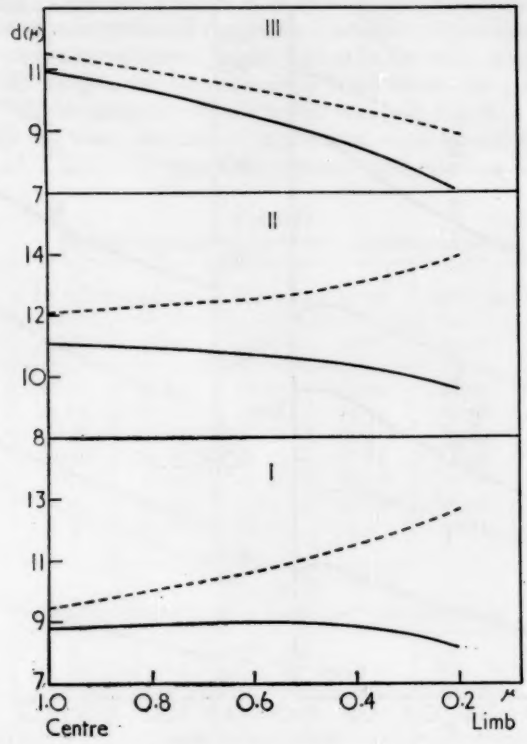

FIG. 3.—*The variation of* $d(\mu)=r_2(\mu)-r_1(\mu)$ *from centre to limb. The full curves represent the variations for a doublet with interlocking and the broken curves those for a doublet without interlocking.*

The A's are given by the simultaneous equations

$$\left.\begin{aligned} (1+\eta_1+\tfrac{2}{3}p_1)A_{11}+(1+\eta_1+\tfrac{2}{3}p_2)A_{12}+\eta_1&=0,\\ (1+\eta_2+\tfrac{2}{3}p_1)A_{21}+(1+\eta_2+\tfrac{2}{3}p_2)A_{22}+\eta_2&=0, \end{aligned}\right\} \tag{6.18}$$

with

$$A_{11}=\frac{q_{22}^2-p_1^2}{q_{21}^2}A_{21}, \quad A_{22}=\frac{q_{11}^2-p_2^2}{q_{12}^2}A_{12}. \tag{6.19}$$

The residual intensities for Cases I–III, calculated by means of equations (6.15)–(6.19), are given in Table IV. Comparing these approximate values with the exact values given in Table II, the proportional errors in the residual intensities,

although large at the extreme limb, are found to lie within ± 1 per cent for values of $\mu > 0{\cdot}2$. The error in $d(\mu) = r_2(\mu) - r_1(\mu)$ is likewise small for $\mu > 0{\cdot}2$, and when $\mu = 0{\cdot}2$ it only amounts to 0·5 per cent of the intensity in the continuous spectrum. Thus the errors of the approximate solution are satisfactorily small in the range of values for μ for which the plane-parallel model applies, and they are sufficiently small to predict the limb effect of Fig. 3.

TABLE IV

Residual intensities for interlocked doublet lines according to Eddington's approximation

μ	I : $\eta_1 = 10$, $\eta_2 = 5$		II : $\eta_1 = 4$, $\eta_2 = 2$		III : $\eta_1 = 1$, $\eta_2 = \frac{1}{2}$	
	$r_1(\mu)$	$r_2(\mu)$	$r_1(\mu)$	$r_2(\mu)$	$r_1(\mu)$	$r_2(\mu)$
0·0	42·35	47·16	61·53	67·94	88·06	92·04
0·1	40·38	46·97	58·43	66·50	84·21	89·69
0·2	38·64	46·27	55·77	64·82	81·06	87·67
0·4	35·74	44·31	51·42	61·53	76·21	84·47
0·6	33·40	42·26	48·04	58·65	72·66	82·07
0·8	31·46	40·36	45·32	56·22	69·96	80·23
1·0	29·84	38·65	43·09	54·18	67·83	78·77

7. *Conclusions.*—The theory and calculations show that there is a limb effect (Fig. 3) in the inner wings of interlocked doublet lines, the difference $d(\mu) = r_2(\mu) - r_1(\mu)$ between the residual intensities of the two lines at the same distance from their centres being smaller than for doublet lines without interlocking. The limb effect for $\mu > 0{\cdot}2$ is also predicted by an approximate solution of the equations of transfer by Eddington's approximation. This suggests that results obtained in this way for the centre-to-limb effects in more complicated multiplets are probably reliable for $\mu > 0{\cdot}2$ and that conclusions drawn from the approximate solution are likely to remain true for the exact solution.

APPENDIX

8. *The principle of reciprocity for the scattering functions.*—In Section 3 we have shown that the scattering functions $S_{rs}(\mu, \mu_i)$ $(r, s = 1, \ldots, k)$ satisfy the equations (3.2), viz.

$$\left[\frac{1+\eta_r}{\mu} + \frac{1+\eta_s}{\mu_i}\right]\frac{S_{rs}(\mu,\mu_i)}{1-\epsilon} = \left\{1 + \sum_{p=1}^{k} \alpha_p \int_0^1 S_{rp}(\mu,\mu')\frac{d\mu'}{2\mu'}\right\} \times \left\{\eta_s + \sum_{q=1}^{k} \alpha_q \eta_q \int_0^1 S_{qs}(\mu',\mu_i)\frac{d\mu'}{2\mu'}\right\}, \quad (8.1)$$

where $r, s = 1, \ldots, k$, and it is known from the theory of coherent scattering that

$$S_{rr}(\mu,\mu_i) = S_{rr}(\mu_i,\mu) \quad (r = 1, \ldots, k). \quad (8.2)$$

We shall now deduce (3.4) from (8.1) and (8.2).*

* In (1), the proof of the principle of reciprocity, which was omitted, is very similar to that given here, but it ends with an appeal to the theory of homogeneous integral equations instead of to the theory of homogeneous linear equations.

Put $s=r$ in (8.1) and interchange μ and μ_i. Then it follows from (8.2) that

$$\left\{1+\sum_{p=1}^{k}\alpha_p\int_0^1 S_{rp}(\mu,\mu')\frac{d\mu'}{2\mu'}\right\}\left\{\eta_r+\sum_{q=1}^{k}\alpha_q\eta_q\int_0^1 S_{qr}(\mu',\mu_i)\frac{d\mu'}{2\mu'}\right\}$$
$$=\left\{1+\sum_{p=1}^{k}\alpha_p\int_0^1 S_{rp}(\mu_i,\mu')\frac{d\mu'}{2\mu'}\right\}\left\{\eta_r+\sum_{q=1}^{k}\alpha_q\eta_q\int_0^1 S_{qr}(\mu',\mu)\frac{d\mu'}{2\mu'}\right\}.$$

This is of the form

$$f(\mu)g(\mu_i)=f(\mu_i)g(\mu),$$

whence

$$f(\mu)/g(\mu)=f(\mu_i)/g(\mu_i)=\text{a constant independent of }\mu.$$

The constant does, however, depend on r and we therefore write

$$\eta_r+\sum_{q=1}^{k}\alpha_q\eta_q\int_0^1 S_{qr}(\mu',\mu)\frac{d\mu'}{2\mu'}=C_r\left\{1+\sum_{p=1}^{k}\alpha_p\int_0^1 S_{rp}(\mu,\mu')\frac{d\mu'}{2\mu'}\right\}. \quad (8.3)$$

From (8.1) and (8.3) we have

$$\left[\frac{1+\eta_r}{\mu}+\frac{1+\eta_s}{\mu_i}\right]\frac{S_{rs}(\mu,\mu_i)}{1-\epsilon}=C_s\left\{1+\sum_{p=1}^{k}\alpha_p\int_0^1 S_{rp}(\mu,\mu')\frac{d\mu'}{2\mu'}\right\}$$
$$\times\left\{1+\sum_{p=1}^{k}\alpha_p\int_0^1 S_{sp}(\mu_i,\mu')\frac{d\mu'}{2\mu'}\right\},$$

and interchanging r and s, μ and μ_i, we get

$$\left[\frac{1+\eta_s}{\mu_i}+\frac{1+\eta_r}{\mu}\right]\frac{S_{sr}(\mu_i,\mu)}{1-\epsilon}=C_r\left\{1+\sum_{p=1}^{k}\alpha_p\int_0^1 S_{sp}(\mu_i,\mu')\frac{d\mu'}{2\mu'}\right\}$$
$$\times\left\{1+\sum_{p=1}^{k}\alpha_p\int_0^1 S_{rp}(\mu,\mu')\frac{d\mu'}{2\mu'}\right\}.$$

From these we have

$$C_rS_{rs}(\mu,\mu_i)=C_sS_{sr}(\mu_i,\mu). \quad (8.4)$$

By (8.4), (8.3) can be written (changing p into q)

$$(\eta_r-C_r)+\sum_{q=1}^{k}(\eta_q-C_q)\alpha_q\int_0^1 S_{qr}(\mu',\mu)\frac{d\mu'}{2\mu'}=0, \quad (8.5)$$

where $r=1,\ldots,k$. This gives k homogeneous equations for the constants (η_r-C_r) $(r=1,\ldots,k)$. The determinant formed by the coefficients is a function of μ and is not identically zero; hence the only solution independent of μ is

$$\eta_r-C_r=0 \quad (r=1,\ldots,k).$$

Thus (8.4) becomes

$$\eta_rS_{rs}(\mu,\mu_i)=\eta_sS_{sr}(\mu_i,\mu),$$

and this is (3.4).

St. Hugh's College,
Oxford:
1953 *July* 9.

University Observatory,
Oxford.

References

(1) I. W. Busbridge, *M.N.*, **113**, 52, 1953.
(2) S. Chandrasekhar, *Radiative Transfer*, Oxford, 1950.
(3) J. Houtgast, *Dissertation*, Utrecht: Schotanus & Jens, 1942.
(4) D. W. N. Stibbs, *M.N.*, **113**, 493, 1953.
(5) R. v. d. R. Woolley and D. W. N. Stibbs, *The Outer Layers of a Star*, Oxford, 1953.

MOTIONS IN THE SUN AT THE PHOTOSPHERIC LEVEL

IV. The equatorial rotation and possible velocity fields in the photosphere

A. B. Hart

(Communicated by the Director, University Observatory, Oxford)

(Received 1953 November 28)

Summary

From spectra of the equatorial photosphere taken near the limb of the Sun between 1950 October and 1952 June, 480 determinations of line-of-sight velocity are made. A careful investigation shows, contrary to an earlier suggestion, that the effect on velocities, of light scattered in the Earth's atmosphere and in the telescope, is negligible. In order that each day on which observations are made should carry equal weight in the final solution, only 334 of the determinations are used to find the mean equatorial velocity. After the elimination of limb effect, the velocity due to solar rotation is found to be 1·91 km sec^{-1} for the mean epoch 1951·5. The individual determinations have a large dispersion about this mean and a statistical discussion shows that the chance is less than one in a thousand that the dispersion is due to errors of measurement. It is therefore highly probable that the velocity varies from point to point in the photosphere. The extreme range in measured velocity is approximately 0·3 km sec^{-1} and successive maxima or minima of velocity appear to be separated by a distance of the order of 75 000 km. Some evidence is found for bands of constant velocity occurring perpendicular to the solar equator, but this is less certain. The existence of such velocity changes may account for the discrepant rates of rotation found by earlier observers.

Introduction.—From visual measures of Doppler displacements, Dunér (**5**) in 1888 made the first spectroscopic determination of solar rotation. The potential accuracy of the method and its applicability to all solar latitudes gave grounds for the belief that the determination of rotation by sunspots would soon be superseded. Discrepant results were, however, obtained by photographic spectroscopy between 1906 and 1913, and since 1915 investigations have been restricted to a determination of equatorial velocity in the hope of elucidating the causes of these discrepancies.

Adams (**2**) at Mt. Wilson between 1906 and 1908 made the first photographic measures and laid the foundations of a method used by many later investigators. Working in the wave-length region 4250 A with a solar image 170 mm in diameter and a dispersion of 0·71 or 0·56 A mm^{-1}, he used two small prisms to bring light from opposite limbs of the Sun into juxtaposition on the slit of the spectroscope. Half the displacement between the same spectral line on the two limbs gave the value of the rotation. The spectra were measured with an ordinary cross-wire micrometer.

This procedure was improved by J. S. Plaskett (**19**), at Ottawa in 1911, who used a triple-prism system. It produced spectra arranged so that the spectrum

from one limb lay between the two spectra from the other, thus removing spurious displacements caused by any non-parallelism of the measuring wire and spectral lines. A series of measures in 1911, 1912 and 1913 was carried out in this way (**18**) and a precisely similar method was adopted at Allegheny by Schlesinger (**20**). It was clear, however, that the small-prism method was still subject to systematic error in that displacements of the prisms might cause them to illuminate the collimator differently and so produce spurious shifts in the spectral lines. By returning to Dunér's original method of using water-vapour lines as standards of zero velocity, H. H. Plaskett (**13**) eliminated this source of error which, unless such a precaution is taken, vitiates any determination of velocity.

With these improvements, in 1915, a variation in the equatorial velocity with amplitude $\pm 0{\cdot}15\,\mathrm{km\,sec^{-1}}$ was shown to exist. Of the reality of the measured change in velocity there can be little doubt, but the change itself was very differently interpreted. On the one hand, it was ascribed by H. H. Plaskett to an actual change in velocity of the photospheric matter and, on the other hand, by R. E. DeLury (**3**) to the superposition of a variable amount of sky spectrum on the limb spectrum.

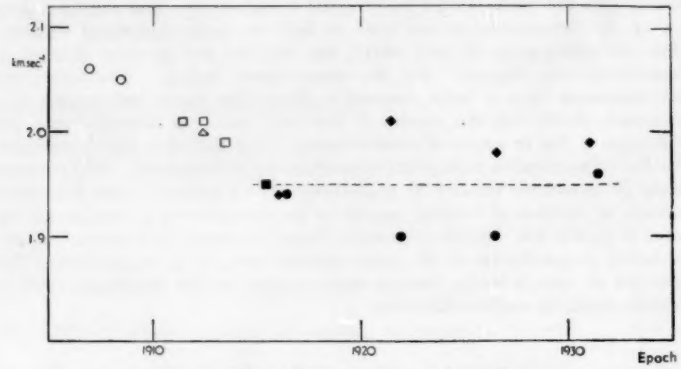

FIG. 1.—*The rotational velocity at the equator.*

○ *W. S. Adams and J. B. Lasby, Mt. Wilson.*
□ *J. S. Plaskett and R. E. DeLury, Ottawa.*
△ *F. Schlesinger, Allegheny.*
● *Mt. Wilson.*
■ *H. H. Plaskett, Ottawa.*
◆ *Edinburgh.*

For many years systematic observations were made on a few days in each year at Mt. Wilson (**12**) and at Edinburgh (**9, 21, 22**), using atmospheric lines as standards, in an effort to obtain a good mean value for the equatorial velocity. The values obtained up to 1935 are shown in Fig. 1. Results from Mt. Wilson and Edinburgh are averaged over the five year periods beginning in 1914, 1919, 1924 and 1929. Determinations using atmospheric standards are shown as filled symbols (the only ones shown after 1914) and the values obtained by some of the earlier workers are shown as unfilled ones. It will be noted that once atmospheric lines were used as standards, the measured equatorial velocity settled down to a mean of $1{\cdot}95\,\mathrm{km\,sec^{-1}}$ with a dispersion $\pm 0{\cdot}05\,\mathrm{km\,sec^{-1}}$. This dispersion has been variously attributed to the effect of superposed sky spectrum, to the vertical apparatus function of the spectroscope and to actual changes in velocity, but no analysis has been made of the relative sizes of these effects.

Consequently, new observations have been made at Oxford with the intention, (1) of obtaining a value of the equatorial velocity together with a critical estimate of its reliability, (2) of determining precisely the effect of superposed sky spectrum on the measured velocities, and (3) of making some investigation of any irregularities in velocity which may occur. The following account of an investigation carried out between 1950 and 1952 is divided into four sections. The first section concerns the observations and the method of measurement and the second the effect of superposed light on measured velocities, a discussion of which is necessary before measured velocities can be converted into velocities on the Sun. The third section contains the details of the calculation of the equatorial velocity and a value of the limb effect, and the last section is a discussion of the residuals in the measured velocities.

1. *Observations and measurements*

1.1. *Observations.*—The observations were made with the Oxford solar telescope (**14**). The telescope is of the vertical Cassegrain type and produces at its focal plane an image 180 mm in diameter giving a linear scale 1 mm = 10″·4 arc. The image is formed in the plane of the spectroscope slit (**15**). The slit lies very nearly in the East–West direction on the image and the precise direction is determined for each series of observations. The position on the image at which the observations are made can be found and accurately maintained throughout an exposure by means of the rocking plate described by H. H. Plaskett.* The spectra were taken in the wave-length region 5900 A where there is a number of suitable unblended solar and water-vapour lines. The dispersion is 1·5 A mm^{-1}.

Spectra of the two limbs were photographed separately, any one plate carrying two (or in the third series, six) exposures of the same limb. The height of the spectroscope slit was limited to 12·5 mm but the solar image did not occupy the whole height. Each spectrum was only 6 to 10 mm high so that the limb proper could be identified on the plate. A metal diaphragm just in front of the dark slide of the plate prevented the light distributed in the vertical apparatus function of the spectroscope during one exposure falling on any other spectrum.

Three series of limb spectra were taken. The first, an exploratory series, consisted of repeated exposures along that chord at each limb, which passes through the equator at the limb proper. In the second series, successive exposures covered an appreciable area of the disk and followed each other as rapidly as possible. The maximum time which elapsed between the first and last of a set of six exposures on any one limb was 10 minutes. Adjacent spectra were separated by 1° latitude at the limb and were arranged so that approximately equal areas North and South of the equator were covered. Fig. 2 shows the arrangement of the slits in this case. The third series was similar to the first. For high resolution on the solar image it is necessary to have good seeing. The second and third series had, in general, seeing 1 or 2 on a scale of 0 to 5 (5 the best, see Paper I), but series I was taken during a bad season and is inferior in this respect. Of the numerous spectra so obtained, three sets made in the best available conditions were selected for measurement. Details are given in Table I. A spectrum of the centre of the Sun, 12·5 mm in height, was taken for use as the standard spectrum in the measuring machine. Ilford Rapid Process Panchromatic plates were used for all

* This is the first paper in the series, Motions in the Sun at the photospheric level. Papers in this series will be referred to by their serial numbers, I (**16**), III (**11**).

the work; they were developed in Kodak Press Contrast Developer or Parkhurst two-solution developer.

In Series I and II, on each day that a set of limb spectra was obtained, at least one " sky brightness " plate was taken to find the ratio of the intensity of the light at a fixed distance outside the limb to that at a fixed distance inside. Each plate consisted of one exposure at the centre of the Sun through a Zeiss calibrated step-wedge and one without it to show any variation in illumination along the slit; then narrow spectra, 3 mm high, were taken of the light from points 40″ arc radially inside and outside the limb. The exposure time was the same for each of the four spectra and suitable densities on the plate were obtained by using N.P.L. calibrated filters. The plates were not developed until 24 hours after they had been taken, so

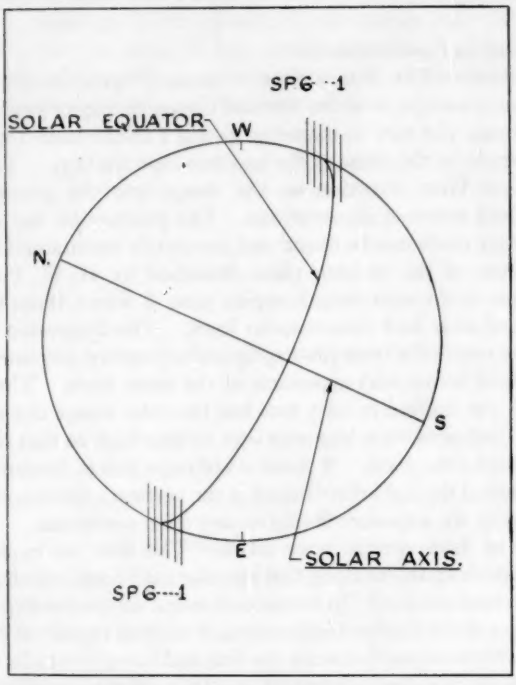

FIG. 2.—*Arrangement of observations in Series II.* (*The diagram is not drawn to scale.*)

that the initial fading of the photographic images did not introduce any spurious differences in density on the plate. Table I, col. (8) shows the ratio of the brightness of the sky spectrum as a percentage of the brightness of the limb spectrum, as found in this way.

1.2. *Measurements.*—Spectra are marked perpendicular to the dispersion, at either end of the spectral region, by a needle attached to a Hilger measuring machine. This determines to approximately 0·01 mm the position on the spectrum and hence the position on the Sun at which measurement is to be made. The height of spectrum measured is defined by a limiting diaphragm of variable aperture in the eye-piece of the Evershed machine (Paper I). Apart from personal equation, error in measurement is chiefly produced by irregularities in the

distribution of silver grains. An investigation showed, as one would expect, that the consistency of measurement increases as the height of the limiting diaphragm increases, up to a certain limit. This limit is approached asymptotically and occurs at about a height of 1 mm. Increase of diaphragm height decreases, however, the resolution on the solar image and in Series II and III the spectra were measured with a diaphragm aperture of 0·75 mm at intervals of 0·75 mm so that the entire spectrum was measured between the first and last marked points. In these series the first point of measurement was 1 mm inside the limb. In the exploratory Series I the diaphragm aperture was 0·3 mm and the measurement was made at intervals of 1 mm. The first point of measurement was a variable distance from the limb, depending on the spectrum, the average distance being 1 mm.

TABLE I

Observations									Measurements		
	(1)	(2)	(3)	(4)	(5)	(6)	(7)	(8)	(9)	(10)	(11)
Series I Exploratory 1950 Oct. 5	W	6	3	0·04	~ 6	$1^h\ 15^m$	0	2·7	6	9 w.v. 9 sol.	36
	E	6	3	0·04	~ 6	$1^h\ 13^m$	0		6	9 w.v. 9 sol.	36
Series IIa 1951 April 24	E	6	2·5	0·04	~ 6	7^m	1^+ 2^-	2·1	7	9 w.v. 10 sol.	42
	W	6	2·5	0·04	~ 6	8^m	1^+ 2^-		7	9 w.v. 10 sol.	42
Series IIb 1951 May 25	E	6	3	0·04	~ 6	10^m	2	2·1	7	9 w.v. 10 sol.	42
	W	6	2·5	0·04	~ 6	8^m	2		7	9 w.v. 10 sol.	42
Series III 1952 April 27	W	10	2	0·04	~10	$3^h\ 46^m$	1	...	12	9 w.v. 10 sol.	120
	E	10	1·5	0·04	~10	$3^h\ 17^m$	1		12	9 w.v. 10 sol.	120

Col. (1) Limb; (2) No. of sp. on each limb; (3) Exp. time in secs; (4) Slit width in mm; (5) Spectrum height in mm; (6) Time interval between first and last spectrum; (7) Seeing on a scale of 5; (8) Percentage sc. light; (9) No. of pts. per spectrum; (10) No. of lines per point; (11) Total no. of measured velocities.

the work; they were developed in Kodak Press Contrast Developer or Parkhurst two-solution developer.

In Series I and II, on each day that a set of limb spectra was obtained, at least one "sky brightness" plate was taken to find the ratio of the intensity of the light at a fixed distance outside the limb to that at a fixed distance inside. Each plate consisted of one exposure at the centre of the Sun through a Zeiss calibrated step-wedge and one without it to show any variation in illumination along the slit; then narrow spectra, 3 mm high, were taken of the light from points 40″ arc radially inside and outside the limb. The exposure time was the same for each of the four spectra and suitable densities on the plate were obtained by using N.P.L. calibrated filters. The plates were not developed until 24 hours after they had been taken, so

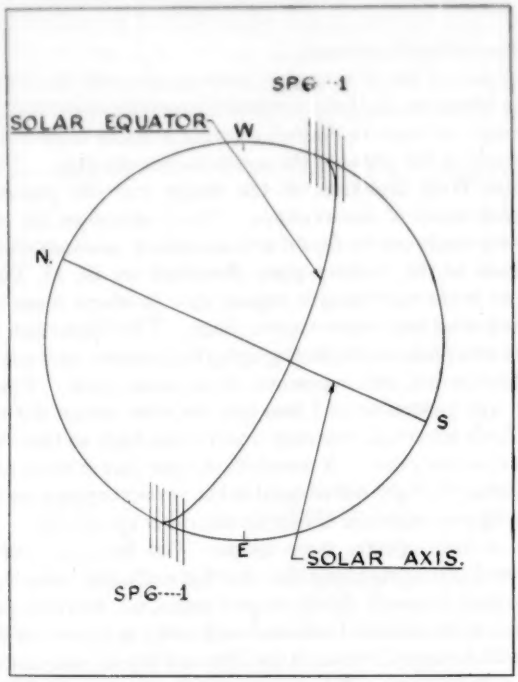

FIG. 2.—*Arrangement of observations in Series II.* (*The diagram is not drawn to scale.*)

that the initial fading of the photographic images did not introduce any spurious differences in density on the plate. Table I, col. (8) shows the ratio of the brightness of the sky spectrum as a percentage of the brightness of the limb spectrum, as found in this way.

1.2. *Measurements.*—Spectra are marked perpendicular to the dispersion, at either end of the spectral region, by a needle attached to a Hilger measuring machine. This determines to approximately 0·01 mm the position on the spectrum and hence the position on the Sun at which measurement is to be made. The height of spectrum measured is defined by a limiting diaphragm of variable aperture in the eye-piece of the Evershed machine (Paper I). Apart from personal equation, error in measurement is chiefly produced by irregularities in the

distribution of silver grains. An investigation showed, as one would expect, that the consistency of measurement increases as the height of the limiting diaphragm increases, up to a certain limit. This limit is approached asymptotically and occurs at about a height of 1 mm. Increase of diaphragm height decreases, however, the resolution on the solar image and in Series II and III the spectra were measured with a diaphragm aperture of 0·75 mm at intervals of 0·75 mm so that the entire spectrum was measured between the first and last marked points. In these series the first point of measurement was 1 mm inside the limb. In the exploratory Series I the diaphragm aperture was 0·3 mm and the measurement was made at intervals of 1 mm. The first point of measurement was a variable distance from the limb, depending on the spectrum, the average distance being 1 mm.

TABLE I

	Observations								Measurements		
	(1)	(2)	(3)	(4)	(5)	(6)	(7)	(8)	(9)	(10)	(11)
Series I Exploratory 1950 Oct. 5	W	6	3	0·04	~ 6	$1^h\ 15^m$	0	2·7	6	9 w.v. 9 sol.	36
	E	6	3	0·04	~ 6	$1^h\ 13^m$	0		6	9 w.v. 9 sol.	36
Series IIa 1951 April 24	E	6	2·5	0·04	~ 6	7^m	1^+ 2^-	2·1	7	9 w.v. 10 sol.	42
	W	6	2·5	0·04	~ 6	8^m	1^+ 2^-		7	9 w.v. 10 sol.	42
Series IIb 1951 May 25	E	6	3	0·04	~ 6	10^m	2	2·1	7	9 w.v. 10 sol.	42
	W	6	2·5	0·04	~ 6	8^m	2		7	9 w.v. 10 sol.	42
Series III 1952 April 27	W	10	2	0·04	~10	$3^h\ 46^m$	1	...	12	9 w.v. 10 sol.	120
	E	10	1·5	0·04	~10	$3^h\ 17^m$	1		12	9 w.v. 10 sol.	120

Col. (1) Limb; (2) No. of sp. on each limb; (3) Exp. time in secs; (4) Slit width in mm; (5) Spectrum height in mm; (6) Time interval between first and last spectrum; (7) Seeing on a scale of 5; (8) Percentage sc. light; (9) No. of pts. per spectrum; (10) No. of lines per point; (11) Total no. of measured velocities.

The relation between distance along the slit and position on the solar image is known when the position of the limb on the plate is known. The problem of finding the position of the limb proper was dealt with in two ways. In the first place, in Series I, microphotometer tracings were made perpendicular to the dispersion. The intensities were found from the calibration curves of the "sky brightness" plates, which are described above. The true position of the limb is then found by comparison with Wanders' distribution (**23**) for suitable values of the scattering parameter. In the second place, the position of the limb on the plate was estimated visually with a cross-wire; this method becomes more accurate as the seeing improves. For Series I, the visually estimated positions differed from the true ones on the average by approximately 0·03 mm and seldom by more than 0·1 mm. The first method takes a prohibitively long time and the average accuracy attained by the second method is comparable. A visual estimate of the position of the limb was made in Series II and III.

Nineteen lines were finally selected and measured at each point on the plates of Series II and III (see Table II). Ten of these are solar lines and they are bracketed by 9 water-vapour lines of comparable intensity which are used as standards of zero velocity. In this way, any errors caused by non-uniform illumination of the collimator are avoided.

TABLE II

Water-vapour lines		*Solar lines*			Km sec^{-1} per micron shift	
Wave-length in A	Rowland intensity	Wave-length in A	Element	Rowland intensity	(Series I)	(All other measurements)
5901·468	6	5905·680	Fe I	4	0·0744	0·0746
5919·055	5	*5909·981	Fe I	1	...	·0748
5919·643	7	5916·258	Fe I	3	·0749	·0751
5924·272	4	5927·796	Fe I	2	·0754	·0757
5932·093	5	5929·682	Fe I	2	·0755	·0758
5946·006	3	5930·190	Fe I	6	·0756	·0758
5947·066	2	5934·665	Fe I	5	·0758	·0760
5957·880	1	5948·548	Si I	6	·0765	·0767
5958·622	1	5952·726	Fe I	4	·0767	·0769
		5956·705	Fe I	4	·0769	·0771

(Wave-lengths taken from Rowland's Revision and corrected according to I.A.U. recommendations.)

* Not measured in Series I.

The spectra were measured at the various points along their height (see Table I) by the Evershed method. Its principal advantages are the elimination of spurious shifts caused by the asymmetrical distortion of the profiles by the horizontal apparatus function of the spectroscope, and the use of an automatic recording device. The machine is fully described in Paper I and all measurements were made with it, except the direct measures of Series I made on the prototype machine.

General questions concerning the accuracy of the method are discussed in Paper I. A comparison between the velocities obtained by two measurers for direct and reversed measures made at 7 points on one of the spectra of Series IIb showed that the large R–D discrepancy of 0·7 km sec^{-1} is inherent in the method, though it should disappear for water-vapour and solar lines of the same intensity.

Such a large value of the R–D difference is objectionable but the mean velocity agreed well with the mean of direct and reversed measures made with a cross-wire on the same spectrum. The root mean square error for a single line for these Evershed measures was $\pm 0{\cdot}23$ km sec^{-1}, which corresponds to a displacement of 3 microns on the plate. This may be compared with the values of $1{\cdot}5\mu$, 2μ and $1{\cdot}5\mu$ obtained at Mt. Wilson 1906–8 (**2**), Ottawa 1911–13 (**18**) and Allegheny 1911 (**20**), respectively. The smaller dispersion of these earlier differential measures may, however, be a result of prepossessions (**17**) which are eliminated by the automatic recording device on the Evershed machine.

A test was also made of the consistency with which a measurement is repeated, by measuring the 84 spectra of Series IIa twice. Table III shows the distribution of velocity differences which was obtained. All the velocity differences are small (which is satisfactory); the average arithmetic difference between the two measures of a single point is $1{\cdot}4\mu \simeq 0{\cdot}1$ km sec^{-1}. This is comparable with the root mean square error of measurement of a single velocity point, given by $\pm 0{\cdot}23/\sqrt{10} = \pm 0{\cdot}08$ km sec^{-1}, since 10 solar lines were used to give the velocity at any point. The average algebraic or systematic difference between the two measures of a point is $0{\cdot}2\mu$, which is negligible.

TABLE III

Limits of the difference interval				No. of velocities in the interval
$\Delta\mu$ microns		Δv km sec^{-1}		
4·0,	3·0	0·31,	0·23	2
3·0,	2·0	0·23	0·15	8
2·0,	1·0	0·15,	0·08	18
1·0,	0·0	0·08,	0·00	18
0·0,	−1·0	0·00,	−0·08	14
−1·0,	−2·0	−0·08,	−0·15	15
−2·0,	−3·0	−0·15,	−0·23	8
−3·0,	−4·0	−0·23,	−0·31	0
−4·0,	−5·0	−0·31,	−0·38	0
−5·0,	−6·0	−0·38,	−0·45	1

Altogether 480 measurements of velocity were made (see Table I). Before they can be used in the calculation of the velocity of solar rotation it is necessary to find the effect of any extraneous light superposed on the spectra.

2. *The effect of scattered light*

The spectrum of the sky remote from the Sun is an integrated spectrum of the whole disk with a mean velocity corresponding to that of the solar centre. If such a sky spectrum be superposed on the spectrum of the limb of the Sun, the resulting blended spectrum will have a mean velocity displacement less than that of the limb alone and the measured rotation will be distorted by an amount approximately linearly proportional to the ratio of the brightness of the sky spectrum to the limb spectrum. This hypothesis, which ignores the mechanism of the scattering by which the sky spectrum is produced and which was apparently never tested, was put forward by DeLury (**3, 4**) to account for the varying values of solar rotation found between 1906 and 1915.

One quantitative test can, however, easily be made. The spectrum of the sky superposed on the limb must be that of the sky immediately adjacent to the limb, i.e. that of the solar aureole. If any distortion of the measured velocities is to occur, the velocity of the sky spectrum must be different from that of the limb. Accordingly, on 1952 September 18 a series of exposures of the West limb of the Sun was made with a rapidly rotating sector, having a 12° aperture, to cut down the flux from the disk to an amount approximately equal to that of the flux from the inner aureole. The height of the slit was limited to 12·5 mm and the image was guided so that the limb fell well within the portion of the slit shielded by the sector, while the aureole, at distances greater than a few seconds of arc from the limb, fell on the unshielded part and was fully exposed. Five of these exposures were made and a narrow spectrum of the centre, 3 mm in height, was taken before and after the series.

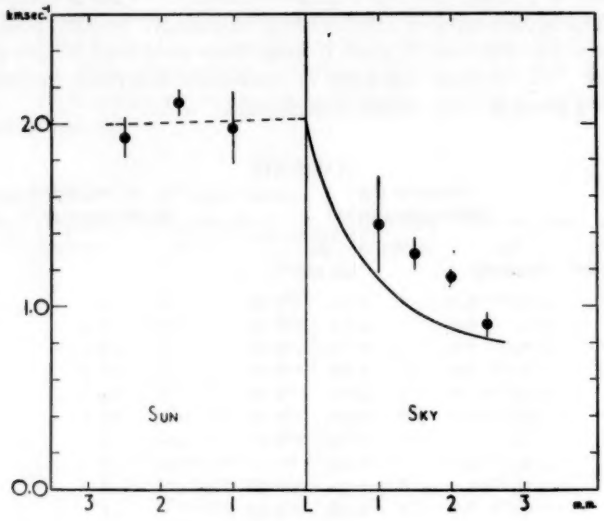

FIG. 3.—*Velocity distribution in the aureole.*

Ordinates: velocities differenced from the centre velocity.
Abscissae: distances from the limb along the E.–W. chord of the solar image.

The spectra so obtained were measured on the Evershed machine with a diaphragm height of 0·75 mm. Inside the limb the spectra were measured at distances of 1 mm, 1·75 mm and 2·5 mm from the limb. Outside the limb, in the spectrum of the aureole, the velocity was again measured at 3 points separated by 0·75 mm intervals. (The first position at which the fully exposed spectrum filled the diaphragm aperture depended on the guiding of the limb.) The 15 measured velocities in the aureole were divided into four groups and the mean velocity and position calculated for each group. For the centre spectra, a diaphragm aperture of 3 mm was used. The resulting velocities are shown by circles in Fig. 3; in each exposure the velocity at the centre was taken as the standard velocity. The length of the vertical line through each circle shows the root mean square error of the velocity.

It will at once be seen that the basic postulate of DeLury's hypothesis is not satisfied. The measured velocities in the aureole, instead of being zero, drop steadily from the velocity of the limb at the limb to reach zero only at a distance of several millimetres from the limb. Since at the places in the aureole where the velocity is measured the vertical apparatus function of the spectroscope accounts for less than one-thousandth of the observed brightness, the results shown in Fig. 3 are essentially due to the aureole alone. Hence if, as in DeLury's hypothesis, the spectrum of the aureole exactly at the limb were superposed on the spectrum of the limb there would be no distortion of the measured velocity at all.

The processes which occur are, however, more complex than pictured by DeLury. Scattering (as opposed to specular reflection) by the telescope mirrors and scattering by the Earth's atmosphere redistribute the light from each point of the Sun over an area in the focal plane of the telescope. By far the greater part of the scattering takes place over small angles and only a minute portion, estimated at 10^{-6} by van de Hulst (**8**), takes place over large angles to form the sky spectrum remote from the Sun. What is observed in the aureole near the solar image is presumably this small-angle, redistributed light. If this be the case, the main effect of scattering on line-of-sight velocities will be to smear out any differences between them and only to a completely negligible amount, as a consequence of second and higher order scattering in the Earth's atmosphere, to superpose an integrated zero velocity spectrum on the limb spectra.

T. D. Kinman has measured the surface brightness of the aureole as a function of its radial distance from the limb (Paper III). His measures are in good agreement with each other and with the surface brightness measures made at a single point (Table I) in the present investigation. From these measures Kinman has calculated the scattering function which must prevail if the aureole is wholly produced by small-angle scattering. If, as we have suggested above, this assumption is true and if there is a negligible amount of superposed zero velocity sky spectrum, then Kinman's scattering function should predict the velocities which are observed in the aureole. Details of this calculation are given in the Appendix and the velocities predicted by the scattering function are shown by the continuous curve in Fig. 3. When it is recalled that Kinman's scattering function refers only to average Oxford conditions, the agreement between the velocities predicted by the function and those actually observed may be considered not unsatisfactory. The difference between the observed and calculated velocities is in the opposite sense to the difference which would arise if there were any appreciable quantity of zero velocity light superposed on the small-angle redistributed light in the aureole. It would therefore appear that small-angle scattering is the dominant mechanism and we need only consider the effect of such scattering on the observed line-of-sight velocities.

The order of magnitude of the effect can readily be calculated (see Appendix) from a simple example. If the equatorial region of the Sun has a uniform rotational velocity of, say, 2·07 km sec^{-1}, then after correction for the Earth's motion, the observed line-of-sight velocity at the limb would be 2·07 km sec^{-1}. The line-of-sight velocity observed (after correction for the Earth's motion) as a result of small-angle scattering from all other regions of the Sun where the line-of-sight velocity is smaller would be 2·03 km sec^{-1}. Hence, at the limb, small-angle scattering produces an error of 0·04 km sec^{-1}. The error decreases as the point at which measurement is made moves further in from the limb and at a

distance of 10″ arc from the limb (1 mm on the Oxford solar image) it would only be 0·03 km sec^{-1}. Since the present observations refer to points 10″ arc or further from the limb, the maximum systematic error, produced by scattering, will not be greater than 0·03 km sec^{-1}, that is, less than one-half the measurement error of 0·08 km sec^{-1} for a single measured velocity.

The nature and effects of scattered light are now clear. Small-angle scattering is the predominant mechanism and its only effect is a smearing out of velocity differences. Any systematic effects are well below the errors of measurement, so that measured velocities can be and are used in the subsequent calculations without further correction.

3. *Solar rotation and limb effect*

Reference to Table I shows that the 480 measured velocities are divided among the various series in the following way: Series I contributes 72 points, each day in Series II 84 points and Series III 240 points. In making a solution for the best values of solar rotation and limb effect for the mean epoch of the investigation it is advisable that approximately equal numbers of velocities should be used from each of the four days for which measurements were made. Accordingly, 4 representative spectra were selected from each limb of Series III so that 96 velocities only from the series are used. The total number of velocities included in the final solution is, therefore, 336.

The conversion of positions on the image to positions on the Sun and of measured line-of-sight velocities to velocities on the Sun are fully explained in Paper I. As shown in the last section, the effects of superposed light are negligible so the measured velocities only need correction for the relative motion of the Earth and Sun. Let this correction to the limb spectra be V_1, and the correction for the standard centre spectrum be V_2 (V_2 includes a correction for a small line-of-sight component of solar rotation at points other than the centre of the image). Then the line-of-sight velocity on the Sun at any point is $V+V_1-V_2$.

For each point the equation of condition may be written

$$(U+u)\cos\gamma_1+v\cos\gamma_2+w\cos\gamma_3=(V+V_1-V_2)-\Delta, \qquad (1)$$

as in Paper I. U is the value of solar rotation, Δ the limb effect, and u, v, w are the components of any local velocity at the point, parallel to axes along the line of latitude, the line of longitude and the solar radius, which make angles γ_1, γ_2, γ_3 respectively, with the line of sight. In a limited latitude zone, U the linear velocity can be represented by the Faye formula $U=(a+b\cos^2 B)\cos B$, where B is the heliographic latitude. Hence the complete equation of condition takes the form

$$(a+b\cos^2 B)\cos B\cos\gamma_1+u\cos\gamma_1+v\cos\gamma_2+w\cos\gamma_3=(V+V_1-V_2)-\Delta, \quad (2)$$

having six unknowns, a, b, u, v, w, Δ.

Since u, v, w are the components of a local velocity there may be no relation between them from point to point, so the equations cannot be grouped together for a solution by the method of least squares. Furthermore, for the range of latitude covered by the observations $|B|\leqslant 6°$, the coefficients of a and b are so nearly equal that the equations are ill-conditioned and a least-squares solution is inadvisable in any case (7). Consequently, a different method of solution has

to be found. The equations are therefore simplified and solved by an iterative method.

Assume that the velocity is independent of latitude and u, v, w are zero. If U^* be the equatorial velocity of rotation, the simplified equation of condition for any point becomes

$$U^* \cos B \cos \gamma_1 = (V + V_1 - V_2) - \Delta, \tag{3}$$

an equation only involving the two most important unknowns, where U^* is constant and Δ is a function only of the fractional distance ρ/ρ_0 from the centre of the disk.

Rewriting this in the form

$$U^* = \frac{V + V_1 - V_2}{\cos B \cos \gamma_1} - \frac{\Delta}{\cos B \cos \gamma_1}, \tag{4}$$

a first approximation to U^* is easily found. The numerical value of $\cos B \cos \gamma_1$ depends mainly on the fractional distance from the centre of the disk, but the sign is opposite in the Western and Eastern halves of the disk. Hence, providing there are equal numbers of observations on the East and West limbs at each value of ρ/ρ_0, a condition roughly satisfied in practice, the first approximation to U^*, say U_1^*, is given by

$$U_1^* = \frac{1}{N} \sum_1^N \frac{V + V_1 - V_2}{\cos B \cos \gamma_1}, \quad N = 336. \tag{5}$$

The resulting value of $U_1^* = 1{\cdot}90$ km sec^{-1} is used to give the first approximation Δ_1 to Δ, from

$$\Delta_1 = (V + V_1 - V_2) - U_1^* \cos B \cos \gamma_1, \tag{6}$$

for each point. For the 334 points lying in the interval $0{\cdot}90 \leqslant \rho/\rho_0 < 0{\cdot}995$, the results so obtained are grouped together at twelve standard positions shown in Table IV ($x = 1 - \rho/\rho_0$ is the fractional distance from the limb). From these results, appropriately weighted, a least-squares solution for a quadratic expression for Δ_1 is calculated, giving

$$\bar{\Delta}_1 = 0{\cdot}236 - 2{\cdot}640x + 2{\cdot}071x^2, \quad 0{\cdot}005 < x \leqslant 0{\cdot}10. \tag{7}$$

TABLE IV

ρ/ρ_0	x	No. of points	Δ_1	ρ/ρ_0	x	No. of points	Δ_1
0·908	0·092	8	+0·01 km sec^{-1}	0·951	0·049	42	+0·12 km sec^{-1}
·916	·084	8	−0·09	·959	·041	41	+0·17
·923	·077	8	+0·12	·967	·033	42	+0·14
·931	·069	8	+0·12	·972	·026	40	+0·14
·938	·062	8	+0·15	·982	·018	42	+0·21
·943	·057	43	+0·06	·988	·012	44	+0·20

Values from this analytical solution are then used to give a second approximation to U^* in each case

$$U_2^* = \frac{V + V_1 - V_2}{\cos B \cos \gamma_1} - \frac{\bar{\Delta}_1}{\cos B \cos \gamma_1}. \tag{8}$$

The mean of the 334 values of U_2^* is 1·91 km sec$^{-1} = \bar{U}_2^*$ say.

So small a change as 0·01 km sec^{-1} in the approximation to U^* will produce a negligible change in the approximation to Δ, so the process has converged rapidly and satisfactorily. We shall adopt $U^* = \bar{U}_2^*$, $\Delta = \bar{\Delta}_1$. The values of

limb effect may be compared with those of M. G. Adam (1). Her interferometric results, necessarily obtained with very low resolution on the solar image, show both a larger value of Δ and a steeper rise to the limb. However, her more recent work with comparable high resolution on the solar image yields results not in disagreement with values found in the present investigation.

Finally, it is necessary to test the assumption of the invariability of velocity with latitude. The individual values of U_2^* are grouped into eight zones of latitude and the mean found for each. Fig. 4 shows the result. The root mean square error of each mean is represented by a vertical line and the number in brackets in each case shows the number of observations used in calculating the mean. Clearly there is no systematic change in velocity and so no correction is needed.

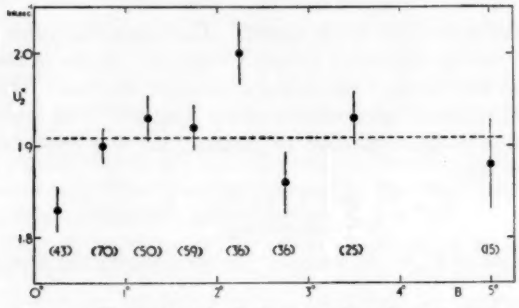

FIG. 4.—*The equatorial velocity; its independence of latitude. Abscissae: heliographic latitude.*

Residuals from the measured line-of-sight velocities were then calculated from the final values of U^* and Δ. The root mean square error of a single solar velocity from 334 observations is $\pm 0{\cdot}18\,\mathrm{km\,sec^{-1}}$. The root mean square error of U^* is $\pm 0{\cdot}01\,\mathrm{km\,sec^{-1}}$, so that the first approximation U_1^* lies within the range of the root mean square error of the final value. One may take, therefore, for the mean epoch 1951·5, the equatorial velocity of solar rotation

$$U^* = 1{\cdot}91 \pm 0{\cdot}01\ \mathrm{km\ sec^{-1}}, \tag{9}$$

and the limb effect in the range $0{\cdot}01 \leqslant x \leqslant 0{\cdot}10$ (where x is the fractional distance from the limb)

$$\Delta = 0{\cdot}236 - 2{\cdot}640x + 2{\cdot}071x^2, \tag{10}$$

as being the best possible values from the material.

4. *Evidence of local variations in velocity*

In the previous section the mean equatorial velocity U^* and the limb effect Δ have been found from 334 line-of-sight velocities measured in Series I, II and III (*cf.* Table I). We now wish to see whether the individual measured values of the equatorial solar velocity, denoted by U, differ significantly from each other. For this purpose attention is confined to the homogeneous set of measures from Series II (168 values of U) and Series III (96 values of U). The 70 measures of Series I, based on different lines measured over a smaller height of spectrum (*cf.* Section 1), are not included in the present discussion, though inspection shows that they support the conclusions which are derived for Series II and III alone.

4.1. *Statistical discussion of errors.*—The 264 values of the rotational velocity U obtained from Series II and III are each the mean velocity from 10 solar lines at a particular place in the equatorial photosphere. We shall call U a *spectrum-velocity*. These 264 values have a dispersion about their mean with a root mean square error for a single spectrum-velocity of $\pm 0{\cdot}17$ km sec^{-1} ($\pm 0{\cdot}18$ km sec^{-1} is obtained for the 334 spectrum-velocities considered in the previous section). Can so large a dispersion arise solely from errors of measurements?

To answer this question we must first make a precise estimate of the errors of measurement. Let the measured velocity from a single line be u, *the line-velocity*. Then the spectrum-velocity, U, and the root mean square error, s, of the line-velocity at any point are given by

$$U=\frac{1}{n}\sum_1^n u_r, \quad s^2=\frac{1}{n-1}\sum_1^n (U-u_r)^2, \qquad \text{(11 a) and (11 b)}$$

where $n=10$, since each spectrum-velocity is the mean of 10 line-velocities u_r. Now the operation of measurement is essentially one of taking samples of n measures at a time from a hypothetical, infinite population of line measures at that particular point in the photosphere. The value of the error of measurement will then be the value σ of the root mean square error of a line-velocity for this infinite population. This cannot be calculated directly from equation (11 b) but an estimate of its size can be made if we suppose that the infinite population of all line-velocities has a Gaussian distribution about a mean μ (which is also unknown).

The probability of obtaining a line-velocity between u and $u+du$ from the population is

$$P(u)\,du=(\sqrt{2\pi}\,.\,\sigma)^{-1}\exp\left[-(u-\mu)^2/2\sigma^2\right]du. \qquad (12)$$

Hence the probability of obtaining a sample of n line-velocities between u_1 and $u_1+du_1, \ldots, u_r$ and $u_r+du_r, \ldots, u_n$ and u_n+du_n respectively, is

$$(\sqrt{2\pi}\,.\,\sigma)^{-n}\exp\left[-\sum_1^n (u_r-\mu)^2/2\sigma^2\right]du_1\ldots du_r\ldots du_n, \qquad (13)$$

since the probabilities of obtaining the individual velocities are independent. Written in terms of the easily calculable sample statistics U and s [equations (11 a) and (11 b)], this becomes

$$(\sqrt{2\pi}\,.\,\sigma)^{-n}\exp\left[-n(U-\mu)^2/2\sigma^2\right]\exp\left[-(n-1)s^2/2\sigma^2\right]du_1\ldots du_r\ldots du_n. \qquad (14)$$

By a purely analytic process (**10**) the product of the differentials can be expressed in terms of the new variables U and s and $n-2$ other variables. After integration with respect to the latter, we find the probability of obtaining the sample is

$$C\exp\left[-n(U-\mu)^2/2\sigma^2\right]dU\,.\,s^{n-2}\exp\left[-(n-1)s^2/2\sigma^2\right]ds, \qquad (15)$$

where C is a constant. Hence the probability that the arithmetic mean of a sample of n line-velocities lies between U and $U+dU$ is independent of the probability that the root mean square error of a single line-velocity, in a sample of n, lies between s and $s+ds$. Normalizing these two independent probabilities we find that the probability of the spectrum-velocity lying between U and $U+dU$ is

$$P_1(U)\,dU=(\sqrt{2\pi}\,.\,\sigma/\sqrt{n})^{-1}\exp\left[-(U-\mu)^2\Big/\frac{2\sigma^2}{n}\right]dU, \qquad (16)$$

and the probability that the root mean square error of a single line-velocity lies between s and $s+ds$ is

$$P_2(s)\,ds = \{2^{(n-3)/2}\Gamma[(n-1)/2]\}^{-1} \cdot [(n-1)/\sigma^2]^{(n-1)/2} \cdot s^{n-2} \exp[-(n-1)s^2/2\sigma^2]\,ds. \quad (17)$$

Integrating this over all s, we find that $\bar{s}$ the mean value of s is given by

$$\bar{s} = [2/(n-1)]^{1/2}\Gamma(n/2)\{\Gamma[(n-1)/2]\}^{-1} \cdot \sigma, \quad (18)$$

so that for samples of $n=10$, $\bar{s}=0{\cdot}973\sigma$ is a very good estimate of the unknown standard error σ. For moderate values of n equation (17) reduces to the Gaussian form

$$P_2(s)\,ds = [\sqrt{2\pi} \cdot \sigma/\sqrt{2(n-1)}]^{-1} \exp\left[-(s-\bar{s})^2 \Big/ \frac{\sigma^2}{n-1}\right] ds. \quad (19)$$

The problem now is to find a reliable value of $\bar{s}$. For this purpose 106 spectrum-velocities are selected from the 264 available observations so that they are fairly divided between the East and West limbs and the three days on which observations were made. The 106 values of s are then calculated according to formula (11 b); the results are plotted as a frequency histogram in Fig. 5,

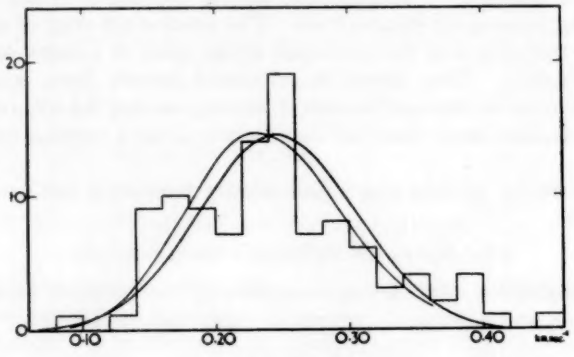

FIG. 5.—*Distribution of sample standard errors.*
Ordinates: number of samples having a given error.
Abscissae: root mean square error expressed in km sec^{-1}.

together with the theoretical distribution $P_2(s)$ (thin line, left-hand curve) from equation (17) for comparison. The mean value of s, $\bar{s}=0{\cdot}25$ km sec^{-1} (which agrees closely with the value 0·23 km sec^{-1} found for a slit position of Series II b and quoted in Paper I) gives for $n=10$ (equation (18)) a value $\sigma=0{\cdot}26$ km sec^{-1}. The next problem is the reliability of the estimate of $\bar{s}$, and hence of σ, which is found from the dispersion of the values of s. This is very easily calculated since the approximate Gaussian form of $P_2(s)$, given in equation (19) and shown as a thick line (right-hand curve) in Fig. 5, fits the observations as well as the exact form does. It gives for the standard error of σ, simply $\sigma/\sqrt{2(n-1)}=0{\cdot}06$ km sec^{-1}. Thus we have as the best estimate of the root mean square error of measurement of a single line-velocity $\pm(0{\cdot}26\pm0{\cdot}06)$ km sec^{-1}. This estimate will be denoted by σ_2.

Consider now the distribution of the sample means. If the value of solar rotation were uniform and constant at all points in the equatorial region, the 264 spectrum-velocities (plotted as a frequency histogram in Fig. 6) would themselves form a sampling distribution of the mean according to equation (16),

with a standard error $\sigma/\sqrt{10}$. Again σ is the unknown root mean square error of a single line-velocity. The theoretical distribution $P_1(U)$ is shown as a smooth curve in Fig. 6. On this hypothesis $\sigma/\sqrt{10} = \pm 0{\cdot}17$ km sec^{-1} or $\sigma = \pm 0{\cdot}54$ km sec^{-1}. Let this estimate of the value of σ be denoted by σ_1.

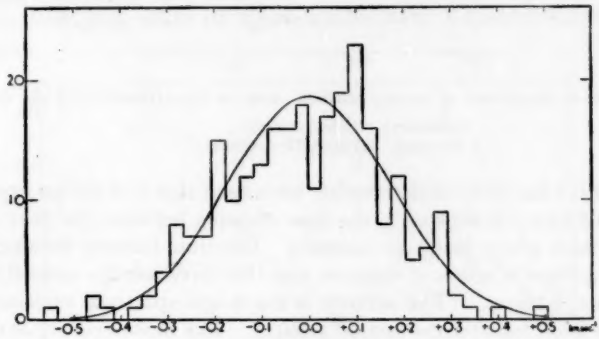

FIG. 6.—*Distribution of sample means.*
Ordinates: number of samples having a given mean.
Abscissae: sample means expressed in km sec^{-1}.

We have thus obtained two values for σ, the standard error of a single line-velocity u. The value $\sigma_2 = \pm (0{\cdot}26 \pm 0{\cdot}06)$ km sec^{-1} is derived from the sampling distribution of the standard error of a single line-velocity, calculated from the 10 lines comprising a single spectrum-velocity. This estimate is independent of any variation of rotational velocity with time or position on the Sun. On the other hand, the estimate from the values of U gives $\sigma_1 = \pm 0{\cdot}54$ km sec^{-1}, but is valid only if the solar rotation is uniform and constant over the equatorial region. It differs from σ_2 by nearly five times the root mean square error of the latter. The probability of the values σ_1 and σ_2 representing the same quantity in the infinite population is, therefore, less than one in a thousand, and we must reject the hypothesis of a uniform and constant rotational velocity throughout the equatorial region. That is to say, the large dispersion in the spectrum-velocities cannot be accounted for solely by errors of measurement and must be a consequence of actual variations in rotational velocity.

4.2. *Distribution of velocity residuals on the solar surface.*—From this point onwards the investigation is purely exploratory, but it is interesting to see if there is any regularity discernible in the variation of velocity from point to point. Series III is obviously best suited to provide an answer to this question. In the solar rotation determination (Section 3) only 4 spectra from Series III are included from each limb, but in the present investigation the entire 10 spectra are included, giving a total of 120 measured velocities at each limb.

The velocity residuals, $U - U^* \cos B \cos \gamma_1 - \Delta$, for one slit position on the East limb are shown in Fig. 7. (The straight lines joining adjacent velocity points have no physical significance and are only intended to serve as a guide to the eye.) The figure shows no regular change in velocity over this portion of the solar surface. It may well be, however, that a regular variation of velocity is being obscured by the superposition of errors of measurement and randomly distributed local solar velocities. If a regular distribution exists, it can be revealed by taking the mean of a sufficient number of observations at any point.

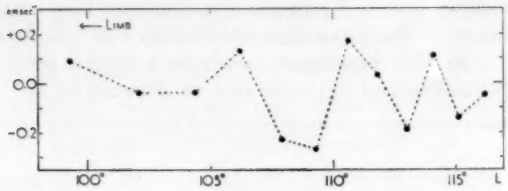

FIG. 7.—*Typical distribution of velocity-residuals along an East–West chord of the solar image.*
Ordinates: residual velocity.
Abscissae: heliographic longitude.

In Series III the times of observation were such that 9 of the 10 exposures on each limb fall into 3 groups of 3, the time elapsing between the first and third exposure in each group being 40 seconds. The time interval between the first and second groups is about 5 minutes and that between the second and third groups about $3\frac{1}{2}$ hours. (The seventh is the single spectrum remaining and it follows a few minutes after the second group.) The mean velocity at each point is calculated for each of the three 40-second groups. Figs. 8 and 9 show the results for the groups at the West and East limbs, respectively. Vertical lines show the root mean square error of the velocity (calculated from the agreement of the three individual velocities) at each point and, once again, adjacent velocity points are joined by straight guiding lines.

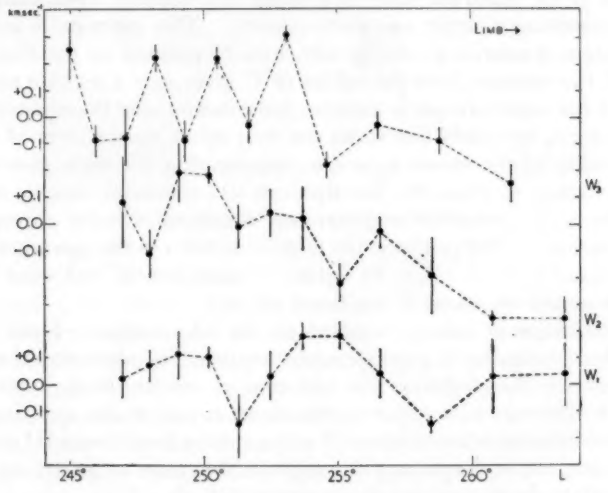

FIG. 8.—*Distribution of mean residual velocities with longitude on West limb.*
Ordinates: residual velocity.
Abscissae: heliographic longitude.

Attention may be drawn to the marked similarity of velocity variation between the three groups E_1, E_2 and E_3 on the East limb. On the West limb there is little similarity between W_1 and W_2, the groups separated by five minutes in time, though there is a similarity between W_2 and W_3, the groups separated by some three and a half hours. The steady variation in velocity at the East

limb over several degrees of longitude approximately equal to a distance of 75 000 km along the solar circumference, together with the marked similarity in velocity pattern in these three groups, seem to point to the existence of a steady velocity field persisting over a period of some hours. The gradual dying-away of the velocity variations near the limb in all six cases presumably arises as a result of the averaging effect of measurement over a greater length of solar circumference.

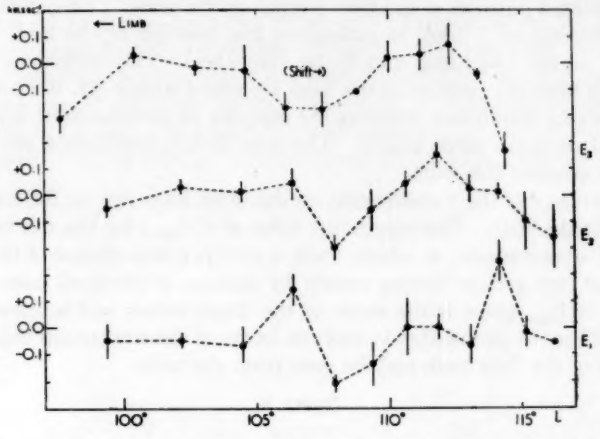

FIG. 9.—*Distribution of mean residual velocities with longitude on East limb.*
Ordinates: residual velocity.
Abscissae: heliographic longitude.

4.3. *Possible systematic error.*—At this point the objection may be made that, despite the precautions which have been taken, the velocity shifts are produced instrumentally. For example, it is conceivable, though not very probable, that a systematic velocity pattern exists in the standard spectrum (*cf.* Section 1) made from the out-of-focus image of the centre of the Sun; it is against this standard spectrum that the limb spectra are measured. Any such spurious velocity pattern is most easily found by taking the average of a large number of velocity residuals at each point on the slit, since for different areas on the Sun at different times the true residual velocities are randomly distributed about zero.

Accordingly, the 264 velocities of Series II and III, included in the solar rotation determination and measured against the same standard spectrum, were divided into 15 groups, the members of each group corresponding to approximately the same point on the slit. The average residual velocity of each group was calculated in order to find the best available estimate of any correction for that region. Over the portion of the slit where a considerable number of independent solar velocities contribute to the mean of the group the correction does not exceed $\pm 0{\cdot}03$ km sec^{-1}. This value should provide an upper limit to the size of any systematic error. Hence there is no evidence for supposing the correction differs significantly from zero and it is clear that the residual velocities cannot be attributed to instrumental causes.

4.4. *Evidence for velocity fields.*—Having confirmed the solar origin of the velocities, it only remains to find the probability of the similarity between W_2

and W_3, E_1, E_2 and E_3 arising by chance. It can be decided by calculating the correlation coefficients r between the various groups. Correlations are calculated for the pairs W_1W_2, W_2W_3, W_3W_1 and for the corresponding groups on the East limb.

In the case of E_1, E_2, E_3 the similarity in pattern is marked, but E_3 appears to be shifted, relative to the other two, by about 1° in longitude. This may be quite a spurious effect, since the longitude assigned to each point depends on the estimated position of the limb proper on the plate. The shift could arise from a difference of 0·1 mm in estimating the position of the limb as between E_1 and E_2 on the one hand, and E_3 on the other. This difference lies within the possible error of estimating the limb by visual means (*cf.* Section 1), and a change in seeing conditions, affecting the estimate of limb position, is not unlikely in a period of some three hours. The correlation coefficients are calculated, taking into account this shift.

The average $\bar{r}$ of the 3 coefficients on the West limb and on the East limb are shown in Table V(*a*). The significant value of r, $\bar{r}_{\text{sign.}}$, for the relevant number of pairs of observations, at which there is a 10 per cent chance of the similarity between the two groups arising purely by chance, is obtained from tables (**6**). The value of $\bar{r}_{\text{sign.}}$ given is the mean of the three values and is shown for comparison. That the probability is only one in ten of the similarities being spurious in the case of the East limb may be seen from the table.

TABLE V

(*a*)

Group	$\bar{r}$
W_1, W_2, W_3	+0·32
E_1, E_2, E_3	+0·52
$\bar{r}_{\text{sign.}}$	+0·46

(*b*)

Series	Limb	$\bar{r}$
II a	W.	+0·26
	E.	+0·34
II b	W.	+0·56
	E.	+0·47
	$\bar{r}_{\text{sign.}}$	+0·28

Finally, we turn to Series II to see if any relation exists between the velocity variations along parallel chords of the disk slightly separated from one another. If the velocity field is steady over the period of some hours the 10 minutes elapsing between the first and last exposure on a limb (*cf.* Table I) is negligible and the six spectra may be regarded as a map of the region. Since only one exposure was made in each position, the observational evidence is very much weaker than in Series III and the results must be treated with reserve.

Fig. 10 shows the velocity residuals along the West limb chords, marked in Fig. 2, for Series II a. Similar variations are shown by the remaining observations of Series II a and by Series II b on West and East limbs. There appear to be bands of velocity occurring approximately perpendicular to the solar equator. That this is not a completely spurious effect is checked by a method similar to that used for Series III. On any one limb, each of the six spectra is in turn used as the standard spectrum, and the value of the correlation of all remaining five velocities at each of the same longitude positions is calculated in this case. The mean of the six coefficients on each limb is listed in Table V (*b*) in the column headed $\bar{r}$ and as before the value is shown at which there is a 10 per cent probability of the similarity being due to chance. The mean observed correlation is well above the 10 per cent significance level, but this should perhaps

be regarded with some reserve since the single spectra being correlated have in them the full effect of errors of measurement and possible fluctuating solar velocities.

An attempt was made to resolve the bands of constant velocity into their u, v, w components (see equation (1) in Section 3). The coefficients of u, v, w do not vary significantly, however, over the area of measurement, so that the equations are ill-conditioned and no solution for u, v, w could be found.

Conclusion.—The general problem presented by measures of the equatorial solar velocity appears to be considerably clarified. The effect on the measured velocities, of light scattered in the Earth's atmosphere and by the telescope, is shown to be only of the order of 0·03 km sec^{-1}. There remain variations in velocity of the order of $\pm$0·17 km sec^{-1} which cannot be accounted for by errors of measurement. These velocity differences are of the same order of magnitude

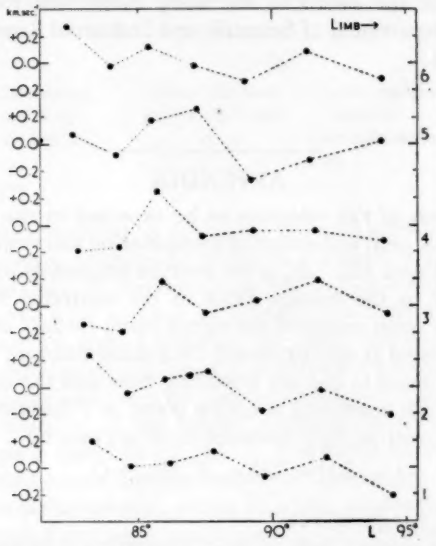

FIG. 10.—*Velocity residuals as a function of longitude and position on disk.*
Ordinates: residual velocity.
Abscissae: heliographic longitude.

as those originally found by H. H. Plaskett. The present observations go further, however, in showing that these differences may arise from velocity fields in the form of bands of constant velocity separated by distances of the order of 75 000 km. These bands possibly extend perpendicular to the equator over distances of not less than 60 000 km.

If such velocity fields exist they might go far towards accounting for the results obtained by earlier workers, shown in Fig. 1. The dispersion of the most reliable values is $\pm$0·05 km sec^{-1} and this is the order of the variation in the mean values found on single days in the present investigation. Such large differences are to be expected for the mean of a few observations made at a single place in a velocity field.

While the presence of velocity fields in the equatorial photosphere is suggested by the present investigation and accounts for the earlier discrepant values of the equatorial rotation, the existence of such velocity fields still requires demonstration from more extensive observations. Some of these observations are now in progress at Oxford.

Acknowledgment is due to Professor H. H. Plaskett, Dr M. G. Adam and Dr T. D. Kinman. Professor Plaskett suggested the problem and planned the investigation; in particular he is responsible for the observational attack on scattered light in Section 2, and the statistical discussion of the results in Section 4. Dr Adam helped in all the observational work and in the discussion of the results. Finally, Dr Kinman helped in the discussion in the Appendix.

I should like to thank the Principal and Fellows of Lady Margaret Hall for a Senior Scholarship 1950–52, the Principal and Fellows of Somerville College and the Donors for the award of the Mary Somerville Research Fellowship 1952–53, and the Department of Scientific and Industrial Research for a maintenance grant 1950–52.

University Observatory,
Oxford:
1953 *November* 20.

APPENDIX

In the calculation of the velocities to be expected in the aureole and inside the limb, the arrangement and extent of the scattering and solar zones are the same as in Section 1 of Paper III. B_n is the average brightness of the nth solar zone from the limb; U_p is the average value of the scattering function in the pth scattering zone, the outer radius of the eighth being $s = 120''$ arc, and beyond this the total light scattered is approximated by a small constant quantity, Q. Let σ_{pn} be the area common to the pth scattering zone and the nth solar zone when the point X, to which scattering is taking place, is a distance x from the limb. Then the total intensity of light scattered to X is given by

$$I(x) = \{\sum_n (\sum_p \sigma_{pn} U_p) B_n\} + Q, \qquad \text{(A 1)}$$

Paper III, Section 1, equation (2).

Each solar zone scatters light of its characteristic velocity; for the nth solar zone let this be V_n. It is calculated from the equatorial velocity of rotation, taken as 2·07 km sec^{-1}, by assuming that the centre showed zero line-of-sight velocity while the limb showed the full value. Hence the product of brightness and velocity for the area of the image included in the scattering zones is

$$\sum_n (\sum_p \sigma_{pn} U_p) B_n \,.\, V_n.$$

For light scattered from outside the area included in the scattering zones the mean velocity is taken to be zero, since the velocity distribution is symmetrical about the solar axis. This approximation improves as X moves further from the limb along a solar radius perpendicular to the axis.

Hence, for points outside the limb in the equatorial region, the observed velocity $V^*(x)$ due to scattered light is given by

$$V^*(x) = \frac{\sum_n (\sum_p \sigma_{pn} U_p) B_n V_n}{\{\sum_n (\sum_p \sigma_{pn} U_p) B_n\} + Q}. \qquad \text{(A 2)}$$

(The validity of this step is discussed later.) The calculations were performed for $x = 7''{\cdot}5$, $15''$ and $25''$ arc along a solar radius, corresponding to distances 0·8 mm, 1·6 mm and 2·7 mm from the limb along the E.–W. line of the telescope. The results are given in Table A I (*a*), and yield the curve given in Fig. 3.

For points inside the limb, however, the light of intensity $I(x)$ and velocity $V^*(x)$ is superposed on that remaining from the true intensity I after scattering has taken place. This residual intensity is approximately 90 per cent and in this paper a factor $0{\cdot}905I$ has been used. The value of I, to a sufficient accuracy, is found from an observed mean limb-darkening curve. If V is the true velocity at the point considered, the observed velocity is

$$V(x) = \frac{0{\cdot}905I \times V + I(x)V^*(x)}{0{\cdot}905I + I(x)}, \qquad (A\,3)$$

and the values of $V(x)$ at points $0''{\cdot}0$ and $10''{\cdot}0$ arc inside the limb are given in Table A I (*b*). These lead to the results discussed in Section 2.

TABLE A I

(*a*)		(*b*)		
Radial distance outside the limb	Calculated velocity	Radial distance inside the limb	Calculated velocity	Velocity without scattering
$7''{\cdot}5$	1·25 km sec^{-1}	$0''{\cdot}0$	2·03 km sec^{-1}	2·07 km sec^{-1}
$15''{\cdot}0$	0·93	$10''{\cdot}0$	2·02	2·05
$25''{\cdot}0$	0·80			

The only point remaining is to justify the assumption in equations (A 2) and (A 3), that a change in intensity produces a linearly proportional change in velocity. This was done by measuring the effect of blending a spectrum of one intensity and velocity with another of differing intensity and velocity. On a narrow (3 mm) spectrum from a point 20″ arc inside the limb a spectrum of the centre of the disk was superposed directly with the same exposure time, the dark slide of the plate holder and the plate position remaining untouched between the exposures. The intensity of the centre spectrum was reduced to a known fraction of its original intensity by N.P.L. calibrated filters. Each plate also carried an unblended centre spectrum and two unblended limb spectra, taken at the same position as the spectra used for blending, to give the velocity difference between the unblended and superposed spectra. Five plates were taken at the West equatorial limb and four at the East equatorial limb.

TABLE A II

Fraction of central intensity	I_C/I_L per cent	$(V_L-V_B)/(V_L-V_C)$ per cent		Calculated $(V_L-V_B)/(V_L-V_C)$ per cent
0·0117	2	3·2	± 3·1	1·6
·0184	4	0·4	3·0	2·8
·0382	7	6·0	2·3	4·6
·0597	11	6·8	3·3	7·0

Column 1 of Table A II shows the fractions of the centre intensity transmitted by four combinations of filters. From a mean limb-darkening curve, the ratio of the intensity (at 6000 A) of the centre of the disk to that at 20″ arc from the limb is 1·9 so that the values of I_C/I_L given in the second column of the table represent the ratio of the superposed centre intensity to the limb intensity. The whole height of each spectrum was measured on the Evershed machine and the

third column shows the values of $V_L - V_B$ expressed as a percentage of $V_L - V_C$ together with the root mean square error of each measurement. V_B, V_C, V_L are the measured velocities of the blend, centre and mean of the two limb velocities, respectively. A least-squares solution was made for a linear relation between these four pairs of values and the point $I_C/I_L = 0$, $(V_L - V_B)/(V_L - V_C) = 0$. The values obtained from the solution are shown in the last column of the table. For values up to $I_C/I_L = 10$ per cent the representation is obviously adequate. We may, therefore, safely assume that addition to a spectrum, of a small quantity of light of differing velocity results in a fractional change in velocity varying linearly as the fractional change in intensity.

References

(1) M. G. Adam, *M.N.*, **108**, 446, 1948; *Comm. Univ. Obs., Oxford*, No. 26.
(2) W. S. Adams and J. B. Lasby, *Rotation of the Sun. Papers of the Mt. Wilson Observatory*, **1**, Part 1, 1911.
(3) R. E. DeLury, *Ap. J.*, **44**, 177, 1916.
(4) R. E. DeLury, *Jour. R.A.S.C.*, **33**, 345, 1939.
(5) N. C. Dunér, *Nova Acta Regiae Societatis Scientiarum Upsaliensis*, Series 3, **14**, 1890–91.
(6) R. A. Fisher and F. Yates, *Statistical Tables for Biological, Agricultural and Medical Research*, 4th edn., Table VI, Edinburgh, Oliver and Boyd, 1953.
(7) D. R. Hartree, *Numerical Analysis*, p. 152, Oxford, 1952.
(8) H. C. van de Hulst, *Atmospheres of the Earth and Planets*, edited by Kuiper, p. 49, Chicago, 1949.
(9) A. Hunter, *M.N.*, **94**, 594, 1933–34.
(10) J. O. Irwin, *Jour. Royal Statistical Society*, **94**, 284, 1931.
(11) T. D. Kinman, *M.N.*, **113**, 613, 1953; *Comm. Univ. Obs., Oxford*, No. 41.
(12) Mt. Wilson, *Director's reports*, 1910–36.
(13) H. H. Plaskett, *Ap. J.*, **43**, 145, 1916.
(14) H. H. Plaskett, *M.N.*, **99**, 219, 1938–39; *Comm. Univ. Obs., Oxford*, No. 14.
(15) H. H. Plaskett, *M.N.*, **112**, 177, 1952; *Comm. Univ. Obs., Oxford*, No. 33.
(16) H. H. Plaskett, *M.N.*, **112**, 414, 1952; *Comm. Univ. Obs., Oxford*, No. 34.
(17) H. H. Plaskett, *Jour. R.A.S.C.*, **10**, 220, 1916.
(18) J. S. Plaskett, *Ap. J.*, **42**, 373, 1915.
(19) J. S. Plaskett and R. E. DeLury, *Ap. J.*, **37**, 73, 1913.
(20) F. Schlesinger, *Publications of the Allegheny Observatory*, **3**, No. 13, p. 99, 1916.
(21) J. Storey, *M.N.*, **92**, 737, 1931–32.
(22) J. Storey and R. Wilson, *M.N.*, **71**, 674, 1910–11.
(23) A. J. M. Wanders, *Zs. f. Astrophys.*, **8**, 108, 1934.

THEORY OF THE METEOR HEIGHT DISTRIBUTION OBTAINED FROM RADIO-ECHO OBSERVATIONS

I. Shower Meteors

T. R. Kaiser

(Communicated by A. C. B. Lovell)

(Received 1953 August 21)

Summary

Apart from a slight influence of the directional properties of the aerial system, the form of the radio-echo height distribution for a homogeneous velocity group of meteors constituting a stream with a well-defined radiant point is found to be a function only of the atmospheric scale height and the mass distribution of the incident meteors. The relation between these parameters and the width of the height distribution (expressed as the r.m.s. deviation from the mean) is derived, hence if one is known the other may be determined from the observed meteor heights. The mean height corresponds to a value of the atmospheric pressure which is related to the physical properties of the meteors, their ionizing efficiency and velocity, and the radio-echo equipment parameters. The theory enables the observed dependence of the mean height on the velocity to be interpreted in terms of the variation of atmospheric pressure with height.

---

1. *Introduction.*—The passage of a meteor through the atmosphere produces a column of ionization which may be detected by the scattering of radio waves from it. In the absence of distortion of the linear trail (by winds, etc.) the reflection is specular, i.e. the important part of the trail is a length of the order of $\sqrt{(R\lambda)}$ (R = range, λ = wave-length) centred about the normal intersection of a radius vector from the observing station with the trail. We will call this the reflection point. The characteristics of the observed radio echo are dependent primarily upon the electron line density in the trail and on the properties of the atmosphere in the vicinity of the reflection point (**1, 2**).

Clegg and Davidson (**3**) have described an apparatus for determining the elevation and range, and hence the height of the reflection points. The purpose of this paper is to develop a theory of the dependence of the observed height distribution on the properties of the incident meteors and of the atmosphere in the meteor ionization region, and on the parameters of the radio equipment. The discussion is restricted here to a homogeneous velocity group of meteors constituting a stream with a well-defined radiant point.

2. *Theory of meteor ionization.*—In passing through the upper atmosphere, a meteor is subject to individual collisions with air molecules, a great proportion of which are trapped in its surface. The heat liberated causes the meteor to evaporate atoms which leave with thermal velocities relative to the meteor surface but carry the meteor velocity relative to the surrounding atmosphere. Subsequent collisions between meteor atoms and air molecules produce ionization and excitation, mainly of the meteor atoms (**4**).

Herlofson (**5**) and Whipple (**6**) have summarized the modern theory of the motion of a meteoric particle in a rarefied atmosphere, from which we obtain the following expression for the rate of evaporation:

$$n=(\mu H)^{-1}mv\cos\chi(p/p_{\max})[1-\tfrac{1}{2}(p/p_{\max})]^2; \quad (1)$$

$p_{\max}$ is the atmospheric pressure at the point of maximum rate of evaporation and is given by

$$p_{\max}=[(2lg)/(\Lambda v^2 A)]m^{1/3}\cos\chi, \quad (2)$$

where $A=\mathscr{A}m^{-2/3}$, $\mathscr{A}$ is the initial cross-sectional area of the meteor in its line of flight in cm^2 and m is its initial mass in g. It should be noted that A, which Whipple calls the " shape factor ", is independent of m, being a function only of the shape of the meteor and of its density. The other quantities appearing in (1) and (2) are as follows:

n (sec^{-1}) = number of meteor atoms evaporated per second,
v (cm sec^{-1}) = meteor velocity,
μ (g) = mass of an individual meteor atom,
l (erg g^{-1}) = latent heat of evaporation of the meteor,
χ = zenith angle of the meteor radiant,
p (dyne cm^{-2}) = atmospheric pressure,
H (cm) = atmospheric scale height,
g (cm sec^{-2}) = gravitational acceleration,
Λ = heat transfer coefficient.

The heat transfer coefficient (**6**) is defined as the ratio (heat energy liberated)/(air mass intercepted by the meteor $\times\frac{1}{2}v^2$). Herlofson takes $\Lambda=1$, i.e. he assumes that all impinging air molecules are trapped in the meteor surface, while Whipple suggests a value of about 0·7.

In deriving (1) and (2) the deceleration of the meteor is assumed to be small, and approximations have been made which require $v^2\gg 12l$. The error at small velocities mainly affects equation (2). The zenith angle is assumed to be constant along the length of the trail, i.e. $(90^\circ-\chi)$ must be at least several degrees.

The electron line density produced by the meteor is $\alpha=\beta n/v$, where β is the probability that a single evaporated meteor atom will give rise to a free electron; β may be a function of v.

We will restrict ourselves to the case of a meteor shower, comprising a homogeneous velocity group of meteors with a well-defined radiant. Writing

$$k_1=\beta/(\mu H), \quad k_2=2lg/(\Lambda v^2 A)$$

we find that α electrons per cm are produced, at pressure p, by a meteor of mass

$$m=\left[\left(\frac{k_2\alpha}{k_1 p}\right)^{1/2}+\frac{p}{3k_2\cos\chi}\right]^3. \quad (3)$$

3. *The meteor mass distribution.*—Since $p_{\max}$ is a function of the meteor mass, the height distribution will depend upon the mass distribution of the incident meteors.

From a statistical analysis of visual observations Watson (**7**, **8**) and Williams (**9**) have shown that, over a wide range of visual magnitudes, the frequency increases by a constant ratio, a, per magnitude. This leads to the mass frequency law

$$v_M=bm^{-s}, \quad (4)$$

where $\nu_M dm$ is the number of meteors in the mass group $m-(m+dm)$, crossing unit area normal to the stream per second, b is a constant and

$$s = 1 + 2{\cdot}5 \log_{10} a. \tag{5}$$

The above authors give values of a between 2 and 4, hence we may expect s to be in the vicinity of 2.

4. *Radio-echo height distribution.*—In the main part of this discussion we shall assume that the sensitivity of the apparatus is such that the majority of the meteor trails detected have electron line densities less than $10^{12}\,\mathrm{cm}^{-1}$ (short-duration echoes) and take the echo amplitude as directly proportional to α. The case where all echoes are from trails of line density greater than $10^{12}\,\mathrm{cm}^{-1}$ will be dealt with in Section 4.5 below.*

On account of the specular reflection from the trails, all of the echoing points lie in a plane ABCD (Fig. 1) passing through the observing station, O, normal to the radiant direction. The constant height (and pressure) contours are slightly curved lines, SS′, in this plane.

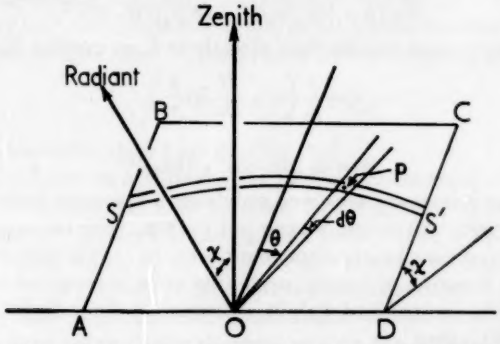

FIG. 1.—*The echo plane ABCD is normal to the radiant direction and is at elevation χ above the horizontal. $\pi/2-\theta$ is the angle in the echo plane, measured from the horizontal.*

4.1. *Height distribution from echoes obtained in the sector $\theta-(\theta+d\theta)$.*—Consider the point P, at height h, in the sector $\theta-(\theta+d\theta)$ of the echo plane (Fig. 1). The minimum electron line density detectable at P is given by

$$\alpha_P = KR^{3/2} S^{-2}(\theta), \tag{6}$$

subject to $\alpha_P < 10^{12}$. $S(\theta)$ represents the aerial polar diagram (amplitude) in the echo plane, $R(\mathrm{cm}) = \mathrm{OP}$, and K is a constant determined by the equipment parameters. It is given (1) by

$$K = 6{\cdot}3 \times 10^{13} (\eta G_m)^{-1} [\epsilon/(P\lambda^3)]^{1/2}, \tag{7}$$

where G_m = aerial power gain (referred to an isotropic radiator) in the direction of the maximum of the beam in the echo plane,

$\lambda(\mathrm{cm})$ = wave-length,

P = peak transmitter power,

ϵ = minimum detectable echo power,

η is a constant which depends on the orientation of the incident electric field vector to the meteor trail. Its value lies between 1·0 for parallel polarization and 2·0 for transverse polarization.

* For a discussion of the variation of echo amplitude and duration with electron line density, see Kaiser and Closs (1); Closs, Clegg and Kaiser (2); and Greenhow (10).

From (3), writing

$$z=(p/k_2)[9\alpha_P\cos^2\chi/(4k_1)]^{-1/3}, \tag{8}$$

we find that the smallest detectable meteor passing through P has a mass

$$m_P=\frac{\alpha_P}{12k_1\cos\chi}(2z^{-1/2}+z)^3. \tag{9}$$

The number of detectable meteors passing per second through unit area at P is obtained by integrating the right-hand side of (4) with respect to m, between limits m_P and infinity. Thus the rate at which meteors will be observed in the sector $\theta-(\theta+d\theta)$, and within the height range $h-(h+dh)$, is $\nu_1\,d\theta\,dh$, where

$$\nu_1=\frac{b}{(s-1)}\left(\frac{12k_1\cos\chi}{\alpha_P}\right)^{s-1}\frac{R}{(R/R_e+\cos\theta\sin\chi)}\frac{1}{(2z^{-1/2}+z)^{3(s-1)}}. \tag{10}$$

R_e is the Earth's radius.

Except for α_P in (8), z varies directly as the pressure. When $z=1$, let $\alpha_P=\alpha_1$, $p=p_1$, $R=R_1$, $h=h_1$. Then

$$z=(p/p_1)(\alpha_1/\alpha_P)^{1/3}=(p/p_1)(R_1/R)^{1/2}.$$

Now R cannot vary more rapidly than directly as h, so putting $R_1/R=h_1/h$ we get

$$z=\frac{p}{p_1}\left(1-\frac{H}{2h_1}\ln\frac{p}{p_1}\right),$$

where

$$p_1=k_2\,[9\alpha_1\cos^2\chi/(4k_1)]^{1/3}. \tag{11}$$

Since meteor echoes are observed only over a few scale heights, with a mean height in the vicinity of 100 km, we can put $z=p/p_1$. For the same reason we find that the only significant height-dependent term in (10) is that containing z and, although R is a function of height, negligible error is involved in putting $R=R_1$ throughout. The normalized height distribution for echoes observed in the sector $\theta-(\theta+d\theta)$ is thus

$$\nu_1{}^*=\left(\frac{3}{2z^{-1/2}+z}\right)^{3(s-1)} \tag{12}$$

and

$$\nu_1\simeq\frac{b}{(s-1)}\left(\frac{4k_1\cos\chi}{9\alpha_1}\right)^{s-1}\frac{R_1}{(R_1/R_e+\cos\theta\sin\chi)}\nu_1{}^*, \tag{13}$$

subject to the restriction that χ does not approach 90°.

In most cases $\cos\theta\sin\chi\gg R_1/R_e$ and

$$\nu_1\simeq\frac{b}{(s-1)}\left(\frac{4k_1\cos\chi}{9\alpha_1}\right)^{s-1}\frac{h_1}{\cos^2\theta\sin^2\chi}\nu_1{}^*. \tag{14}$$

4.2. *Properties of the height distribution* $\nu_1{}^*$.—Putting $x_1=-\ln z$ we have

$$\nu_1{}^*=\left(\frac{3e^{x_1}}{2e^{3x_1/2}+1}\right)^{3(s-1)}, \tag{15}$$

where, for constant scale height,

$$x_1=(h-h_1)/H. \tag{16}$$

Fig. 2 gives $\nu_1{}^*$ as a function of x_1 for a range of values of s. The most probable height occurs at $x=0$, i.e. at height h_1, pressure p_1, and is independent of s. It is easily shown that α_1, the minimum line density detectable at range $R_1=h_1/(\cos\theta\sin\chi)$, is that produced by the meteor which has a maximum rate of

evaporation at pressure p_1. The width of the height distribution is a function only of s and of the scale height.

Due to the slight asymmetry of the height distribution, the mean value of x_1 is not zero. Denoting it by $\bar{x}_1$ we have

$$\bar{x}_1=(\bar{h}-h_1)/H=\frac{\int_{-\infty}^{\infty}x_1\nu_1^*\,dx_1}{\int_{-\infty}^{\infty}\nu_1^*\,dx_1}. \tag{17}$$

The r.m.s. deviation of x_1 from the mean value we will denote by δx_1. Thus

$$(\delta x_1)^2=\frac{\int_{-\infty}^{\infty}(x_1-\bar{x}_1)^2\nu_1^*dx_1}{\int_{-\infty}^{\infty}\nu_1^*\,dx_1}. \tag{18}$$

Both $\bar{x}_1$ and δx_1 are independent of θ, being functions only of s. They have been determined by numerical integration and are given in Fig. 3.

The integral of ν_1^* with respect to x_1 will be of interest for later work concerned with the total meteor echo rate. To a good approximation it is given by

$$\int_{-\infty}^{\infty}\nu_1^*\,dx_1=2{\cdot}3\,(s-1{\cdot}13)^{-1/2}, \tag{19}$$

which is accurate to better than 1 per cent for $s>\frac{4}{3}$.

4.3. *Complete height distribution, polar diagram symmetrical about* $\theta=0$.—The complete height distribution, ν, is obtained by integrating ν_1 with respect to θ, remembering that ν_1^*, through x_1 and h_1, is a function of θ. To avoid confusion, we will let the values of h_1, α_1, p_1 for $\theta=0°$ be denoted by h_m, α_m, p_m, and put $x=(h-h_m)/H$. Thus they are related by the same equations (11) and (16).

Anticipating that the normalized distributions will not be strongly dependent upon the exact form of the polar diagram and on the other θ-dependent terms multiplying ν_1^* in (13) and (14), we will restrict ourselves to consideration of (14) and neglect the variation of h_1 with θ. Thus we can put

$$\alpha_1=\alpha_m[\cos^{3/2}\theta\,S^2(\theta)]^{-1}=\alpha_m f^{-2}(u), \tag{20}$$

where $u=\tan\theta$, $f(u)=\cos^{3/4}\theta S(\theta)$ and α_m is the minimum detectable line density at range $h_m/\cos\chi$ in the direction of the principal maximum of the aerial beam (in the echo plane). Hence ν is proportional to

$$\int_{-\infty}^{\infty}f^{2(s-1)}(u)\,\nu_1^*\,du.$$

Now $$x_1=-\ln(p/p_1)=-\ln(p/p_m)-\ln(p_m/p_1)=x-\tfrac{1}{3}\ln(\alpha_m/\alpha_1).$$

Therefore
$$x_1=x-\tfrac{2}{3}\ln f(u), \tag{21}$$

and
$$\nu(x)\propto\int_{-\infty}^{\infty}\left[\frac{e^x}{2f^{-1}(u)e^{3x/2}+1}\right]^{2(s-1)}du. \tag{22}$$

Mean height

The mean height is given by

$$\bar{x}=(\bar{h}-h_m)/H=\frac{\iint xf^{2(s-1)}(u)\nu_1^*\,du\,dx_1}{\iint f^{2(s-1)}(u)\nu_1^*\,du\,dx_1}, \tag{23}$$

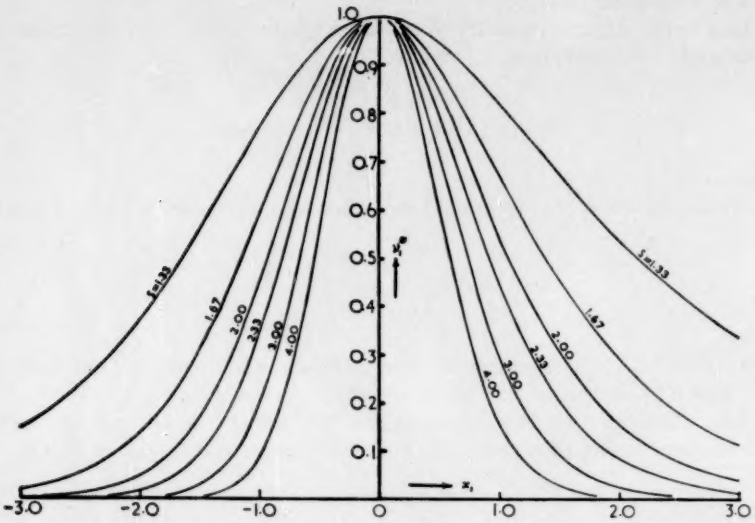

FIG. 2.—*Normalized distribution in height, v_1^*, of echoes observed in the sector $\theta-(\theta+d\theta)$ of the echo plane. $x_1=(h-h_1)/H$.*

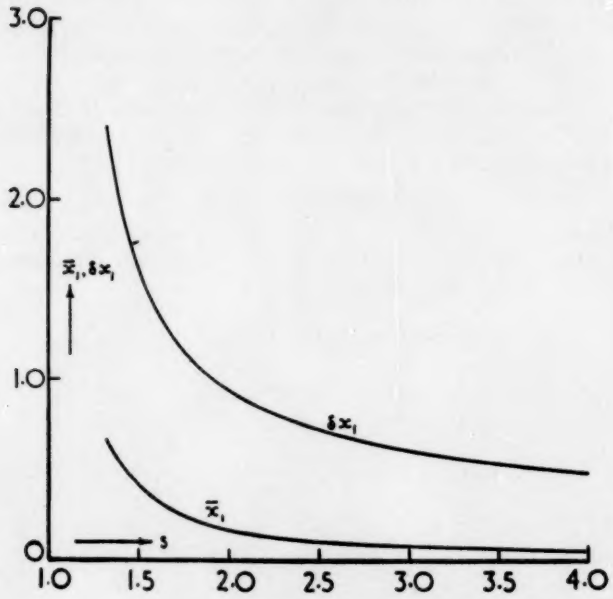

FIG. 3.—*Parameters of the distribution v_1^* as a function of s.*

the integrals being taken for both u and x between $-\infty$ and $+\infty$. Substituting (21) in (23) and remembering that

$$\int_{-\infty}^{\infty} x_1 \nu_1^* \, dx_1 \quad \text{and} \quad \int_{-\infty}^{\infty} v_1^* dx_1$$

are independent of θ, we have

$$\bar{x} - \bar{x}_1 = \frac{2}{\vartheta} \frac{\int_{-\infty}^{\infty} f^{2(\vartheta-1)}(u) \ln f(u) \, du}{\int_{-\infty}^{\infty} f^{2(\vartheta-1)}(u) \, du}. \tag{24}$$

R.m.s. height deviation from the mean

The r.m.s. deviation of x from $\bar{x}$, denoted by δx, is obtained from the elementary height distribution, ν_1^*, through

$$(\delta x)^2 = \frac{\iint (x-\bar{x})^2 f^{2(\vartheta-1)}(u) \nu_1^* \, du \, dx_1}{\iint f^{2(\vartheta-1)}(u) \nu_1^* \, du \, dx_1}.$$

Using the previous expansion (21) for x_1, we find

$$(x-\bar{x})^2 = (x_1-\bar{x}_1)^2 - 2(x_1-\bar{x}_1)(\bar{x}-\bar{x}_1) + (\bar{x}-\bar{x}_1)^2 + \tfrac{4}{\vartheta}(x_1-\bar{x}) \ln f(u) + \tfrac{4}{\vartheta} \ln^2 f(u),$$

leading to

$$(\delta x)^2 = (\delta x_1)^2 - (\bar{x}-\bar{x}_1)^2 + \frac{4}{\vartheta} \frac{\int_{-\infty}^{\infty} f^{2(\vartheta-1)}(u) \ln^2 f(u) \, du}{\int_{-\infty}^{\infty} f^{2(\vartheta-1)}(u) \, du}. \tag{25}$$

The value of (24) and (25) is that they enable the mean height and the r.m.s. height deviation to be evaluated in terms of the corresponding quantities for the elementary distribution ν_1^*, eliminating the necessity for evaluating ν^* explicitly.

Simple physical considerations show that the main effect of the polar diagram on the height distribution derives from the behaviour of $f(u)$ in the vicinity of $u = 0$. For this reason, the parameters of the height distribution have been determined for the following forms of $f(u)$:

(a) $(1+c^2u^2)^{-1}$ (b) $\exp(-c^2u^2)$ (c) $\cos^2 cu$ for $-\pi/2 < cu < \pi/2$ and zero otherwise.

All vary as $(1-c^2u^2)$ for small u but approach zero at different rates as $u \to \infty$. $\bar{x}$ and δx have also been evaluated numerically for $S(\theta) = \cos(\pi/2 \sin\theta)$, which corresponds approximately to the case of a horizontal half-wave dipole spaced $\leqslant \lambda/4$ above a reflecting ground plane. Almost any actual polar diagram will lead to a function $f(u)$ between the limits of (a) and (c). For example, the polar diagrams derived from (a), (b) and (c) for $c^2 = 1{\cdot}61$ are given in Fig. 4 (*a*), with $\cos(\pi/2 \sin\theta)$ (which has the same form near $\theta = 0$) for comparison (curve (*d*)). The case of $c^2 \gg 1$, when we can put $\theta \simeq \sin\theta \simeq \tan\theta$, is given in Fig. 4 (*b*) together with the polar diagram $[\sin(c\sqrt{6}\theta)]/(c\sqrt{6}\theta)$ for comparison (curve (*d*)).

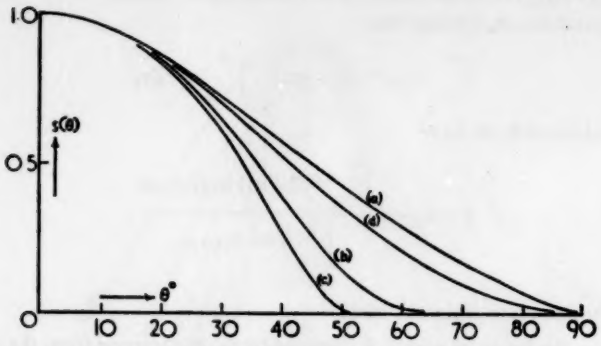

FIG. 4 (*a*).—*Aerial polar diagram, $S(\theta)$, in the echo plane.*
(*a*) $f(u)=(1+1{\cdot}61u^2)^{-1}$, (*b*) $f(u)=\exp(-1{\cdot}61u^2)$, (*c*) $f(u)=\cos^2(1{\cdot}27u)$, (*d*) $S(\theta)=\cos(\pi/2\sin\theta)$.

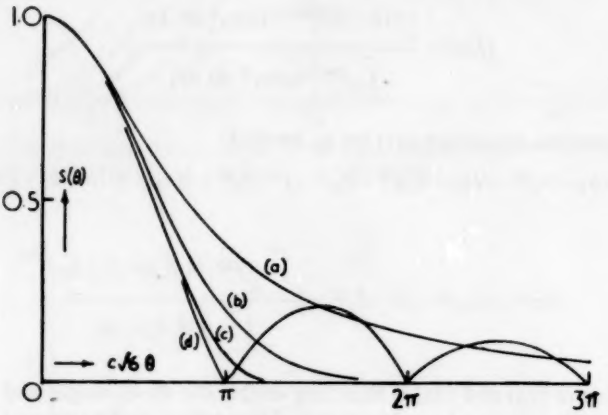

FIG. 4 (*b*).—*Aerial polar diagram, $S(\theta)$, in the echo plane for a beam sufficiently narrow that* $\theta \simeq \sin\theta \simeq \tan\theta$.
(*a*) $f(u)=(1+c^2u^2)^{-1}$, (*b*) $f(u)=\exp(-c^2u^2)$, (*c*) $f(u)=\cos^2(cu)$, (*d*) $S(\theta)=[\sin(c\sqrt{6\theta})]/(c\sqrt{6\theta})$.

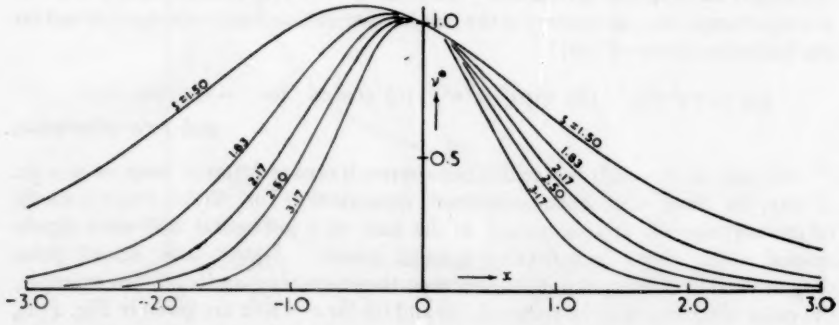

FIG. 5.—*Height distribution, v^*, as a function of x for an aerial polar diagram (in the echo plane) represented by* $f(u)=(1+c^2u^2)^{-1}$. $x=(h-h_m)/H$.

Case (a) $f(u)=(1+c^2u^2)^{-1}$

The integrals which we require for the evaluation of $\bar{x}$ and δx become, using the substitutions $cu=\tan v$, $q=4s-6$,

$$\int_{-\infty}^{\infty} f^{2(s-1)}(u)\,du=\frac{2}{c}\int_0^{\pi/2}\cos^q v\,dv, \tag{26}$$

$$\int_{-\infty}^{\infty} f^{2(s-1)}(u)\ln f(u)\,du=\frac{4}{c}\int_0^{\pi/2}\cos^q v\ln(\cos v)\,dv, \tag{27}$$

$$\int_{-\infty}^{\infty} f^{2(s-1)}(u)\ln^2 f(u)\,du=\frac{8}{c}\int_0^{\pi/2}\cos^q v\ln^2(\cos v)\,dv. \tag{28}$$

For integral values of q, (26) is easily evaluated, and for (27) and (28) we obtain the recurrence formulae:

$$q\int_0^{\pi/2}\cos^q v\ln(\cos v)\,dv=(q-1)\int_0^{\pi/2}\cos^{q-2}v\ln(\cos v)\,dv+\int_0^{\pi/2}\cos^{q-2}v\,dv - \int_0^{\pi/2}\cos^q v\,dv, \tag{29}$$

$$q\int_0^{\pi/2}\cos^q v\ln^2(\cos v)\,dv=(q-1)\int_0^{\pi/2}\cos^{q-2}v\ln^2(\cos v)\,dv +2\int_0^{\pi/2}\cos^{q-2}v\ln(\cos v)\,dv-2\int_0^{\pi/2}\cos^q v\ln(\cos v)\,dv. \tag{30}$$

These integrals have been evaluated numerically for $q=0$, 1.

From (22) the height frequency distribution, normalized to unity at $x=0$, is found to be

$$\nu^*(x)=e^{-x/4}\left[\frac{3e^x}{2e^{3x/2}+1}\right]^{3s-7/2}, \tag{31}$$

which is plotted in Fig. 5 for various values of s.

Case (b) $f(u)=\exp(-c^2u^2)$

Putting $cu=v$, we have

$$\int_{-\infty}^{\infty} f^{2(s-1)}(u)\,du=\frac{2}{c}\int_0^{\infty}e^{-2(s-1)v^2}\,dv,$$

$$\int_{-\infty}^{\infty} f^{2(s-1)}(u)\ln f(u)\,du=-\frac{1}{2c(s-1)}\int_0^{\infty}e^{-2(s-1)\,v^2}\,dv,$$

$$\int_{-\infty}^{\infty} f^{2(s-1)}(u)\ln^2 f(u)\,du=\frac{3}{8c(s-1)^2}\int_0^{\infty}e^{-2(s-1)v^2}\,dv,$$

hence

$$\bar{x}=\bar{x}_1-\frac{1}{6(s-1)}, \tag{32}$$

$$(\delta x)^2=(\delta x_1)^2+\frac{1}{18(s-1)^2}. \tag{33}$$

The function ν^* has not been determined for this case.

Case (c) $f(u)=\cos^2 cu$

Putting $cu=v$, $q=4(s-1)$, we obtain the same equations as for Case (a), namely (26), (27), (28).

Equation (22) is integrable for integral values of $3s-7/2$, giving

$$v^*(x) \propto e^{(3s-7/2)x}\left[\sin^{-1}y - y\sqrt{(1-y^2)}\sum_{n=1}^{3s-7/2}\left(1+\frac{2.4.6....2n}{3.5.7....(2n+1)}y^{2n}\right)\right], \quad (34)$$

where $y=2e^{3x/2}+1$, which is given in Fig. 6 for various values of s.

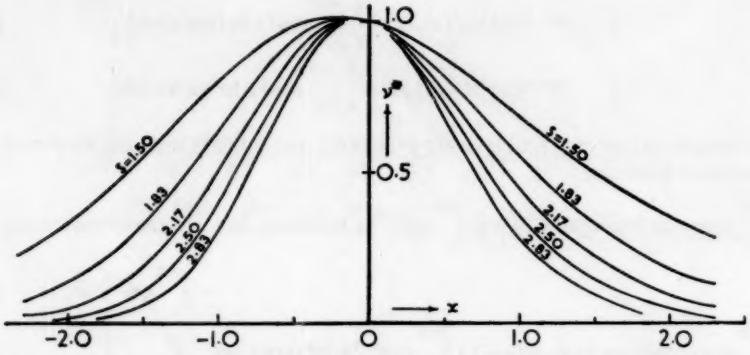

FIG. 6.—*Height distribution, v^*, as a function of x for an aerial polar diagram (in the echo plane) represented by $f(u)=\cos^2 cu$. $x=(h-h_m)/H$.*

Figs. 7 (*a*) and 7 (*b*) show $\bar{x}$ and δx as a function of s for the cases considered above. It will be noted that, as anticipated, the height distribution is remarkably insensitive to the exact form of $f(u)$, and hence of the polar diagram. For the same reason, the complete height distribution for v_1 given by (13) will not be significantly different from those derived above.

4.4. *Complete height distribution, polar diagram symmetrical about $\theta=\theta_0$.*—In this section we will let h_m, α_m, etc., be the values of h_1, α_1, etc., at $\theta=\theta_0$, i.e. as before, the quantities appropriate to the direction of the principal maximum of the aerial beam in the echo plane. Since the foregoing has shown that the height distribution is not critically dependent on the exact form of the function of θ multiplying v_1^* in (13) and (14), we will restrict the discussion to the case of an aerial beam sufficiently narrow that we may write $\alpha_1 \simeq \alpha_m S^{-2}(\theta')$, $\cos\theta \simeq \cos\theta_0$, where $\theta'=\theta-\theta_0$. Hence, from (14),

$$v_1 \simeq \frac{b}{(s-1)}\left(\frac{4k_1\cos\chi}{9\alpha_1}\right)^{s-1}\frac{h_1}{\sin^2\phi}v_1^*, \quad (35)$$

where $\sin\phi=\cos\theta_0\sin\chi$, i.e. ϕ is the elevation of the principal maximum of the beam in the echo plane. Putting $\tan\theta'=u$, $f(u)\simeq S(\theta')$, v^* is given by (22), i.e. is identical with the previous case, and the characteristics of the height distributions for the various $f(u)$ are given by Figs. 5, 6 and 7.

As the elevation ϕ tends to zero, v_1 may be found from (13), which, provided θ_0 does not approach 90°, leads to a result identical with (35) except that the factor $h_1/\sin^2\phi$ is replaced by R_e.

4.5. *Equipment sensitivity such that $\alpha_m \gg 10^{12}$ cm^{-1}.*—We will deal briefly with this case for which only the long-duration echoes are observed.

We proceed as before, except that instead of (6) we find $\alpha_p^{1/4}$ to be proportional to $R^{3/2}S^{-2}(\theta)$ (1). Thus $\alpha_1=\alpha_m[\cos^6\theta\, S^8(\theta)]^{-1}$. Equations (13) and (14) remain

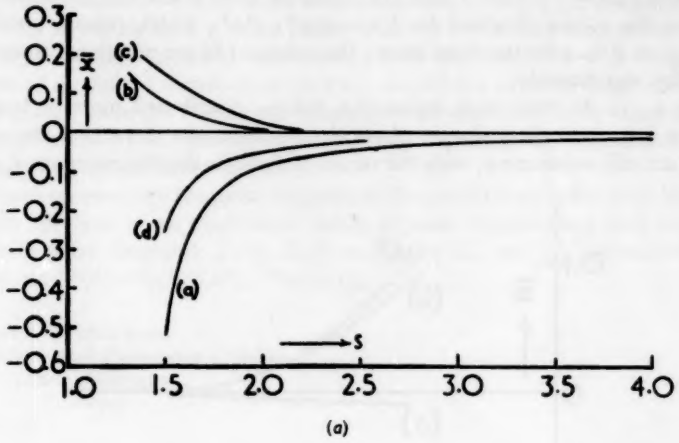

(a)

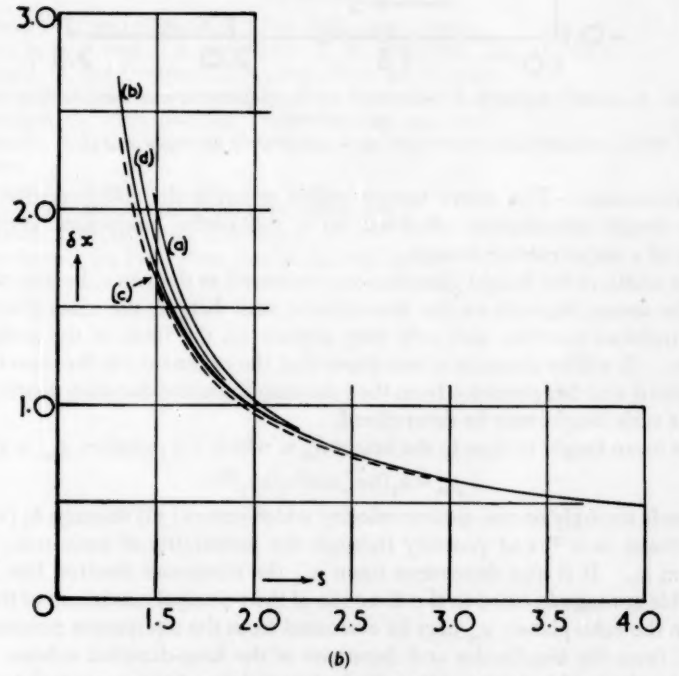

(b)

FIGS. 7 (*a*) *and* (*b*).—*Parameters of the height distribution as a function of s for an aerial polar diagram (in the echo plane) represented by:*

(*a*) $f(u)=(1+c^2u^2)^{-1}$, (*b*) $f(u)=\exp(-c^2u^2)$, (*c*) $f(u)=\cos^2 cu$, (*d*) $S(\theta)=\cos[(\pi/2)\sin\theta]$. *The broken curve in Fig.* 7 (*b*) *gives the r.m.s deviation,* δx_1, *for the elementary distribution* v_1^*.

valid, as does the remainder of the analysis except that $f^4(u)$ replaces $f(u)$ throughout. For $f(u)=(1+c^2u^2)^{-1}$ and $f(u)=\cos^2 cu$ both $\bar{x}$ and δx are more nearly equal to the values obtained for $f(u)=\exp(-c^2u^2)$, which remain unchanged. Fig. 8 gives $\bar{x}$ vs. s for the three cases; the values of δx are not given, since they do not differ significantly.

For α_m in the transition region (i.e. echoes distributed more or less evenly between the two types) simple physical considerations show that the previous results are still satisfactory, with the values of $\bar{x}$ and δx slightly nearer to $\bar{x}_1$ and δx_1.

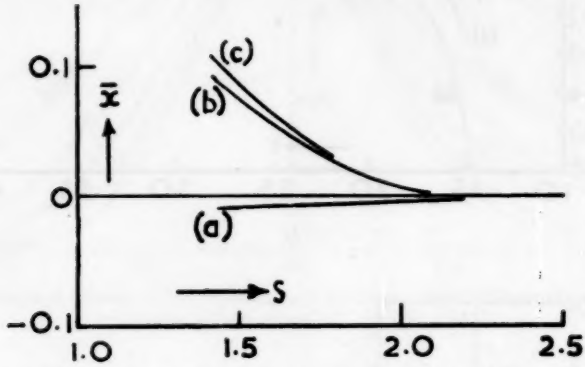

FIG 8.—$\bar{x}=(\bar{h}-h_m)/H$ *as a function of s for an equipment of such low sensitivity that* $\alpha_m \gg 10^{12}\ cm^{-1}$.
(*a*) $f(u)=(1+c^2u^2)^{-1}$, (*b*) $f(u)=\exp(-c^2u^2)$, (*c*) $f(u)=\cos^2 cu$.

5. *Discussion.*—The above theory makes possible the interpretation of the meteor height distribution observed on a radio-echo equipment during the activity of a major meteor stream.

The width of the height distribution, expressed as the r.m.s. height deviation from the mean, depends on the atmospheric scale height, the mass distribution of the incident meteors, and only very slightly on the form of the aerial polar diagram. It will be shown in a later paper that the exponent s in the mass law may be obtained with fair precision from the echo amplitude and duration distributions; thus the scale height may be determined.

The mean height is close to the height h_m at which the pressure, p_m, is given by

$$p_m = k_2[9\alpha_m \cos^2\chi/4k_1]^{1/3}. \tag{36}$$

It depends strongly on the meteor velocity which enters (36) through k_2 (which is proportional to v^{-2}) and possibly through the probability of ionization, β, contained in k_1. It is also dependent upon α_m, the minimum electron line density detectable at range $h_m/\sin\phi$ in the direction of the principal maximum of the aerial beam in the echo plane; α_m may be evaluated from the equipment parameters or derived from the amplitudes and durations of the long-duration echoes. Thus p_m can be obtained in terms of the physical properties of the meteors (latent heat, density, velocity), the radiant zenith angle χ, the heat transfer coefficient and the probability of ionization. The latter need not be known with great accuracy, since it enters (36) as the cube root.

The zenith angle χ has been treated throughout as constant. It is thus desirable that the height distribution be measured over a selected time interval

during the passage of the radiant across the sky, sufficiently short that the variation of χ may be neglected. This is not a severe restriction, since p_m is proportional to $\cos^{2/3}\chi$. As an example, if χ varies from 35° to 55°, the mean height changes by about 0·25 scale heights and if observations were extended over this range of χ, the width of the height distribution for $s \sim 2$, would not be more than some three per cent greater than the theoretical values derived above. The assumption of a well-defined radiant point merely requires the spread in meteor radiants to be small compared with the aerial beam width.

We have represented the polar diagram of the aerial beam in the echo plane by $S(\theta)$. In the case of an equipment using separate transmitting and receiving aerials with polar diagrams $S_T(\theta)$, $S_R(\theta)$ and gains G_T and G_R respectively, we simply write $S^2(\theta) = S_T(\theta)\, S_R(\theta)$, $G^2 = G_T\, G_R$.

University of Manchester,
Jodrell Bank Experimental Station,
Lower Withington,
Cheshire:
1953 *July*.

References

(1) Kaiser, T. R. and Closs, R. L., *Phil. Mag.*, **43**, 1, 1952.
(2) Closs, R. L., Clegg, J. A. and Kaiser, T. R., *Phil. Mag.*, **44**, 313, 1953.
(3) Clegg, J. A. and Davidson, I. A., *Phil. Mag.*, **41**, 77, 1950.
(4) Kaiser, T. R. and Greenhow, J. S., *Proc. Phys. Soc.* B, **66**, 150, 1953.
(5) Herlofson, N., *Phys. Soc. Rep. Prog. Phys.*, **11**, 444, 1948.
(6) Whipple, F. L., *Advances in Geophysics*, I, p. 119, Academic Press Inc., New York, 1952.
(7) Watson, F., *Harv. Ann.*, **105**, 623, 1937.
(8) Watson, F., *Between the Planets*, Blakiston, 1941.
(9) Williams, J. D., *A.J.*, **92**, 424, 1940.
(10) Greenhow, J. S., *Proc. Phys. Soc.* B, **65**, 169, 1952.

THEORY OF THE METEOR HEIGHT DISTRIBUTION OBTAINED FROM RADIO-ECHO OBSERVATIONS

II. Sporadic Meteors

T. R. Kaiser

(Communicated by A. C. B. Lovell)

(Received 1953 August 21)

Summary

The theory of the meteor height distribution is extended to the case of a selected velocity group of sporadic meteors.

The width of the height distribution (r.m.s. deviation from the mean) is determined as a function of the atmospheric scale height and the mass distribution of the incident meteors. This latter is shown to be almost exactly inverse square. For a given velocity the mean height is shown to occur at a value of the atmospheric pressure which is related to the physical properties of the meteors and of the ionization process and to the radio-echo equipment parameters.

The measurement of meteor heights by the radio-echo technique is suggested as a new and important method for determination of the atmospheric pressure and scale height in the meteor ionization region.

---

1. *Introduction.*—In Part I (1) we have derived the height distribution of radio echoes from the trails formed by meteors belonging to a homogeneous velocity group, constituting a stream with a well-defined radiant point. In this paper the theory is extended to the case of a selected velocity group of meteors whose radiants are distributed over the celestial sphere. On account of the specular reflection property of the trails, only those meteors will be observed whose radiant points correspond to echo planes intersecting the aerial beam. Thus, referring to Fig. 1, the radiant points of meteors observed in the conical element of solid angle of half angle ψ must lie within the shaded strip of the celestial sphere of width 2ψ.

We will make the assumption that the geocentric radiants are uniformly distributed over the celestial sphere. At any instant, the radiants for a given velocity group will in fact tend to be concentrated about the apex of the Earth's way to an extent dependent upon the heliocentric radiant and velocity distributions. However, if the meteors are observed over an extended period of time from a station in northern latitudes with an aerial beam directed northwards, the instantaneous radiant distribution will sweep across the shaded region of Fig. 1 and the effect will be similar to the case of a uniform distribution. In any case, the relatively small differences between the results obtained in the following for sporadic meteors and those given in Part I for shower meteors show that the height distribution is not very sensitive to the exact form of the radiant distribution.

On the above assumptions, the flux of meteors per second crossing unit area normal to their direction of motion, with velocities v to $(v+dv)$, masses m to $(m+dm)$ and with radiants within a solid angle $d\Omega$ is $\nu_M\, dv\, dm\, d\Omega$, where, as in Part I, we may write

$$\nu_M = b(v)m^{-s}. \tag{1}$$

The discussion in this paper is restricted to the case of a radio-echo equipment with sensitivity such that echoes from trails with electron line densities less than 10^{12} cm^{-1} may be detected over most of the solid angle covered by the aerial beam. Thus the minimum detectable electron line density at a point P, distant R cm from the observer, is (2)

$$\alpha_P = KR^{3/2}S^{-2}(\phi, \vartheta), \tag{2}$$

where ϕ, ϑ are respectively the elevation and azimuth of P relative to the observer, the zero of ϑ being chosen as the optimum azimuthal direction of the aerial beam.

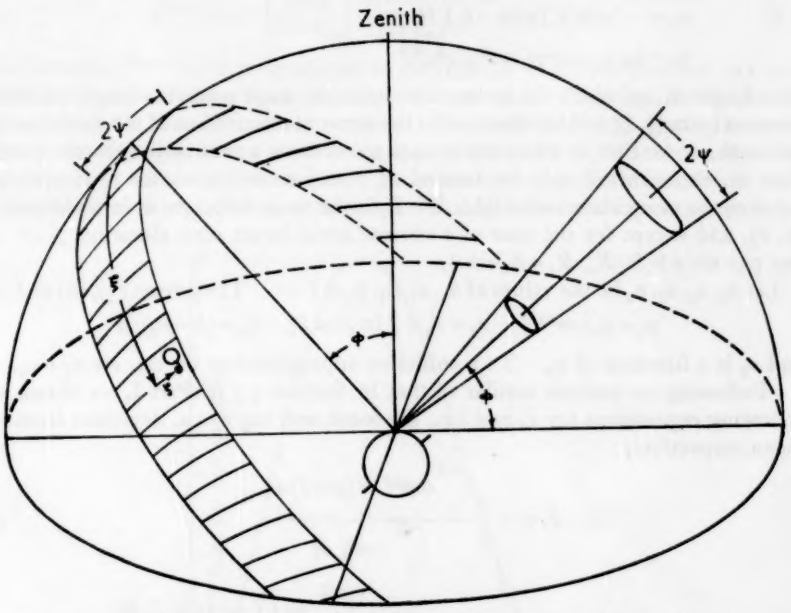

FIG. 1.—*Meteors observed in the conical element of the aerial beam with semi-angle ψ have radiant points Q (coordinates (ξ, ζ)) within the shaded strip of the celestial sphere.*

$S(\phi, \vartheta)$ is the aerial polar diagram (amplitude) and is normalized to unity at $(\phi_m, 0)$, K is as defined in (7) of Part I, the gain G_m referring to the direction $(\phi_m, 0)$. The elevation, ϕ_m, will be taken as the maximum of the distribution of echo elevations. It is not, in general, identical with the elevation of the aerial beam maximum (especially for a vertically directed beam), hence on the above definition the maximum value of $S(\phi, \vartheta)$ may be greater than unity.

2. *Meteors observed in a cone of solid angle $d\omega$ at elevation ϕ.*—We will first consider those meteors, radiating from the element $d\xi\, d\zeta$ at Q on the celestial sphere, which are observed in the narrow cone of half angle ψ at elevation ϕ (Fig. 1).

The rate of echoes from meteors with velocities v to $(v+dv)$ observed in a sector θ to $(\theta+d\theta)$ of the echo plane corresponding to Q (see Fig. 1, Part I) and in the height range h to $(h+dh)$ is $\nu_1\,dv\,dh\,d\theta\,d\xi\,d\zeta$, where ν_1 is given by equation (13) of Part I. Now the cone intercepts an angle $2(\psi^2-\zeta^2)^{1/2}$ of the echo plane, hence, by putting $\cos\chi=\cos\phi\cos\xi$, where χ is the zenith angle of Q, $\pi\psi^2=d\omega$, in (13) of Part I and integrating with respect to ξ and ζ, the rate of echoes observed in an element of solid angle $d\omega$, having coordinates (ϕ,ϑ), in the height range h to $(h+dh)$, is $\nu_2\,dv\,dh\,d\omega$, where, in the notation of Part I,

$$\nu_2\simeq\frac{b(v)}{(s-1)}\left(\frac{4k_1\cos\phi}{9\alpha_1}\right)^{s-1}\frac{R_1}{(R_1/R_e+\sin\phi)}\int_{-\pi/2}^{\pi/2}\cos^{s-1}\xi\nu_1^*\,d\xi, \tag{3}$$

$$\nu_1^*(x_1)=\left[\frac{3e^{x_1}}{2e^{3x_1/2}+1}\right]^{3(s-1)}, \tag{4}$$

$$\alpha_1=KR_1^{3/2}S^{-2}(\phi,\vartheta), \tag{5}$$

$$x_1=-\ln(p/p_1)=(h-h_1)/H, \tag{6}$$

$$p_1=k_2(9\alpha_1\cos^2\phi\cos^2\xi/4k_1)^{1/3}. \tag{7}$$

The height h_1, at which the pressure is p_1, is the most probable height at which meteors from (ξ,ζ) will be observed in the element $d\omega$. Thus h_1 is a function of ξ although, as in Part I, wherever it appears only as a multiplying factor (rather than an exponent) it may be treated as constant and taken as approximately equal to the mean observed height, $\bar{h}$. R_1 is the range to height h_1 in the direction (ϕ,ϑ), and except for the case of a narrow aerial beam with elevation $\lesssim 10°$ we can put $\sin\phi\gg R_1/R_e$, $R_1=h_1/\sin\phi$.

Let h_2, α_2, x_2, p_2 be the values of h_1, α_1, x_1, p_1 at $\xi=0$. Thus, from (5), (6) and (7),

$$p_1=p_2\cos^{2/3}\xi,\quad x_1=x_2+\tfrac{2}{3}\ln(\cos\xi),\quad x_2=(h-h_2)/H$$

and ν_2 is a function of x_2. To a sufficient approximation we can set $\alpha_1=\alpha_2$.

Following an analysis similar to that in Section 4.3 of Part I, we obtain the following expressions for $\bar{x}_2$ and δx_2, the mean and the r.m.s. deviation from the mean respectively:

$$\bar{x}_2-\bar{x}_1=-\frac{2}{3}\frac{\int_0^{\pi/2}\cos^q\xi\ln(\cos\xi)\,d\xi}{\int_0^{\pi/2}\cos^q\xi\,d\xi}, \tag{8}$$

$$(\delta x_2)^2-(\delta x_1)^2=-(\bar{x}_2-\bar{x}_1)^2+\frac{4}{9}\frac{\int_0^{\pi/2}\cos^q\xi\ln^2(\cos\xi)\,d\xi}{\int_0^{\pi/2}\cos^q\xi\,d\xi}, \tag{9}$$

where $q=s-1$. The quantities $\bar{x}_1$ and dx_1, which refer to the function $\nu_1^*(x_1)$, have been evaluated in connection with the shower meteor height distribution (see Part I), as have the integrals in (8) and (9), for a range of values of q.

3. *Complete sporadic meteor height distribution.*—From (3), making the approximation $\sin\phi\gg R_1/R_e$, we may write

$$\nu_2(x_2)\propto(\cos\phi/\alpha_2)^{s-1}\sin^{-2}\phi\,\nu_2^*(x_2), \tag{10}$$

where ν_2^* is normalized to unity at $x_2=0$. The complete height distribution, ν, is obtained by integrating (10) with respect to ϕ and ϑ, remembering that α_2

is a function of (ϕ, ϑ). The aerial polar diagram function $S(\phi, \vartheta)$ can in most cases be adequately represented as a product $S_e(\phi)S_a(\vartheta)$ of the polar diagram functions in the principal planes of the beam. Thus $S_a(0)=S_e(\phi_m)=1$.

Let the values of h_2, α_2, p_2 in the direction $(\phi_m, 0)$ be h_m, α_m, p_m and put $x=(h-h_m)/H$. Now α_2 is the minimum line density detectable at range $h_2/\sin\phi$ in the direction (ϕ, ϑ), thus, neglecting the small dependence of h_2 on (ϕ, ϑ), we obtain, using (5),

$$\alpha_2=\alpha_m(\sin\phi_m/\sin\phi)^{3/2}S_e^{-2}(\phi)S_a^{-2}(\vartheta). \tag{11}$$

From (10) and (11), with $d\omega=\cos\phi\, d\phi\, d\vartheta$, we obtain, for the complete height distribution,

$$\nu(x)\propto\int_0^{\pi/2}\int_{-\pi}^{\pi}[F(\phi)S_a(\vartheta)]^{2(s-1)}\nu_2^{s}(x_2)\, d\phi\, d\vartheta, \tag{12}$$

where

$$F^{2(s-1)}(\phi)=\left(\frac{\cos\phi}{\cos\phi_m}\right)^{s}\left(\frac{\sin\phi}{\sin\phi_m}\right)^{(3s-7)/2}S_e^{2(s-1)}(\phi). \tag{13}$$

The function $F^{2(s-1)}(\phi)$ is proportional to the number of echoes observed per unit elevation interval; thus ϕ_m is the elevation at which $F(\phi)$ has its maximum value, which we have normalized to unity. It is clear from (13) that ϕ_m is not in general the elevation of the aerial beam maximum, however, it becomes approximately so for a narrow elevated beam. As an example, the theoretical distribution in elevation of echoes observed with a horizontal half-wave dipole situated $\lambda/4$

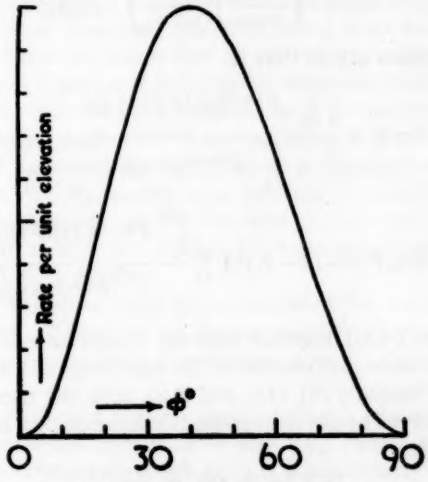

FIG. 2.—*Theoretical distribution in elevation of sporadic meteors observed with a half-wave dipole aerial situated $\lambda/4$ above ground.*

above a reflecting surface, for $s=2$, is given in Fig. 2. In this case $\phi_m\simeq 40°$, whereas the maximum of the aerial polar diagram is at $\phi=90°$. The form of $F(\phi)$ will not, in general, depend strongly on s.

The mean value of x $(=\bar{x})$ and the r.m.s. deviation from the mean can be evaluated in two steps.

Let

$$\nu_3^*(x_3) \propto \int_{-\pi}^{\pi} S_a^{2(s-1)}(\vartheta)\nu_2^*(x_2)\,d\vartheta, \tag{14}$$

and let h_3, α_3, x_3, p_3 be the values of h_2, α_2, x_2, p_2 at $\vartheta = 0$. From (5), (6), (7),

$$\alpha_2 = \alpha_3 S_a^{-2}(\vartheta), \quad p_2 = p_3 S_a^{-2/3}(\vartheta), \quad x_2 = x_3 - \tfrac{2}{3}\ln S_a(\vartheta), \quad x_3 = (h-h_3)/H,$$

hence, following Section 4.3 of Part I,

$$\bar{x}_3 - \bar{x}_2 = \frac{2}{3}\frac{\int_{-\pi}^{\pi} S_a^{2(s-1)}(\vartheta)\ln S_a(\vartheta)\,d\vartheta}{\int_{-\pi}^{\pi} S_a^{2(s-1)}(\vartheta)\,d\vartheta}, \tag{15}$$

$$(\delta x_3)^2 - (\delta x_2)^2 = -(\bar{x}_3 - \bar{x}_2)^2 + \frac{4}{9}\frac{\int_{-\pi}^{\pi} S_a^{2(s-1)}(\vartheta)\ln^2 S_a(\vartheta)\,d\vartheta}{\int_{-\pi}^{\pi} S_a^{2(s-1)}(\vartheta)\,d\vartheta}. \tag{16}$$

Finally, we have

$$\nu(x) \propto \int_0^{\pi/2} F^{2(s-1)}(\phi)\nu_3^*(x_3)\,d\phi. \tag{17}$$

Using (6), (7) and (11), we obtain

$$p_3 = p_m G^{-2/3}(\phi), \quad x_3 = x - \tfrac{2}{3}\ln G(\phi),$$

where

$$G(\phi) = \left(\frac{\cos\phi_m}{\cos\phi}\right)\left(\frac{\sin\phi}{\sin\phi_m}\right)^{3/4} S_s(\phi); \tag{18}$$

hence, following Section 4.3 of Part I,

$$\bar{x} - \bar{x}_3 = \frac{2}{3}\frac{\int_0^{\pi/2} F^{2(s-1)}(\phi)\ln G(\phi)\,d\phi}{\int_0^{\pi/2} F^{2(s-1)}(\phi)\,d\phi}, \tag{19}$$

$$(\delta x)^2 - (\delta x_3)^2 = -(\bar{x} - \bar{x}_3)^2 + \frac{4}{9}\frac{\int_0^{\pi/2} F^{2(s-1)}(\phi)\ln^2 G(\phi)\,d\phi}{\int_0^{\pi/2} F^{2(s-1)}(\phi)\,d\phi}. \tag{20}$$

Equations (9), (16), (20), together with the computed value of δx_1, determine the r.m.s. height deviation, δx (in units of the scale height), for a given aerial polar diagram $S(\phi, \vartheta)$. Similarly (8), (15) and (19), with the computed value of $\bar{x}_1$, enable the mean observed height to be related to the height h_m, at which the pressure is given, from (7), by

$$p_m = k_2[9\alpha_m \cos^2\phi_m/4k_1]^{1/3}, \tag{21}$$

where

$$\alpha_m = K(h_m/\sin\phi_m)^{3/2}. \tag{22}$$

Since α_m appears in (21) as the cube root (and since $\bar{h}$ differs only slightly from h_m), it may be taken as the minimum detectable line density at range $\bar{h}/\sin\phi_m$ in the direction $(\phi_m, 0)$. The function $F(\phi)$ will in general be approximately symmetrical about ϕ_m, which may therefore be taken as the mean observed elevation.

3.1. *Beamed aerial system.*—As in Part I, we will assume various forms for the aerial polar diagram and evaluate $\bar{x}$ and δx as a function of s. We consider here the case of an elevated aerial beam with zero (or low) gain at $\phi = 0°$, $90°$; thus ϕ_m will correspond approximately to the beam maximum and the controlling factor in the expressions for $F(\phi)$, $G(\phi)$ is $S_e(\phi)$. We will anticipate that the values of $\bar{x}$ and δx will not be strongly dependent on the exact form of these functions, and put $F(\phi) = G(\phi)$ (as the beam width tends to zero, both $F(\phi)$ and $G(\phi)$ tend to $S_e(\phi)$).

In order to obtain an estimate of the variation of the parameters of the height distribution with the form of the aerial polar diagram, we will consider several cases which between them should encompass the range of variation likely to be met with in practice (see Part I). They are:

$$\left.\begin{array}{lll} \text{(a)} & F(\phi) = (1 + c_e^2\phi'^2)^{-1}, & S_a(\vartheta) = (1 + c_a^2\vartheta^2)^{-1}, \\ \text{(b)} & F(\phi) = \exp(-c_e^2\phi'^2), & S_a(\vartheta) = \exp(-c_a^2\vartheta^2), \\ \text{(c)} & F(\phi) = \cos^2(c_e\phi'), & S_a(\vartheta) = \cos^2(c_a\vartheta), \end{array}\right\} \qquad (23)$$

where $\phi' = \phi - \phi_m$, c_e and c_a are constants determining the beam width, and in (c) the functions are as specified for $c_e\phi'$ and $c_a\vartheta$ between $-\pi/2$ and $\pi/2$ and are zero otherwise.

The integrals appearing in (8), (9), (15), (16), (19) and (20) for the above cases have been evaluated in connection with the shower meteor height distribution. The resulting values of the parameters $\bar{x}$ and δx are given in Figs. 3(*a*) and 3(*b*) for a range of values of s.

It is apparent from Fig. 3 that the lower the mean height in relation to h_m, the greater is the r.m.s. deviation, the effect being most marked for the smaller values of s. The reason for this is that an aerial beam which falls slowly to zero at its extremities (e.g. Case (a) of (23)) tends to see relatively more large meteors which occur, in the main, below the maximum of the height distribution. This trend is also noticeable in the case of shower meteors discussed in Part I.

3.2. *Horizontal half-wave dipole, $\lambda/4$ above a reflecting surface.*—In this case we cannot express $S(\phi, \vartheta)$ exactly as a product $S_e(\phi) \cdot S_a(\vartheta)$; however, to a sufficiently good approximation we can take $S_e(\phi) = S(\phi, 0)$, $S_a(\vartheta) = S(\phi_m, \vartheta)$, where $\phi_m \simeq 40°$. Although when $\phi = \pi/2$, $G(\phi)$ now goes to infinity, the integrands in (19) and (20) all go to zero.

The values of $\bar{x}$ and δx have been computed for $s = 2{\cdot}0$ and are given in Figs. 3(*a*) and 3(*b*). These points do not quite fit the general trend referred to in Section 3.1, the reason being that whereas $\phi_m = 40°$, the aerial beam maximum is at $\phi = 90°$.

4. *Height distribution for meteors observed within a selected elevation interval.*—By selecting a narrow elevation interval about ϕ_m (which in this case need not necessarily be the elevation at which $F(\phi)$ is a maximum) we can eliminate the final step in Section 3 which requires knowledge of $S_e(\phi)$, $F(\phi)$ and $G(\phi)$. It is sufficient to restrict the range of ϕ to that for which $G(\phi)$ is substantially constant (say, to within 30 per cent), in which case the expressions on the right-hand sides of (19) and (20) are negligible and $\nu^* = \nu_3^*$, $\bar{x} = \bar{x}_3$, $\delta x = \delta x_3$, which can be evaluated from (15) and (16) with $S_a(\vartheta) = S(\phi_m, \vartheta)$.

The parameters of the height distribution are given in Figs. 4(*a*) and 4(*b*) for the three forms of $S_a(\vartheta)$ defined in (23), as well as for a horizontal half-wave dipole, $\lambda/4$ above ground (in this latter case for $s = 2{\cdot}0$ only).

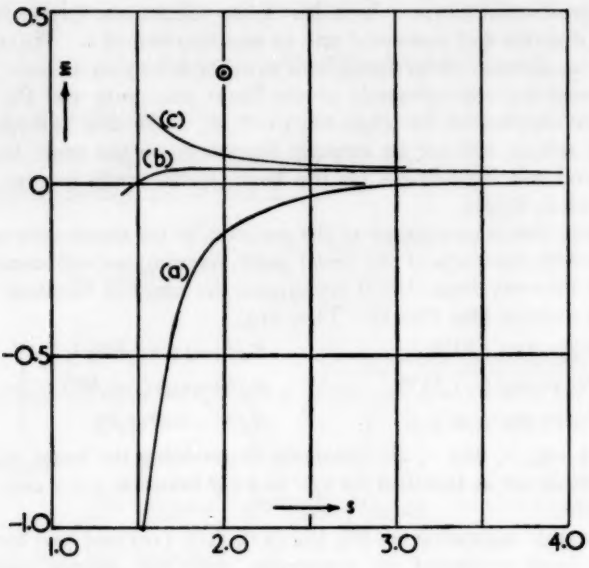

(a)

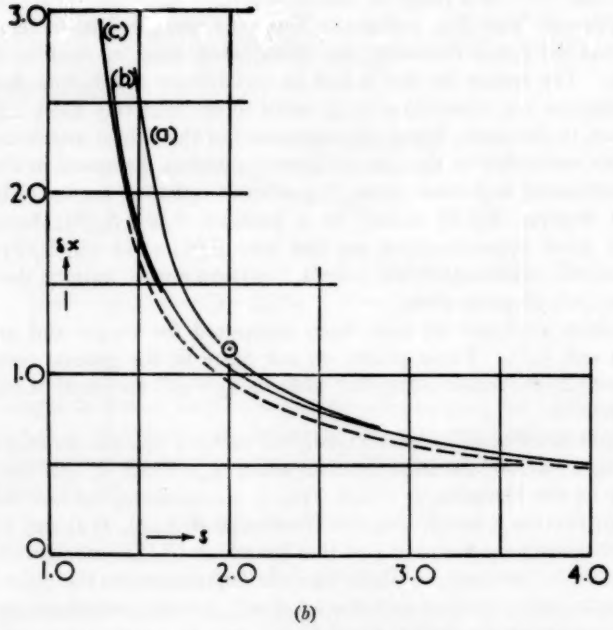

(b)

FIGS. 3 (a) and (b).—*Parameters of the sporadic meteor height distribution.*
(a), (b), (c)—*Aerial polar diagram defined by* (23) (a), (b), (c) *respectively.*
⊙—*Half-wave dipole aerial,* $\lambda/4$ *above ground.*
The broken curve in Fig. 3 (b) *is the r.m.s. deviation,* δx_1, *for the elementary distribution* ν_1^*.

It will be noted that if the azimuths of the meteors were also known, the effect of the aerial polar diagram could be completely eliminated by selecting, in addition, a sufficiently narrow range of ϑ, in which case $\bar{x}=\bar{x}_2$, $\delta x=\delta x_2$. It would seem, however, that this would unnecessarily complicate the experimental apparatus.

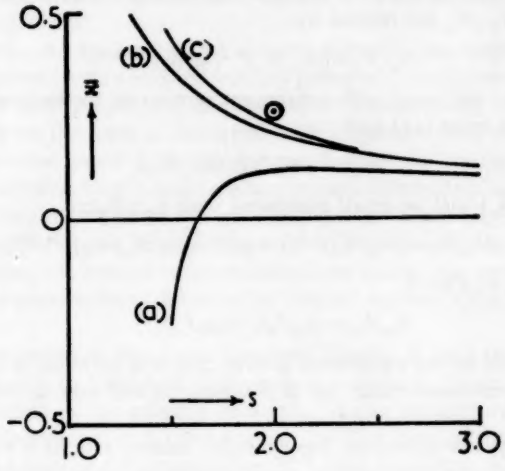

(*a*)

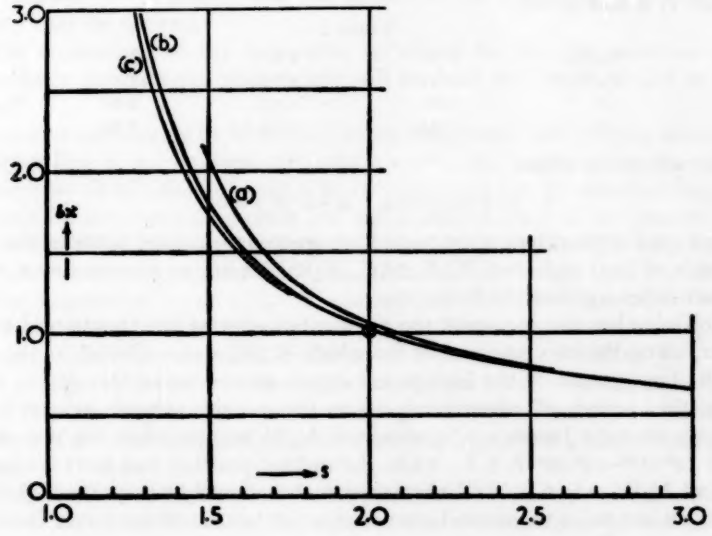

(*b*)

FIG. 4 (*a*) *and* (*b*).—*Parameters of the height distribution of sporadic meteors observed in a selected elevation interval.*
(*a*), (*b*), (*c*)—*Azimuthal aerial polar diagram defined as in* (23) (*a*), (*b*), (*c*) *respectively.*
⊙—*Half-wave dipole aerial,* $\lambda/4$ *above ground* (*selected elevation* $\phi_m=40°$).

5. *Sporadic meteor mass distribution.*—The total observed echo rate, N sec^{-1}, can be related to the incident flux of meteors by integrating (3) with respect to v, h, ϕ, ϑ, over the complete range of variation of these quantities.

If we have two equipments, A and B, with aerials of identical polar diagram, but with sensitivities defined by K_a and K_b, then using (3) and (5) with $h_1 \simeq \bar{h}$, the echo rates N_a ,N_b are related by

$$N_a/N_b = (K_b/K_a)^{s-1}(\bar{h}_b/\bar{h}_a)^{(3s-5)/2}.$$

The mean height will vary with equipment sensitivity to the same extent as the height h_m, hence from (21) and (22)

$$\bar{h}_b \simeq \bar{h}_a + \tfrac{1}{3}H \ln (K_a/K_b),$$

and since $(\bar{h}_b - \bar{h}_a)$ will be small compared with $\bar{h}_a \simeq \bar{h}_b \simeq \bar{h}$,

$$N_a/N_b = (K_b/K_a)^{s-1}[1 + \tfrac{1}{3}(H/\bar{h}) \ln (K_a/K_b)]^{(3s-5)/2}, \tag{24}$$

where, from (7) of Part I,

$$K_a/K_b = (\epsilon_a P_b \lambda_b{}^3)/(\epsilon_b P_a \lambda_a{}^3). \tag{25}$$

The second factor in the right-hand side of (24) will be close to unity, hence we may use an approximate value for $H/\bar{h}$ which we will take as 0·07 ($\bar{h} \sim 100$ km, $H \sim 7$ km).

McKinley (3) has measured the sporadic meteor rate as a function of transmitter power (in one case with a small change in wave-length). The results, together with the values of s derived from them (using (24)), are given in Table I. The parameter, a, which defines the meteor magnitude distribution (see equation (5), Part I) is also given.

TABLE I

K_b/K_a	2·5	4·0	43
N_a/N_b	2·53	3·79	45
s	2·02	1·97	2·02
a	2·54	2·44	2·54

We will adopt the values

$$s = 2{\cdot}00 \pm 0{\cdot}02, \quad a = 2{\cdot}51 \pm 0{\cdot}04. \tag{26}$$

To a good approximation we could have ignored the second factor on the right-hand side of (24) and used $N_a/N_b \simeq (K_b/K_a)^{s-1}$ leading to $s = 1{\cdot}99 \pm 0{\cdot}02$, which does not differ significantly from (26).

McKinley has also measured the relative rates during the Quadrantid meteor shower, using the two equipments for which $K_b/K_a = 43$. Owing to the large sporadic background on the high-power equipment he found that N_a/N_b varied during the period of observation. For the period 09^h 00^m–24^h 00^m E.S.T. (Canada) on 1951 January 3 he obtained $N_a/N_b = 25{\cdot}2$, while for the shorter period 12^h 00^m–19^h 00^m E.S.T., when the radiant position was most favourable, he found $N_a/N_b = 19{\cdot}6$. McKinley states that the hourly rate on the high-power equipment was twice the normal sporadic rate for the same hours during December and January. Depending upon the period of observation to which this applies, the true ratio for Quadrantid meteors becomes either 17·5 or 12·5, leading to $s = 1{\cdot}76$, $a = 2{\cdot}02$ or $s = 1{\cdot}67$, $a = 1{\cdot}85$ respectively.

In the above we have assumed that all of the equipments used by McKinley were capable of detecting the short-duration decay-type echoes over most of the

solid angle covered by the aerial polar diagram. That this must be so is indicated by the good agreement between the values of s deduced for the three different sensitivity ratios (Table I). Confirmation is provided by the values of α_m for the various equipments calculated from McKinley's data (with $\phi_m = 40°$, $G_m = 2{\cdot}1$ for the dipole aerial $\lambda/4$ above ground, $\bar{h} \sim 95$ km, $\eta = 1{\cdot}0$), namely 10^{10}, $2{\cdot}5 \times 10^{10}$, $4{\cdot}0 \times 10^{10}$, $4{\cdot}3 \times 10^{11}$ cm^{-1}.

6. *Discussion.*—As in the case of shower meteors, the width of the height distribution observed with a selected velocity group of sporadic meteors depends on the atmospheric scale height and the mass distribution of the incident meteors, but only slightly on the form of the aerial polar diagram. For the assumed mass distribution (inverse power law) it is independent of the equipment sensitivity. Since an accurate value for the exponent in the mass distribution has been obtained, the radio-echo height measurements provide a powerful technique for determination of the atmospheric scale height in the meteor ionization region. The complete height distribution, ν^*, has not been evaluated explicitly; however, it is clear that it will be of the same general form as for shower meteors (Part I), but slightly wider.

The relation between the mean observed height, $\bar{h}$, and the height, h_m, at which the pressure is p_m (equation (21)) has been evaluated. Since $k_2 \propto v^{-2}$ (Part I), p_m depends strongly on the selected velocity. It also depends on the probability of ionization, β (contained in k_1) and upon α_m. The form of the pressure-height variation may be obtained by integrating H^{-1} with respect to height, hence it is necessary to know β for one velocity only in order to obtain the pressure variation over a range of heights (limited by the range of meteor velocities, which is about 20–60 km sec^{-1}). It follows that the probability of ionization as a function of velocity may be derived.

The application of the radio-echo technique to the determination of the atmospheric pressure and scale height will be dealt with by S. Evans in a later paper.*

From measurements by McKinley, using equipments with varying sensitivities corresponding to α_m between 10^{10} and 4×10^{11}, the exponent in the sporadic meteor mass distribution is found to be $s = 2{\cdot}00 \pm 0{\cdot}02$, i.e. the absolute frequency increases by $a = 2{\cdot}51 \pm 0{\cdot}04$ times per visual magnitude. If we assume that a meteor of zenithal magnitude $+5$ produces about 10^{12} electrons per cm, then it is clear that the inverse-square mass law must hold accurately over the range of zenithal magnitudes $+5$ to $+10$. The above result is in good agreement with the most recent value given for telescopic meteors by Watson (**4**), namely $a = 2{\cdot}5$, but is in marked disagreement with the value $a = 2{\cdot}08$ derived by Williams (**5**).

In contrast to the radio-echo measurements, the visual and telescopic observations require large corrections, including subjective factors, in converting observed to absolute rates and values of a ranging from 2·0 to 4·0 have been quoted by various authors.

The exponent in the mass law for the Quadrantid meteor shower is found to be 1·67 or 1·78, depending upon the correction to the experimental results which should be made for the sporadic meteor background. It is clear that the exponent is considerably less than that for sporadic meteors, i.e. there is a relatively greater proportion of bright meteors in the shower, in agreement with visual and telescopic observations.

* See p. 63.

An extension of the theory developed in these papers (I and II), enabling the observed echo rate to be related to the absolute incident meteor flux, to the total rate of meteor ionization, etc., together with a more detailed investigation of the mass distribution of sporadic and shower meteors, will be presented elsewhere.

Acknowledgments.—The author is indebted to Mr S. Evans, with whom he has had many stimulating discussions on the meteor height problem, and to Messrs I.C.I. Limited for a Research Fellowship.

University of Manchester,
Jodrell Bank Experimental Station,
Lower Withington,
Cheshire:
1953 *August.*

References

(1) Kaiser, T. R., *M.N.*, **114**, 39, 1954.
(2) Kaiser, T. R. and Closs, R. L., *Phil. Mag.*, **43**, 1, 1952.
(3) McKinley, D. W. R., *Can. Jour. Phys.*, **29**, 403, 1951.
(4) Watson, F., *Between the Planets*, Blakiston, 1941.
(5) Williams, J. D., *A.J.*, **92**, 424, 1940.

SCALE HEIGHTS AND PRESSURES IN THE UPPER ATMOSPHERE FROM RADIO-ECHO OBSERVATIONS OF METEORS

S. Evans

(Communicated by A. C. B. Lovell)

(Received 1953 August 21)

Summary

A split beam radio-echo technique has been used to measure the heights of the reflecting points of meteor trails. The measured width of the distribution of heights has been used in conjunction with the theories previously developed by Kaiser to determine the atmospheric scale height. The observations of sporadic meteors have been divided into velocity groups and values of the scale height have been calculated for each. A value of the atmospheric pressure at the mean height of each group is calculated from the evaporation theory of meteors. For purposes of comparison these results are converted into atmospheric densities which are compared with those obtained from rocket flights and meteor photographs made in New Mexico and Massachusetts. The present results for scale heights and densities are in close agreement with those obtained in New Mexico. In view of this a latitude variation in the density profile, which has been suggested as an explanation of the difference between the New Mexico and Massachusetts results, now seems unlikely.

---

1. *Introduction.*—This paper is concerned with the measurement of atmospheric pressure and scale height in the region 88 to 100 km altitude, determined from the observations of meteor heights with a radio-echo height-finding equipment. In two previous papers (**1**, **2**) Kaiser has developed a theory of the distribution of heights of meteors observed on a radio-echo equipment. The first (referred to as Paper I) deals with shower meteors, and the second (Paper II) with sporadic meteors. In these papers Kaiser, following Herlofson (**3**), shows that the pressure p, at the height of maximum ionization of a meteor of velocity v, producing a maximum of α electrons/cm path, is given by

$$p=\frac{2gl}{\Lambda A}\frac{\cos^{2/3}\chi}{v^2}\left(\frac{9H\mu\alpha}{4\beta}\right)^{1/3}, \tag{1}$$

where

H is the atmospheric scale height in centimetres,
μ is the mean mass of a meteor atom in grams,
β is the probability of ionization of an evaporated meteor atom,
χ is the zenith distance of the meteor trail,
g is the gravitational acceleration in cm sec^{-2},
l is the energy required in erg g^{-1} to vaporize the meteoric material,
Λ is the heat transfer coefficient (see Paper I), and
A, the shape factor, is defined by $A=\mathscr{A}m^{-2/3}$, where $\mathscr{A}$ is the cross-sectional area of the meteor in the line of flight, and m is the mass.

In principle this expression could be used to measure a series of values of p at different altitudes, but in the experimental measurement of meteor heights the reflecting point does not necessarily lie at the point of maximum ionization to which (1) applies. However, Kaiser's theory shows that the mean height observed for a large number of meteors moving with the same velocity is close to the height at which the smallest detectable meteor produces its maximum ionization (referred to as the characteristic height, h_m). The determination of h_m from the observed mean heights is discussed in Section 5. The smallest detectable value of the line density can be calculated from the parameters of the apparatus, and hence if h_m is determined for a series of values of v, the relationship between pressure and altitude can be obtained from (1), provided the other quantities are known.

Kaiser also shows that the width of the height distribution is a function of the size distribution of the incident meteors and the atmospheric scale height, H. In Paper II Kaiser has derived a size distribution for sporadic meteors and this is used in Section 4 to determine the scale height from the measured height distribution.

In the case of sporadic meteors, an integration over a range of zenith distances is taken in deriving the theoretical distribution of heights. The value of χ to be used in calculating the pressure from (1) is shown to be the most probable elevation of the reflecting points. Since the equipment measures the individual elevations, it is sufficient to take the mean value of these. The remaining constants, l, Λ, A, μ and β can be determined from data on photographic meteors given by Jacchia, and from correlations between visual and radio-echo observations.

2. *Apparatus.*—The observations presented in this paper have been obtained with the radio-echo height-finding equipment described by Clegg and Davidson (**4**). The transmitter works on a frequency of 69 Mc/s and radiates pulses of 6 μs duration and 50 kW peak power from a single dipole which floodlights a major portion of the northern sky. A conventional receiver, switching rapidly between two aerials, is used. The ratio of the signals received in the two aerials enables the elevation and hence the height of the effective echoing point to be measured. The limitations and accuracy of the method have been discussed by Clegg and Davidson. Considerable improvement in accuracy has been attained in the present work by the use of a photographic recorder of the type described by Davies and Ellyett (**5**). The error in a single height measurement is $\pm$ 1 km. Some of the observations on major showers have been taken with a similar equipment using a slightly different aerial arrangement which can be set up at different azimuths, and working on a frequency of 36·6 Mc/s. The accuracy is of the same order.

3. *Observations.*—Observations of the heights of sporadic meteors have been carried out using the 69 Mc/s equipment at Jodrell Bank during the period 1952 January to July. Echoes for which it was possible to measure the velocity by the technique of Davies and Ellyett (**5**) comprised about 10 per cent of the total. Table I shows the number of meteors used in this analysis for each period of the day, for each month. These were divided into the seven velocity groups shown in Table II. The mean height, mean velocity and r.m.s. deviation of the heights are given here for each group.

In Paper II it is shown that the scale height can be calculated from the width of a sporadic height distribution if the observations are selected to cover a range of elevations over which the gain of the aerials is roughly constant. Fig. 1 shows a

number distribution of the elevations of all the echoes given in Table II. The peak at 23° may well be due to the fact that at this elevation the ratio of the signals in the two aerials is unity and the chance of recognizing a velocity-type echo much greater. Accepting this explanation, echoes at elevations less than 20° or greater than 36° were rejected. These echoes are indicated by asterisks in Table II; the heights and r.m.s. deviations calculated after their exclusion are given in the lower section of the table.

TABLE I

Numbers of sporadic meteors used in this analysis

Period of day	$00^h\ 00^m$–$06^h\ 00^m$	$06^h\ 00^m$–$12^h\ 00^m$	$12^h\ 00^m$–$18^h\ 00^m$	$18^h\ 00^m$–$24^h\ 00^m$	Totals
1952					
January	56	37	4	21	118
February	28	21	3	10	62
March	20	7	3	2	32
April	32	17	2	4	55
May	24	45	6	3	78
June	13	...	5	1	19
July	10	7	...	...	17
Totals	183	134	23	41	381

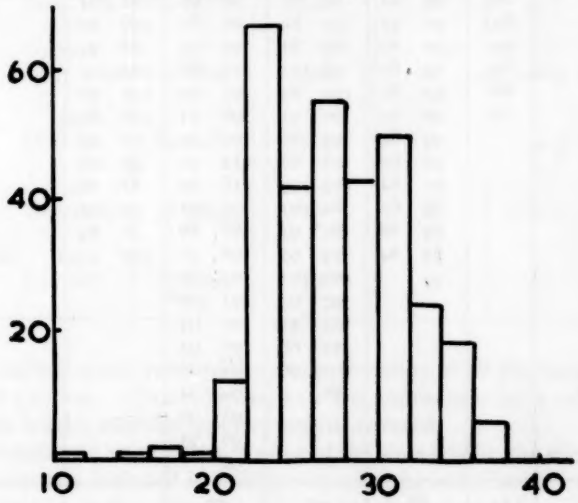

FIG. 1.—*Distribution of elevations.*

Ordinates: Numbers of meteors.
Abscissae: Elevation in degrees.

Table III gives similar data for four major showers. Further analysis and discussion of the astronomical significance of these results will be given in another paper. The data for the Perseid stream are used in Section 5 to estimate the behaviour of the aerial system.

TABLE II

Heights of sporadic meteors

Velocity group (km/sec)	20–24	25–29	30–34	35–39	40–44	45–49	50–59
Mean velocity (km/sec)	22	27	32	37	42	47	53†
Heights (km)	72	73 97	87 107	97 95	101 103	97 100	108 103
	94	92 92	84 107	95 93	95 91	99 102	107 92
	93	65* 98	101 96	100 103	100 99	100 90	99 101
	103	96 91	88 100	83 105	96 105	97 99	99 107
	95	95 97	95 89	92 94	100 103	93 101	100 94
	88	99 95	97 100	98 97	98 102	89 99	103 113
	83	99 100*	87 100	87 94	89 99	102 106	99 97
	84	92 95	98 100	91 100	92 105	100 99	102 105
	90	88 84	94 89	99 90	100 102	106 92	93 109
	78	96 95	102 103	94 105	97 103	101 89	98 100
	95	93 88	82 91	94 94	97 100	96 97	101 108
	90	88 103	98 100	76* 92	101 96*	91 100	118 92
	96	95 100	110 92	87 106	98 113	89 76	103 92
	86	88 98	94 97	91 77	95 92	100 93	130 108
	97*	82 87	87 86	79 94	102 82	83 105	91 103
	86	88 95	94 77	105 90	100 99	101 109	91 100
	93	103 99	89 88	90 97	100 95*	100 103	109 86
	97	96 94	102 95	85* 81	97 109	104	97 104
	89	95 88	89 91	96 99*	100 107		100 104
	84	90 93	95 89	96 89	106 92		81 94
	90	90 86	89 81	90 94	98 93		90
	83	92 87	96 102	116 88	101 110		
	88	92 81	101 85	95 92	101 98		
	88	90 75	90 91	96 97	106 85		
		97 84	93 86	92* 95	70 94		
		90 93	78 88	113 90	92 103		
		91 84	103 79	116 99	81 99		
		89 82	84 101	95 91	94 93		
		85 86	83* 95	88 86	96 84		
		85 84	79 97	98 91	100		
			100 101	103 90			
			97 93	91 100*			
			103 95	100 94			
			93 88	98 94			
			101 96	94 100			
			86	99 94			
				92 90			
				96 93			
				91			
Number	24	60	71	77	59	35	41
Mean height	89·2	90·7	93·2	94·4	97·6	97·3	100·7
R.m.s. deviation	6·63	7·05	7·47	7·22	7·22	7·35	8·45
Selected elevations							
Number	23	58	70	72	57	35	41
Mean height	89·0	90·5	93·3	94·7	97·6	97·3	100·7
R.m.s. deviation	6·58	6·12	7·44	7·13	7·36	7·35	8·45

† There is some difficulty in recognizing high-velocity meteors on the 69 Mc/s height-finding equipment, causing the numbers to be asymmetrically distributed in this group. There are insufficient numbers in higher velocity groups as yet.

The velocities are given to the nearest km/sec from the results of radio-echo measurements made at Jodrell Bank (**6, 7**).

4. *Determination of scale height.*—If the mass distribution of the meteors incident upon the Earth follows a law of the form $dN = m^{-s}\,dm$, where dN is the number of meteors in the mass group m to $m + dm$, it has been established by Kaiser in Paper II that for sporadic meteors the value of s is $2{\cdot}00 \pm 0{\cdot}02$. Referring to Fig. 4(*b*), Paper II, it can be seen that if δh is the r.m.s. deviation in a height distribution of sporadic meteors of uniform velocity and selected elevations, then for this value of s

$$\delta h = (1{\cdot}05 \pm 0{\cdot}02)\,H, \qquad (2)$$

where H is the atmospheric scale height. The probable error quoted is due partly to the uncertainty in the value of s and partly to the uncertainty in the aerial polar diagram. The latter error is small, but it will be shown later that a curve lying somewhere between Case (*a*) and Case (*b*) of Fig. 4(*b*), Paper II, is most appropriate to the equipment used here.

TABLE III

Shower	Equipment used	Number of echoes	Velocity (km/sec)	Mean height (km)	R.m.s. deviation (km)
Daytime Arietids 1952 June 8–9	69 Mc/s	210	38	92·7	5·5
Perseids 1952 Aug. 7–10	36 Mc/s	190	60	100·3	12·0
Geminids 1951 Dec. 14	69 Mc/s	110	36	94·3	9·5
Geminids 1952 Dec. 11–12	36 Mc/s	180	36	95·0	9·5
Quadrantids 1953 Jan. 2–3	36 Mc/s	210	39	95·7	9·2

The weighted mean value of the r.m.s. deviation of all the velocity groups in Table II is 7·17 km. Thus (2) gives, as a first approximation, a value of 6·80 km for the scale height, over the range of heights covered.

In determining a more accurate value of the scale height, the effect of the finite range of velocities included in each group must be considered. Apart from v, the only quantity in equation (1) which may be velocity-dependent is β, the probability of ionization of a meteor atom. Adopting a law of the form

$$\beta = av^n, \text{ where } a \text{ is a constant,} \qquad (3)$$

then

$$p = \text{const.}/v^{2+n/3}.$$

Hence

$$\frac{1}{H} = -\frac{d\ln p}{dh} = (2 + n/3)\frac{d\ln v}{dh}. \qquad (4)$$

In estimating n, consider the two extreme velocity groups in Table II. Substituting the approximate value of H derived above we find $(2+n/3)=1{\cdot}99$. As a first approximation a value of $n=0$ has been adopted, i.e. the probability of ionization is a constant and p varies inversely as v^2.

If δh is the true r.m.s. deviation, let suffix m refer to measured values, suffix v to velocity variations, and suffix e to errors of measurement. Then $\delta h^2=\delta h_m{}^2-\delta h_e{}^2-\delta h_v{}^2$ since the distributions are approximately Gaussian. δh_e is of the order of 1 km.

TABLE IV

Mean velocity (km/sec)	Mean height (km)	Measured r.m.s. deviation (km)	Corrected r.m.s. deviation (km)	Scale height (km)	Number of observations
22	89·0	6·58	6·43	6·12	23
27	90·5	6·12	6·00	5·71	58
32	93·3	7·44	7·32	6·98	70
37	94·7	7·13	7·02	6·68	72
42	97·6	7·36	7·25	6·93	57
47	97·3	7·35	7·24	6·93	35
53	100·7	8·45	8·30	7·90	41

The corrected r.m.s. deviations for each group are shown in Table IV. Values of the scale height have been calculated for each, using equation (2), and these are plotted against altitude in Fig. 2. The weighted mean value is $6{\cdot}70\pm0{\cdot}3$ km at 94·7 km altitude. The errors in the individual values of δh used are of the order of $(2N)^{-1/2}\delta h$, where N is the number of observations in a single distribution. This error is much larger than that due to the uncertainty in the value of s and the aerial polar diagram, but can clearly be reduced by taking more observations. The magnitude of the error is indicated by the horizontal lines in Fig. 2.

The full line shows the linear relation fitted to these data by least squares and represents the values which will be adopted in this analysis. The broken line shows the smoothed values adopted by the Rocket Panel (8).

It is unlikely that the selection of a particular type of echo would have a serious effect on the height distribution. In order to check this, the r.m.s. deviation of 92 sporadic velocity-type echoes of all velocities was found to be $(9{\cdot}5\pm1)$ km. The r.m.s. deviation of 106 sporadic echoes of all types obtained during the same period was found to be $(9{\cdot}8\pm1)$ km. If this small difference is found to be real as more data become available, it will be necessary to apply a small correction to the figures given in Table IV. In the meantime it is assumed that the velocity selection has no effect.

5. *Determination of characteristic heights.*—As discussed in Section 1, the atmospheric pressure can be calculated at the characteristic height, h_m, which has to be determined from the measured mean heights. The theoretical deviation of the measured mean height from h_m is shown in Fig. 4(*a*), Paper II.

For values of s of the order of 2 it can be seen that there is a difference of $0{\cdot}12H$ in this deviation for the curves relating to the two extreme types of aerial polar diagrams considered. The polar diagram of the height-finding aerials cannot

easily be represented by a single curve, but the behaviour of the system can be derived in the following way.

An appropriate value of s for the Perseid meteor stream is obtained first from the r.m.s. deviation of the height distribution given in Table III. This is 12 km or, using the value of scale height determined in Section 3, $1{\cdot}65\,H$. Fig. 7 (*b*), Paper I, then shows the value of s to be $1{\cdot}55 \pm 0{\cdot}05$.

Unfortunately sufficient numbers of sporadic meteors of the same velocity as the Perseids are not available, but we can extrapolate from the highest velocity group available. It was shown in Section 4 that the pressure is inversely proportional to v^2.

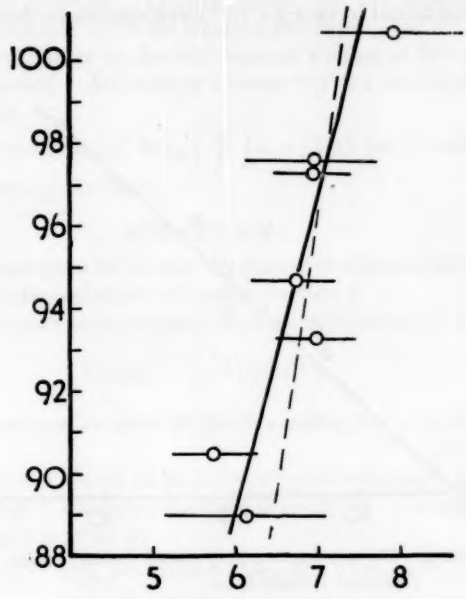

FIG. 2.—*Atmospheric scale heights.*

The full line has been fitted by least squares to the present results. The broken line represents the smoothed values adopted by the Rocket Panel.

Ordinates: Altitude in km.
Abscissae: Scale height in km.

We have
$$\frac{1}{H} = -\frac{d\ln p}{dh}.$$

Hence
$$h_1 - h_2 = 2H \ln v_1/v_2. \qquad (5)$$

Thus we should expect the mean height of sporadic meteors of velocity 60 km/sec to be 102·5 km. The mean height of the Perseids is 100·3 km. The difference is 2·2 km or $0{\cdot}3H$, and this we attribute to the difference in the value of s. A comparison of Fig. 7 (*a*), Paper I with Fig. 4 (*a*), Paper II, shows that the behaviour of the height-finding system is best represented by a line lying about half-way between curves (*a*) and (*b*). Thus for sporadic meteors of selected elevations the observed mean height is $(0{\cdot}15 \pm 0{\cdot}05)H$ above the characteristic height.

The values of h_m for each velocity group are plotted in Fig. 3.

The above argument presupposes that the behaviour of the 69 Mc/s equipment used for the sporadic observations and the 36·6 Mc/s equipment used for the Perseid observations is identical. The polar diagram of the 36 Mc/s equipment in an echo plane of elevation 45° will be sufficiently near to the azimuthal polar diagram of the 69 Mc/s equipment at constant elevation 27°·5. The low-frequency equipment is intrinsically of greater sensitivity but was operated at lower gain. In order to trigger the photographic recorder and provide a satisfactory height measurement the received echo must be of the order of five times noise. By measuring the peak power of the transmitter and the sensitivity of the receiver and using the formula of Lovell and Clegg (**9**) the minimum detectable line density at the mean elevation and mean height was found to be $2{\cdot}3 \times 10^{11}$ electrons/cm for both equipments.

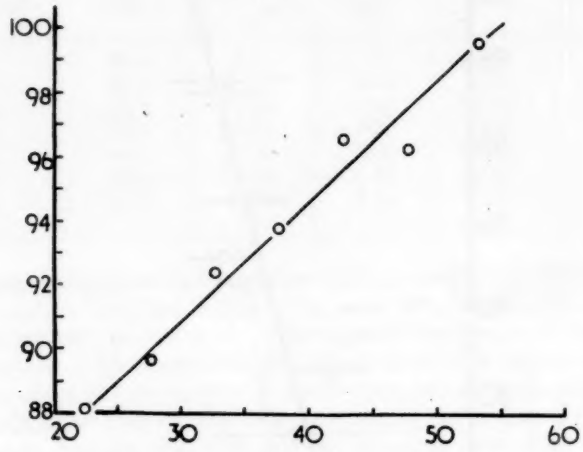

FIG. 3.—*Characteristic heights of sporadic velocity groups.*
Ordinates: Altitude in km.
Abscissae: Mean geocentric velocity in km/sec.

6. *Determination of constants.*—Before equation (1) can be used to determine the absolute pressure/height relationship a knowledge of the constant

$$Q = \frac{l}{\Lambda A}\left(\frac{\mu}{\beta}\right)^{1/3} \tag{6}$$

is required. This can be determined from photographic meteor data and radio-visual correlations.

Jacchia (**10**) has given values of

$$\log_{10} K_m = -11{\cdot}75 \pm 0{\cdot}02,$$

where $K_m = \dfrac{\Lambda}{2\gamma l}$ and γ is the drag coefficient, and $\log_{10}(\gamma A)^3 \tau_0 = -9{\cdot}43$, where τ_0 is defined by $\tau = \tau_0 v$ and τ is the luminous efficiency. Thus (6) can be written

$$\log_{10} Q = \log_{10} 0{\cdot}5 - \log_{10} K_m - \tfrac{1}{3}\log_{10}(\gamma A)^3 \tau_0 + \tfrac{1}{3}\log_{10}\left(\frac{\tau_0 \mu}{\beta}\right). \tag{7}$$

The visual magnitude of an object at 100 km emitting light of intensity I erg/sec uniformly in all directions is given by

$$M = 24{\cdot}6 - 2{\cdot}5 \log_{10} I. \tag{8}$$

For a meteor
$$I = \tau \frac{dm}{dt} \frac{v^2}{2} \tag{9}$$

and
$$\alpha = \frac{\beta}{\mu v} \frac{dm}{dt}. \tag{10}$$

Hence
$$M = 25{\cdot}35 - 2{\cdot}5 \log_{10} \left(\frac{\tau_0 \mu}{\beta}\right) - 10 \log_{10} v - 2{\cdot}5 \log_{10} \alpha. \tag{11}$$

Greenhow and Hawkins (11) have shown that the zenithal magnitude of a meteor can be related directly to the electron line density and from the observations of Millman and McKinley on Perseid meteors a value of $M = 3$ for $\alpha = 7{\cdot}3 \times 10^{12}$ electrons/cm is quoted. An error of a factor 1·5 in α would produce an error of only 0·05 in $\log_{10} p$.

Hence from equation (11) $\log_{10} \left(\frac{\tau_0 \mu}{\beta}\right) = -31{\cdot}05$ for Perseid meteors. Substituting in equation (7) we find

$$\log_{10} Q = 4{\cdot}24.$$

This value will be adopted for all velocity groups in this analysis since the value of β was shown to be independent of velocity in Section 4.

7. *Absolute pressure versus height.*—Rewriting equation (1) we have

$$p = 2gQ \frac{\cos^{2/3} \chi}{v^2} (9H\alpha)^{1/3}. \tag{12}$$

Using an inverse-square law from the Earth's centre, the value of g is 951 cm sec^{-2} at 95 km altitude.

The value of α was shown to be $2{\cdot}3 \times 10^{11}$ electrons/cm in Section 5.

Referring to Fig. 1, the mean elevation is $\chi = 27°{\cdot}5$. Hence the pressure at the characteristic height is given by

$$\log_{10} p = 11{\cdot}42 + \tfrac{1}{3} \log_{10} H - 2 \log_{10} v.$$

The pressures calculated from this equation are plotted in Fig. 4. The smooth curve was fitted to these points for the minimum algebraic sum of the residuals in $\log_{10} p$. The form of the curve was obtained, by integration, from the scale height curve in Fig. 2.

8. *Comparison with other results.*—In Fig. 2 the present measurements of scale heights are compared with the New Mexico rocket results. It can be seen that, at a given height, the difference in the scale heights is only of the order of the standard deviations. Thus there is no significant difference in the results of the two methods of measurement.

In order to calculate the air temperature it is necessary to assume a value for the mean molecular weight of air molecules. At these altitudes partial dissociation of molecular oxygen may be expected, but to a first approximation we can use the molecular weight measured at ground level, which is 29 g/mole. Using $H = 6{\cdot}70$ km at 95 km altitude the air temperature is 220 deg. K. Because of the narrow range of heights available the temperature gradient cannot be estimated with any accuracy but it is between 2 deg. and 6 deg./km, increasing upwards.

Photographic meteor results fundamentally measure air densities, and thus for purposes of comparison the Jodrell Bank results have been converted into densities using

$$p = \rho Hg. \tag{13}$$

It will be seen that with a direct measure of H it is not necessary to use a value of the mean molecular weight in order to derive the gas density.

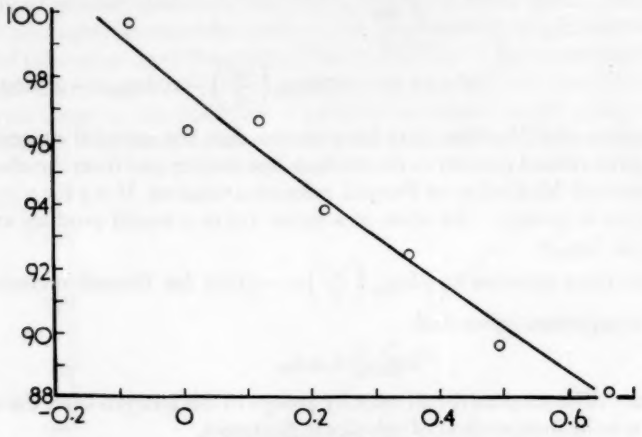

FIG. 4.—*Atmospheric pressures.*

The circles represent absolute values of the pressure calculated from velocity groups. The form of the smooth curve which is adopted here was obtained by integration of the scale height curve in Fig. 2.

Ordinates: Altitude in km.
Abscissae: $\log_{10}$ pressure (dyn cm^{-2}).

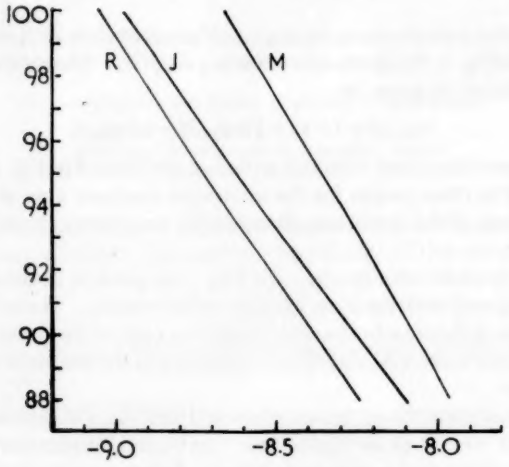

FIG. 5.—*Atmospheric densities.*

R, density profile from rocket and photographic meteor observations over New Mexico, latitude 32° N.
M, profile from photographic meteor observations over Massachusetts, latitude 42° N.
J, profile from radio-echo meteor observations at Jodrell Bank, latitude 53° N.

Ordinates: Altitude in km.
Abscissae: $\log_{10}$ density (g cm^{-3}).

Photographic meteor data obtained by Jacchia in New Mexico are now in agreement with the rocket data, but meteor data from Cambridge, Massachusetts, reduced in an identical manner, show a systematic difference. In Fig. 5, R is the most recent profile from rocket flights over New Mexico (**12**), M is the profile over Massachusetts from photographic meteor data, and J is the profile from the Jodrell Bank observations.

It was pointed out by the Rocket Panel that the difference between the New Mexico and Massachusetts results may be due to a latitude effect or to the differing location with respect to upper atmospheric circulation patterns. The rocket site in New Mexico has a latitude of 32°, Cambridge, Massachusetts, has a latitude of 42°, and Jodrell Bank, 53°. Thus, in view of the present results, a monotonic variation with latitude is unlikely. Results from other sites will clearly be awaited with great interest. Further observations to establish the seasonal effect at Jodrell Bank are now being carried out.

Acknowledgments.—The author is particularly indebted to Dr T. R. Kaiser of Jodrell Bank for many helpful discussions, also to Professor A. C. B. Lovell for his encouragement and advice in the preparation of this paper, and to the Department of Scientific and Industrial Research for the award of a maintenance grant which has enabled him to carry out this work. Miss J. Almond assisted with the Arietid and sporadic analysis.

University of Manchester,
Jodrell Bank Experimental Station,
Lower Withington,
Cheshire :
1953 *August.*

References

(1) Kaiser, T. R., *M.N.*, **114**, 39, 1954.
(2) Kaiser, T. R., *M.N.*, **114**, 52, 1954.
(3) Herlofson, N., *Phys. Soc. Rep. Prog. Phys.*, **11**, 444, 1948.
(4) Clegg, J. A. and Davidson, I. A., *Phil. Mag.*, **41**, 77, 1950.
(5) Davies, J. G. and Ellyett, C. D., *Phil. Mag.*, **40**, 614, 1949.
(6) Hawkins, G. S. and Almond, M., *M.N.*, **112**, 219, 1952.
(7) Davies, J. G. and Greenhow, J. S., *M.N.*, **111**, 26, 1951.
(8) Rocket Panel, *Phys. Rev.*, **88**, No. 5, 1027, 1952.
(9) Lovell, A. C. B. and Clegg, J. A., *Proc. Phys. Soc.*, **10**, 491, 1948.
(10) Jacchia, L. G., *H.C.O. and Cent. Anal. M.I.T. Tech. Rep.*, No. 3 (H.R. Ser. II–31), 1949.
(11) Greenhow, J. S. and Hawkins, G. S, *Nature*, **170**, 355, 1952.
(12) Jacchia, L. G., *H.C.O. and Cent. Anal. M.I.T. Tech. Rep.*, No. 10 (H.R. Ser. II–44), 1952.

AN ANALYSIS OF BURSTS OF SOLAR RADIO EMISSION AND THEIR ASSOCIATION WITH SOLAR AND TERRESTRIAL PHENOMENA

R. D. Davies

(Received 1953 December 24)*

Summary

Solar radio emission records on seven frequencies in the range 60 to 10 000 Mc/s were studied over a period of 18 months. The analysis, which includes a number of histograms, shows that many of the properties of bursts change with frequency. A study of the time delay between bursts on different frequencies revealed that 3 000 Mc/s bursts often occur first; a simultaneous up and down movement of ionized material from the level of zero refractive index at that frequency is postulated. It is found that bursts were more frequent than flares, fadeouts and crochets and that they almost always accompanied these effects. The commencement of bursts appears to be simultaneous with that of flares and crochets but precedes that of fadeouts by about two minutes. In addition, there is a rough correlation between the intensity of bursts, flares, fadeouts and crochets.

---

1. *Introduction.*—In the course of routine observations of radio emission from the Sun taken at the Radiophysics Laboratory, Sydney, a considerable accumulation of records has become available covering a large frequency range. Although a day-by-day summary of these records is published in the *Quarterly Bulletin of Solar Activity*, there is no opportunity to present in that publication a detailed analysis of outstanding occurrences, in particular the bursts of radio emission characteristic of the records. Such an analysis seems worth while in order to find what generalizations emerge from the data and how the recorded bursts are related to other solar and terrestrial phenomena.

Previous work on this subject includes detailed studies of (*a*) many bursts at one frequency (**1, 2, 3**), (*b*) occasional observations of simultaneous bursts on several frequencies (**4, 5**), and (*c*) spectrum analyser observations at the lower frequencies (**6, 7, 8**). However, no systematic investigation of bursts recorded over a wide frequency range has been described.

In the present paper a detailed analysis is made of bursts recorded in the period 1950 January to 1951 June. The records were taken at seven frequencies in the range 60 to 10 000 Mc/s. The analysis includes a detailed study of the correlation of bursts with flares, sunspots, ionospheric fadeouts and magnetic crochets. In most cases no attempt has been made to draw physical conclusions from the analysis. However, certain results which appear to be of immediate interest are discussed briefly in the final section.

The main analysis is given in Section 4. In treating a long series of largely disconnected properties, no attempt has been made to maintain continuity or to discuss each item fully. The essential results are presented in the accompanying diagrams and tables and only the main conclusions are stated in the text.

* Received in original form 1953 August 24.

2. *The data.*—The radio data, most of which were tabulated by Davies and Hindman (**9**), were obtained mainly from records at 200*, 600, 1 200, 3 000 and 9 400 Mc/s; these were extended to 62 and 98 Mc/s in a later part of the analysis. The following burst properties were measured as a preliminary to the analysis.

(i) Time of start—the time when the radio noise rose to 5 per cent of the maximum burst intensity.

(ii) Time of upswing—the time at which the major part of the burst (lasting more than 10 per cent of the total life-time) rose to 20 per cent of the peak intensity.

(iii) Maximum (peak) burst intensity.

Flare and sunspot information was obtained from the *Quarterly Bulletin* of the I.A.U. and the *Monthly Bulletin* of the Tokyo Observatory.

Fadeouts, observed as a fall in intensity of the received galactic radiation, were derived from 18 Mc/s galactic noise records obtained at this laboratory. Observed fadeout intensities measured in decibels were corrected for obliquity of ray path through the ionosphere by multiplying by the secant of the Sun's zenith distance.

Magnetic solar flare effect (crochet) information was obtained from the magnetograms of Toolangi Magnetic Observatory. The quarterly reports in the *Journal of Geophysical Research* and the 1950 *Bulletin* of I.A.T.M.E. were also used.

In a few cases complete burst, flare, fadeout and crochet information is available. Two typical examples are given in Fig. 1. In other cases the data are incomplete but are used in the statistics.

3. *Qualitative properties of bursts.* (a) *Definitions.*—The occurrence called a burst in this paper is any clear-cut solar radio emission rising above the daily level. In view of the close relationship of bursts with flares (discussed in Section 4, Part B), many may be identified with the "outbursts" studied by other workers (**6, 10, 11**).

(b) *Burst outline.*—A characteristic of some bursts is their "jaggedness"—short-duration rises and falls in intensity. The degree of jaggedness decreases with increasing frequency, as can be seen in Fig. 1. In an average burst at 200, 600 or 1 200 Mc/s about two peaks were observed each minute. However, bursts at 3 000 and 9 400 Mc/s consisted of a smooth rise and fall. This decrease of the amplitude of fluctuations with increasing frequency was also noted by Covington and Medd (**12**).

Burst traces at the lower frequencies may be considered to consist of fluctuations superposed on a smooth minimum level. The smoothed minima are similar in shape to the burst outlines at the higher frequencies.

Burst activity is more profuse at 200 Mc/s than at the higher frequencies. Over some periods as many as 25 separate bursts, most of which were not coincident with activity on the higher frequencies, were recorded each hour. Therefore the statistics applied to 200 Mc/s in Part A of the analysis (Section 4) relate only to bursts which coincided with those on the higher frequencies or with flares. In sections where all bursts (irrespective of their coincidence and flare associations) are analysed, the 200 Mc/s data have been excluded altogether. This applies to Sections 4 A (a) and 4 B (a).

A number of bursts of long duration were examined to determine the extent to which the shape was preserved on different frequencies. The smoothed outlines were similar on all frequencies and also the similarity was more pronounced the closer the frequencies. The fine detail, as seen on high-speed records, does not

* The 200 Mc/s records came from the Commonwealth Observatory, Mt. Stromlo.

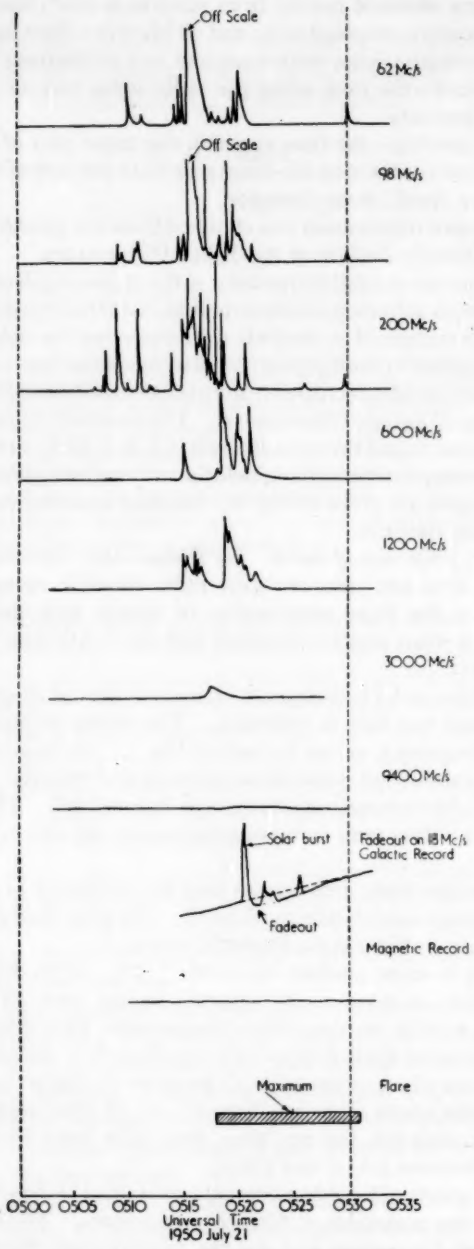

FIG. 1 (*a*).—*Burst, fadeout, crochet and flare observations on* 1950 *July* 21.

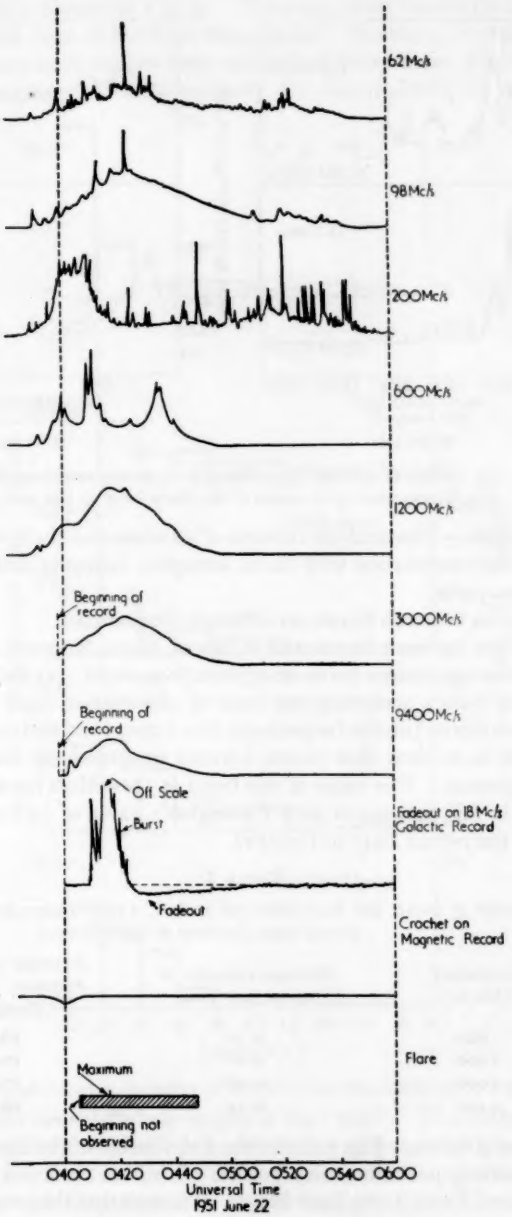

FIG. 1 (*b*).—*Burst, fadeout, crochet and flare observations on* 1951 *June* 22.

correspond on different frequencies. These effects are illustrated in Fig. 2, which shows a burst occurring on 600 and 1 200 Mc/s.

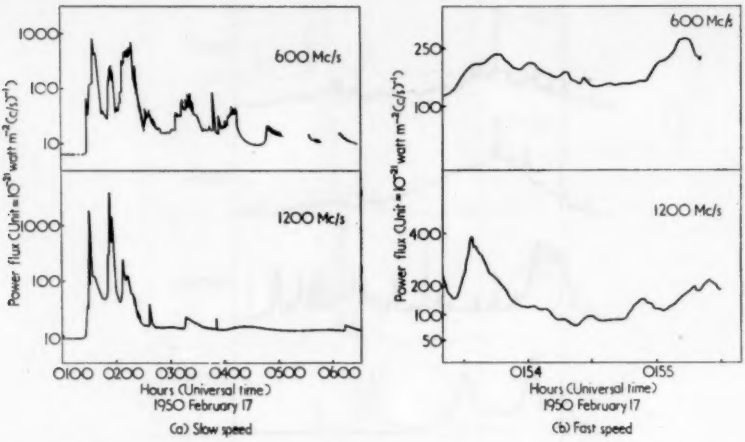

FIG. 2.—(*a*) *Outline of burst on* 1950 *February* 17, *at* 600 *and* 1 200 *Mc/s.*
(*b*) *A comparison of a section of the above burst at* 600 *and* 1 200 *Mc/s.*

4. *The analysis.*—The analysis consists of a systematic study of the properties of bursts and their correlation with flares, sunspots, fadeouts and crochets. The analysis has two parts:

(A) Relations between bursts on different frequencies.

(B) Relations between bursts and sunspots, flares, fadeouts and crochets.

Part A: Relations between bursts on different frequencies. (a) *Rate of occurrence.*—The number of bursts occurring per hour of observation (and also the average interval between bursts) on the frequencies 600, 1 200, 3 000 and 9 400 Mc/s is given in Table I. It is evident that bursts become progressively less frequent with increasing frequency. The value of one burst at 3 000 Mc/s for each 17 hours of observation is in fair agreement with Covington's value of 23 hours estimated at 2 800 Mc/s for the period 1947 to 1950 (1).

TABLE I

The average number of bursts per hour observed at 600, 1 200, 3 000 *and* 9 400 *Mc/s in the period* 1950 *January to* 1951 *June*

Frequency (Mc/s)	Average number of bursts per hour	Average interval between bursts (hours)
600	0·10	10
1 200	0·08	12
3 000	0·06	17
9 400	0·04	26

(b) *Lifetime of bursts.*—Fig. 3 shows the distribution of the lifetimes (defined as the time between $\frac{1}{10}$ peak intensity points) of bursts recorded on the five frequencies 200, 600, 1 200, 3 000, 9 400 Mc/s. It is seen that the proportion of bursts of short duration (say less than four minutes) is greatest at the lower frequencies. On the other hand, an examination of individual bursts showed no clear relationship between lifetime and frequency.

(c) *Time of decay of bursts.*—The distribution of averaged "decay times" (determined by fitting sections of the tail of each burst to an exponential form $e^{-t/\tau}$) for 40 bursts is plotted in Fig. 4. The mean decay time at the low frequencies is shown to be less than at the high frequencies. However, it was observed that the smoothed minima of the low frequencies had decay times of the same order as the high frequencies. At no frequency did the majority of bursts show an

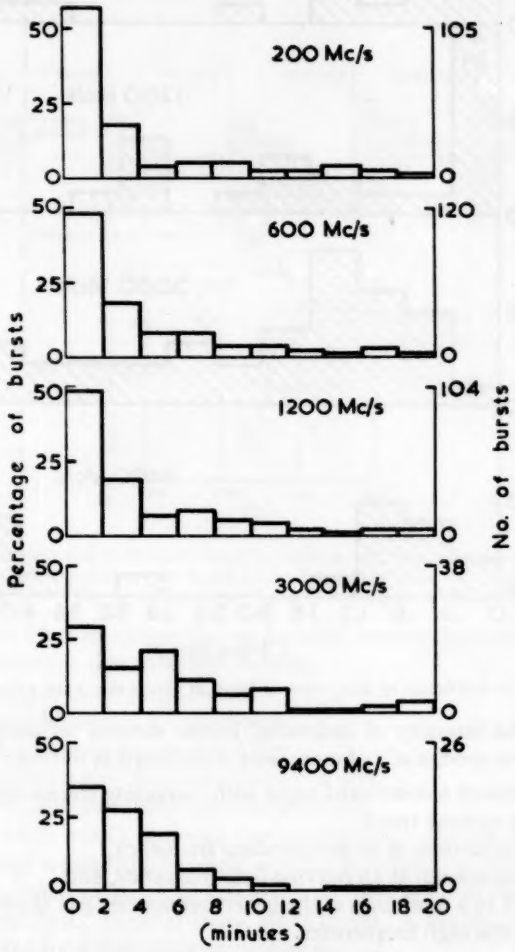

FIG. 3.—*The distribution of lifetime of bursts at* 200, 600, 1 200, 3 000 *and* 9 400 *Mc/s.*

exponential decay over the whole length of the "tail". The manner in which the decay time changed over the tail of a burst did not vary significantly with frequency.

(d) *Intensity of bursts.*—Histograms showing the distribution of peak burst intensities at various frequencies are shown in Fig. 5 (*a*). The modal values are plotted as a function of frequency in Fig. 5 (*b*). The mean spectrum obtained by joining these points (full line) is seen to show a minimum at 1 200 Mc/s in contrast to the smooth downward trend of the intensity of the quiet Sun (dotted line).

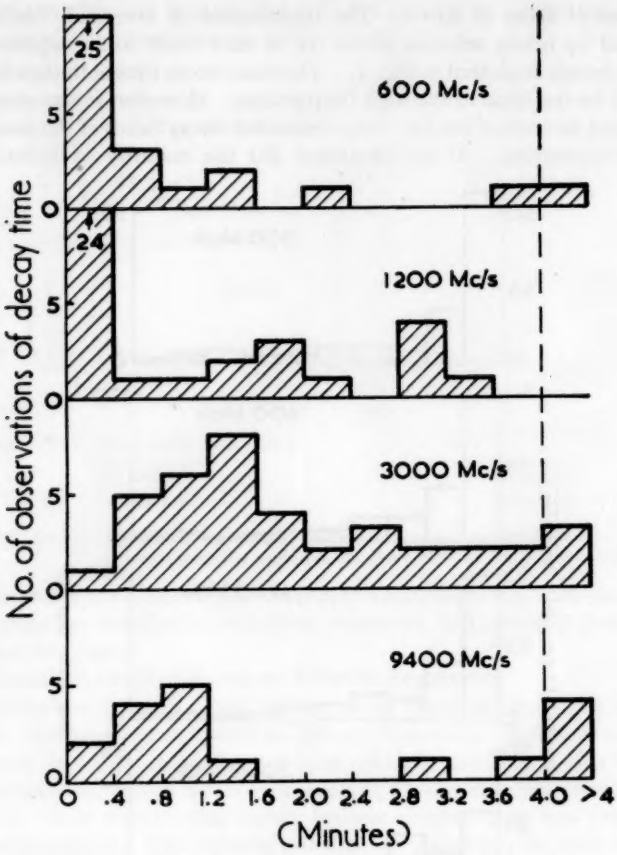

FIG. 4.—*The distribution of decay times of bursts at* 600, 1 200, 3 000 *and* 9 400 *Mc/s.*

However, the intensity of individual bursts showed no unique trend with frequency. The spectra of 44 bursts were distributed as follows:

8 showed a downward trend with increasing frequency,
7 an upward trend,
7 a maximum at an intermediate frequency,
14 a minimum at an intermediate frequency, and
8 fell to a minimum at the lower frequencies and showed a maximum at the high frequencies.

(e) *Time delays between bursts on different frequencies.* (i) *Time of start.*—In order to discover the time relationship between bursts, delay times were calculated relative to 1 200 Mc/s, the middle frequency. The distribution of the delay of times of start is shown in the dotted histograms in Fig. 6. They are symmetrical about coincidence on all frequencies except 9400 Mc/s, which shows a lag. This unexpected 9400 Mc/s lag was further tested by comparison with 3000 Mc/s. The times of start and maximum intensity of 9400 Mc/s were found to be delayed ½ minute behind 3000 Mc/s.

(ii) *Time of upswing.*—Most bursts at 200 and 600 Mc/s which preceded those at 1 200 Mc/s in the dotted histograms of Fig. 6 showed preliminary activity of low intensity before the sudden upswing characteristic of the lower frequencies. The results of a comparison of times of upswing (as defined in Section 2) with 1 200 Mc/s are given in the full-line histograms in Fig. 6. Although a large number of bursts are coincident within the error of measurement there is a tendency for 200 and 600 Mc/s to lag behind 1 200 Mc/s.

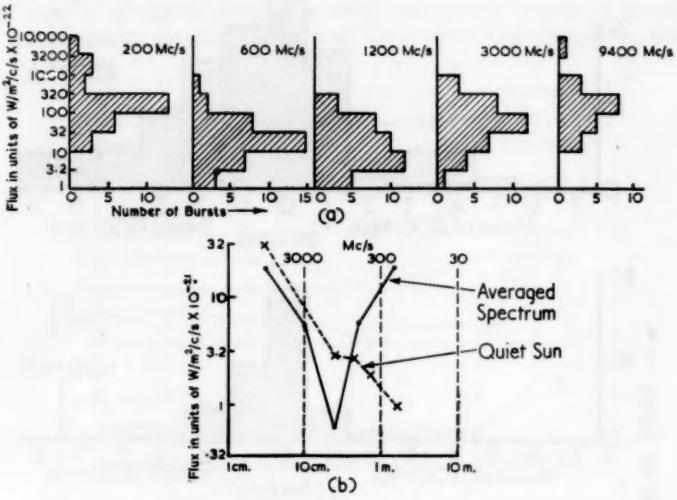

FIG. 5.—(*a*) *The distribution of the intensities of* 44 *bursts on* 200, 600, 1200, 3000 *and* 9400 *Mc/s.*
(*b*) *The full curve gives the modal intensities derived from Fig.* 5 (*a*) *plotted against frequency. The dotted line gives the intensity spectrum of the quiet Sun.*

The sequence of times of upswing on different frequencies was determined for 35 bursts. They were distributed as follows:

(*a*) 7 coincident on all frequencies.
(*b*) 4 lowest frequencies occurred first.
(*c*) 15 highest frequencies occurred first.
(*d*) 9 an intermediate* frequency occurred first.
(*e*) 0 an intermediate* frequency occurred last.

1200 and 3000 Mc/s bursts occurred first most often. Double bursts with two clear-cut upswings separated by several minutes sometimes occurred at the lower frequencies. In some cases, all of group (*b*), the first burst of the pair appeared to fit the sequence best; in other cases, all of group (*c*), the second. The latter effect was observed by Reber (**5**) in one occasion.

Part B: Relations between bursts and sunspots, flares, fadeouts and crochets. (a) *Sunspot statistics and the rate of occurrence of bursts.*—To make possible a comparison of the radio data with sunspot data, an estimate was made of the average number of bursts per hour for each month. In Fig. 7 are displayed three-month running means of 600, 1200, 3000 and 9400 Mc/s burst indices along with monthly average sunspot areas and numbers.† It is concluded from the figure that

* A frequency other than highest or lowest recorded.
† Obtained from Washington Naval Observatory circulars.

(i) time plots of the burst index are similar at different frequencies; and

(ii) the burst index correlates well with sunspot area and number; the number of bursts per hour at any frequency may be used as an index of solar activity.

(b) *Coincidence of bursts, flares, fadeouts and crochets.* (i) *Bursts and flares.*—The distribution of 261 coincidences between bursts and flares is given in Table II.

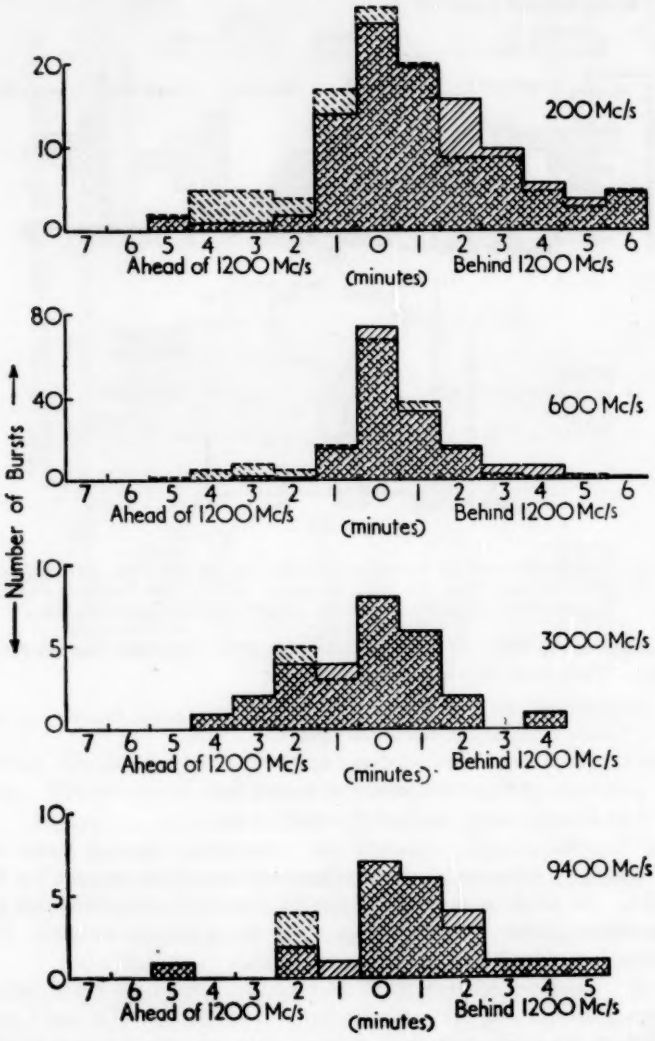

FIG. 6.—*The dotted histograms give the distributions of times of start on 200, 600, 3000 and 9400 Mc/s relative to 1200 Mc/s. The full-line histograms are for the times of upswing.*

Three flares only were unaccompanied by excess radio noise at one or more frequencies in the range 60 to 10 000 Mc/s and in two of these cases the radio records were incomplete. Thus at least 99 per cent of all flares are accompanied by excess radio emission in some part of the frequency range. However, the

possibility that this high correlation could be due in part to chance coincidences requires special examination, especially when activity was recorded only on one of the low frequencies where activity may persist over long periods. As shown in Table II, 31 out of the 222 flares were accompanied by extended activity on 200 Mc/s. In these cases it was difficult to recognize a discrete burst and it is possible that in some of them a significant coincidence did not exist.

These results extend those of Dodson, Hedeman and Owren (**13**), who observed that 78 per cent of all flares were associated with energy excess at 200 Mc/s. Flares are more often coincident with low- than with high-frequency bursts.

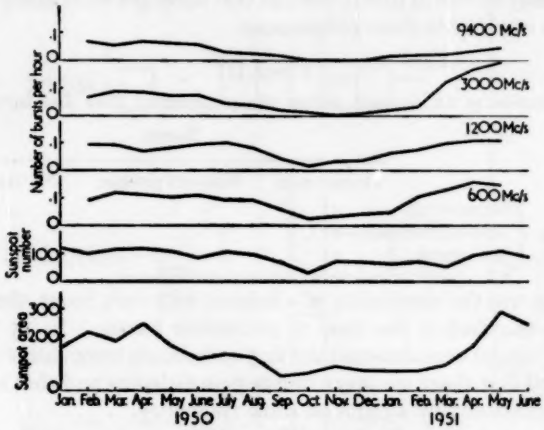

FIG. 7.—*A comparison of the three-month running means (number of bursts per hour) with the monthly average sunspot areas and numbers for the period January 1950 to June 1951.*

TABLE II

The distribution amongst the classes (a), (b) and (c) of flares and bursts on each of the frequencies 200, 600, 1 200, 3 000 and 9400 Mc/s

		Class (*a*) Flares with bursts	Class (*b*) Flares without bursts	Class (*c*) Bursts without flares	Totals
200 Mc/s	number	180	36	29	245
	percentage	74	14	12	100
600 Mc/s	number	109	61	34	204
	percentage	53	30	17	100
1 200 Mc/s	number	94	79	28	201
	percentage	47	39	14	100
3000 Mc/s	number	21	50	4	75
	percentage	28	67	5	100
9400 Mc/s	number	40	44	3	87
	percentage	47	50	3	100
All frequencies	number	211*	11†	39	261
	percentage	81	4	15	100

* These included 31 flares accompanied by extended activity on 200 Mc/s.
† 8 of these 11 have associated burst activity on 98 and 62 Mc/s.

However, a burst on a high frequency is more likely to be accompanied by a flare than one on a low frequency. Thirty-nine bursts with a wide range of intensities were unaccompanied by flares of importance 1^- (the minimum value reported) or greater. In order to test whether these bursts were accompanied by less intense

flare-like activity, 200 Mc/s records were searched at the times of flares of importance 0.* Of 20 flares 0, 7 were associated with distinct bursts and 7 with prolonged intense activity. Thus, less pronounced forms of flare-like activity can produce excess radio noise.

(ii) *Fadeouts, bursts and flares.*—Sixty-eight galactic fadeouts (sudden absorption by the ionosphere of galactic radiation) were reported in the period 1950 July to 1951 June. They are compared with Tokyo flare records and burst data in Table III. Of 68 fadeouts, only one was not coincident with a burst, and then the fadeout intensity was small. Fadeouts are more often associated with bursts than flares; this may be due in part to the fact that flares are more easily missed, and in part to effects intrinsic to these phenomena.

TABLE III

The distribution of 68 fadeouts among the 9 classes of flare and burst conditions

		Bursts		
		Occurrence	Non-occurrence	No record
Flares	Occurrence	25	...	...
	Non-occurrence	11	...	...
	No record	31	1	...

In order to test the association of a fadeout with each burst, the galactic radio records were searched at the time of 20 intense bursts. In 15 cases fadeouts (larger than average) were detected and in 5 no fadeouts were visible on the records. It is concluded that there are more bursts than fadeouts and that all fadeouts are probably accompanied by a burst on some frequency.

(iii) *Crochets, flares and bursts.*—The coincidence between flares, bursts and the crochets visible on the magnetograms of the Toolangi Magnetic Observatory, near Melbourne, are given in Table IV. The feature of this table is that more crochets are associated with bursts (67) than with flares (35). This is due to the smaller optical observing time and to the fact that bursts occur without an observed flare.

TABLE IV

The distribution of 92 crochets amongst various classes of flare and burst conditions

		Bursts			
		Occurrence	Non-occurrence	No record	Total
Flares	Occurrence	29	...	6	35
	Non-occurrence	11	1	2	14
	No record	27	1	15	43
	Total	67	2	23	92

(c) *Time delays between bursts, flares, fadeouts and crochets.* (i) *Bursts and flares.*—The differences between the times of start of flares (I.A.U. data) and the times of upswing of the corresponding bursts on 200, 600, 1200, 3000 and 9400 Mc/s were determined and the distributions plotted in Fig. 8. The histograms show no marked asymmetry at any frequency. This agrees with the results of Dodson, Hedeman and Owren (**13**) who found that the starting times of most types of bursts seem to cluster about the rise in Hα brightness.

* Phenomena less intense than flares of importance 1⁻, recorded in the Mount Stromlo spectrohelioscope log.

(ii) *Bursts and fadeouts.*—To determine the time relationship between fadeouts and bursts the times of starts of the galactic fadeouts were compared with the burst upswing on the frequency which occurred first. The distribution of time differences is shown in Fig. 9 along with the fadeout-flare comparison. The burst-fadeout histogram (Fig. 9 (*a*)) shows a smaller spread than the burst-flare histogram (Fig. 8) or the flare-fadeout histogram (Fig. 9 (*b*)). The median delay of fadeouts after bursts is 1·5 minutes.

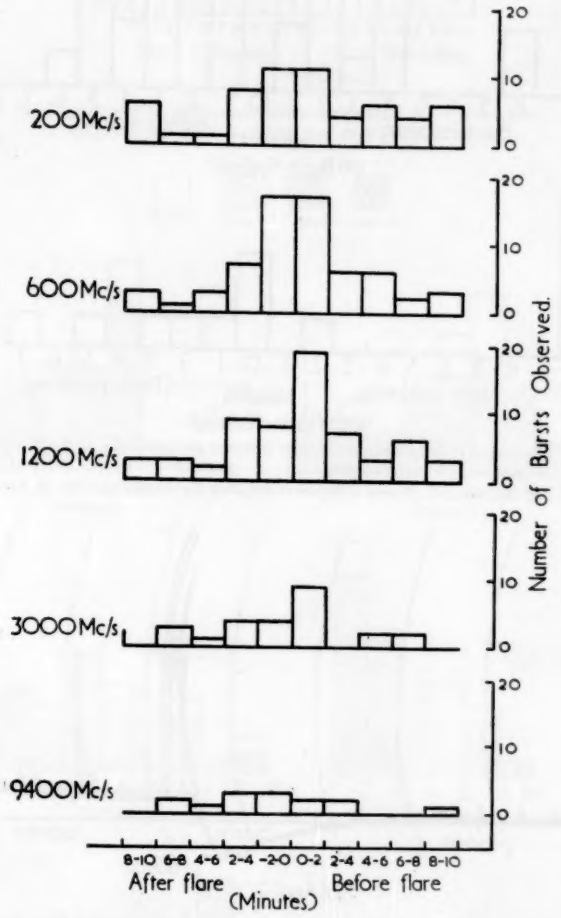

FIG. 8.—*The distribution of the times of start of flares and the upswing of the corresponding bursts on* 200, 600, 1200, 3000 *and* 9400 *Mc/s.*

Fig. 10 shows an example of a burst preceding a fadeout. Hey, Parsons and Phillips (3), however, found that on the average the commencement of radio-communication fadeouts, as distinct from galactic fadeouts, preceded by 13 minutes bursts at 4·1 metres in the period 1946–47.

(iii) *Bursts and crochets.*—The distribution of the differences between the time of upswing of the burst (on the frequency which occurred first) and the time of start of the corresponding crochet is given in Fig. 11. The median delay of the crochets after the bursts is about ½ minute.

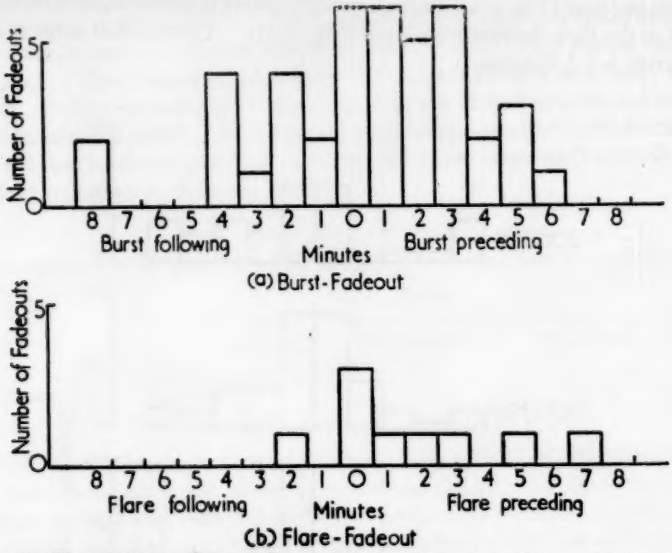

FIG. 9.—(*a*) *The distribution of time differences between the start of a fadeout and the upswing of the burst which occurred first.*
(*b*) *The distribution of time differences between the commencement of flares and fadeouts.*

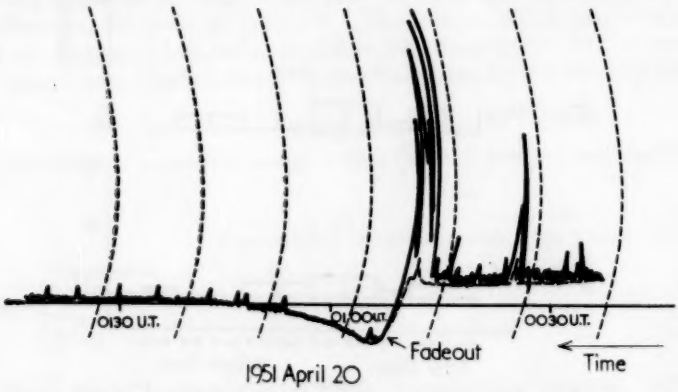

FIG. 10.—*An 18 Mc/s galactic record showing a fadeout preceded by a burst. The dotted curve is a record from an aerial directed away from the Sun (the burst is consequently smaller and the beginning of the fadeout is visible).*

(d) *Intensity relations between bursts, flares, fadeouts and crochets.* (i) *Burst intensity and flare importance.*—The distribution of burst intensities among the 4 flare classes (no flare, and flares of importance 1, 2 and 3) is shown in Fig. 12. Flares of the various classes are seen not to be restricted to any burst intensity range; nevertheless, small flares tend, on the average, to give smaller bursts.

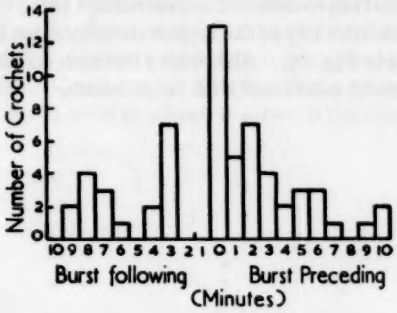

FIG. 11.—*The distribution of time differences between the start of the crochet and the upswing on the frequency which occurred first in the related burst.*

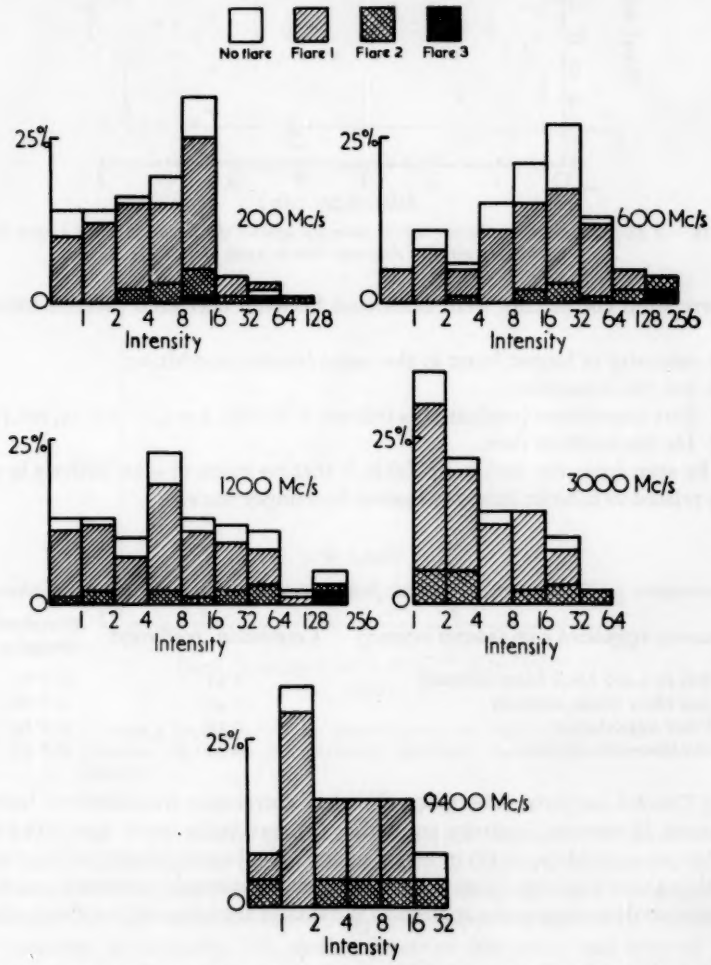

FIG. 12.—*The distribution of flares amongst the various ranges of burst intensity at* 200, 600, 1200, 3000 *and* 9400 *Mc/s. The intensity scales are in arbitrary units.*

(ii) *Fadeout and burst intensities.*—The corrected* value of fadeout intensity is compared with the peak intensity of the largest simultaneous burst observed in the range 600 to 9400 Mc/s in Fig. 13. Although a close correlation does not exist, the intense fadeouts tend to be associated with large bursts.

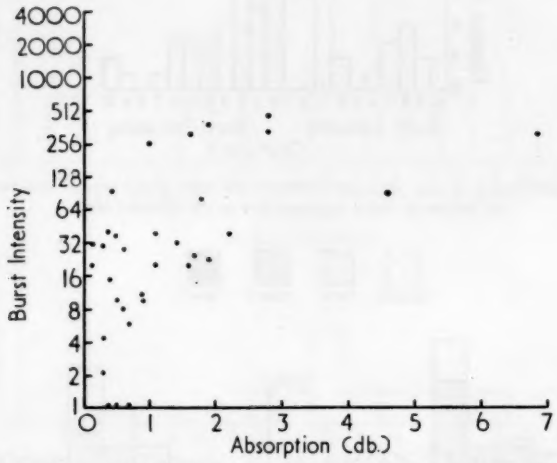

FIG. 13.—*A plot of corrected galactic fadeout intensity against the intensity of the largest burst which occurred in the range 600 to 9400 Mc/s.*

Correlation coefficients were calculated between corrected fadeout intensity and

(*a*) intensity of largest burst in the range 600 to 9400 Mc/s;
(*b*) 200 Mc/s intensity;
(*c*) flare importance (evaluated as follows, $1^- = 0{\cdot}67$, $1 = 1$, $1^+ = 1{\cdot}33$, etc.);
(*d*) Hα linewidth of flare.

It can be seen from the results in Table V that no index of solar activity is more closely related to fadeout intensity than is flare importance.

TABLE V

Correlation coefficients between galactic fadeout intensity and burst and flare indices

Quantity correlated with fadeout intensity	Correlation coefficient	Standard deviation
600 to 9400 Mc/s burst intensity	0·51	±0·12
200 Mc/s burst intensity	0·40	±0·16
Flare importance	0·56	±0·14
Hα linewidth of flare	0·14	±0·25

(iii) *Crochet and burst intensities.*—No clear correlation was observed between the crochet *H*-element intensity and either (*a*) maximum burst intensity in the range 600 to 9400 Mc/s, or (*b*) intensity of 200 Mc/s bursts (shown in Fig. 14 (*a*)). McNish (**14**) has postulated that the size of a crochet is roughly proportional to the simultaneous daily magnetic variation. We should then expect that the quotient,

* See Section 2.

H-element intensity divided by the daily variation, might show a correlation with burst intensity. Fig. 14(*b*) shows that high quotient values tend to occur only with large bursts, though a detailed correlation is not present.

A note on the correlations between bursts and the geomagnetic phenomena, magnetic storms and world-wide crochets, is given in the Appendix.

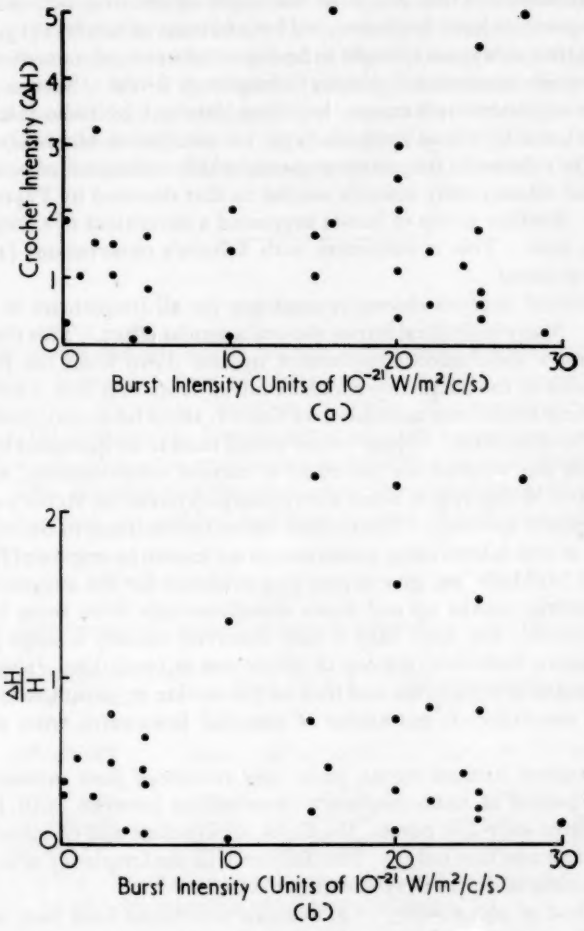

FIG. 14.—(*a*) *H-element intensity of crochet plotted against 200 Mc/s burst intensity.*
(*b*) *Quotient (H-element intensity/daily variation) plotted against 200 Mc/s burst intensity.*

5. *Discussion.* (a) *Change of characteristics with frequency.*—The outstanding feature is the occurrence of the jaggedness at only the low frequencies and the consequent smaller decay times observed at those frequencies. The jaggedness decreases in intensity with increasing frequency while the smoothed (minimum) burst increases in intensity. At the extremes of frequency one type of burst

activity can occur without the other. Thus it is suggested that there may be two separate components of bursts, one which shows rapid fluctuations and preponderates at the low frequencies, and one which is smooth and is characteristic of the high frequencies (although it may occur at low frequencies also). The latter has a spectrum similar to that of the quiet Sun and may possibly be thermal in origin. It is possible that plasma oscillations give rise to the jagged burst component.

(b) *Delay times.*—Time delays of the order of minutes between bursts on different frequencies have been observed by a number of workers (**15, 12, 6, 4, 5, 16**). These time delays are thought to be due to the outward movement of ionized material through successive "plasma" frequency levels. Such a movement, followed by an inward movement, has been detected by radio interferometric methods (**11**) and by visual methods (**17**). A number of bursts studied in the present analysis showed a frequency sequence which corresponded to a movement outwards and subsequently inwards similar to that detected by Payne-Scott and Little (**11**). Another group of bursts suggested a movement of exciting material towards the Sun. This is consistent with Ellison's observations (**17**) of surge prominence material.

The statistical analysis showed a tendency for all frequencies to lag behind 3000 Mc/s. Many individual bursts showed a similar effect. This time sequence would suggest a simultaneous movement up and down from the level of zero refractive index at the frequency which occurred first. At 600, 1200, 3000 and 9400 Mc/s these levels were calculated by Smerd (**18**) to be 10 000, 5000, 3000 and 500 km for the quiet Sun. These values would need to be increased by a factor of approximately five to allow for the effect of coronal condensations, supposed by Waldmeier and Müller (**19**) to occur above sunspots (from the vicinity of which the ionized material is ejected). The revised values approximate to the heights of the top of flares, at which level surge prominences are known to originate (Ellison (**17**)). Dodson and McMath (**20**) give supporting evidence for the suggestion that the radiating material moves up and down simultaneously from some levels in the solar atmosphere. On 1951 May 8 they observed visually a surge prominence associated with a limb flare, the top of which was at 10 000 km; ionized material rose to 50 000 km at 700 km/sec and then to 200 000 km at 300 km/sec; in addition there was a simultaneous movement of material downwards from the 5000 km level.

(c) *Association between bursts, flares and terrestrial flare accompaniments.*—During the period of radio-frequency observations between 1950 January and 1951 June there were 400 bursts, 300 flares, 92 crochets and 68 galactic fadeouts (the latter cover one year only). The difference in the frequency of occurrence of these phenomena is due to the following effects:

(*a*) Method of observation—e.g. overcast conditions limit flare observations and magnetic storminess prevents the detection of crochets.

(*b*) Intrinsic differences in the frequency of occurrence—even under favourable observing conditions more bursts can be detected than flares, fadeouts or crochets. Nearly all flares and their terrestrial accompaniments are coincident with bursts. (The proportion of flares, fadeouts and crochets unaccompanied by bursts is 1 per cent, 1 per cent and 2 per cent respectively). Hence bursts are a sensitive indicator of solar activity and may be used to confirm doubtful fadeouts and crochets. Eighty-one per cent of bursts are simultaneous with flares of importance 1⁻ or greater. Some of the remaining bursts are accompanied by less intense

forms of flare activity while others accompany phenomena (fadeouts and crochets) normally associated with flares. It is thus concluded that bursts are caused not only by flares of importance 1⁻ or greater but also by less intense flare-like activity, perhaps in the bright floccular regions near sunspots.

6. *Acknowledgments.*—Thanks are due to many in this Division who have helped in the maintenance of equipment and the taking of radio observations. The author wishes to thank Dr Woolley, the Commonwealth Astronomer, for making available the 200 Mc/s data, and Mr R. F. Thyer, Chief Geophysicist of the Bureau of Mineral Resources, for allowing use of the Toolangi magnetograms. The author is indebted to Mr C. A. Shain of this Laboratory for his help in the interpretation of the 18 Mc/s galactic radiation data. Particular thanks are due to Dr J. L. Pawsey, Assistant Chief of the Radiophysics Division and to Mr W. N. Christiansen for their help and encouragement during the course of this work.

APPENDIX

Magnetic storms and world-wide crochets.—Normally it is difficult to establish the association between a flare or burst and the sudden commencement of a magnetic storm a day later. However, if these phenomena occur in a quiet solar period, the relationship may be detected. On four occasions tabulated in Table VI, a sudden commencement was preceded by a burst although no flare was observed. This substantiates the conclusion above that weak flare-like activity (which can produce the sudden commencements) as well as larger flares may cause bursts.

TABLE VI

Sudden commencement of magnetic storms accompanied by bursts but not by flares

Sudden commencement of a magnetic storm (U.T.)		Burst (U.T.)		Time delay between burst and S.C.	Flare records I.A.U.	Tokyo
1950						
Sept.	$15^d\ 10^h\ 18^m$	Sept.	$14^d\ 05^h\ 05^m$	$29^h\ 13^m$	N.F.*	N.F.*
1951						
Feb.	$5^d\ 04^h\ 22^m$	Feb.	$4^d\ 07^h\ 24^m$	$20^h\ 58^m$	N.R.†	N.R.†
April	$16^d\ 06^h\ 52^m$	April	$17^d\ 05^h\ 21^m$	$25^h\ 31^m$	N.F.*	N.R.†
June	$25^d\ 04^h\ 27^m$	June	$24^d\ 07^h\ 15^m$	$22^h\ 12^m$	N.F.*	N.R.†

* N.F. No flare observed although the Sun was watched.
† N.R. No recording with spectrohelioscope.

It is known to geophysical workers that a crochet observed in the sunlit hemisphere of the Earth may sometimes be accompanied by a simultaneous effect in the dark hemisphere. Such world-wide crochets are rare and their association with flares is not well established. Sixteen world-wide crochets observed at the Toolangi Magnetic Observatory were associated with observations at daylight stations; a flare was simultaneous with only one of these. Eleven world-wide crochets not accompanied by a reported flare were associated with bursts and are listed in Table VII.

TABLE VII

A list of world-wide crochets accompanied by bursts but not by flares

Time (U.T.) 1950		Time (U.T.) 1950	
Feb.	$17^d\ 23^h\ 08^m$	July	$21^d\ 00^h\ 46^m$
March	$25^d\ 04^h\ 53^m$	Aug.	$2^d\ 22^h\ 04^m$
May	$5^d\ 05^h\ 50^m$	Aug.	$3^d\ 01^h\ 20^m$
May	$20^d\ 20^h\ 15^m$	Aug.	$9^d\ 00^h\ 04^m$
May	$20^d\ 20^h\ 36^m$	Nov.	$15^d\ 06^h\ 45^m$
July	$19^d\ 00^h\ 33^m$		

These phenomena thus appear to be genuine and may be supposed to have a flare-like origin judging from their association with bursts.

Division of Radiophysics,
Commonwealth Scientific and Industrial Research Organization,
Sydney, Australia:
1953 *December* 21.

Jodrell Bank Experimental Station,
Lower Withington, Macclesfield,
Cheshire.

References

(1) A. E. Covington, *J. Roy. Astron. Soc. Canada*, **45**, 15, 1951.
(2) R. Payne-Scott, *Aust. J. Sci. Res.* A, **2**, 214, 1949.
(3) J. S. Hey, S. J. Parsons and J. W. Phillips, *M.N.*, **108**, 354, 1948.
(4) W. N. Christiansen, J. V. Hindman, A. G. Little, R. Payne-Scott, D. E. Yabsley and C. W. Allen, *Aust. J. Sci. Res.* A, **4**, 51, 1951.
(5) G. Reber, *Science*, **113**, 312, 1951.
(6) J. P. Wild, *Aust. J. Sci. Res.* A, **3**, 399, 1950.
(7) J. P. Wild, *Aust. J. Sci. Res.* A, **3**, 541, 1950.
(8) J. P. Wild, *Aust. J. Sci, Res.* A, **4**, 36, 1951.
(9) R. D. Davies and J. V. Hindman, R. P. R. 127, available on request to the Chief of the Radiophysics Laboratory, C.S.I.R.O., University Grounds, Sydney, Australia.
(10) C. W. Allen, *M.N.*, **107**, 386, 1947.
(11) R. Payne-Scott and A. G. Little, *Aust. J. Sci. Res.* A, **5**, 32, 1952.
(12) A. E. Covington and W. J. Medd, *J. Roy. Astron. Soc. Canada*, **43**, 106, 1949.
(13) H. Dodson, R. Hedeman and L. Owren, Reported to U.R.S.I. Xth General Assembly, Sydney, 1952.
(14) A. G. McNish, *Terr. Mag.*, **42**, 109, 1937.
(15) R. Payne-Scott, D. E. Yabsley and J. G. Bolton, *Nature*, **160**, 256, 1947.
(16) J. P. Hagen and N. Hepburn, *Nature*, **170**, 244, 1952.
(17) M. A. Ellison, *M.N.*, **109**, 3, 1949.
(18) S. F. Smerd, *Proc. I. E. E.*, **97**, 447, 1950.
(19) M. Waldmeier and H. Müller, *Zs. f. Ap.*, **27**, 58, 1950.
(20) H. Dodson and R. R. McMath, *Ap. J.*, **115**, 78, 1952.

THE HELIUM STAR HD 168476

A. D. Thackeray

(Received 1953 October 27)

Summary

Wave-lengths of 206 absorption lines have been measured in HD 168476 between 3700 and 6700 A. No lines of hydrogen or oxygen are found, while lines of He I, C II and Ne I are prominent. A list is given of the various elements represented. A large range of excitation and ionization potentials is exhibited. Ti II, with the same I.P. as H and O I, is definitely present. Except for H and O, a fair match with the spectrum of the B5 supergiant 67 Oph can be made, but equivalent widths in HD 168476 are about twice those in the supergiant; this corresponds roughly to increasing the number of atoms above the photosphere by a factor 10. The observations are consistent with a great deficiency of hydrogen causing increased transparency and the spectral characteristics of a supergiant.

The velocity −165 km/s appears to be constant. In view of the large positive velocity of HD 160641, a similar H-weak star, these stars must be regarded as high-velocity objects rather than as exhibiting peculiar atmospheric motions. Proper motion data suggest an absolute magnitude of −2 or brighter; this is supported by evidence from a line in HD 168476 which is probably due to interstellar calcium.

---

1. *Introduction.*—There are now three high-temperature stars known in whose spectra no lines of hydrogen, in emission or absorption, can be found.

These stars, in order of discovery, are:

HD	m_v	Sp.	Reference
124448	10·1	B2	D. Popper, *P.A.S.P.*, **54**, 160, 1942; **59**, 320, 1947.
160641	9·8	O	W. Bidelman, *Ap. J.*, **116**, 227, 1952.
168476	8·9	B	A. D. Thackeray and A. J. Wesselink, *Obs.*, **72**, 248, 1952.

The present paper is concerned with the spectrum of the brightest of the three, HD 168476, as recorded with the Cassegrain 2-prism spectrograph of the Radcliffe 74-inch reflector. Seventeen plates with the *f*/3·7 camera (49 A/mm at Hγ) and five plates with the *f*/6 camera (29 A/mm at Hγ) are available. The latter plates have been measured thoroughly for identification of absorption lines, while the lower dispersion plates have been used primarily for measures of velocity. One two-hour exposure with the *f*/6 camera, taken in excellent conditions, is heavily overexposed in the ordinary photographic region, but permits a study of the interesting region 3700–3900 A at the relatively high dispersion of about 16 A/mm. Another plate on 103 aF emulsion permits a study of the region 5000–6700 A.

2. *Identification and representation of elements.*—A total of 206 absorption lines have been measured between 3700 and 6700 A. Of these, 39 lines, in addition to being recorded only once (chiefly because only one plate was available for the relevant region), are marked as of questionable reality. But many of them can be identified with some confidence as weaker members of multiplets known to be

present. In all, some 170 lines have been identified in HD 168476 and no strong lines remain unidentified.

The list of measured wave-lengths and identifications is not published here as it is hoped that eventually the star may be studied with still higher dispersion. But a list has been deposited with the Society, and duplicated copies will be issued on request to the author.

Identifications were made with the help of Mrs Moore-Sitterly's *Revised Multiplet Table* in the usual manner. The representation of the various elements is as follows:

H — No Balmer lines are recorded, not even on spectra widened more than usual which would bring out broad shallow features. It can be stated that if Hγ had a normal profile with equivalent width 0·15 A it should have been measured on at least one plate; the limit might be put even lower at about 0·10 A. The upper limit for Hα is much larger owing to the lower dispersion in the red.

H_2 — Although it is excessively unlikely that hydrogen could exist in molecular form at the temperature of HD 168476, this question was investigated by searching for lines of H_2 of intensity 10 in the list by Gale, Monk and Lee. Only one coincidence occurred with a faint unidentified line in HD 168476 and this must be attributed to chance.

He I — All accessible lines in the *R.M.T.* except the forbidden appear. The diffuse singlets are very strong relative to the triplets. The diffuse series $2\,^1P^0 - n\,^1D$ appears strongly in the ultra-violet and probably extends beyond the laboratory limit of 3756 ($n = 14$). Details of identifications of this line and the next two with extrapolated wave-lengths are as follows:

λ measured	Int.	Suggested identification (with blends)
3756·80	Bd. NN	He 66 56·10, Fe II 154 55·56, (Ca II 8 55·6, ?Cr II 20 54·59)
3745·92	4	He p 45·8, V II 15 45·81, ?Fe I 5 45·56
3736·98	4	He p 37·3 Ca II 3 36·90, ?Fe I 5 37·13

The line 3756 appears as a remarkably diffuse shallow feature, attributable to blending to a large extent. However, it seems possible that the diffuseness is partly connected with the fact that the upper state 14 ^{1}D lies only 0·02 cm^{-1} from 14 ^{3}D; the upper state may thus be broadened by perturbation. The corresponding line in the diffuse triplet series is at 3487 A and lies outside the scope of the present investigation.

He II — Not found.

C I — Not found, but no good lines are accessible.

C II — Well represented by strong lines. Components of the following *R.M.T.* multiplet numbers are present: 2, 4, 5, 6, (13, 15), 16, ?17, (18, 22), 28, 33, 36, ?37, (39, 40), ?45. Numbers in brackets, here and in the following, refer to possible contributions to blends.

C III — Probably absent. 4650 is suspected as an extremely weak feature on one plate.

N I — Present; multiplets 10, ?16, 21. The blend at 6483 is moderately strong; this feature has been found strong in the hydrogen-weak star υ Sgr.

N II — Present; multiplets 5, 6, (8), 12, 15, (17), ?19, (48), ?(58, 59).

N III — Not found.

O I, II, III Not found. A strong broad feature is measured at 4075·76 but this is attributed entirely to the C II blend of multiplet 36. This is supported by the measured wave-length and by the fact that none of the other expected O II lines (e.g. 4649, 4414, etc.) are found.* It would be of interest to search for the strong O I triplet at 7774 A, since the level of ionization in HD 168476 is probably near the I.P. of O I.

Ne I Present; multiplets 1, 3, 5, 6, ?9, ?19. Although the lines do not appear strongly, on account of the low dispersion in the red, they must be enormously strong relative to other B stars. Several Ne lines are assigned the same visual intensity (3) as He 5876; the latter line appears strongly in the Michigan tracing of β Ori, while the Ne lines appear on the margin of visibility. These lines of Ne I are also strongly recorded by Greenstein in υ Sgr, the first star in which they were astrophysically observed.

Ne II Not found.

Na I Presence in stellar or interstellar form is masked by C II.

Mg I Not found, although 3838 might contribute weakly to a blend.

Mg II Present; multiplets 4, ?5, ?9, 10, ?18, (19), 20, (21), ?25, 26.

Al II Present; multiplets (1), ?45, ?46, 57. The evidence rests mainly on the line at 6201 A.

Si I The line 3905 is very doubtfully present as a contributor to a blend.

Si II Present; multiplets 1, 2, 3, (4), 5.

Si III May be represented by multiplet 2, 4552 being blended with N II, 4567 appearing on the margin of visibility.

P II Possibly represented weakly by members of multiplet 6 but 5253 is not found. Higher dispersion in the green is required to settle the question.

S I Not found.

S II Well represented by numerous faint lines; multiplets 6, ?8, 9, 11, 14, 19, (26), ?29, ?36, 40, ?43, 44, 45, 49, 59.

A I A few lines of multiplet 2 appear to be present.

A II Not found.

K II Not found.

Ca I The resonance line 4226 is not found.

Ca II H and K strong; multiplets 3 and 8 also found in the ultra-violet but blended.

Ca III The few accessible lines have E.P. 30 volts and are probably absent.

Sc II Possibly represented weakly by the lines 4246 and 4314.

Ti II Present; multiplets 13, 19, 20, 34, 41, (82), ?104, ?105. The presence of this ion of a relatively rare element is of special interest in view of the fact that its ionization potential is practically identical with that of H and of O I, which are not found.

V II Probably represented by the multiplets ?10 (15).

Cr II 4558 possibly appears weakly on one plate, and two lines of multiplet 20 may contribute to blends.

Mn II Not found; the best lines lie beyond the ultra-violet limit.

* It appears probable that the same argument applies to the feature at 4075 in HD 124448 which Popper attributes entirely to O II. None of the other expected O II lines are measured by Dr Wesselink in his Radcliffe spectra of HD 124448.

Fe I May be represented by the strongest lines in multiplets 4, 5; there are no other satisfactory identifications for lines at 3719·69 (int. ?4n), and 3860·23 (?2n); other lines may contribute to blends.

Fe II Well represented by fairly weak lines; multiplets 27, 28, 37, 38, ?40, 42, 48, 49, 154, ?172, 173, ?190.

Fe III 4419 is a weak line, and 4396 may contribute to a blend. Some lines of multiplet 118 (E.P. = 20·5) also seem to be present.

Ni II 4067 and 3849 may be weakly present.

Other elements; not found.

In general there appears to be fair correlation between the estimated intensities in HD 168476 and Struve's* estimates in the supergiant 67 Oph (B5 HD; B8s Vict.; B5 Ib MK) except for H and O II. In Fig. 1 the visually estimated intensities in these two stars are plotted against each other. Note that the groups of lines with widely different excitation potentials have a fairly random scatter about a straight line. Note also that the estimated intensities in HD 168476 run systematically higher than for 67 Oph despite the much lower dispersion used for the former star; (Struve used in part Mt. Wilson Coudé spectra).

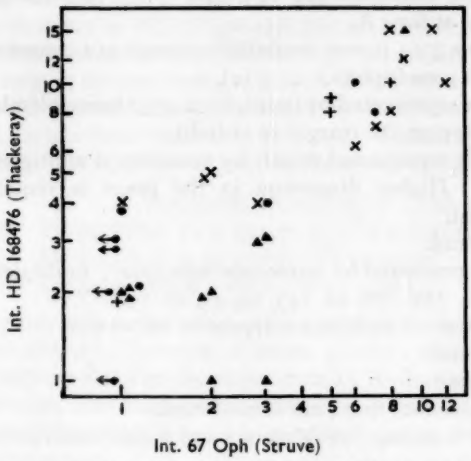

FIG. 1.—*Comparison of visual intensities in HD 168476 and 67 Oph.*

●	*Fe* II, *Ca* II	*E.P.* 0–3
+	*Mg* II, *Si* II	*E.P.* 8–10
▲	*N* II, *S* II, *C* II	*E.P.* 14–19
×	*He* I	*E.P.* 20–21

Arrows to the left indicate lines not observed in 67 Oph. The Balmer lines would appear outside the figure below the right-hand corner.

3. *Measures of equivalent widths.*—A few selected lines have been measured for equivalent width, the plates having been calibrated with a tube sensitometer. These measures must be regarded as highly provisional and it is hoped to replace them eventually with more extensive ones of higher dispersion. The accompanying table gives the results, which depend in most cases on one plate only.

* O. Struve, *Ap. J.*, **74**, 230, 1931.

TABLE I

Provisional equivalent widths in HD 168476 (*angstroms*)

Line	E.W.	Line	E.W.
Si II 3853	0·33	He I 3964	0·74
Si II 3856	0·59	N II 3995	0·30
Si II 3862	0·48	He I 4120	0·54
He I 3927	1·2	Si II 4130	0·56
Ca II 3933	0·76	He I 4143	2·1
Ca II 3968	0·62	C II 4267	0·92

The helium lines and C II 4267 are stronger than in any star in Williams' list.* The lines with widths greater than 1 A have wings, perhaps due to Stark effect. All lines have sharp cores.

The ultra-violet Si II triplet lines have theoretical relative intensities 1 : 9 : 5 and since the strongest, 3856, is practically equal to Ca II 3968, they can be combined with *H* and *K* to give a rough idea of the shape of the curve of growth in the range 0·3 to 0·8 A, with a range in *Nf* of relative intensity 18 : 1. The mean slope ($\Delta \log W/\lambda : \Delta \log Nf$) is about 0·3.

4. *Excitation and ionization.*—The lower excitation potentials of lines appearing strongly in HD 168476 range from 0·0 (*H* and *K*) to 21·1 (He I) and 24·3 (C II). The ionization potentials of well-established ions range from 11·8 (Ca II) to 29·5 (N II); but outside this range there is doubtful evidence for Fe I (7·86 volts), ?Mg I (7·61) and Si I (8·11), and at the high level, Fe III (30·5) and Si III (33·3).

The excitation and ionization potentials represented are illustrated in Fig. 2, the joining lines or dashes giving a rough indication of the intensities of the corresponding lines. There are two points requiring special mention concerning this figure. First, the wide range in excitation and ionization, which would probably be still better indicated were higher dispersion available, has a parallel in the wide range exhibited by the star *υ* Sgr and emphasized by Greenstein and Adams.† Secondly, the range in E.P. easily includes those of the Balmer lines and also includes near the upper limit those of strong lines of O II which have not been found. Moreover, the ionization potentials of H and O I are both practically identical with that of the relatively rare ion Ti II which is observed. As with *υ* Sgr, but to an exaggerated degree, there appears to be no escape from the conclusion that hydrogen really is extremely deficient in the atmosphere of HD 168476, being far less abundant than helium, probably less than carbon and neon, and that oxygen is less abundant than carbon. It is unfortunate that the present observations do not cover the ultra-violet series limit of helium where Popper‡ has observed a depression in the spectrum of the similar star HD 124448, but there can be little doubt that the same effect could be observed in HD 168476.

5. *Consequences of hydrogen deficiency.*—The cosmic abundance of hydrogen has so many important consequences that one would expect to see many marked peculiarities in a hydrogen-weak atmosphere. The effects have been considered, for instance, by H. N. Russell§ when he originally put forward the evidence for the great abundance of hydrogen in his classical papers.

The first effect is due to the fact that in the atmosphere of a normal late B type star hydrogen provides essentially all the electrons and is thus the most important

* E. G. Williams, *Ap. J.*, **83**, 279, 1936.

† J. L. Greenstein and W. S. Adams, *Ap. J.*, **106**, 339, 1947; see esp. p. 349.

‡ D. Popper, *P.A.S.P.*, **59**, 320, 1947.

§ H. N. Russell, *Ap. J.*, **78**, 239, 1934 (esp. last two paragraphs p. 297).

source of opacity. If the hydrogen were removed, all lines due to other elements would be strengthened, due to the increased transparency. But the lowering of the electron pressure would increase the state of ionization and produce effects normally attributed to a supergiant atmosphere.

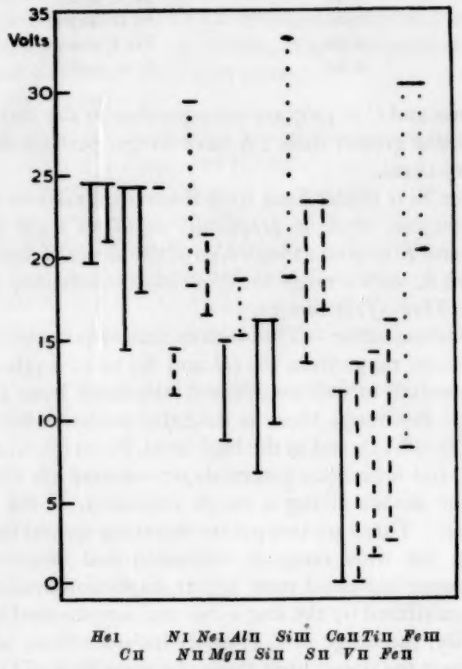

FIG. 2.—*Representation of excition and ionization potentials in HD* 168476.
Strong lines are represented by continuous lines joining the I.P. and lower E.P. Intermediate lines are represented by dashes and weak lines by dots.

In HD 168476 we observe such effects. All lines in such supergiants as 67 Oph and β Ori, with the exception of H and O II, appear to be strengthened. Increased transparency of the atmosphere compared even with a supergiant is definitely indicated.

Secondly, there is the question of the hydrogen convection zone. If hydrogen should be less abundant than say carbon, then presumably helium would replace hydrogen as the effective agent in setting up a convection zone. At the temperature of HD 168476 this would presumably lie chiefly below the photosphere, just as does the hydrogen convection zone in the Sun. However, Eddington* has shown how the solar convection zone can extend itself into much higher layers than the limits given by Unsöld's original calculations. It seems reasonable to suppose that the helium convection zone in HD 168476 extends up into the observable portion of the atmosphere. This, as well as the transparency of the atmosphere, may contribute to the large range in excitation and ionization in the observed spectrum.

* A. S. Eddington, *M.N.*, **101**, 177, 1941; **102**, 154, 1942.

Thirdly, a deficiency of hydrogen might have a marked effect upon the damping portion of the curve of growth. Collisional damping, which may vary from line to line, is dependent in a normal atmosphere on the density of hydrogen and of electrons. It is hoped eventually to construct a curve of growth for HD 168476 from plates of high dispersion. But what evidence there is at present available suggests that the damping portion of the curve of growth is not reached by lines as strong as *H* and *K* (see Section 3).

6. *The transparency of the atmosphere.*—We can make a rough estimate of the increased transparency by means of the equivalent widths in Table I. HD 168476 is matched much better by 67 Oph than by β Ori, but unfortunately no equivalent widths are available for 67 Oph. Instead, the following indirect approach is adopted. Struve's visual estimates in β Ori were calibrated by measuring the equivalent widths on the Michigan *Atlas* tracings of this star. It was then assumed that Struve's visual estimates for 67 Oph followed the same calibration. The widths derived in this way for 67 Oph (W_{67}) were then compared with the widths directly measured in HD 168476 (W^*). We thus find:

Line	3933	3964	3995	4120	4130	4143	4267
log W^*/W_{67}	+·40	+·31	+·39	+·25	+·34	(+·62)	+·28

Excluding the strongly winged line 4143 we find as a mean value

$$\log W^*/W_{67} = +0{\cdot}33 \pm 0{\cdot}02.$$

Thus the E.W.'s in HD 168476 are about twice those of corresponding lines in 67 Oph. This ratio applies to the portion of the curve of growth covered by the Si II and *H* and *K* lines, whose slope is about 0·3. Hence it would need a reduction by a factor 10 in the number of atoms above the photosphere of HD 168476 to bring the equivalent widths in this star to equality with those in the supergiant 67 Oph. This could be taken as a measure of the relative transparencies of the atmospheres of the two stars, provided the parameters of the curves of growth (turbulence, temperature, etc.), are effectively the same.

7. *The radial velocity.*—As announced in the discovery note, the velocity of HD 168476 is high. From 21 plates we find a velocity relative to the Sun of

$$-165{\cdot}0 \pm 0{\cdot}8 \text{ (m.e.)}.$$

Some of the earlier plates suggested possible variations in velocity over intervals of some months, but from the present evidence the velocity should probably be regarded as constant. The range in velocity for 4 "b" plates (29 A/mm) is 7·7 km/s, for 17 "c" plates (49 A/mm) 18·7 km/s. The differences between individual plates may arise in part from the influence of faint blending lines, especially if the lines vary slightly in intensity—a circumstance for which there is some evidence. If the differences are real they cannot be reconciled with any period in excess of a day. There is no evidence for systematic residuals for different lines which could not be attributed to blending. In particular there is no evidence for duplicity of the star.

It is of particular interest to note that the other two hydrogen-poor stars, HD 124448 and 160641, also have high velocities of −65 and about +100 km/s respectively. The positive velocity of HD 160641 is important as indicating that in these three stars we are not dealing with peculiar expanding atmospheres.

They must be regarded as high-velocity objects. It has already been pointed out that the proper motions of HD 168476 and 124448 are both small and apparently normal for B type stars of their apparent magnitude.

8. *The luminosity and colour.*—It is exceedingly difficult to draw any secure conclusions regarding the luminosity of HD 168476. Popper has suggested an absolute magnitude of about $-2{\cdot}5$ to -4 for HD 124448, partly from spectroscopic criteria and partly from the radial velocity which could be attributed to the effect of galactic rotation. However, since these stars are apparently high-velocity objects, the latter argument is quite inconclusive; and it seems dangerous to apply spectroscopic criteria to such peculiar spectra. Hydrogen deficiency will, as mentioned above, tend to produce the characteristics of a supergiant.

However, it does not appear that the absolute magnitude can be fainter than -1. A tangential velocity of 100 km/s at 1400 parsecs would yield an annual proper motion of $0''{\cdot}015$ of arc, which should be perceptible. The proper motion data suggest absolute magnitudes of the order of -2 or brighter.

Another line of approach lies in the intensity of interstellar lines, but here the high galactic latitude ($-20°$) of HD 168476 is a drawback. A line of intensity 2 is recorded at 3970·51 (allowing for a velocity of -165 km/s). No satisfactory identification is possible, the contributions of C II 3970·20 and S II 3970·69 being probably negligible. It is more reasonable to attribute the line to interstellar Ca II with a velocity of -10 km/s. Unfortunately the corresponding *K* component is lost entirely in the strong stellar line He 3935·9. Thus the normal circumstance that interstellar *K* can be measured more accurately than interstellar *H* is reversed.

The equivalent width of the "3970 line" has been measured on one plate as 0·20 A. Assuming it to be entirely due to interstellar Ca II, the width of interstellar *K* should be between 0·30 and 0·35 A. Münch* gives a distance of 550 parsecs for the star HD 84567 at $b = +18°$, with equivalent width 0·14 for the *K* line.

It is probably safe to conclude that if the "3970 line" in HD 168476 is correctly identified with interstellar calcium, then the star must lie at a distance of the order of a kiloparsec, or more; this gives a distance of 340 parsecs from the galactic plane, which would take it outside most of the gaseous substratum. An absolute magnitude $M = -1$ or brighter is indicated.

Dr Wesselink has very kindly undertaken at my request photoelectric measures of the star. He has derived a colour index on the Cape 1953 S system of $-0{\cdot}36$. Using the linear relationship in *Cape Mimeogram* No. 3, this corresponds to $B-V = -0{\cdot}05$ on the Johnson system. The colour matches that of a normal late B type star.

9. *Acknowledgments.*—I am much indebted to Dr A. J. Wesselink, Dr M. W. Feast and Mr A. Morrisby for obtaining six plates of HD 168476 on closely adjacent nights in 1953 for the purpose of studying possible short-period variations in radial velocity; also to Dr Wesselink for undertaking the photoelectric measures of colours of the star. The author is responsible for the other plates and all spectroscopic measures and reductions.

Radcliffe Observatory,
Pretoria:
1953 *October* 22.

* G. Münch, *P.A.S.P.*, **64**, 312, 1952.

PHOTOMETRIC EFFECTS OF REFLECTION IN CLOSE BINARY SYSTEMS

Zdeněk Kopal

(Received 1953 November 17)

Summary

The aim of the present investigation has been to study the mutual illumination of two luminous spheres, reflecting light in accordance with Lambert's law, by taking into account the finite angular size of the light source.

After an expository section containing an outline of our problem (Section 1), exact expressions will be set up which govern the amount of light of one sphere reflected by the other for any geometrical configuration (Section 2). In Section 3 we shall specify the flux of radiation incident upon the fully illuminated as well as penumbral zones of the reflecting component; while in the subsequent Section 4 the exact results of Section 3 will be simplified to the order of accuracy to which two fluid components of a close binary system can be regarded as spheres.

Section 5 will then contain a derivation of the law governing the variation of the amount of reflected light with the phase; while the concluding Section 6 will be devoted to a brief analysis of this law, as well as to an outline of its generalization to the case of distorted binary systems, or to systems exhibiting eccentric orbits.

---

1. *Introduction.*—It is inevitable in close binary systems that a part of the radiation of either component, sent out in every direction, will be intercepted by the surface of its mate where it will be absorbed and re-emitted (or scattered). This fact is bound to cause the hemisphere of each star exposed to incident light to be brighter than that turned away; and as the components revolve, the amount of light* "reflected" in the direction of the line of sight should vary with the phase. This effect has, in turn, long been known to give rise to by far the most intricate part of the theory of eclipsing variables. Even for a plane exposed to parallel light the law of angular distribution of re-emitted radiation is not yet known exactly (1); and in close binary systems the difficulty is greatly increased by the large fractional size of their components. In point of fact, the problem of mutual illumination of two finite spheres alone becomes geometrically so complicated that no other aspect of the interpretation of light curves of eclipsing binary systems has confronted us with greater difficulties.

In the simplest case of the incident light forming a parallel beam (which would correspond to an infinite distance of the illuminating source) and re-emitted in accordance with Lambert's law, the solution of our problem is, of course, well known and had been investigated in connection with planetary phases many years ago (2). A first attempt at taking account of the convergence of the incident beam (which must be considered if the light source is placed at a finite distance from the

* Under this term we shall hereafter understand "integrated radiation in all wave-lengths".

reflecting star) was due to Takeda (**3**), who regarded the secondary component as a non-dimensional light-point illuminating the primary which (as seen from the light source) exposed to the incident light an apparent disk of finite angular size. Takeda carried through an approximate solution of this problem to quantities of the fourth order in the fractional radius of the primary (reflecting) component (i.e. to the order of accuracy to which a distortion of this star due to its own axial rotation as well as to the tidal action of its companion can be ignored). In doing so Takeda committed, however, a mistake of extending the cone of incident light beyond the horizon of visibility of the illuminating light source at the primary star—an oversight which vitiated his fourth-order term and which was eventually corrected by Sen (**4**).

A reconnaissance of the effects of a finite angular size of the illuminating component on the amount of reflected light was first undertaken by Russell (**5**), by an approximate method which was essentially incapable of generalization and which merely permitted a surmise that the contribution of the penumbral zone (where the apparent disk of the illuminating component would appear partly set for an observer on the primary star) is likely to amount to less than one per cent of the total light reflected. Two years later a discussion of the same problem was resumed by Matukuma (**6**). Like Russell, Matukuma did not aim at a derivation of the phase-law of the reflected light, but limited himself to ascertaining the proportion of the total incident light to that reflected in all directions (expressed by what Matukuma called the "criterion formula"). However, in concluding his paper already quoted, Matukuma mentioned that . . . "recently the writer had taken up this problem" (i.e. of the derivation of phase-law) "and has almost completed the necessary calculations. But some minute point, which is obscure in a physical sense, makes him postpone publishing his results". Unfortunately, shortly after writing these words, Matukuma died—apparently without being able to clear up his doubts; and an examination of his "criterion formula" reveals that its derivation was in error*, invalidating his result.

These reasons led the present writer to open up the problem *de novo*, and to work out a detailed theory of the mutual illumination of two finite spheres reflecting in accordance with Lambert's law. Such a theory should, in particular, reveal a variation of the amount of reflected light with the phase, taking account of the finite angular size of the illuminating component. Its application to astrophysical cases will be limited, on one hand, by the extent to which the actual reflecting properties of stellar outer layers depart from Lambert's law; and, on the other, by the assumed spherical shape of both components. Approximate solutions of the problem of radiative transfer of reflected light in stellar atmospheres (**1**) reveal indeed the existence of departures from Lambert's law which should be taken into account in more refined work. Such refinements could, however, be carried through only at the expense of detailed numerical integrations. On the other hand, the assumption that the components possess spherical shape, implying the neglect of first-order rotational and tidal distortion, will restrict the correctness of our work to quantities of the fourth order in the fractional radii of the components. A general theory developed below could, in principle, be extended to distorted stars without essential modification—at the expense of

* The integral for N_1 in Matukuma's equation (13)′ has been evaluated incorrectly—its true value being $(2r_1/3\pi\rho)\sin^3\psi$ rather than $2(r_1/\pi\rho)\sin\psi$ as given by Matukuma—and this slip avalanched through the rest of his paper.

nothing else but additional algebraic work. At present we propose, however, to limit ourselves to a consideration of both components as spheres, and to postpone complications arising from their distortion to subsequent communications.

2. *Geometry of the problem.*—In order to fix our ideas, let us adopt a rectangular frame of reference XYZ, with origin O_1 at the centre of gravity of a star to which we shall hereafter refer as the primary component, and oriented so that the X-axis is constantly in the direction of the secondary (illuminating) component, while the Z-axis is perpendicular to the orbital plane. Let, furthermore, r, η, ϕ be the spherical polar coordinates in this system, related with the rectangular ones by means of the relations

$$\left.\begin{aligned} x &= r\cos\phi\sin\eta, \\ y &= r\sin\phi\sin\eta, \\ z &= r\cos\eta, \end{aligned}\right\} \qquad (1)$$

such that η denotes the polar distance of an arbitrary point P on the surface of the primary (see Fig. 1); and ϕ, its longitude measured from the "principal meridian" in the XY-plane.

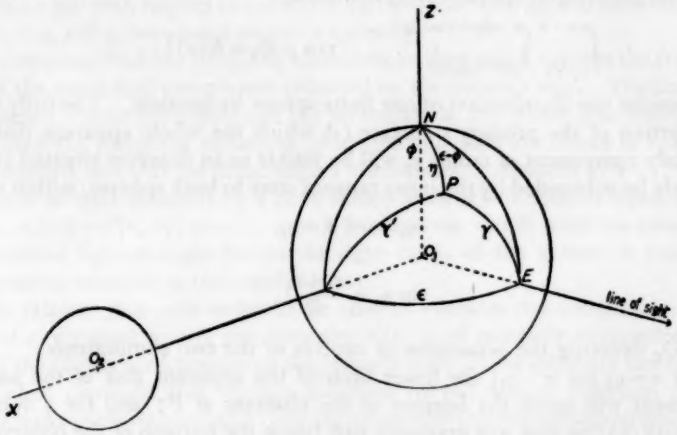

FIG. 1.

As the components revolve, this system of axes will evidently rotate with respect to a fixed line of sight. Let the direction of the latter be described by the direction cosines

$$\left.\begin{aligned} l_0 &= \cos\psi\sin i, \\ m_0 &= \sin\psi\sin i, \\ n_0 &= \cos i, \end{aligned}\right\} \qquad (2)$$

where ψ denotes the true anomaly of the secondary component in its relative orbit (measured from the moment of inferior conjunction), and i the inclination of the orbital plane to the celestial sphere. The angle ϵ between this line and the X-axis joining the centres of both components (whose direction cosines are, therefore, 1, 0, 0) will evidently be given by

$$\cos\epsilon = l_0 = \cos\psi\sin i. \qquad (3)$$

Moreover, the amount $\mathscr{L}$ of the secondary's light "reflected" from the primary

component in the direction of the line of sight should then depend on the true anomaly ψ only through ϵ, and be generally expressible as

$$\mathscr{L} = \int_{\mathbf{C}} \mathscr{I} \cos\gamma \, ds_1, \tag{4}$$

where $\mathscr{I}$ denotes the intensity distribution of reflected light; γ, the angle of foreshortening; and ds_1, the corresponding surface element of the reflecting star; while the domain **C** of integration is to be extended over the crescent visible to a distant observer at any particular phase.

Consistent with the foregoing definitions, the angle γ of foreshortening can be solved for from the spherical triangle NPE (Fig. 1) in the form

$$\cos\gamma = \sin\eta \cos(\epsilon - \phi), \tag{5}$$

while

$$ds_1 = r_1^2 \sin\eta \, d\eta \, d\phi, \tag{6}$$

where r_1 denotes the (constant) radius of the primary component.

As to the limits of integration in both variables let us, for the sake of brevity, introduce the integral operator $K(x)$ defined by

$$\int_{\epsilon-\pi/2}^{\cos^{-1}x} \int_{\sin^{-1}(x\sec\phi)}^{\pi-\sin^{-1}(x\sec\phi)} \ldots\ldots \cos\gamma \, ds_1 = K(x)\{\ldots\}, \tag{7}$$

and consider the illumination of one finite sphere by another. The fully illuminated portion of the primary's surface (at which the whole apparent disk of the secondary component of radius r_2 will be visible to an observer situated at P) will evidently be subtended by the inner tangent cone to both spheres, within which

$$\eta_1 \leqslant \eta \leqslant \pi - \eta_1, \tag{8}$$

where

$$\sin\eta_1 = \frac{r_1 + r_2}{R}, \tag{9}$$

$R \equiv \overline{O_1O_2}$ denoting the separation of centres of the two components.

For $\eta = \eta_1$ (or $\pi - \eta_1$) the lower limb of the apparent disk of the secondary component will touch the horizon of the observer at P; and for η outside the inequality (8) this disk will gradually sink below the horizon of the observer until, for $\eta = \eta_2$ (or $\pi - \eta_2$) such that

$$\sin\eta_2 = \frac{r_1 - r_2}{R}, \tag{10}$$

it disappears completely. Therefore, as long as

$$\eta_1 \leqslant \epsilon \leqslant \pi - \eta_1, \tag{11}$$

the *fully illuminated zone* will eventually be delimited by an application of the integral operator $K(\sin\eta_1)$; while the *penumbral zone* (illuminated by only a part of the apparent disk of the secondary) should be delimited by an application of the operator $K(\sin\eta_2) - K(\sin\eta_1)$.

The foregoing statements are, to be sure, exact as only as long the phase angle ϵ continues to lie between the limits of the foregoing inequality (11); for when

$$-\eta_1 \leqslant \epsilon \leqslant \eta_1, \tag{12}$$

the fully illuminated zone becomes completely exposed to the external observer,

and the lower limit $\epsilon - 90°$ of integration with respect to η in the operator $K(\sin \eta_1)$ should be replaced by $-\cos^{-1}(\sin \eta_1)$.* When, on the other hand,

$$\pi - \eta_1 \leqslant \epsilon \leqslant \pi + \eta_1, \tag{13}$$

the whole fully illuminated zone becomes invisible and the integral $K(\sin \eta_1)\{\dots\}$ then vanishes. Similarly, when

$$-\eta_2 \leqslant \epsilon \leqslant \eta_2, \tag{14}$$

the limb of the penumbral zone becomes a circle, and the lower limit $\epsilon - 90°$ of integration with respect to η in the operator $K(\sin \eta_2)$ should be replaced by $-\cos^{-1}(\sin \eta_2)$. When, ultimately,

$$\pi - \eta_2 \leqslant \epsilon \leqslant \pi + \eta_2 \tag{15}$$

and $r_1 > r_2$, the whole penumbral zone will be lost out of sight of our external observer, and the integral $K(\sin \eta_2)\{\dots\}$ will consequently vanish. Should, on the other hand, the illuminating component be the larger of the two the penumbral zone will not disappear for ϵ constrained by (15) but will continue to surround the primary component with an illuminated ring—obtained again by replacing the lower limit $\epsilon - 90°$ with respect to η in $K(\sin \eta_2)$ by $-\cos^{-1}(\sin \eta_2)$ and remembering that, for $r_1 < r_2$, $\sin \eta_2$ becomes a negative quantity.

It may be added that the foregoing equations, as they stand, express the fraction of light of the secondary component reflected by the primary star. The fraction of the primary's light reflected from the secondary at any phase can likewise be deduced from the foregoing equations, provided only that the values of r_1 and r_2 are interchanged, and that the phase angle ϵ is consistently replaced by $\pi - \epsilon$. The total amount of light reflected by a close binary system will then be equal to the sum $\mathscr{L}(r_1, r_2; \epsilon) + \mathscr{L}(r_2, r_1; \pi - \epsilon)$; and it is this sum which must be taken out of the observed light changes before the light curve of the system is analysed for photometric elements in the usual manner.

3. *The incident flux.*—In order to be able to evaluate the integral (4) as a function of ϵ, we must specify the intensity $\mathscr{I}(\phi, \eta)$ of radiation reflected at any point P of the illuminated portion of the primary star. This intensity can indeed be established provided that we can ascertain (i) the flux of radiation of the secondary component incident at P; and (ii) its transfer (by absorption-re-emission, or scattering) outwards consistent with the requirement that the heat-albedo of the stellar surface must necessarily be unity. This second part of our problem, first considered by Milne (7), has recently become the subject of renewed investigation (1); but its proper solutions are so far only approximately known. In what follows we shall, therefore, by-pass this physical difficulty by assuming that the reflected radiation is uniformly distributed (which is always true to a first approximation), and that its intensity varies in accordance with Lambert's cosine law

$$\mathscr{I}(\phi, \eta) = S \cos \alpha, \tag{16}$$

where πS denotes the flux, per unit area normal to it, originating in the secondary component; and α is the angle of incidence (*cf.* Fig. 2). In the present section our problem will, therefore, be limited to expressing both S and α in terms of our angular variables ϕ, η.

* This case is, however, largely academic; for if $|\epsilon| < |\eta_1|$, the secondary component is going to eclipse the primary star; and if $r_2 > 0$, a part of the reflected light will be lost by eclipse —a situation whose analysis is outside the scope of the present paper.

In order to do so, consider a new rectangular system of axes, with origin at P (see Fig. 2), whose Z-axis coincides with $\overline{O_2P}\equiv\rho$, and the XZ-plane coincides with that of the triangle O_2PQ (i.e. with the plane of the diagram); the Y-axis being perpendicular to it. The direction cosines of an arbitrary radius-vector from O_1 through P then are

$$\cos\alpha,\ \sin\alpha,\ 0;$$

while the direction cosines of $\overline{PQ'}\equiv\rho'$ in the same system become

$$\cos\beta,\ \sin\beta\cos\omega,\ \sin\beta\sin\omega,$$

where β denotes the angle O_2PQ between the vectors ρ and ρ', and $\omega=\angle QP'Q'$ (see Fig. 2).

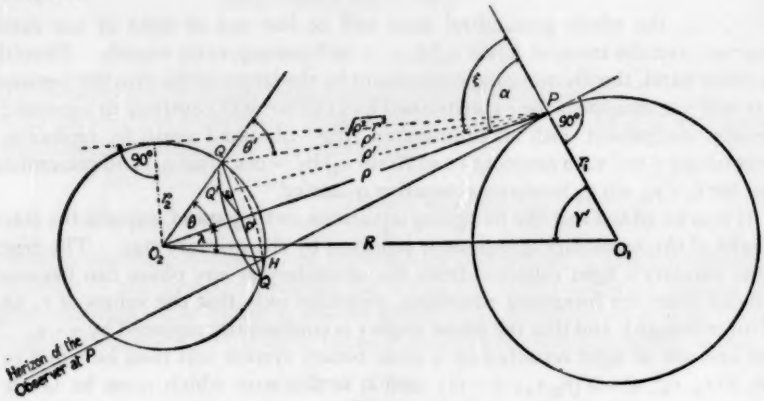

FIG. 2.

If so, the angle ζ between ρ' and the surface normal at P will evidently be specified by

$$\cos\zeta=\cos\alpha\cos\beta+\sin\alpha\sin\beta\cos\omega, \tag{17}$$

where, from $\triangle O_2PQ$,

$$\sin\beta=\frac{r_2}{\rho}\sin\theta' \text{ and } \cos\beta=\frac{\rho-r_2\cos\theta}{\rho'}, \tag{18}$$

while (from the same triangle) it follows that

$$\cos\theta'=\frac{\rho^2-r_1^2-\rho'^2}{2\rho' r_2}=\frac{\rho\cos\theta-r_2}{\rho'}. \tag{19}$$

Therefore,

$$\rho'=\rho^2+r_2^2-2r_2\rho\cos\theta, \tag{20}$$

while (from $\triangle O_1O_2P$)

$$\rho^2=R^2+r_1^2-2r_1R\cos\gamma, \tag{21}$$

where $\gamma'=\angle O_2O_1P$, defined by

$$\cos\gamma'=\sin\eta\cos\phi; \tag{22}$$

and, ultimately,

$$\cos\alpha=\frac{R\cos\gamma'-r_2}{\rho}. \tag{23}$$

The last three equations (21)–(23) define α as a function of ϕ and η; while the flux πS incident at P can be ascertained as follows. Let the distribution of brightness $I(\theta')$ over the apparent disk of the secondary component vary in accordance with the well-known cosine law of limb-darkening as

$$I(\theta') = I(0)\{1 - u + u\cos\theta'\}, \tag{24}$$

where $I(0)$ denotes the intensity at the apparent centre of the illuminating star and u, its coefficient of darkening. The intensity $\mathcal{I}(\phi, \eta)$ of light reflected at P can then be expressed as

$$\mathcal{I}(\phi, \eta) = I(0)\{(1-u)J_1 + uJ_2\}, \tag{25}$$

where

$$\pi J_n = \int \frac{\cos\zeta \cos^n\theta'}{\rho'^2}\, ds_2, \tag{26}$$

the surface element ds_2 of a (spherical) secondary component being, in turn, expressible as

$$ds_2 = r_2^2 \sin\theta\, d\theta\, d\omega = r_2(\rho'/\rho)\, d\rho'\, d\omega; \tag{27}$$

while $\cos\zeta$ and ρ' continue to be defined by (17) and (20).

As long as the whole apparent disk of the secondary component remains visible to the observer at P, the limits of integration in ω extend from 0 to 2π. If so, however, the integration with respect to ω clearly annihilates the second part of the right-hand side of (26) arising from the second term on the right-hand side of the equation (17) for $\cos\zeta$, leaving us with

$$\pi J_1 = \int_{\rho_1}^{\rho_2}\int_0^{2\pi} \frac{\cos\alpha\cos\beta}{\rho'^2}\,\frac{\rho^2 - r_1^2 - \rho'^2}{2\rho}\, d\rho'\, d\omega, \tag{28}$$

where

$$\left.\begin{aligned} \rho_1 &= \rho - r_2, \\ \rho_2 &= (\rho^2 - r_2^2)^{1/2}, \end{aligned}\right\} \tag{29}$$

and $\cos\alpha$ as well as $\cos\beta$ have already been defined in terms of our variables of integration. Integrating, we thus establish that

$$J_1 = \frac{\cos\alpha}{2\rho^2}\int_{\rho_1}^{\rho_2} \frac{(\rho^2 - r_2^2)^2 - \rho'^4}{\rho'^3}\, d\rho' = \frac{r_2^2}{\rho^2}\cos\alpha; \tag{30}$$

while, similarly,

$$\begin{aligned} J_2 &= \int_{\rho_1}^{\rho_2}\int_0^{2\pi} \frac{\cos\alpha\cos\beta}{\rho'^2}\left\{\frac{\rho^2 - r_1^2 - \rho'^2}{2r_2\rho'}\right\}^2 \frac{r_2\rho'}{\pi\rho}\, d\rho'\, d\omega \\ &= \frac{2}{3}\frac{r_2^2}{\rho^2}\cos\alpha. \end{aligned} \tag{31}$$

Inserting (30) and (31) in (25) we find, eventually, that

$$\mathcal{I}(\phi, \eta) = \frac{L_2\cos\alpha}{\pi\rho^2}, \tag{32}$$

where

$$L_2 = \pi r_2^2 I(0)\{1 - \tfrac{1}{3}u\} \tag{33}$$

represents the apparent luminosity of the secondary component. At any point of the *fully illuminated zone* the flux incident upon P proves to be proportional

to the total light of the secondary component, and inversely proportional to the square of the distance of its centre from P; so that, by (32) and (21)–(23),

$$\mathscr{I}(\phi, \eta) = \frac{L_2}{\pi} \frac{R\mu - r_1}{(R^2 + r_1^2 - 2r_1 R\mu)^{3/2}}, \tag{34}$$

where we have abbreviated

$$\mu = \cos \gamma' = \sin \eta \cos \phi. \tag{35}$$

In the *penumbral zone* the situation becomes complicated by virtue of the fact that the secondary component now undergoes eclipse by the horizon of the observer (which acts as a straight occulting edge), and only the light of the uneclipsed portion will continue to illuminate the surface element at P. In order to evaluate the intensity of light reflected from any point of the penumbral zone, let us write again

$$\mathscr{I}'(\phi, \eta) = I(0)\{(1-u)J_1' + uJ_2'\}, \tag{36}$$

where now

$$\pi J_n' = 2r_2^2 \int_{\lambda}^{\cos^{-1}(r_2/\rho)} \int_{0}^{\cos^{-1}(\sin\lambda \csc\theta)} (\rho')^{-2} \cos\zeta \cos^n \theta' \sin\theta \, d\theta \, d\omega, \tag{37}$$

the limits of integration being now adjusted so as to extend over the visible portion of the secondary's disk visible to the observer at P. The (plane) angle λ, which will hereafter play the role of a "geometrical depth of the eclipse" is, in turn, defined by the triangle HPO_2 (*cf.* Fig. 2) as

$$\lambda = \alpha - \cos^{-1}(\rho/r_2) \cos\alpha, \tag{38}$$

and normalized so as to vary between $\pm \cos^{-1}(r_2/\rho)$ as the apparent disk of the secondary component continues to set behind the horizon of the observer. We shall, moreover, reckon λ so that its lower limit corresponds to the beginning of the eclipse (i.e. to the observer situated at the boundary between the fully illuminated and penumbral zones).

The integration of (37) with respect to ω offers again but little difficulty; for inserting $\cos\zeta$ from (17) we readily establish that

$$J_n' = M_n \cos\alpha + N_n \sin\alpha, \tag{39}$$

where

$$\pi M_n = 2r_2^2 \int_{\lambda}^{\cos^{-1}(r_2/\rho)} \frac{\cos\beta}{\rho'^2} \cos^{-1}\left(\frac{\sin\lambda}{\sin\theta}\right) \cos^n \theta' \sin\theta \, d\theta \tag{40}$$

and

$$\pi N_n = 2r_2^2 \int_{\lambda}^{\cos^{-1}(r_2/\rho)} \frac{\sin\beta}{\rho'^2} (\sin^2\theta - \sin^2\lambda)^{1/2} \cos^n \theta' \, d\theta, \tag{41}$$

respectively. Unlike the case of flux in the fully illuminated zone, however, the second integration of the foregoing expression with respect to θ can no longer be performed in a closed form without appeal to certain simplifications which we shall presently proceed to discuss.

4. *Solution of the equations.*—In the two foregoing sections we have formulated rigorously the problem of mutual illumination of two spheres reflecting in accordance with Lambert's law. The expressions for the flux and limits of integration could, in fact, be used to study the reflection of light from two spheres in actual contact, or from a sphere illuminated by an infinite wall—in both of which cases there would be no fully illuminated zone, but only a penumbral zone (extending, in the latter case, over the entire surface of the reflecting sphere).

Such extreme cases would, however, be of little or no astrophysical interest, since two stars brought so close together could not possibly retain spherical shape, and their mutual distortion would render the geometry of our preceding sections inexact. As was mentioned in the introductory paragraphs of the paper, it is our intention to carry through the solution of our problem only to the order of accuracy to which both components of our binary system can be regarded as spherical (i.e. to quantities of the fourth order in their fractional radii). In doing so, we surmise, in particular, that the amount of light reflected from the penumbral zone will represent a small quantity whose square and higher powers become negligible within the scheme of our approximation.

If, however, only terms of the lowest order are to be retained, we may evidently set

$$\left.\begin{aligned} \sin\beta &\simeq (r_2/\rho)\sin\theta, \\ \cos\beta &\simeq 1, \\ \cos\theta' &\simeq \cos\theta, \\ \rho' &\simeq \rho, \end{aligned}\right\} \tag{42}$$

in virtue of which the flux of radiation incident on the penumbral zone may be approximated by

$$\begin{aligned} M_1 &= \frac{2r_2^2}{\pi\rho^2}\int_\lambda^{\pi/2} \cos^{-1}\left(\frac{\sin\lambda}{\sin\theta}\right)\sin\theta\cos\theta\,d\theta \\ &= \frac{r_2^2}{\rho^2}\left\{\frac{1}{2} - \frac{\lambda+\sin\lambda\cos\lambda}{\pi}\right\} \end{aligned} \tag{43}$$

and

$$\begin{aligned} N_1 &= \frac{2r_2^2}{\pi\rho^3}\int_\lambda^{\pi/2} (\sin^2\theta - \sin^2\lambda)^{1/2}\sin\theta\cos\theta\,d\theta \\ &= \frac{2r_2^3}{3\pi\rho^3}\cos^3\lambda \end{aligned} \tag{44}$$

for uniformly bright disks, while

$$\begin{aligned} M_2 &= \frac{2r_2^2}{\pi\rho^2}\int_\lambda^{\pi/2} \cos^{-1}\left(\frac{\sin\lambda}{\sin\theta}\right)\sin\theta\cos^2\theta\,d\theta \\ &= \frac{r_2^2}{3\rho^2}\left\{1 - \sin\lambda\left(1 + \frac{\cos^2\lambda}{2}\right)\right\} \end{aligned} \tag{45}$$

and

$$\begin{aligned} N_2 &= \frac{2r_2^3}{\pi\rho^3}\int_\lambda^{\pi/2} (\sin^2\theta - \sin^2\lambda)^{1/2}\sin\theta\cos^2\theta\,d\theta \\ &= \frac{r_2^3}{8\rho^3}\cos^4\lambda \end{aligned} \tag{46}$$

for disks completely darkened at the limb.

Inserting the foregoing equations in (39) we are then in a position to assert that, within the scheme of our approximation,

$$J_1' = \frac{r_2^2}{\rho^2}\left\{\frac{1}{2} - \frac{\lambda+\sin\lambda\cos\lambda}{\pi}\right\}\cos\alpha + \frac{2r_2^3}{3\pi\rho^3}\cos^3\lambda\sin\alpha, \tag{47}$$

$$J_2' = \frac{r_2^2}{3\rho^2}\left\{1 - \sin\lambda\left(1 + \frac{\cos^2\lambda}{2}\right)\right\}\cos\alpha + \frac{r_1^3}{8\rho^3}\cos^4\lambda\sin\alpha, \tag{48}$$

where, to the order of accuracy we are working,

$$-\frac{\pi}{2} \leqslant \lambda \leqslant \frac{\pi}{2}. \tag{49}$$

If $\lambda = -90°$ (corresponding to the boundary between full-light and penumbral zone), the foregoing expressions reduce to

$$J_1'\left(-\frac{\pi}{2}\right) = \frac{r_1^2}{\rho^2}\cos\alpha, \tag{50}$$

$$J_2'\left(-\frac{\pi}{2}\right) = \frac{2}{3}\frac{r_1^2}{\rho^2}\cos\alpha, \tag{51}$$

in agreement with the results established previously by equations (30) and (31) for J_1 and J_2 in the fully illuminated zone; whereas if $\lambda = +90°$

$$J_1'\left(\frac{\pi}{2}\right) = J_2'\left(\frac{\pi}{2}\right) = 0, \tag{52}$$

as they should, since the eclipse of the secondary component has now become complete.

In order to simplify further the foregoing expressions for $J_{1,2}$ it should be remembered that within the penumbral zone α will be in the neighbourhood of 90°, thus rendering $\cos\alpha$ a small quantity of the order of r_2/ρ. If so, equation (38) defining λ can be replaced by

$$\lambda = \sin^{-1}(R/r_2)\cos\alpha \tag{53}$$

and, in terms of the order of $(r_2/R)^2$, we may approximate $\sin\alpha \simeq 1$, while $\cos\alpha \simeq r_2/R$. In consequence, equations (47) and (48) may be rewritten as

$$J_1' = \frac{r_2^3}{R^3}\left\{\frac{\sin^{-1}x + x(1-x^2)^{1/2}}{\pi} - \frac{1}{2}\right\} + \frac{2r_2^3}{3\pi R^3}(1-x^2)^{3/2}, \tag{54}$$

$$J_2' = \frac{r_2^3}{R^3}\left\{\frac{x}{6}(1-x)(x^2+x-2) + \tfrac{1}{8}(1-x^2)^2\right\}, \tag{55}$$

and expressed in terms of the single variable $x \equiv \sin\lambda$ which, consistent with (53), can be approximated by

$$x = \sin\lambda = (R/r_2)\cos\alpha, \tag{56}$$

and is by (49) constrained to vary within $-1 \leqslant x \leqslant 1$.

Moreover, an appeal to equation (23) discloses that, to the order of accuracy we are working,

$$\frac{R}{r_2}\cos\alpha = \frac{R}{r_2}\mu - \frac{r_1}{r_2}, \tag{57}$$

where, as before, $\mu = \cos\gamma' = \cos\phi\sin\eta$. If, furthermore, L_2 stands again for the luminosity of the secondary component—as defined by equation (33) above—the equation (36) governing the intensity of light reflected by the penumbral zone will, with the aid of the foregoing expressions for $J'_{1,2}$, ultimately assume the form

$$\mathscr{I}'(\phi,\eta) = \frac{3(1-u)}{3-u}\mathscr{I}^{\mathbf{U}}(\phi,\eta) + \frac{2u}{3-u}\mathscr{I}^{\mathbf{D}}(\phi,\eta), \tag{58}$$

where, as before, u denotes the secondary's coefficient of limb-darkening, and

$$\mathscr{I}^{\mathbf{U}}(\phi,\eta) = \frac{r_2 L_2}{6\pi^2 R^3}\{6x(\sin^{-1}x + x\sqrt{1-x^2} - 3\pi) + 4(1-x^2)^{3/2}\}, \tag{59}$$

while

$$\mathscr{I}^{\mathbf{D}}(\phi,\eta) = -\frac{r_2 L_2}{24\pi R^3}(1-x)^2(7x^2+14x+3), \tag{60}$$

respectively. As x can, by means of (56) and (57), be readily expressed as a

function of $\mu \equiv \cos\phi \sin\eta$, the requisite explicit forms of $\mathscr{I}^{U,D}(\phi, \eta)$—and, therefore, of $\mathscr{I}'(\phi, \eta)$—as functions of our angular variables are thereby established.

5. *The phase-law.*—A possession of the foregoing results puts us at last in a position to ascertain the fraction of light of one component of a close binary system from the other at any phase; for this task calls merely for an application of the K-operator, as defined by equation (7), to the expressions for $\mathscr{I}(\phi, \eta)$ established in the preceding two sections.

In the *fully illuminated* zone, $K \equiv K(\sin\eta_1)$, while the intensity $\mathscr{I}(\phi, \eta)$ of reflected radiation is known to be given by equation (34). Moreover, an expansion of the right-hand side of this latter equation in ascending powers of r_1/R in terms of the Legendre polynomials $P_j(\mu)$ of $\mu = \sin\phi \cos\eta$, permits us to replace the closed form of (34) by

$$\mathscr{I}(\phi, \eta) = \frac{L_2}{\pi R^2}\left\{ P_1(\mu) + 2\frac{r_1}{R} P_2(\mu) + 3\frac{r_1^2}{R^2} P_3(\mu) + \dots \right\}, \tag{61}$$

correctly to the order of accuracy adopted in Section 4. Hence, the corresponding amount of light of the secondary component reflected from the fully illuminated portion of the primary star in the direction of the line of sight should be given by

$$\mathscr{L}_1(r_1, r_2; \epsilon) = K(\sin\eta_1)\left\{ P_1(\mu) + 2\frac{r_1}{R} P_2(\mu) + 3\frac{r_1^2}{R^2} P_3(\mu) + \dots \right\}\frac{L_2}{\pi R^2}. \tag{62}$$

Performing the actual integration in a closed form we find that

$$K(\sin\eta_1)\{P_1(\mu)\} = \tfrac{2}{3} r_1^2\{\Phi_2 - \Phi_3 \sin^3\eta_1\}\cos\epsilon + \tfrac{2}{3} r_1^2 F \cos^2\eta_1, \tag{63}$$

$$\begin{aligned} K(\sin\eta_1)\{P_2(\mu)\} = {} & \tfrac{1}{4} r_1^2 \Phi_1 P_2(\cos\epsilon) \\ & + \tfrac{1}{8} r_1^2 \Phi_3 (1 + 3\sin^2\eta_1)\cos^2\eta_1 \cos\epsilon \\ & + \tfrac{1}{4} r_1^2 F(\tfrac{1}{2} + 3\cos^2\eta_1)\sin\eta_1, \end{aligned} \tag{64}$$

$$\begin{aligned} K(\sin\eta_1)\{P_3(\mu)\} = {} & r_1^2 \Phi_3 \sin^3\eta_1 \cos^2\eta_1 \cos\epsilon \\ & + r_1^2 F \sin^2\eta_1 \cos^2\eta_1 - \tfrac{1}{3} r_1^2 F^3, \end{aligned} \tag{65}$$

where we have abbreviated

$$\Phi_1 = \cos^{-1}(\sin\eta_1 \csc\epsilon), \tag{66}$$

$$\Phi_2 = \cos^{-1}(-\sec\eta_1 \cos\epsilon), \tag{67}$$

$$\Phi_3 = -\cos^{-1}(\tan\eta_1 \cot\epsilon) \tag{68}$$

and

$$F = (\sin^2\epsilon - \sin^2\eta_1)^{1/2}. \tag{69}$$

Since, however,

$$\Phi_1 = \frac{\pi}{2} - \sin\eta_1 \csc\epsilon - \tfrac{1}{6}\sin^3\eta_1 \cos\epsilon - \dots, \tag{70}$$

$$\Phi_2 = \pi - \epsilon + \tfrac{1}{2}\sin^2\eta_1 \cot\epsilon + \tfrac{1}{8}\sin^4\eta_1 (\cot^2\epsilon + 3)\cot\epsilon + \dots, \tag{71}$$

$$\Phi_3 = -\frac{\pi}{2} + \sin\eta_1 \cot\epsilon + \tfrac{1}{6}\sin^3\eta_1 (\cot^2\epsilon + 3)\cot\epsilon + \dots, \tag{72}$$

and

$$F = \sin\epsilon - \tfrac{1}{2}\sin^2\eta_1 \csc\epsilon - \tfrac{1}{8}\sin^4\eta_1 \csc^3\epsilon - \dots, \tag{73}$$

correctly to quantities of the fourth order in $\sin\eta_1$, it follows that, within the scheme of our approximation,

$$\mathscr{L}_1(r_1, r_2; \epsilon) = L_2\left\{\frac{2}{3}\left(\frac{r_1}{R}\right)^2 \frac{(\pi-\epsilon)\cos\epsilon + \sin\epsilon}{\pi} + \frac{1}{8}\left(\frac{r_1}{R}\right)^3 (3\cos^2\epsilon + 2\cos\epsilon - 1) + \left(\frac{r_1}{R}\right)^4 \frac{\sin\epsilon\cos^2\epsilon}{\pi} - \frac{r_1^2 r_2^2}{R^4}\frac{\sin\epsilon}{\pi} + \ldots\right\} \tag{74}$$

for any phase angle ϵ within

$$\sin^{-1}\frac{r_1+r_2}{R} \leqslant \epsilon \leqslant \pi - \sin^{-1}\frac{r_1+r_2}{R}. \tag{75}$$

In the immediate neighbourhood of the inferior conjunction, when

$$-\sin^{-1}\frac{r_1+r_2}{R} \leqslant \epsilon \leqslant \sin^{-1}\frac{r_1+r_2}{R}, \tag{76}$$

the K-operator (7) must be modified as explained in Section 2, in order to account for the fact that the fully illuminated zone should become completely exposed to the external observer (though it is bound to be partially masked by eclipses); and the result of such integration reveals that, during this phase,

$$\mathscr{L}_1(r_1, r_2; \epsilon) = L_2\frac{r_1^2}{R^2}\left\{\frac{2}{3} + \frac{r_1+r_2}{2R} + \ldots\right\}\cos\epsilon, \tag{77}$$

correctly to the same order of accuracy.* If, ultimately,

$$\pi - \sin^{-1}\frac{r_1+r_2}{R} \leqslant \epsilon \leqslant \pi + \sin^{-1}\frac{r_1+r_2}{R} \tag{78}$$

and the fully illuminated zone becomes completely invisible to our observer, the foregoing expression for $\mathscr{L}_1(r_1, r_2; \epsilon)$ is indeed seen to vanish for $\epsilon = \pi$, and to become an ignorable quantity of the fifth order in r/R for all other ϵ's within the limits of the inequality (78).

The fraction $\mathscr{L}_2(r_1, r_2; \epsilon)$ of the secondary's light reflected from the *penumbral zone* of the primary star may, in turn, be decomposed into

$$\mathscr{L}_2(r_1, r_2; \epsilon) = \frac{3(1-u)}{3-u}\mathscr{L}_2^{\mathbf{U}} + \frac{2u}{3-u}\mathscr{L}_2^{\mathbf{D}}, \tag{79}$$

where u denotes, as before, the coefficient of limb-darkening of the illuminating star, and

$$\mathscr{L}_2^{\mathbf{U},\mathbf{D}} = \{K(\sin\eta_2) - K(\sin\eta_1)\}\{\mathscr{I}^{\mathbf{U},\mathbf{D}}(\phi, \eta)\}. \tag{80}$$

Now the expression (59) for $\mathscr{I}^{\mathbf{U}}$ can be expanded in ascending powers of x to yield

$$\mathscr{I}^{\mathbf{U}}(\phi, \eta) = \frac{r_2 L_2}{\pi R^3}\left\{\frac{2}{3\pi} + \frac{x}{2} + \frac{x^2}{\pi} - \frac{x^4}{12\pi} - \ldots\right\} \tag{81}$$

within an error of less than one per cent for the extreme values attainable by x; and equation (57) permits us to convert the foregoing expansion into a series of the form

$$\mathscr{I}^{\mathbf{U}}(\phi, \eta) = \frac{r_2 L_2}{\pi R^3}\sum_{n=0}^{\infty} C_n^{\mathbf{U}}\left(\frac{R\mu}{r_2}\right)^n, \tag{82}$$

* A part of this light will, of course, be lost by the eclipse.

where

$$\left.\begin{aligned}
\pi C_0^{\mathbf{U}} &= \frac{2}{3} - \frac{\pi}{2}\left(\frac{r_1}{r_2}\right) + \left(\frac{r_1}{r_2}\right)^2 - \frac{1}{12}\left(\frac{r_1}{r_2}\right)^4 + \ldots,\\
\pi C_1^{\mathbf{U}} &= \frac{\pi}{2} - 2\left(\frac{r_1}{r_2}\right) + \frac{1}{3}\left(\frac{r_1}{r_2}\right)^2 + \ldots,\\
\pi C_2^{\mathbf{U}} &= 1 \qquad\quad - \frac{1}{2}\left(\frac{r_1}{r_2}\right)^2 + \ldots,\\
\pi C_3^{\mathbf{U}} &= \qquad \frac{1}{3}\left(\frac{r_1}{r_2}\right) + \ldots,\\
\pi C_4^{\mathbf{U}} &= -\frac{1}{12} + \ldots.
\end{aligned}\right\} \tag{83}$$

On the other hand, by virtue of (60),

$$\begin{aligned}
\mathscr{I}^{\mathbf{D}}(\phi_1\eta) &= \frac{r_2 L_2}{\pi R^3}\left\{\frac{3}{16} + \frac{x}{2} + \frac{3x^2}{8} - \frac{x^4}{16}\right\}\\
&= \frac{r_2 L_2}{\pi R^3}\sum_{n=0}^{4} C_n^{\mathbf{D}}\left(\frac{R\mu}{r_2}\right)^n,
\end{aligned} \tag{84}$$

where

$$\left.\begin{aligned}
C_0^{\mathbf{D}} &= \frac{3}{16} - \frac{1}{2}\left(\frac{r_1}{r_2}\right) + \frac{3}{8}\left(\frac{r_1}{r_2}\right)^2 \qquad - \frac{1}{16}\left(\frac{r_1}{r_2}\right)^4,\\
C_1^{\mathbf{D}} &= \frac{1}{2} - \frac{3}{4}\left(\frac{r_1}{r_2}\right) \qquad + \frac{1}{4}\left(\frac{r_1}{r_2}\right)^3,\\
C_2^{\mathbf{D}} &= \frac{3}{8} \qquad - \frac{3}{8}\left(\frac{r_1}{r_2}\right)^2,\\
C_3^{\mathbf{D}} &= \qquad \frac{1}{4}\left(\frac{r_1}{r_2}\right),\\
C_4^{\mathbf{D}} &= -\frac{1}{16}.
\end{aligned}\right\} \tag{85}$$

Now as the reader can easily verify,

$$K(a)\{\mu^n\} = K(0)\{\mu^n\} - \frac{2r_1^2}{n+1}a^{n+1}\sin\epsilon + \ldots, \tag{86}$$

by virtue of which

$$\begin{aligned}
&\{K(\sin\eta_2) - K(\sin\eta_1)\}\{\mathscr{I}^{\mathbf{U},\mathbf{D}}(\phi_1\eta)\}\\
&\quad = 2\frac{L_2}{\pi}\frac{r_1^2 r_2}{R_2}\sum_{n=0}^{\infty}\frac{C_n^{\mathbf{U},\mathbf{D}}}{n+1}\left(\frac{R}{r_2}\right)^n(\sin^{n+1}\eta_1 - \sin^{n+1}\eta_2)\sin\epsilon \qquad (87)\\
&\quad = \frac{2}{\pi}\left(\frac{r_1 r_2}{R^2}\right)^2 L_2\sin\epsilon\sum_{n=0}^{\infty}\frac{C_n^{\mathbf{U},\mathbf{D}}}{n+1}\left\{\left(\frac{r_1+r_2}{r_2}\right)^{n+1} - \left(\frac{r-r_2}{r_2}\right)^{n+1}\right\},
\end{aligned}$$

where all $C_n^{\mathbf{U}}$'s for $j>4$ are identically zero. Inserting the appropriate coefficients C_n, as given by the foregoing equations (83) and (85), in (87) we find, moreover, that the whole summation on the right-hand side of (87) reduces to π^{-1} in the case of a uniformly bright secondary component ($u=0$), and to 0·3 in the case of complete darkening ($u=1$). In consequence, the requisite amount of light reflected by the

penumbral zone of the primary component may, to the order of accuracy we have been working, be approximated by

$$\mathscr{L}_2^{\mathrm{U}}(r_1, r_2\ ;\ \epsilon) = \left\{\frac{2r_1r_2}{\pi R^2}\right\}^2 L_2 \sin\epsilon + \ldots, \tag{88}$$

$$\mathscr{L}_2^{\mathrm{D}}(r_1, r_2\ ;\ \epsilon) = \frac{6}{5\pi}\left\{\frac{r_1r_2}{R^2}\right\}^2 L_2 \sin\epsilon + \ldots, \tag{89}$$

so that the amount of light, reflected by the penumbral zone, incident from a secondary component arbitrarily darkened at the limb becomes

$$\mathscr{L}_2(r_1, r_2\ ;\ \epsilon) = \frac{12}{5}\left\{\frac{r_1r_2}{\pi R^2}\right\}^2 \left\{\frac{5+(\pi-5)u}{3-u}\right\} L_2 \sin\epsilon + \ldots \tag{90}$$

for any phase angle ϵ within the limits of the inequality (75). The total amount of light $\mathscr{L}(r_1, r_2\ ;\ \epsilon)$ reflected from the fully illuminated as well as the penumbral zones of the primary component is naturally represented by the sum

$$\mathscr{L}(r_1, r_2\ ;\ \epsilon) = \mathscr{L}_1(r_1, r_2\ ;\ \epsilon) + \mathscr{L}_2(r_1, r_2\ ;\ \epsilon), \tag{91}$$

where the quantities $\mathscr{L}_1$ and $\mathscr{L}_2$ are (within the scheme of our approximation) given by equations (74) and (90); which means that the geometrical solution of our problem which we set out to obtain in Section 4 is now complete.

6. *Discussion of the results.*—The phase law (91) with its constituents as given by equations (74) or (77) and (90) represents the final outcome of our investigation. The first term on the right-hand side of (74)—of the order of $(r_1/R)^2$—is, of course, well known from planetary photometry. The next term, of the order of $(r_1/R)^3$, was first deduced by Takeda (**3**), and that of the order of $(r_1/R)^4$ by Sen (**4**). The terms of the order of $(r_1r_2/R^2)^2$ in both (74) and (90) are new, and their sum represents the first-order photometric effect of finite angular size of the secondary (illuminating) component. These terms are approximately $(r_2/R)^2$ times smaller than the first-order reflection effect. If we consider $r_2/R = 0{\cdot}3$—a realistic value in close binary systems—the penumbral zone, in particular, turns out to contribute approximately 10 per cent of the total reflected light. Russell's conjecture that . . . "the penumbral effect on the reflected light may be neglected unless the precision of observation surpasses one part in a thousand" (**5**) proves, therefore, to be ill-founded; in actual fact the penumbral zone is relatively much more important.

The ensemble of these terms renders, to be sure, our phase-law exact only as far as quantities of fifth and higher orders in fractional radii of both components are negligible. The geometrical analysis of Sections 2 and 3 is, however, rigorous and free from any approximation; and the general formulae given there could be developed to any order of accuracy—at the expense only of rather troublesome algebraic work. If, however, such an extension were to be physically meaningful, it would be necessary to take account of the departures of both components from spherical form, due to their axial rotation and mutual tidal action. In more precise terms, according to the equilibrium theory of tides, the radius of a centrally condensed primary component rotating with the Keplerian angular velocity should, to the first order in small quantities, be given by

$$r_1(\phi, \eta) = r_{10}\left\{1 - \frac{1}{3}\left(1 + \frac{m_2}{m_1}\right)\left(\frac{r_{10}}{R}\right)^3 P_2(\cos\eta) + \frac{m_2}{m_1}\sum_{n=2}^{4}\left(\frac{r_{10}}{R}\right)^{n+1} P_n(\cos\phi\sin\eta)\right\}, \tag{92}$$

where m_2/m_1 denotes the ratio of masses of the two components, and r_{10} the radius of a sphere having the same volume as the distorted ellipsoid (**8**).

The foregoing expression for $r_1(\phi, \eta)$ should be introduced in equation (21) and its sequel; and the fact that it is no longer constant will affect also the limits of the illuminated crescent visible at any phase. The corresponding distortion of the secondary component will, in turn, affect not only the geometry of our problem, through equation (20), but also the flux of the incident radiation; for the apparent surface brightness of a distorted star should—apart from limb-darkening—vary also in proportion to local gravity (**9**). All these phenomena are bound to render a determination of the proper amount of reflected light much more involved, but will have to be considered in any attempt to establish the specific form of the terms of the order of $(r/R)^5$ or higher in the corresponding phase-law. This, however, constitutes a task which must necessarily be postponed for future investigation.

In order to facilitate application of the results established in the preceding section to practical cases, let us expand the phase-law (91) in ascending powers of $\cos\epsilon$ in a series of the form

$$\mathscr{L}(r_1, r_2;\ \epsilon) = L_2 \sum_{n=0}^{\infty} C_n \cos^n\epsilon, \tag{93}$$

where, within the scheme of our approximation,

$$\left.\begin{aligned}
C_0 &= \frac{2}{3\pi}\left(\frac{r_1}{R}\right)^2 - \frac{1}{8}\left(\frac{r_1}{R}\right)^3 - \frac{k}{\pi}\left(\frac{r_1 r_2}{R^2}\right)^2 + \ldots,\\
C_1 &= \frac{1}{3}\left(\frac{r_1}{R}\right)^2 + \frac{1}{4}\left(\frac{r_1}{R}\right)^3 + \ldots,\\
C_2 &= \frac{1}{3\pi}\left(\frac{r_1}{R}\right)^2 + \frac{3}{8}\left(\frac{r_1}{R}\right)^3 + \frac{1}{\pi}\left(\frac{r_1}{R}\right)^4 + \frac{k}{2\pi}\left(\frac{r_1 r_2}{R^2}\right)^2 + \ldots,\\
C_3 &= 0,\\
C_4 &= \frac{1}{36\pi}\left(\frac{r_1}{R}\right)^2 - \frac{1}{2\pi}\left(\frac{r_1}{R}\right)^4 + \frac{k}{8\pi}\left(\frac{r_1 r_2}{R^2}\right)^2 + \ldots,
\end{aligned}\right\} \tag{94}$$

where we have abbreviated

$$k = 1 - \frac{12}{5\pi}\,\frac{5+(\pi-5)u}{3-u}. \tag{95}$$

Alternatively, by expanding our phase-law (91) in a Fourier cosine series we get

$$\mathscr{L}(r_1, r_2;\ \epsilon) = L_2 \sum_{n=0}^{\infty} C_n' \cos n\epsilon, \tag{96}$$

where

$$\left.\begin{aligned}
C_0' &= \frac{8}{3\pi^2}\left(\frac{r_1}{R}\right)^2 + \frac{1}{16}\left(\frac{r_1}{R}\right)^3 + \frac{2}{3\pi^2}\left(\frac{r_1}{R}\right)^4 - \frac{2k}{\pi^2}\left(\frac{r_1 r_2}{R^2}\right)^2 + \ldots,\\
C_1' &= \frac{1}{3}\left(\frac{r_1}{R}\right)^2 + \frac{1}{4}\left(\frac{r_1}{R}\right)^3 + \ldots,\\
C_2' &= \frac{16}{27\pi^2}\left(\frac{r_1}{R}\right)^2 + \frac{3}{16}\left(\frac{r_1}{R}\right)^3 + \frac{4}{15\pi^2}\left(\frac{r_1}{R}\right)^4 + \frac{4k}{3\pi^2}\left(\frac{r_1 r_2}{R^2}\right)^2 + \ldots,\\
C_3' &= 0,\\
C_4' &= \frac{16}{675\pi^2}\left(\frac{r_1}{R}\right)^2 - \frac{52}{105\pi^2}\left(\frac{r_1}{R}\right)^4 + \frac{4k}{15\pi^2}\left(\frac{r_1 r_2}{R^2}\right)^2 + \ldots,
\end{aligned}\right\} \tag{97}$$

etc.

The phase-law (91) or its foregoing expansions (93) or (96) represents the amount of light of one (the secondary) component reflected at any phase from its mate. The corresponding amount of light of the primary component reflected from the secondary is, however, bound to be given by the same equations provided that the radii r_1 and r_2 are interchanged, the phase angle ϵ is replaced by $\pi-\epsilon$, and L_2 is replaced by L_1. The total amount of light added by reflection to the intrinsic light of a close binary system is, of course, represented by the *sum* of $\mathscr{L}(r_1, r_2;\ \epsilon)+\mathscr{L}(r_2, r_1;\ \pi-\epsilon)$; and it is this sum which should be removed from the observed light changes of a close eclipsing system before its light curve is analysed for the geometrical elements. The explicit form of this sum is so easily written down with the aid of the expressions already given that it need not be repeated here. The reader may, however, notice that the difference of 180° between the phase of the primary and secondary component will change the sign of all odd functions of ϵ in (91), but not of even functions. As a result, the terms arising from reflection of light of one star from another and varying as odd functions of the phase, i.e. odd powers of $\cos\epsilon$ in (93), or cosines of odd multiples of ϵ on the right-hand side of (96), will tend to neutralize each other in the combined light of a close binary system, while those varying as even functions of ϵ will always reinforce. In the particular case of a system whose components are equal in size and brightness all odd terms arising from reflection should cancel, and the surviving even terms should closely simulate the photometric effects of ellipticity produced by tidal distortion.

In concluding the present investigation, one last point deserves explicit notice. All expressions derived above for the amount of reflected light and its variation with the phase hold good irrespective of whether the relative orbit of the two components is circular or eccentric. If it is circular, the phase-angle ϵ is simply proportional to the time and the radius-vector R is constant. Should, on the other hand, this orbit happen to be an ellipse, it is easy to show (**9**) that equation (3) should be rewritten as

$$\cos\epsilon=\sin(v+w)\sin i, \tag{98}$$

where v denotes the true anomaly of the secondary (illuminating) component in its relative orbit around the primary star, and w stands for the longitude of periastron. Furthermore, the separation R of centres of the components will vary so that

$$\frac{r_{1,2}}{R}=\frac{r_{1,2}}{h}(1+e\cos v), \tag{99}$$

where h denotes the semi-latus rectum of the relative orbit, and e its eccentricity. In consequence, the reflection effect in eccentric binary systems will no longer be symmetrical with respect to conjunctions; and its observed asymmetry may indicate to us an approximate position of the periastron.*

Ultimately, it should be recalled that the reflection effect—like the ellipticity—is bound to give rise to continuous variation of light of close binary systems, irrespective of whether or not the system happens to be an eclipsing variable; and this variation should disappear only under certain special circumstances. If, for instance, the relative orbit of the two stars is circular and the line of sight happens to be perpendicular to the orbital plane (i.e. $i=0°$), then $\epsilon=90°$ all

* For an illustrative example of such a case, the reader is referred to a study of the reflection effect in the system of ξ Aurigae ($e=0{\cdot}41$) by K. Walter, *Zs. f. Ap.*, **14**, 62, 1937.

the time, and the reflected light continues to contribute a constant amount to the intrinsic light of the system. Should, however, the relative orbit happen to be an ellipse, the amount of this additive light will vary (approximately) as R^{-2}, being greatest at the time of periastron passage, and smallest at apastron—a fact which, if observed, should indicate by inspection an approximate orientation of the apsidal line.

Department of Astronomy,
University of Manchester :
1953 *November* 16.

References

(1) *Cf.* Chandrasekhar, S., *Ap. J.*, **101**, 348, 1945.
(2) *Cf.*, e.g., Schönberg's chapter on theoretical photometry in *Handb. der Astroph.*, Erste Hälfte, Zweiter Teil, **1**, pp. 62–65.
(3) Takeda, S., *Kyoto Mem.*, **A17**, 197, 1934.
(4) Sen, H. K., *Proc. U.S. Nat. Acad. Sci.*, **34**, 311, 1948.
(5) Russell, H. N., *Harv. Obs. Circ.*, No. 452, 1949.
(6) Matukuma, T., *Sendai Astronomiaj Raportoj*, **2**, No. 10, 1950.
(7) Milne, E. A., *M.N.*, **87**, 43, 1926.
(8) Chandrasekhar, S., *M.N.*, **93**, 469, 1933.
(9) *Cf.*, e.g., the writer's *Introduction to the Study of Eclipsing Variables*, Harvard Univ. Press, 1946, Sections 52 and 65.

Addendum.—After this paper had been read before the Society, T. G. Cowling pointed out to the writer that, in order to obtain a consistent phase-law complete to quantities of the order of $(r_1r_2/R^2)^2$, we should adjoin to (74) the effects of "secondary reflection"—i.e. the amount of the primary's light reflected from the secondary component back to the primary star. This can indeed be done when we ensure that if L_2 denotes, in equation (74), the intrinsic luminosity of the secondary component, its actual luminosity increased by reflection at "full" phase ($\epsilon = 0$) will be equal to

$$L_2 + L_1\left\{\frac{2}{3}\frac{r_2^2}{R} + \frac{1}{2}\frac{r_2^3}{R} + \dots\right\}.$$

In consequence, to the phase-law as represented by equation (74) should be added the term

$$L_1'(r_1, r_2;\ \epsilon) = \left\{\frac{2}{3}\frac{r_1r_2}{R^2}\right\}^2\left\{\frac{(\pi-\epsilon)\cos\epsilon + \sin\epsilon}{\pi}\right\}L_1 + \dots$$

$$= \left\{\frac{2}{3}\frac{r_1r_2}{R^2}\right\}^2\left\{\frac{1}{\pi} + \frac{\cos\epsilon}{2} + \frac{\cos^2\epsilon}{2\pi} + \frac{\cos^4\epsilon}{24\pi} + \dots\right\}L_1, \quad (98)$$

which represents the phase effect of secondary reflection.

Within the scheme of our approximation, the foregoing equation (98) alone would represent the light reflected by an eclipsing system whose secondary component was completely dark; for the latter would still be bound to intercept a part of the radiation of the primary star, and to illuminate it back by reflection in very much the same way as lunar ashen light illuminates our Earth. Tertiary reflection (arising from reflection of the secondary's light on the primary, back to the secondary, and returned to the primary again) would clearly constitute a quantity of the order of $(r_1^2r_2/R^3)^2L_2$, and therefore negligible within the scope of our accuracy.

INTERMEDIATE COUPLING LINE STRENGTHS

R. H. Garstang

(Communicated by the Director of the University of London Observatory)

(Received 1954 January 28)

Summary

Relative line strengths for the $3s$–$3p$ and $3p$–$3d$ transitions in O II and Ne II and the $4s$–$4p$ transitions in S II and A II have been calculated by quantum mechanics, using the intermediate coupling approximation. Landé g-values have been calculated and compared with experimental values. The parameters in the calculations have been determined empirically from observational spectroscopic data. Absolute strengths have been calculated by the Coulomb approximation. The strengths of the arrays $3p$–ns are discussed. Applications are made to the curve of growth of γ Pegasi.

---

1. *Introduction.*—The theoretical analysis of stellar spectra requires a knowledge of the strengths of a large number of spectral lines. In some cases (e.g. iron) experimental values are available for many lines, but for most of the lighter atoms and for most ionized atoms experimental techniques do not permit of the measurement of either relative or absolute line strengths. Recourse must then be had to theoretical calculations. General formulae have been obtained for a large number of possible transitions when it is permissible to assume that the atom or ion obeys Russell-Saunders (LS) coupling (i.e. that spin-orbit interaction and configuration interaction are negligible) (**1**). For many atoms of astrophysical interest the assumption of LS coupling is insufficiently accurate and appreciable departures from LS coupling are observed for some arrays of atoms in the first row of the Periodic Table. In astrophysical work such departures are major contributors to the large scatter of points around a curve of growth. Dr L. H. Aller pointed out to the writer that the $3p$–$3d$ array in O II appears to show substantial departures from LS coupling, and for heavier atoms it is well known that many strong lines in astrophysical sources have a theoretical strength of zero in LS coupling.

It is evidently desirable to attempt to carry out more accurate calculations, including the effects of spin-orbit interaction but neglecting configuration interaction. Atoms for which such calculations provide a fair representation of the physical state are said to obey intermediate coupling (IC). IC theory is now standard and is described by Condon and Shortley (**2**). Very few applications have been attempted, largely because of the considerable labour involved and the need to consider individually each array of each atom. Most of the work has to be done numerically, and numerical results for one array are of little help when studying some other array. Shortley (**3**) described much of the general theory, worked out in detail the array $3s$–$3p$ in Ne I and compared his results with dispersion measurements of Ladenburg and Levy. His results were not wholly satisfactory, the calculated intensities were sensitive to the

assumed values of the parameters involved. Gottschalk (4) studied the $3d^7 4s$–$3d^7 4p$ array in Fe I and obtained results which represented a considerable advance on LS coupling calculations. His results gave much better agreement with experiment for many line strengths and for the Landé g-values. For a large number of intercombination lines he obtained finite strengths, and many of these agreed with experimental data.

It is concluded from this work that while, in some cases at least, reliable values of the line strengths are difficult to attain, in all cases the introduction of IC gives a great improvement over LS calculations. (In spite of the defect of sensitivity mentioned above, Shortley's IC results are much better than the LS values for all but one or two faint lines.) Considerable confidence is felt in the value of extending this type of calculation to other ions even if no experimental data are available for comparison. Indeed, the need for acquiring data for ions which cannot be studied experimentally is the main justification for the work described in this paper.

2. *Method of calculation.*—Line strengths in intermediate coupling can be calculated from the strengths in LS coupling if we know the transformation matrices. These matrices are obtained by diagonalizing the complete energy matrix (including both electrostatic and spin interactions). Let φ_i, φ_f be the LS wave functions of the initial and final configurations. φ_i and φ_f are represented by column matrices. Let the transformations to intermediate coupling be written

$$\psi_i = A\varphi_i, \qquad \psi_f = B\varphi_f.$$

Then the matrices of the square roots of the line strengths are related by the equation

$$(S^{1/2})_{IC} = B(S^{1/2})_{LS}\widetilde{A},$$

where $\widetilde{A}$ is the transpose of A.

If H is the energy matrix of the initial configuration in LS coupling, A is determined by making $AH\widetilde{A}$ diagonal. Similarly B is determined for the final configuration. The diagonal elements of $AH\widetilde{A}$ give the IC energies of the initial configuration.

The following arrays were chosen for numerical calculations of line strengths:

O II	$2p^2 3s$–$2p^2 3p$
	$2p^2(^3P)3p$–$2p^2(^3P)3d$
Ne II	$2p^4 3s$–$2p^4 3p$
	$2p^4(^3P)3p$–$2p^4(^3P)3d$
S II	$3p^2 4s$–$3p^2 4p$
A II	$3p^4 4s$–$3p^4 4p$

The first step in the calculation is the determination of the matrices of spin-orbit interaction. Condon and Shortley (2) describe the method in detail and give the matrices for the $p^2 s$ configuration. We have followed their method through for the $p^2 p$ configuration.* Throughout this paper we use a prime ($^2D'$) to denote a spectral term based on a ^1D parent and a double prime ($^2S''$) to denote a term based on a ^1S parent. Terms based on a ^3P parent are written without a prime. In the $p^2 p$ configuration $\zeta_{p'}$ refers to the outer electron.

* The writer will gladly supply a copy of these matrices to any interested investigators.

One approximation made by Gottschalk (**4**) was to neglect the interactions between spectral terms based on different parents. In the s–p transitions we shall retain these interactions and investigate their effect on the line strengths. In the p–d arrays, which are more complicated, we shall neglect interparental interactions. Examination of the s–p results shows that interparental transitions are weak. Their neglect for p–d is likely to be a good approximation and gives a valuable reduction in the computational labour involved. Johnson (**5**) gave a method which is immediately applicable if we take the LS values of the parent term (^{3}P) as playing the part of the first electron in his formulae. Using Johnson's method and Condon and Shortley's determination of absolute term values (**6**) we obtain the matrix for the $p^2 d$ configuration.*

The matrices for $p^4 s$, $p^4 p$ and $p^4 d$ are obtained from those for $p^2 s$, $p^2 p$ and $p^2 d$ respectively by changing the sign of ζ_p and leaving the signs of ζ_p' and ζ_d unchanged.

The complete energy matrix is obtained by adding to each diagonal term of the spin-orbit matrix the appropriate electrostatic energy (the centre of gravity of the multiplet).

The next problem is to fix the numerical values of the spin-orbit parameters (ζ) and the centres of gravity of the multiplets. This is, in many cases, the most difficult and critical step in the calculations. In the $p^2 s$ and $p^4 s$ configurations the departures from LS coupling are small. It is sufficient to work to the second-order terms in ζ_p. We have five parameters to adjust, ζ_p and four centres of gravity. In principle, all the parameters could be calculated from wave functions. Generally, however, wave functions are not available, and an empirical approach must be adopted. We choose the parameters to give the best possible fit to the spectroscopic energy levels. The observational data are taken from the recent publications of C. E. Moore (**7**). The observed energies are equated to theoretical expressions written down by second-order perturbation theory. The set of eight equations is solved by a least squares process or a method of trial and error. Having determined the five parameters, we compute from them the theoretical energies and compare with the eight observed energies to check the adequacy of fit. The adopted parameters for the $p^2 s$ and $p^4 s$ configurations are given in Table I. E(^{4}P) denotes the centre of gravity (electrostatic energy) of the ^{4}P term. With the exception of A II $3p^4(^1\mathrm{D})4s\ ^2\mathrm{D}'$ the fit obtained is excellent. The A II ^{2}D′ doublet is predicted to have a separation of 12 cm^{-1}, but is observed to be 222 cm^{-1}. No reasonable choice of parameters would remove this discrepancy.

TABLE I

Adopted parameters for $p^2 s$ and $p^4 s$ configurations

Ion	O II	Ne II	S II	A II
Configuration	$2p^2\ 3s$	$2p^4\ 3s$	$3p^2\ 4s$	$3p^4\ 4s$
E(^{4}P)	185 402·0	219 452	110 019	134 795
E(^{2}P)	189 010·1	224 291	113 289	138 587
E(^{2}D′)	206 971·0	246 391	121 515	148 689
E(^{2}S″)	226 849	276 664	136 800†	167 242
ζ_p	190·5	615	524	1 030

* The writer will gladly supply a copy of these matrices to any interested investigator.
† Estimated from the S III spectrum.

In the p^2p and p^4p configurations we have two spin-orbit parameters and ten centres of gravity of multiplets, to be chosen to give as good a fit as possible for 21 energy levels. The values of the spin-orbit parameters for the outer electrons were rather difficult to set. An examination of the energy levels arising from the ^{1}D parent indicated that the parameter ζ_{3p} for O II and Ne II should be estimated theoretically, wave functions being available from unpublished work of D. R. Bates for O II and of the writer for Ne II. Numerical integrations gave $\zeta_{3p} = 23\,\text{cm}^{-1}$ for O II and $46\,\text{cm}^{-1}$ for Ne II, using the standard formula

$$\zeta_{np} = \frac{eh^2}{8\pi^2m^2c^2} \int_0^\infty \left(-\frac{1}{r}\frac{\partial V}{\partial r}\right) P^2(np)\, dr.$$

For the purposes of calculation values of $20\,\text{cm}^{-1}$ and $40\,\text{cm}^{-1}$ were adopted for O II and Ne II, taking into consideration the observed energy levels. Values of $\zeta_{4p} = 80\,\text{cm}^{-1}$ and $100\,\text{cm}^{-1}$ were adopted for S II and A II respectively. These latter values, based on the observations, are quite uncertain; they are appreciably smaller than the core parameters ζ_{3p} and no appreciable error is likely to result from their adoption. The remaining parameters were estimated by a process of trial and error. In some cases second-order perturbation theory was used. This was insufficiently accurate for many of the configurations. For the latter a method of successive partial diagonalization was used. Using a preliminary set of parameters the energy matrix was set up numerically. A series of unitary matrices $\boldsymbol{P}$, $\boldsymbol{Q}$, $\boldsymbol{R}$, ... was constructed by inspection in such a way as to reduce or eliminate one by one the large off-diagonal elements in the energy matrix when the series of transformations $\boldsymbol{PHP}$, $\boldsymbol{QPHP}\widetilde{\boldsymbol{P}}\widetilde{\boldsymbol{Q}}$, $\boldsymbol{RQPHP}\widetilde{\boldsymbol{P}}\widetilde{\boldsymbol{Q}}\widetilde{\boldsymbol{R}}$, ... was performed. Eventually a matrix $[\ldots\boldsymbol{RQP}]$ is found which reduces $\boldsymbol{H}$ to a new matrix with small off-diagonal elements. The calculation of the energies and the final transformation matrix is completed by second-order perturbation theory. This method is especially suited to our work because we have to begin with a matrix $\boldsymbol{H}$ computed on the basis of assumed parameters. These parameters must be varied to give the best possible fit of the calculated and observed energies. When one of the parameters is altered, we compute a new matrix $\boldsymbol{H}$ and immediately apply the transformation $[\ldots\boldsymbol{RQP}]$ obtained previously, finishing the calculation by second-order perturbation theory. This method makes the trial of new parameters a relatively simple operation. It would be possible to apply a least squares technique in the final stages of the adjustment of parameters; but this refinement was not felt to be justified in the present series of calculations.

The adopted parameters for the p^2p and p^4p configurations are given in Table II. On the whole excellent fits were obtained, but considerable discrepancies were encountered in the ^{2}P and ^{2}P′ levels in Ne II, S II and A II. No satisfactory explanation of these discrepancies has been found.

The p^2d and p^4d configurations in O II and Ne II respectively were studied by the above method. Only terms based on the ^{3}P parent were considered. The adopted parameters are listed in Table III. The spin-orbit parameter ζ_{3d} could not be obtained from the observed energy levels. ζ_{3d} was computed from a wave function for Ne II. The value obtained was $0{\cdot}3\,\text{cm}^{-1}$; accordingly it was sufficient to put ζ_{3d} zero for O II and Ne II. The observed and calculated energies agree remarkably well for O II. For Ne II the agreement is rather poor. Unfortunately, the calculated energy levels are very sensitive to the adopted parameters. In choosing trial values for the parameters special care was taken to

ensure that the levels with any given J came out in the correct order of increasing energy, as judged by the observed energies. This appears to be essential if transition probabilities are to be computed. It is possible that further adjustments of the parameters might improve the Ne II energies, but in view of the general sensitivity of the calculations and the labour involved, further work did not seem justified at the present time.

The matrices which transform LS coupling to intermediate coupling were computed, using second-order perturbation theory, combined, where necessary, with the approximate matrices [$\ldots \boldsymbol{RQP}$] already obtained for many of the configurations.

TABLE II

Adopted parameters for $p^3\,p$ and $p^4\,p$ configurations
(units : cm^{-1})

Ion	O II	Ne II	S II	A II
Configuration	$2p^2\,3p$	$2p^4\,3p$	$3p^2\,4p$	$3p^4\,4p$
E(^{3}S)	203 945	252 852	125 520	160 845
E(^{3}P)	214 214	254 139	133 379	159 900
E(^{3}D)	211 635	251 206	130 962	158 820
E(^{4}S)	212 165	252 956	131 047	160 990
E(^{4}P)	208 431	246 366	129 999	155 365
E(^{4}D)	206 899	249 410	128 318	157 730
E(^{3}F′)	228 736	274 385	140 267	170 430
E(^{3}D′)	229 957	277 332	140 712	173 335
E(^{3}P′)	232 500	276 385	143 532	172 465
E(^{3}P″)	250 253*	305 400	156 750*	191 350*
ζ	204	628	552	1 075
ζ'	20	40	80	100

* Estimated.

TABLE III

Adopted parameters in $p^3\,d$ and $p^4\,d$ configurations

Ion	O II	Ne II
Configuration	$2p^2(^3P)3d$	$2p^4(^3P)3d$
E(^{3}P)	233 470	281 506
E(^{3}D)	234 425	280 560
E(^{3}F)	232 880	280 442
E(^{4}P)	232 554	281 040
E(^{4}D)	232 726	279 305
E(^{4}F)	231 430	280 495
ζ_{3p}	192	620
ζ_{3d}	0	0

There is an independent check which can be applied to our work. Using the transformation matrices we can compute Landé g-values in intermediate coupling (8). In LS coupling the g-values are given by the usual formula

$$g(SLJ)=1+\frac{J(J+1)-L(L+1)+S(S+1)}{2J(J+1)}.$$

The IC g-values for p^2s and p^4s configurations do not differ very greatly from the LS values. The IC g-values for the p^2p and p^4p configurations are given in Table IV, together with such experimental values as are available (7). The critical case is A II $3p^4\,4p$, where there are both large deviations from LS coupling and adequate comparison data. Inspection of the results for A II in Table IV shows

that the introduction of intermediate coupling has made a great improvement in the Landé g-values. We find

$$\sum_{\text{array}} (g_{\text{obs}} - g_{\text{LS}})^2 = 0{\cdot}219\,1$$

$$\sum_{\text{array}} (g_{\text{obs}} - g_{\text{IC}})^2 = 0{\cdot}015\,6$$

This provides a remarkable demonstration of the increase in accuracy gained by the use of intermediate coupling theory. For the d configurations experimental g-values are available for only two levels, for which the results are

Ne II $2p^4\,3d$	g_{LS}	g_{IC}	g_{obs}
$^2P_{1/2}$	0·667	0·707	0·70
$^2P_{3/2}$	1·333	1·293	1·25

The general improvement of the g-values and the reasonable fit obtained for the majority of the energy levels encourages us to proceed to the calculation of intermediate coupling line strengths.

TABLE IV

Landé g-factors for $p^2\,p$ and $p^4\,p$ configurations*

Level	g_{LS}	O II $2p^2\,3p$	Ne II $2p^4\,3p$	S II $3p^2\,4p$	A II $3p^4\,4p$
$^2S_{1/2}$	2·000	2·000	1·958 (1·96)	2·000	1·670 (1·695)
$^2P_{1/2}$	0·667	0·667	0·709 (0·71)	0·668	0·985 (0·983)
$^2P_{3/2}$	1·333	1·333	1·337 (1·33)	1·332	1·179 (1·244)
$^2D_{3/2}$	0·800	0·801	0·808 (0·80)	0·810	1·102 (0·918)
$^2D_{5/2}$	1·200	1·200	1·204 (1·20)	1·207	1·243 (1·241)
$^4S_{3/2}$	2·000	1·999	1·989 (...)	1·984	1·970 (1·987)
$^4P_{1/2}$	2·667	2·665	2·662 (2·67)	2·658	2·639 (2·638)
$^4P_{3/2}$	1·733	1·733	1·732 (1·73)	1·735	1·724 (1·720)
$^4P_{5/2}$	1·600	1·599	1·598 (1·60)	1·591	1·593 (1·599)
$^4D_{1/2}$	0·000	0·002	0·005 (0·00)	0·007	0·032 (0·000)
$^4D_{3/2}$	1·200	1·201	1·199 (1·20)	1·203	1·179 (1·199)
$^4D_{5/2}$	1·371	1·372	1·369 (1·37)	1·373	1·330 (1·334)
$^4D_{7/2}$	1·429	1·429	1·428 (1·43)	1·428	1·427 (1·427)
$^2P'_{1/2}$	0·667	0·667	0·667 (0·67)	0·667	0·669 (0·677)
$^2P'_{3/2}$	1·333	1·333	1·333 (1·33)	1·334	1·331 (1·332)
$^2D'_{3/2}$	0·800	0·800	0·801 (0·80)	0·801	0·805 (0·804)
$^2D'_{5/2}$	1·200	1·200	1·200 (1·20)	1·197	1·201 (1·202)
$^2F'_{5/2}$	0·857	0·857	0·857 (0·86)	0·861	0·859 (0·857)
$^2F'_{7/2}$	1·143	1·143	1·143 (1·14)	1·143	1·143 (1·140)
$^2P''_{1/2}$	0·667	0·667	0·667 (0·67)	0·667	0·666 (...)
$^2P''_{3/2}$	1·333	1·333	1·333 (1·33)	1·333	1·333 (...)

* Experimental values in brackets.

A difficulty was encountered in the A II $3p^4\,4p$ calculations. An attempt was made to use the Landé g-values as a guide to the parameters to be adopted. This attempt was not successful. It was found that as certain parameters (particularly E(^{2}D)) were changed in such a way as to improve the calculated energy levels the agreement of the Landé g-values became worse. There seemed to be no point in attempting any further improvement in the calculations. This difficulty does not affect our general conclusion that the intermediate coupling calculations represent a decided improvement over the LS calculations. It is, however, an excellent illustration of the uncertainties which are present in this type of work, and it is a warning against over-confidence in the numerical results of the work.

The final stage in the calculations is the transformation of the line strengths to intermediate coupling. The matrices of the square roots of line strengths are written down from the formulae of Condon and Shortley (**9**) and of Goldberg (**10**). Using the matrices previously obtained the transformation is carried out.

3. *Numerical values of relative line strengths.*—The relative line strengths for all the arrays are collected in Tables V and VI. The numerical values are expressed as multiples of σ^2, the radial integral whose value will be obtained later for each array. We have omitted a number of intercombination lines which are much too weak to appear in the *Revised Multiplet Table* (**11**). Many lines of moderate strength have been included even if they do not appear in the *R.M.T.*

TABLE V

Relative line strengths of s–p arrays in O II, Ne II, S II *and* A II
(All expressed in units of the radial integral σ^2)

Line	LS	Intermediate Coupling			
		O II	Ne II	S II	A II
		$3s$–$3p$	$3s$–$3p$	$4s$–$4p$	$4s$–$4p$
$^4P_{5/2}$–$^4P_{5/2}$	4·20	4·43	4·61	4·63	5·00
3/2 – 3/2	0·53	0·57	0·79	0·34	1·10
1/2 – 1/2	0·33	0·30	0·28	0·27	0·21
5/2 – 3/2	1·80	1·94	1·67	2·69	1·50
3/2 – 1/2	1·67	1·70	1·71	1·73	1·73
3/2 – 5/2	1·80	1·57	1·39	1·30	1·00
1/2 – 3/2	1·67	1·49	1·55	0·95	1·39
$^4P_{5/2}$–$^4D_{7/2}$	8·00	8·00	8·00	8·00	8·00
3/2 – 5/2	4·20	4·43	4·56	4·71	4·30
1/2 – 3/2	1·67	1·79	1·90	1·93	2·05
5/2 – 5/2	1·80	1·57	1·38	1·29	0·83
3/2 – 3/2	2·13	2·05	1·95	1·96	1·62
1/2 – 1/2	1·67	1·70	1·72	1·73	1·79
5/2 – 3/2	0·20	0·16	0·13	0·10	0·08*
3/2 – 1/2	0·33	0·30	0·28	0·27	0·21
$^4P_{3/2}$–$^4S_{3/2}$	1·33	1·37	1·22	1·67	1·18
1/2 – 3/2	0·67	0·72	0·54	1·11	0·40
5/2 – 3/2	2·00	1·90	2·16	1·18	2·35
$^2P_{3/2}$–$^2D_{5/2}$	6·00	6·00	5·93	5·93	5·12
1/2 – 3/2	3·33	3·42	3·03	3·54	0·93*
3/2 – 3/2	0·67	0·58	0·95	0·45	2·84*
$^2P_{3/2}$–$^2S_{1/2}$	1·33	1·35	0·97	1·40	1·93
1/2 – 1/2	0·67	0·65	1·02	0·60	0·018*
$^2P_{3/2}$–$^2P_{3/2}$	3·33	3·41	2·97	3·52	1·00*
1/2 – 1/2	1·33	1·35	0·98	1·40	1·96
3/2 – 1/2	0·67	0·65	1·02	0·60	0·021*
1/2 – 3/2	0·67	0·58	0·93	0·44	2·92*
$^2D'_{5/2}$–$^2F'_{7/2}$	8·00	8·00	7·98	8·00	8·00
3/2 – 5/2	5·60	5·57	5·57	5·26	5·53
5/2 – 5/2	0·40	0·43	0·43	0·74	0·46
$^2D'_{5/2}$–$^2P'_{3/2}$	3·60	3·61	3·52	3·64	3·36
3/2 – 1/2	2·00	2·00	2·00	1·99	1·99
3/2 – 3/2	0·40	0·39	0·39	0·35	0·62

TABLE V (*cont.*)

Line	LS	Intermediate Coupling			
		O II	Ne II	S II	A II
		$3s-3p$	$3s-3p$	$4s-4p$	$4s-4p$
$^2D'_{5/2}-{}^2D'_{5/2}$	5·60	5·57	5·57	5·26	5·53
3/2 — 3/2	3·60	3·61	3·52	3·65	3·37
5/2 — 3/2	0·40	0·39	0·48	0·35	0·63
3/2 — 5/2	0·40	0·43	0·43	0·74	0·47
$^2S''_{1/2}-{}^2P''_{3/2}$	4·00	4·00	4·00	4·00	4·00
1/2 — 1/2	2·00	2·00	2·00	2·00	2·00
$^2P_{3/2}-{}^4D_{5/2}$	...	...	0·064	...	0·88*
3/2 — 3/2	...	...	0·003	...	0·14
1/2 — 3/2	...	...	0·014	...	0·11*
$^4P_{5/2}-{}^2D_{5/2}$	...	...	0·018	0·054	0·18
5/2 — 3/2	...	...	...	0·011	0·001
3/2 — 3/2	...	...	0·009	0·002	0·10
3/2 — 5/2	...	...	0·046	0·014	0·70
1/2 — 3/2	...	...	0·008	0·004	0·13*
$^2P_{3/2}-{}^4S_{3/2}$	...	0·006	0·070	0·035	0·023
1/2 — 3/2	...	0·001	0·024	0·004	0·040
$^4P_{5/2}-{}^2P_{3/2}$	...	0·002	0·035	0·016	0·055
3/2 — 3/2	...	0·003	0·029	0·016	0·002
$^4P_{3/2}-{}^2S_{1/2}$	...	...	0·011	...	0·040
$^2P_{3/2}-{}^4P_{3/2}$	...	...	...	0·065	0·002
3/2 — 1/2	...	...	0·009	...	0·043
$^2P_{3/2}-{}^2P'_{3/2}$	...	...	...	0·002	0·007
3/2 — 1/2	...	...	...	0·003	0·003
1/2 — 1/2	...	...	...	0·001	0·005
$^2D'_{3/2}-{}^2P_{1/2}$	...	...	...	0·004	0·005
$^2D'_{5/2}-{}^4P_{3/2}$	...	...	0·001	0·004	0·011
3/2 — 1/2	...	...	...	0·001	0·003
$^2S''_{1/2}-{}^4S_{3/2}$	...	...	...	0·001	0·004

* Indicates a line particularly sensitive to adopted parameters. Numerous other lines have a small, but finite, strength. All lines with strengths exceeding 0·02 have been included.

There are certain sum-rules valid in intermediate coupling. These provide useful numerical checks on the computations but do not provide any check on the physical validity of the transformation matrices.

On examining the results of the computations for the $s-p$ arrays it is seen that intercombination lines are fairly weak. They are particularly weak if the initial and final terms are based on different parents. It follows that it is a good approximation to neglect interactions between terms based on different parents. A second conclusion which may be drawn from Tables V and VI is that in general weak lines are very much more sensitive to departures from LS coupling than are strong lines. This conclusion was anticipated: the effect of IC is to redistribute

TABLE VI

Relative line strengths for O II $2p^2(^3P)3p-2p^2(^3P)3d$ *and for* Ne II $2p^4(^3P)3p-2p^4(^3P)3d$

(All expressed in units of the radial integral σ^2)

Line	LS Coupling	Intermediate Coupling		Estimated intensities	
		O II	Ne II	O II	Ne II
$^2S_{1/2}-{}^2P_{3/2}$	13·33	13·24	9·01	8	4
1/2 — 1/2	6·67	6·51	7·99	7	5
$^2D_{5/2}-{}^2F_{7/2}$	48·00	45·90	31·90	8	5
5/2 — 5/2	2·40	1·79	1·30*	3	2
3/2 — 5/2	33·60	29·45	4·88*	7	2
$^2D_{5/2}-{}^2D_{5/2}$	8·40	8·81	7·99	7	4
3/2 — 3/2	5·40	5·19	4·84	4	3
5/2 — 3/2	0·60	0·48	0·17	1	...
3/2 — 5/2	0·60	0·47	4·22*	1	3
$^2P_{3/2}-{}^2P_{3/2}$	8·33	7·28	5·39	5	4
1/2 — 1/2	3·33	3·42	1·71	4	2
3/2 — 1/2	1·67	1·61	1·81	2	2
1/2 — 3/2	1·67	2·65	8·24	3	4
$^2P_{3/2}-{}^2D_{5/2}$	27·00	26·73	14·75	7	7
1/2 — 3/2	15·00	13·91	7·71	5	6
3/2 — 3/2	3·00	4·32	3·86	3	5
$^2D_{5/2}-{}^2P_{3/2}$	0·60	0·71	0·82	...	2
3/2 — 1/2	0·33	0·38	0·18	...	2
3/2 — 3/2	0·066	0·003	0·044	...	1
$^4D_{7/2}-{}^4F_{9/2}$	60·00	60·00	60·00	10	8
5/2 — 7/2	41·14	42·16	28·99	8	5
3/2 — 5/2	26·88	27·72	7·08	6	2
1/2 — 3/2	16·80	17·42	11·99	4	3
7/2 — 7/2	6·86	5·86	2·77	5	3
5/2 — 5/2	8·78	8·02	1·76*	3	4
3/2 — 3/2	6·72	6·26	3·83*	4	...
7/2 — 5/2	0·34	0·25	0·20*	0	2
5/2 — 3/2	0·48	0·36	0·011*	0	3
$^4D_{7/2}-{}^4P_{5/2}$	0·80	1·75	1·04	...	4
5/2 — 3/2	0·42	1·80	1·07*	1	0
3/2 — 1/2	0·17	1·12	0·42	1	...
5/2 — 5/2	0·18	0·37	0·010*	4	2
3/2 — 3/2	0·21	0·16	0·89*	1	4
1/2 — 1/2	0·17	0·087	0·11	1	...
3/2 — 5/2	0·020	0·14	0·33	2	3
1/2 — 3/2	0·033	0·16	3·35*	2	3
$^4D_{7/2}-{}^4D_{7/2}$	10·29	10·84	12·87	7	4
5/2 — 5/2	5·19	4·46	6·20	5	3
3/2 — 3/2	2·40	2·34	2·91	3	3
1/2 — 1/2	1·50	1·44	1·34	3	1
7/2 — 5/2	1·71	0·71	1·51	3	2
5/2 — 3/2	2·10	0·80	1·63	1	1
3/2 — 1/2	1·50	0·48	1·12	5	2
5/2 — 7/2	1·71	1·25	0·53	2	...
3/2 — 5/2	2·10	1·25	0·78*	2	2
1/2 — 3/2	1·50	1·16	0·61	3	2

TABLE VI (*cont.*)

Line	LS Coupling	Intermediate Coupling		Estimated intensities	
		O II	Ne II	O II	Ne II
$^4P_{5/2}-{}^4P_{5/2}$	10·50	3·85	6·33	4	...
$3/2-3/2$	1·33	0·34	0·47	0	...
$1/2-1/2$	0·83	5·26	1·30	4	...
$5/2-3/2$	4·50	1·79	2·19	3	...
$3/2-1/2$	4·17	0·84	3·94	2	...
$3/2-5/2$	4·50	13·29	5·96	7	...
$1/2-3/2$	4·17	9·54	3·67	6	...
$^4S_{3/2}-{}^4P_{5/2}$	20·00	16·57	16·65	6	7
$3/2-3/2$	13·33	10·11	7·40	5	4
$3/2-1/2$	6·67	4·66	5·95	4	4
$^4P_{5/2}-{}^4D_{7/2}$	36·00	33·80	34·36	8	5
$3/2-5/2$	18·90	8·49	15·11	5	6
$1/2-3/2$	7·50	1·93	5·29	4	5
$5/2-5/2$	8·10	13·62	12·12	3	4
$3/2-3/2$	9·60	10·79	11·30	7	4
$1/2-1/2$	7·50	3·14	7·09	5	4
$5/2-3/2$	0·90	3·59	1·92	2	3
$3/2-1/2$	1·50	4·69	2·32	3	...
$^2D_{5/2}-{}^4D_{7/2}$	...	2·12	0·24	4	1
$3/2-5/2$	...	4·51	...	5	...
$5/2-5/2$	...	0·24	0·05	2	...
$^4S_{3/2}-{}^4D_{5/2}$	...	2·73	0·22	2	2
$3/2-3/2$	...	3·39	0·18	2	1
$3/2-1/2$	...	2·28	0·04	3	...
$^4P_{5/2}-{}^2F_{7/2}$	...	1·49	0·03	1	...
$3/2-5/2$	...	1·60	0·29	3	...
$5/2-5/2$	...	1·91	0·11	4	...
$^4D_{7/2}-{}^2F_{7/2}$	...	0·43	1·56	0	2
$5/2-5/2$	...	0·65	3·08*	4	3
$7/2-5/2$	...	0·14	0·021*	4	1
$5/2-7/2$	...	0·18	14·50	3	5
$3/2-5/2$	...	0·32	16·36*	3	5
$^4S_{3/2}-{}^2F_{5/2}$	...	0·27	1·21*	1	2
$^4D_{5/2}-{}^2D_{5/2}$	...	...	1·86*	...	2
$3/2-3/2$	...	...	0·95	...	3
$3/2-5/2$	...	...	5·07*	...	3
$1/2-3/2$	...	...	2·50	...	3
$5/2-3/2$	...	...	0·13	...	...
$7/2-5/2$	...	...	0·09	...	...
$^2D_{5/2}-{}^4F_{7/2}$	...	...	15·83	...	6
$3/2-5/2$	...	...	22·84	...	6
$5/2-5/2$	...	...	1·30	...	2
$3/2-3/2$	...	...	0·38	...	...

TABLE VI (*cont.*)

Line	LS Coupling	Intermediate Coupling		Estimated intensities	
		O II	Ne II	O II	Ne II
$^2D_{5/2}-{}^4P_{5/2}$	...	...	0·28	...	1
$3/2-5/2$	...	...	1·43	...	4
$3/2-3/2$	...	...	1·12	...	...
$5/2-3/2$	...	...	0·22	...	...
$^2S_{1/2}-{}^4F_{3/2}$	...	...	0·49	...	1
$^2S_{1/2}-{}^2D_{3/2}$	...	0·10	2·08	...	3
$^2S_{1/2}-{}^4P_{3/2}$	...	0·08	0·19	1	1
$1/2-1/2$	...	0·03	0·21	0	...
$^4S_{3/2}-{}^4F_{5/2}$	...	...	1·47	...	4
$3/2-3/2$	...	...	3·94*	...	4
$^4S_{3/2}-{}^2D_{5/2}$	...	...	1·60*	...	3
$3/2-3/2$	...	...	0·86	...	2
$^4S_{3/2}-{}^2P_{3/2}$	...	...	0·04	...	1
$3/2-1/2$	...	...	0·05	...	1
$^2P_{3/2}-{}^4F_{5/2}$	...	...	0·55*	...	2
$3/2-3/2$	...	...	0·31	...	...
$^2P_{3/2}-{}^2F_{5/2}$	...	...	8·76*	...	5
$^2S_{1/2}-{}^4D_{1/2}$	...	0·03	0·05	1	...
$^4P_{5/2}-{}^4F_{7/2}$	...	0·006	0·41	0	...
$5/2-5/2$	...	...	0·78	...	...
$5/2-3/2$	...	...	0·87	...	...
$3/2-5/2$	...	...	0·11	...	...
$3/2-3/2$	...	...	0·08	...	...
$1/2-3/2$	...	...	2·12	...	...
$^4P_{1/2}-{}^2P_{1/2}$	...	0·07	0·16	1	...
$1/2-3/2$	...	0·09	0·16	0	...
$^2P_{3/2}-{}^4P_{5/2}$	...	...	3·78	...	4
$1/2-3/2$	...	...	2·27	...	4
$3/2-3/2$	...	...	0·95	...	...
$^4D_{1/2}-{}^2P_{3/2}$	...	...	0·12	...	...
$3/2-1/2$	...	...	0·06	...	...
$5/2-3/2$	...	...	0·09	...	...
$^4P_{5/2}-{}^2D_{5/2}$	...	...	0·51	...	...
$5/2-3/2$	...	...	0·23	...	...
$3/2-5/2$	...	...	0·09	...	...
$3/2-3/2$	...	...	0·16	...	...
$1/2-3/2$	...	...	0·12	...	...

* Denotes a line particularly sensitive to adopted parameters. This table includes all lines mentioned in the ***Revised Multiplet Table*** and all others with strengths not less than 0·06.

energy among various possible transitions and a weak line will be subject to a greater proportional change. In the *p–d* arrays, however, there are a number of strong lines with strengths substantially different from the LS values. The multiplet ^4P–^4P of O II is of especial interest in this connection. Furthermore there are a number of very strong intercombination lines in the *p–d* arrays of both O II and Ne II.

There are, unfortunately, no tables of accurate laboratory intensities for any of the transitions which we have studied. The available eye-estimates (**11**) have been included in Table VI. In some multiplets (e.g. ^2P–^2P in O II and Ne II and ^4P–^4P in O II the IC strengths give much better agreement with the estimated

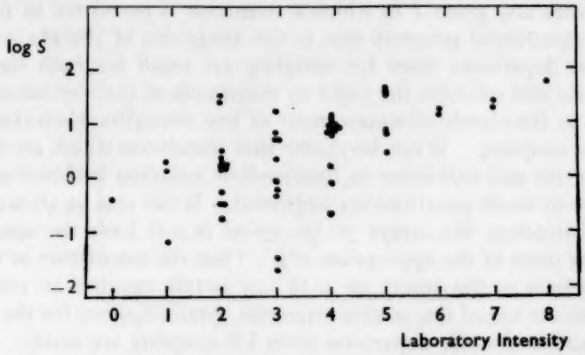

FIG. 1.—*Relation between the logarithm of the LS coupling strength and the laboratory intensity estimates for Ne II 3p–3d.*

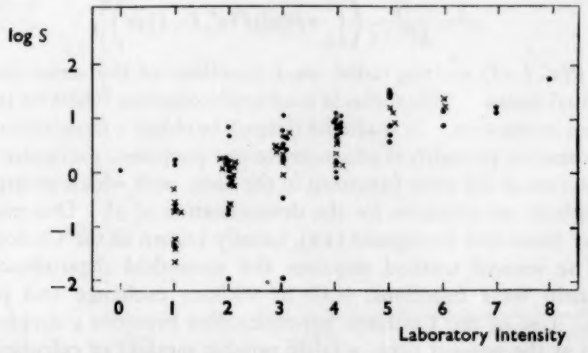

FIG. 2.—*Relation between the logarithm of the IC strength and the laboratory intensity estimates for Ne II 3p–3d. Filled circles denote lines allowed in LS coupling—the same lines as in Fig. 1. Crosses denote intercombination lines.*

intensities than that given by LS strengths. In others (e.g. ^4D–^4F in Ne II) the agreement is disappointing. The most encouraging feature, however, is the behaviour of the intercombination lines in Ne II. The theoretical strengths obtained for the ^4D–^2F multiplet (amongst others) in Ne II are excellent. To illustrate this Figs. 1 and 2 show the relation between the logarithms of the calculated relative strengths and the estimated intensities. In Fig. 2, intercombination lines have been distinguished from lines allowed in LS coupling. The agreement of the general relationships between strength and intensity for the two groups of lines is very satisfactory and gives added confidence in the

results of the calculations. There is a large residual scatter, due to a combination of the uncertainties in the calculations and the unknown errors in the intensity estimates.

4. *The transition arrays* $3p$–ns.—The spectra of some early-type stars (for example, the B2 supergiant 55 Cygni) contain not only lines from the array $3s$–$3p$ of O II but also some lines of O II $3p$–$4s$. It is of interest to consider the line strengths of the latter transition in intermediate coupling. The matrix of the square roots of the line strengths, when expressed in the appropriate σ as unit, is the same for all the arrays $3s$–$3p$, $3p$–ns ($n \geqslant 4$). This matrix has the special property that for any given level of the $3p$ configuration there is only at most one level in ns with any given J to which a transition is permitted in LS coupling. This is an exceptional property due to the simplicity of the $p^2 s$ configuration. Assume that departures from LS coupling are small for both the $3p$ and ns configurations and consider the order of magnitude of the various contributions which arise in the matrix of square roots of line strengths when transformed to intermediate coupling. It can be shown that transitions which are forbidden in LS coupling are also forbidden in intermediate coupling if contributions of the second order of small quantities are neglected. It can also be shown that to the same approximation, the arrays $3s$–$3p$, $3p$–ns ($n \geqslant 4$) have the same strengths (expressed in units of the appropriate σ^2). Thus the calculation of the absolute strengths of lines in the arrays $3p$–ns ($n \geqslant 4$) merely requires an estimate of σ^2, together with the use of the relative strengths obtained above for the $3s$–$3p$ array and a verification that the departures from LS coupling are small.

5. *Absolute strengths.*—The calculations so far discussed have been concerned with the relative strengths of lines expressed in multiples of σ^2, where

$$\sigma^2 = \frac{1}{4l^2 - 1}\left(\int_0^\infty r P(nl) P(n', l-1)\, dr\right)^2,$$

and $P(nl)$, $P(n', l-1)$ are the radial wave functions of the series electron in its initial and final states. This formula is an approximation based on the neglect of configuration interaction. It would be difficult to obtain a more accurate formula. The approximation probably is adequate for our purposes, particularly as there is little cancellation of the wave functions in the cases with which we are concerned.

Two methods are available for the determination of σ^2. One method is that described by Bates and Damgaard (**12**), usually known as the Coulomb approximation. The second method requires the numerical determination of self-consistent field wave functions, with or without exchange and polarizability corrections. Use of the Coulomb approximation provides a simple and, as far as is known at the present time, a fairly reliable method of calculating σ^2. We shall confine ourselves to this method. The method has been applied to the transitions in O II, S II and A II and the results, together with the author's (**13**) earlier results for Ne II, are given in Table VII.

TABLE VII

Ion	Array	σ^2 (atomic units)
O II	$3s$–$3p$	4·2
	$3p$–$3d$	1·17
Ne II	$3s$–$3p$	3·3
	$3p$–$3d$	0·99
S II	$4s$–$4p$	6·5
A II	$4s$–$4p$	5·2

The relative strengths of the lines given in Tables V and VI can be converted to absolute strengths by multiplication of the relative strength by the appropriate σ^2. Transition probabilities and f-values can then be calculated, if required, using standard formulae.

6. *Curves of growth for γ Pegasi.*—One of the principal applications of the strengths of large numbers of spectral lines is the construction of curves of growth for individual stars. Among the numerous studies of this type the work of Aller (**14**) on γ Pegasi is of special interest in connection with our computations on O II.

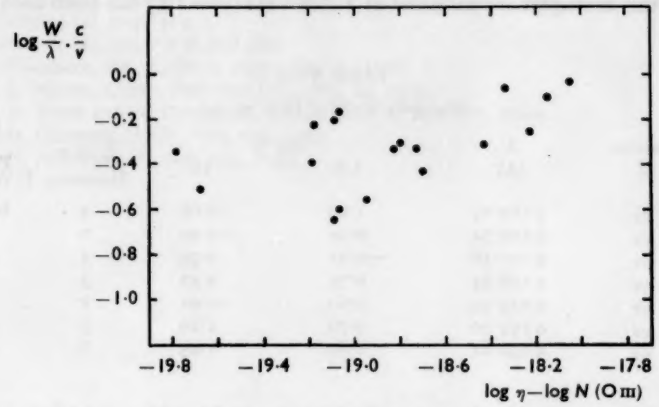

FIG. 3.—*Curve of growth for O II 3p–3d in γ Pegasi, using LS coupling strengths.*

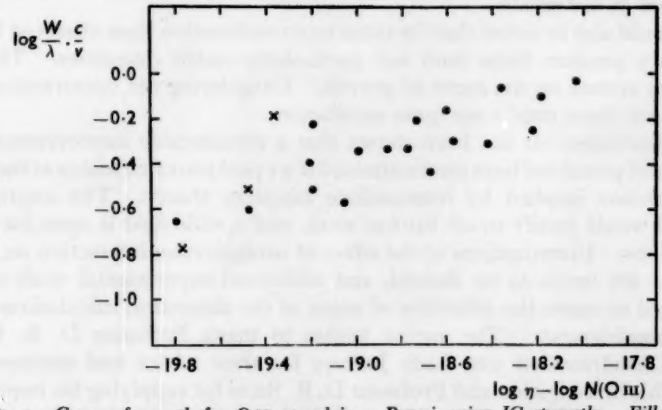

FIG. 4.—*Curve of growth for O II 3p–3d in γ Pegasi, using IC strengths. Filled circles denote lines allowed in LS coupling—the same lines as in Fig. 3. Crosses denote intercombination lines.*

Aller measured the equivalent widths of a large number of lines and constructed curves of growth for various ions. Examination of his data for O II shows that while the $3s$–$3p$ array gives a curve of growth with the observational points scattered reasonably closely about the theoretical curve, the $3p$–$3d$ array observations show a disturbingly large scatter. Part of this scatter is presumably due to observational errors and part may be due to errors in the assumed f-values. The latter source of scatter can now be investigated using our new f-values. We have re-plotted the curves of growth for the $3p$–$3d$ array in O II using LS and IC

line strengths and the results are shown in Figs. 3 and 4. The notation and method of calculation are the same as used by Aller. It will be seen that there is an appreciable reduction of scatter when the IC strengths are used. Unfortunately the remaining scatter is rather large and a theoretical curve cannot be well fitted to the observations. The writer understands that Aller is obtaining new intensity measurements with greater accuracy and further detailed discussion of the bulk of the stellar data at the present time does not seem justified.

The most important changes introduced in IC are in the ^4P–^4P multiplet. Data for this multiplet are collected in Table VIII ($\sigma^2 = 1{\cdot}17$ has been used).

TABLE VIII

Multiplet ^4P–^4P *of* O II $3p$–$3d$

Designation J	Designation J	λ (A)	log S LS	log S IC	*R.M.T.* Intensity	Aller γ Peg E.W. (mA)
5/2	5/2	4 169·23	1·09	0·66	4	blend
3/2	3/2	4 140·74	0·19	−0·40	0	...
1/2	1/2	4 121·48	−0·01	0·79	4	28
5/2	3/2	4 156·54	0·72	0·32	3	16
3/2	1/2	4 129·34	0·69	−0·01	2	14
3/2	5/2	4 153·30	0·72	1·19	7	44
1/2	3/2	4 132·81	0·69	1·05	6	40

The improvement in the strengths is very considerable, and gives increased confidence in our results.

It should also be noted that for three intercombination lines observed by Aller the theory predicts finite (and not particularly small) intensities. These are plotted as crosses on the curve of growth. Considering the uncertainties of the calculations these results are quite satisfactory.

7. *Conclusion.*—It has been shown that a considerable improvement in the strengths of permitted lines can be attained if we perform calculations at the level of approximation implied by intermediate coupling theory. The improvement obtained would justify much further work, and a wide field is open for routine calculations. Investigations of the effect of configuration interaction on the line strengths are much to be desired, and additional experimental work must be performed to assess the reliability of many of the theoretical calculations.

Acknowledgments.—The author wishes to thank Professor D. R. Hartree, Dr S. Chandrasekhar and Lady Jeffreys for their advice and encouragement during this investigation and Professor D. R. Bates for supplying his unpublished wave function. This work was begun during the tenure of an Isaac Newton Studentship of the University of Cambridge and a Studentship from Gonville and Caius College. A small part of the calculations was performed at the Yerkes Observatory while the writer was in receipt of financial support from the Geophysics Research Directorate of the U.S.A.F. Cambridge Research Laboratories. The calculations were completed at the University of London Observatory.

University of London Observatory,
Mill Hill Park,
London, N.W. 7:
1954 *January* 26.

References

(1) For LS Coupling see L. H. Aller, *Astrophysics*, Ronald Press, New York, pp. 134–142, 1953.
(2) E. U. Condon and G. H. Shortley, *Theory of Atomic Spectra*, Cambridge, 1935 and 1952, Chapter XI.
(3) G. H. Shortley, *Phys. Rev.*, **47**, 295, 1935.
(4) W. M. Gottschalk, *Ap. J.*, **108**, 326, 1948.
(5) M. H. Johnson, *Phys. Rev.*, **38**, 1628, 1931.
(6) Reference (2), page 196.
(7) C. E. Moore, *National Bureau of Standards*, Circular 467, 1949.
(8) Reference (2), page 385.
(9) Reference (2), pages 238 and 277.
(10) L. Goldberg, *Ap. J.*, **82**, 1, 1935; **84**, 11, 1936.
(11) C. E. Moore, *Contr. Princeton Obs.*, No. 20, 1945.
(12) D. R. Bates and A. Damgaard, *Phil. Trans.* A, **242**, 101, 1949.
(13) R. H. Garstang, *M.N.*, **110**, 612, 1950.
(14) L. H. Aller, *Ap. J.*, **109**, 244, 1949.

MEAN AREAS AND HELIOGRAPHIC LATITUDES OF SUNSPOTS IN THE YEAR 1950

Royal Greenwich Observatory

(Communicated by the Astronomer Royal)

(Received 1954 February 5)

The following results are in continuation of those given in *M.N.*, **113**, 786, 1953, and are derived from the measurement at Herstmonceux of photographs taken at the Royal Observatories of Greenwich and the Cape and at the Kodaikanal Observatory, India. The Greenwich photographs were all taken at the new site at Herstmonceux Castle.

Table I gives the mean daily areas of umbrae, whole spots and faculae for each synodic rotation of the Sun included in the year 1950; the means for the year as a whole are included in Table II, which summarizes the yearly values since the last sunspot minimum of 1944.

TABLE I

No. of rotation	Rotation commenced U.T. 1949–50	Days photographed	Mean daily areas: Projected* Umbrae	Projected* Whole spots	Projected* Faculae	Corrected for foreshortening† Umbrae	Corrected for foreshortening† Whole spots	Corrected for foreshortening† Faculae
1288	Dec. 20·18	28	266	1691	1838	192	1235	2269
1289	Jan. 16·52	27	274	1559	1810	206	1186	2220
1290	Feb. 12·86	27	564	3429	2013	422	2607	2541
1291	Mar. 12·19	28	389	2215	1752	300	1728	2232
1292	Apr. 8·49	27	514	3300	1781	365	2334	2227
1293	May 5·74	27	328	1922	1742	250	1480	2150
1294	June 1·96	27	246	1441	1600	182	1091	1966
1295	June 29·15	27	264	1543	1467	198	1165	1806
1296	July 26·36	28	294	1774	1270	212	1260	1600
1297	Aug. 22·59	27	133	743	1184	103	579	1437
1298	Sept. 18·84	27	144	780	1127	103	567	1361
1299	Oct. 16·13	27	148	900	886	111	685	1038
1300	Nov. 12·43	28	182	1112	882	129	806	1060

* Expressed in millionths of the Sun's disk.

† Expressed in millionths of the Sun's hemisphere.

Table III gives for each rotation in the year 1950 the mean daily area of the whole spots (corrected for foreshortening) and the mean heliographic latitude of the spotted areas for both northern and southern hemispheres.

The mean heliographic latitude of the entire spotted area and the mean distance from the equator of all spots are also tabulated. The mean values for the year 1950 are included in Table IV.

Tables II and IV are in continuation of similar tables in *Monthly Notices*: for the years *1874* to *1888*, **49**, 381, 1889: *1889* to *1902*, **63**, 465, 1903: *1901* to *1914*, **76**, 402, 1916: *1913* to *1924*, **85**, 1007, 1925: *1923* to *1933*, **94**, 870, 1934: and *1933* to *1945*, **110**, 501, 1950.

The rotations in Tables I and III are numbered in continuation of Carrington's series.

TABLE II

Year	No. of days: Photographed	No. of days: Without spots	Mean daily areas: Projected*: Umbrae	Projected*: Whole spots	Projected*: Faculae	Corrected for foreshortening†: Umbrae	Corrected for foreshortening†: Whole spots	Corrected for foreshortening†: Faculae
1944	366	157	30	160	284	23	126	344
1945	365	14	102	560	774	78	429	940
1946	365	0	389	2381	1794	291	1817	2188
1947	365	0	558	3559	2326	405	2637	2894
1948	366	0	419	2618	1849	314	1977	2331
1949	365	0	485	2873	2140	356	2129	2597
1950	365	3	274	1638	1421	203	1222	1754

* Expressed in millionths of the Sun's disk.
† Expressed in millionths of the Sun's hemisphere.

TABLE III

No. of rotation	Rotation commenced U.T. 1949–50	Spots north of the equator: Mean daily area	Spots north of the equator: Mean heliographic latitude	Spots south of the equator: Mean daily area	Spots south of the equator: Mean heliographic latitude	Mean latitude of entire spotted area	Mean distance from equator of all spots
			°		°	°	°
1288	Dec. 20·18	1022	13·87	213	6·06	+10·44	12·53
1289	Jan. 16·52	960	14·55	226	11·42	+ 9·60	13·95
1290	Feb. 12·86	1820	12·20	787	14·27	+ 4·21	12·82
1291	Mar. 12·19	1083	18·07	646	12·77	+ 6·55	16·09
1292	Apr. 8·49	1362	13·56	972	14·07	+ 2·06	13·77
1293	May 5·74	1164	11·01	315	12·59	+ 5·98	11·35
1294	June 1·96	521	9·79	570	17·98	− 4·72	14·07
1295	June 29·15	808	13·42	357	13·82	+ 5·08	13·54
1296	July 26·36	433	12·46	826	11·21	− 3·06	11·64
1297	Aug. 22·59	272	15·32	307	10·23	+ 1·78	12·62
1298	Sept. 18·84	354	15·45	212	10·28	+ 5·81	13·51
1299	Oct. 16·13	295	13·47	390	10·75	− 0·31	11·93
1300	Nov. 12·43	475	15·04	331	12·59	+ 3·70	14·04

TABLE IV

Year	Days photographed	Spots north of the equator: Mean daily area	Spots north of the equator: Mean heliographic latitude	Spots south of the equator: Mean daily area	Spots south of the equator: Mean heliographic latitude	Mean latitude of entire spotted area	Mean distance from equator of all spots
1944	366	42	19·00	83	22·81	−8·70	21·53
1944	366 Old Cycle	7	4·17	6	7·61	−1·14	5·72
1944	366 New cycle	35	22·18	77	24·02	−9·63	23·45
1945	365	121	20·13	309	20·26	−8·92	20·22
1946	365	1127	20·74	690	18·79	+5·73	20·00
1947	365	992	16·58	1645	17·86	−4·91	17·38
1948	366	936	14·92	1041	13·53	−0·06	14·19
1949	365	1178	14·30	951	12·14	+2·49	13·33
1950	365	771	13·62	452	13·05	+3·77	13·41

The chief features of the record for the year 1950 are as follows :—

(1) The mean daily area of sunspots, corrected for foreshortening (Table II), although still large, shows a marked decrease as compared with the previous year amounting to 42·6 per cent. The decrease from the maximum year (1947) amounts to 53·6 per cent.

The mean area of faculae for 1950 likewise shows a considerable decrease though not so marked as for sunspots. As compared with 1949 the drop in mean daily area is 32·5 per cent and as compared with the maximum year 39·4 per cent.

The ratio of mean corrected areas of faculae/sunspots is 1·44.

A very large and active group with a mean area of 1853 millionths of the Sun's hemisphere and central meridian passage on February 20 contributed to the high area value of 2607 millionths for Rotation No. 1290 (Table I).

Two other large spots with respective mean areas of 1527 and 1011 were present during Rotation No. 1292. Thereafter, the mean areas for the synodic rotations were appreciably less, especially after Rotation 1297.

(2) On three days there were no sunspots present, viz. December 21, 22 and 23, and no faculae were seen on October 22.

(3) The mean weighted latitude of all spots 13°·4 (Table IV) was almost the same as in the previous year, thus representing what is, no doubt, a temporary halt in the latitude progression towards the equator. This irregularity is shown particularly by the southern spots. The latitudes of the three largest spot groups were +10°·1, +13°·4 and −12°·0.

Table IV also shows that the ratio of areas of northern spots/southern spots for 1950 is 1·71.

(4) The number and distribution, northern and southern hemispheres, of spot groups of (*a*) two days' duration or longer; (*b*) one day only; are as follows :

	(*a*)	(*b*)
Northern spots	189	33
Southern spots	126	27
Total	315	60

The range in latitude for the longer-lived spots was from 0° to 40°. The latitudes of the 1-day spots ranged from 1° to 35°.

A short descriptive survey of the sunspots of 1950 has been given in *Monthly Notices*, **111**, 233, 1951.

An appended table gives the mean daily areas of sunspots and of faculae (corrected for foreshortening and expressed in millionths of the Sun's hemisphere) for each calendar month of 1950.

Monthly mean daily areas of sunspots and faculae

1950

Month	Spots	Faculae	Month	Spots	Faculae
Jan.	1416	2278	July	1256	1837
Feb.	1927	2262	Aug.	1069	1496
Mar.	1660	2330	Sept.	488	1350
Apr.	2359	2155	Oct.	571	1220
May	1578	2230	Nov.	745	842
June	1048	1931	Dec.	610	1145

Royal Greenwich Observatory,
Herstmonceux Castle, Sussex :
1954 *January* 29.

CONTENTS

PAGE

Meeting of 1954 January 8 :
Fellows elected 1
Junior Member elected 1
Presents announced 1
Award of the Gold Medal to Dr W. Baade 1

I. W. Busbridge and D. W. N. Stibbs, On the intensities of interlocked multiplet lines in the Milne–Eddington Model 2

A. B. Hart, Motions in the Sun at the photospheric level. IV. The equatorial rotation and possible velocity fields in the photosphere 17

T. R. Kaiser, Theory of the meteor height distribution obtained from radio-echo observations. I. Shower meteors 39

T. R. Kaiser, Theory of the meteor height distribution obtained from radio-echo observations. II. Sporadic meteors 52

S. Evans, Scale heights and pressures in the upper atmosphere from radio-echo observations of meteors 63

R. D. Davies, An analysis of bursts of solar radio emission and their association with solar and terrestrial phenomena 74

A. D. Thackeray, The helium star HD 168476 93

Zdeněk Kopal, Photometric effects of reflection in close binary systems 101

R. H. Garstang, Intermediate coupling line strengths 118

Royal Greenwich Observatory, Mean areas and heliographic latitudes of sunspots in the year 1950 134

Printed in London by Taylor & Francis, Ltd., 1954 October